UNIVERSITY OF NOTTINGHAM

DEPARTMENT OF CIVIL ENGINEERING

PERMANENT DEFORMATION RESISTANCE OF GRANULAR LAYERS IN PAVEMENTS

by

Francis Wai Kun Chan B.Sc., M.Sc., MIHT

Thesis submitted to the University of Nottingham
for the degree of Doctor of Philosophy

September 1990

TABLE OF CONTENTS

TABLE OF CONTENTS (Continued)

TABLE OF CONTENTS (Continued)

TABLE OF CONTENTS (Continued)

TABLE OF CONTENTS (Continued)

TABLE OF CONTENTS (Continued)

ABSTRACT

Research was carried out to improve the current understanding about the permanent deformation behaviour of granular bases. The main approach to the work was divided into two parts. In the first part, four series of large scale experiments involving 17 different flexible pavement sections with thin asphalt surfacings were carried out in the Nottingham Pavement Test Facility (PTF) to investigate the permanent deformation resistance of geosynthetic-reinforced granular bases. The experiments included the study of the effect of prestressing geosynthetic as well as prerutting the granular base with and without the reinforcement. In the second part, the effect of shear stress reversal on the permanent deformation behaviour of a scaled down granular material was investigated by means of a substantially modified repeated load hollow cylinder apparatus (HCA). The work necessitated major effort on the development of both laboratory equipment and testing technique, which are described in detail. Tests were also performed to evaluate the resilient stress-strain behaviour of the granular material under the general stress conditions where principal plane rotation occurred.

From the experiments in the PTF, test data from individual test sections were compared and the influences on the permanent deformation of the granular base due to prestressing, prerutting, stiffness, types and location of geosynthetics are discussed. Rankings of the performance of pavement sections according to their permanent deformation resistance were made. For tests carried out by the HCA, comparison of permanent strain response was made between tests involving triaxial, uni- and bi-directional shear reversal conditions. A comparison of results was also made between tests carried out by the HCA and the more conventional repeated load triaxial test apparatus. The results of the resilient strain tests were analysed by means of a contour model developed from results of triaxial tests. The applicability of the model to results from the HCA tests was evaluated and some modifications were suggested.

ACKNOWLEDGEMENTS

The author wishes to express his sincere gratitude to all those who have provided help and advice in this research project and in the preparation of this thesis. In particular he would like to thank:

Professor S F Brown, as Head of Department of Civil Engineering, for providing all the excellent facilities in the Department and, as project supervisor, for his continued helpful supervision and guidance throughout the project;

Mr A R Dawson and Dr R W Sparrow for their advice in the area of geosynthetic and granular material behaviour respectively;

Mr B V Brodrick and Mr A Leyko for their technical advice and generous assistance in work carried out in the Nottingham Pavement Test Facility;

Mr J Moody and Mr G Hanley, whose expertise in equipment construction, maintenance and electronics has ensured the successful modification and operation of the repeated load Hollow Cylinder and Triaxial Apparatus;

Mr J N Preston for his advice on the English and, occasionally, French language;
Mr M J Raybould for reading the draft of the thesis;
Miss R Allen and Miss C Brayley for preparing some of the figures;
Miss J Adams for her assistance in typing this thesis;

and to all other members of the Pavement Research Group whose friendliness and excellent company have certainly made this rather physically demanding research project easier to bear.

Finally, this research project would not have been possible without the generous financial support from the United States National Co-operative Highway Research Programme, the United States Air Force and the Science and Engineering Research Council of the United Kingdom. Generous sponsorships in terms of raw materials were also received from Amey Roadstone Corporation and Steetley Construction Materials. All this help is gratefully acknowledged.

LIST OF ABBREVIATIONS

B	Bottom of Granular Base
M	Middle of Granular Base
A/D	Analogue to Digital
AC	Asphaltic Concrete
GD	Geogrid
GX	Geotextile
PR	Prerutted
PS	Prestressed
ALF	Accelerated Loading Facility
CBR	California Bearing Ratio
CIV	Clegg Impact Value
DCP	Dynamic Cone Penetrometer
HCA	Hollow Cylinder Apparatus
HRA	Hot Rolled Asphalt
HVS	Heavy Vehicle Simulator
PTF	Pavement Test Facility
RAM	Random Access Memory
STF	Slab Test Facility
VMA	Void in Mix Aggregate
LVDT	Linear Variable Differential Transformer

LIST OF SYMBOLS

A,B	Coefficients used in Loach's resilient stress-strain model for soil
E_r	Subgrade elastic stiffness
G	Shear modulus
G_s	Specific gravity
G1	Coefficient for shear modulus in Contour model
H	Height of hollow cylinder specimen
K	Bulk modulus
K1	Coefficient for bulk modulus in Contour model
L	Gauge length for LVDTs on hollow cylinder specimen
M_T	Torque on hollow cylinder specimen
R^2	Coefficient of correlation
Sg	Stiffness of geosynthetic at 5% axial strain
S_r	Degree of saturation
W	Axial load on hollow cylinder specimen
a,b	Internal, external radius of hollow cylinder specimen
b	Intermediate principal stress parameter
d	Averaged diameter of hollow cylinder specimen
l	Displacement over the gauge length L, defined above
m	Coefficient for shear modulus in Contour model
n	Coefficient for bulk modulus in Contour model
p, p_m	Bulk, mean bulk stress
p_i, p_o	Inner and outer cell pressure in HCA
q	Deviator stress
q_{oct}	Octahedral shear stress
t	Thickness of the wall of hollow cylinder specimen
u	suction
w	water content
α	Angle of rotation of major principal stress from vertical
α	Coefficient used in Loach's resilient stress-strain model for soil
α_ϵ	Angle of rotation of major principal strain from vertical
β	Coefficient for bulk modulus in Contour model
γ	Engineering shear strain
δ	Prefix - meaning "change in"

LIST OF SYMBOLS (continued)

$\varepsilon_r, \varepsilon_z, \varepsilon_\theta, \varepsilon_{45}$	Normal strains in hollow cylinder specimen
$\varepsilon_{\theta z}$	Pure shear strain in θ-z plane
$\varepsilon_1, \varepsilon_2, \varepsilon_3$	Principal strains
ε_h	Horizontal strain $= \varepsilon_r + \varepsilon_z$ in hollow cylinder specimen $= 2\,\varepsilon_r$ in triaxial specimen
ε_s	Octahedral shear strain
ε_v	Volumetric strain
ε_{max}	Maximum shear strain in the θ-z plane
ε_t	Resilient longitudinal strain at the bottom of the asphalt layer
η_m	Mean shear stress ratio, $(q_{oct})_m/p_m$
$\sigma_r, \sigma_z, \sigma_\theta$	Normal stresses in hollow cylinder specimen
$\sigma_1, \sigma_2, \sigma_3$	Principal stresses
σ_c	Confining stress in triaxial specimen
σ_{oct}	Octahedral normal stress
$\tau_{\theta z}$	Torsional shear stress in θ-z plane

Suffices

m	mean
p	Permanent (strain)
r	in the radial direction
r	repeated (stress) or resilient (strain)
z	in the axial direction
θ	in the circumferential direction
max	maximum
failure	at failure

LIST OF FIGURES

LIST OF FIGURES (continued)

LIST OF FIGURES (continued)

LIST OF FIGURES (continued)

LIST OF FIGURES (continued)

LIST OF FIGURES (continued)

LIST OF FIGURES (continued)

CHAPTER ONE

INTRODUCTION

Rutting is the result of an accumulation of permanent deformation in the various pavement layers, both bound and unbound. It is not only due to vertical strain in each layer, but also occurs transversely due to the lateral spreading of the pavement materials. In the United Kingdom, one of the criteria to signal the end of the service life of a flexible pavement is taken to be a 20mm rut depth in the nearside wheel track. A 10mm rut or the onset of wheel track cracking, on the other hand, will mark the point known as the "Critical Life" when strengthening of the pavement should be carried out so that the pavement's structural integrity may be retained (Powell et al, 1984). In order to design for a particular life for the pavement, therefore, the prediction of changes in the pavement profiles has to be made.

The prediction of rut depth, however, is an extremely complicated business, especially so when one compares it with the simple task of measuring the rut depth using a straight edge and a steel rule. The problem is not only one of suitable material characterisation, but also one of accurate assessment of the environmental conditions and calculation of the appropriate stress distribution during the pavement life. In light of these complexities, most contemporary pavement design methods do not involve the direct calculation of rut depth using an analytical procedure. Instead, they commonly rely on semi-empirically developed rut indicators to ensure that excessive rutting will not occur during the design life of the pavement. These indicators are normally based on the back-analysis of pavements with known performance. However, the limitation of this method is that once it cannot be extrapolated with confidence beyond experience, it will no longer be considered reliable.

In most flexible pavements constructed in the United Kingdom, rutting is associated mainly with permanent deformation in the bituminous layers (Lister,1972). The permanent deformation resistance of granular layers often does not constitute a major problem. This is due to the fact that these pavements usually incorporate a rather substantial thickness of bituminous materials above the granular sub-base. As a result, only small peak stresses are transmitted to the underlying layers. However, there are many situations when thin or low stiffness bituminous layers are combined with very heavy wheel loads. Under these circumstances, permanent deformation in the granular layers becomes an important problem. Examples of these may be found:

1. during construction of pavement foundation;
2. in aircraft or similarly heavily loaded pavements;
3. in highways in the tropical or subtropical countries which have to cope with inhospitable high surface temperature or;
4. in the numerous thinly paved roads in a lot of the developing countries where, traffic intensities are admittedly often smaller, but axle loads are frequently much heavier.

Furthermore, the performance of most haul roads is very much dependent on the permanent deformation resistance of both the unbound granular materials and the subgrade. However, since the loading (on the granular base) and maintenance philosophy adopted for these roads are different from those for permanent roads, the approach to the rutting problem may not be the same.

Research into the behaviour of granular material in pavements has attracted a great deal of world-wide attention for the past 20 years. A lot of progress has been made during this time in the understanding and mathematical modelling of the resilient stress-strain behaviour of granular materials (Crockford et al 1988). This has led to successes in the

analysis of the elastic behaviour of pavements with granular bases (Brown and Pappin, 1985, Sweere et al, 1987). However, characterisation of the permanent deformation behaviour which is related to rut formation still remains as a challenge to be conquered. This is due partially to the fact that many material investigations have been limited in range of applied stress and lack of reference to material structure (e.g. grading, density and aggregate type etc. [Barrett 1976]). The fragmentation of research efforts and the paucity of information about the build-up of permanent strain in granular material is also attributed to the nature of the permanent strain test itself which is time-consuming and basically destructive. Therefore, unlike most resilient strain tests where a test specimen can be tested under hundreds of different stress conditions, the construction of a new laboratory specimen or pavement test section is required for a permanent strain test in order to study the new values of each parameter.

No doubt the stress condition is one of the most important parameters affecting the permanent deformation behaviour of granular materials in pavements. Therefore, most research into this problem uses devices which can simulate the stress conditions underneath a loaded wheel. Some approaches relate the permanent deformation resistance, empirically, to static behaviour, such as shear strength. The use of the California Bearing Ratio or Plate Bearing Test devices are typical examples. Others may contain a dynamic element. These include the use of impact devices such as the Clegg Hammer or the Dynamic Cone Penetrometer (DCP). The most realistic approach, however, involves those which reproduce, on an accelerated time scale, the repeated stresses caused by a moving wheel load. Full-scale pavement test facilities, like the South African Heavy Vehicle Simulator, HVS (Maree et al 1982a) and the Australian Accelerated Loading Facility, ALF (Kadar,1987) have proved to be effective tools for the purpose. These devices are powerful and flexible but are expensive, both in terms of initial and running costs. Therefore, their role tends to be one of validation of theory or innovative idea rather than to study the fundamental behaviour.

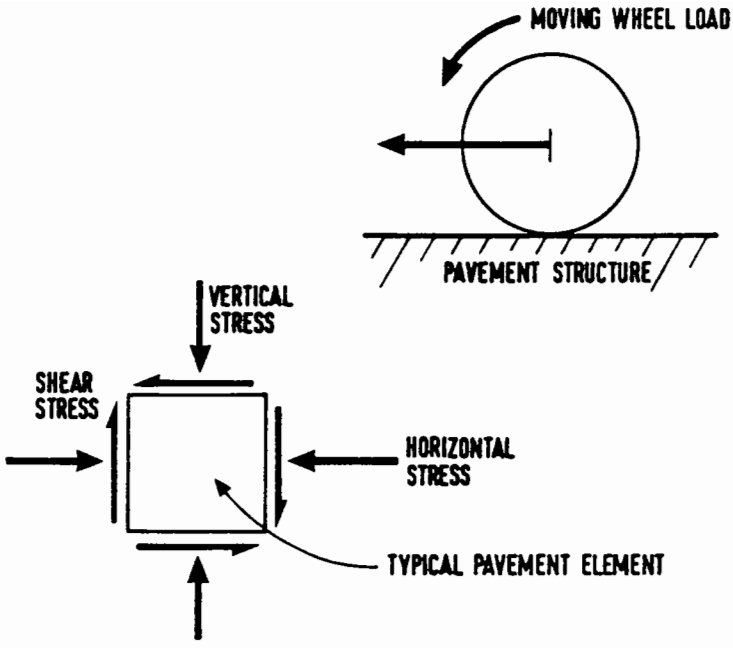

a. Stresses on Pavement Element.

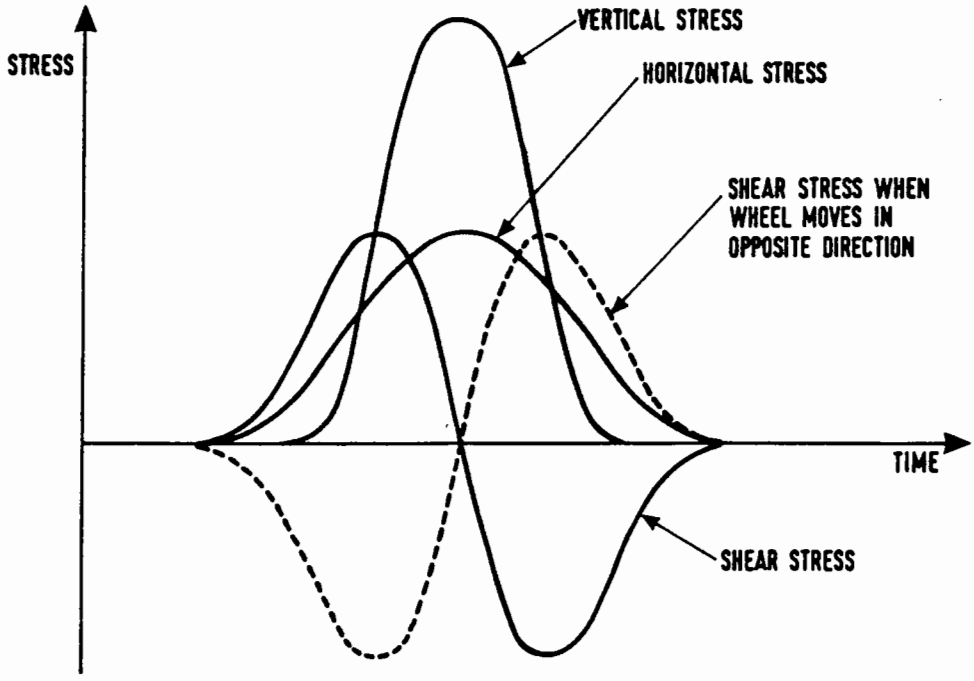

b. Variation of Stresses with Time.

Figure 1.1 Stresses induced by a Moving Wheel Load on a Vertically Oriented Element of Granular Material.

While the search for the appropriate means and technique to model the permanent strain may continue, there is a strong need at the moment by the road industry to develop practical methods to improve the permanent deformation resistance of granular layers. One method which has attracted considerable interest involves the use of geosynthetics - a group of artificially manufactured materials which include geotextiles, geogrid and geomembranes. The application of geosynthetics in earth structures has gained reasonably good acceptance in recent years. Research had already indicated that the fatigue life and rutting resistance of asphaltic materials could be improved by placement of a geogrid within the layer (Brown et al 1985). Geosynthetics have also proved to be very effective in the reduction of permanent deformation in granular pavements with weak subgrades (Webster and Watkins 1977, Potter and Currer 1981). However, in surfaced roads with good subgrades, the benefit to the granular bases is much less apparent. In fact, the merit of using geosynthetics as reinforcement became in doubt when greater permanent deformation (Brown et al 1982) and lack of improvement (Ruddock et al 1982) had been reported in some experiments.

With the above background in mind, the aim of the research presented in this dissertation was to improve the current understanding of the permanent deformation characteristics of granular materials. The main approach of the project was divided into two parts, both of which were experimentally designed to make use of the wide range of laboratory equipment that was uniquely available at the University of Nottingham.

The first part involved a study of the effect of geosynthetics, as highlighted earlier, on permanent deformation resistance of granular materials. The aim here was to provide the urgently required factual information concerning the use of the improvement method. To achieve this, a series of large scale experiments on instrumented test sections were conducted in the Nottingham Pavement Test Facility (PTF). A parallel theoretical study on geosynthetic reinforcement of granular bases in flexible pavements

was carried out by Georgia Institute of Technology in the United States (Barksdale et al 1989). This latter study which was not within the scope of this thesis, was performed by means of a comprehensive finite element program which analyzed mostly the elastic responses of the reinforced pavement structure.

In the second part of this project, the approach was more fundamental. The importance of reversed shear stresses on the permanent deformation of granular materials was first highlighted by means of large scale rutting tests. This was followed by element testing in the laboratory using a substantially modified repeated load HCA and a repeated load triaxial test apparatus. The use of an HCA necessitated major effort on the development of both laboratory equipment and testing technique. The overall emphasis of the element testing, however, was directed toward a study of the effect of shear stress reversal on the permanent deformation behaviour. HCA tests were also performed to evaluate the resilient stress- strain behaviour of the granular material under the general conditions where principal plane rotation occurred.

This dissertation is divided into eleven chapters. Chapter two reviews literature relevant to the project. The next six chapters are divided into two parts covering the two approaches adopted for this project. Part A, incorporating Chapter three and four, is dedicated to the method of improvement of permanent deformation resistance by means of geosynthetics. Details of the full scale experiments and their results are presented and discussed. In Chapter five to eight, which form Part B, attention is mainly focussed on the effect of reversed shear stresses on the permanent deformation characteristics of granular materials. The modified Nottingham HCA, the test programme and the results are described in detail. Chapter nine then summarises the accomplishments and conclusions from the project. Finally, Chapter ten discusses the practical implications of the results from both parts of the investigation and Chapter eleven presents recommendations for further research.

CHAPTER TWO

LITERATURE REVIEW

2.1 GENERAL DEFORMATION CHARACTERISTICS OF GRANULAR MATERIALS

A granular material is basically an assembly of different sizes and shapes of particles consisting of one or more types of minerals with voids occupied by either water or air or both. When a granular material is under loading (either static or dynamic), deformation will occur in the form of particle sliding, crushing, rolling and bending. These modes of physical interactions may in turn result in both volume changes and shear deformation - two important factors which account for the development of permanent strain in granular materials.

Particle bending is important in the case of flaky particles, especially when a group of them act as struts whose resistance to deformation depends both on the particles bending resistance and on the strength of the junctions at their ends.

The importance of grain crushing increases with particle size and load magnitude. Because of the wide dispersion of the magnitudes of interparticle contact forces, particle crushing is a progressive process that can start at relatively low applied stress levels. The resistance to grain crushing or breakage depends on the strength of the particles, which in turn depends on mineralogy. Studies of this mode of deformation in sands and gravels under triaxial stresses to more than 20 MPa (Lee and Farhroomand, 1967) indicate that:

1. Coarse granular materials compress more than fine materials.
2. Materials with uniform grading crush more than those which are well-graded.

3. Materials with angular particles show more crushing than those with rounded particles.
4. Under a given load, crushing continues indefinitely at a decreasing rate.
5. Interparticle contacts occur most frequently in a direction parallel to the major principal stress. As a result, deformation during compression depends mainly on the value of this stress and is independent of the principal stress ratio, σ_1/σ_3.

The basic factor responsible for the resistance to particle rolling and sliding is the friction between granular particles in contact. The magnitude of this resistance depends, for a given material, on the effective stress and the volume change tendencies, which in turn are controlled by the applied stresses and the packing conditions of the particle assembly. At high porosity, or low density some grain rearrangement may occur prior to development of large deformation as particles roll and slide along planes inclined at various angles. However, in the densest state, most deformation requires sliding at contacts and there is very little rolling of grains (Rowe, 1962). Furthermore, large deformation in this state requires volume expansion against the confining stress, thus giving a high contribution of the deformation resistance to dilation.

Apart from the factors mentioned above, the deformation characteristics of granular materials are also dependent on the fabric, or structure of the material. The difference in fabrics between granular materials used in construction or laboratory testing can be a direct result of the different methods of compaction or specimen preparation. Therefore, it should be appreciated that analyses based on properties determined from the same material but with a different structure may be totally in error.

2.2 PERMANENT STRAIN BEHAVIOUR OF GRANULAR BASES UNDER REPEATED LOADING

For the past 20 years, many research workers have attempted to correlate the permanent strain behaviour of granular roadbase material as measured in repeated load tests to simple static load tests (Morgan [1972], Gerrard et al [1975], Lentz and Baladi [1980], Sweere [1990]). However, as the behaviour is very complex, and as dynamic and static loads do not necessarily induce the same structural changes in the materials, such an approach, despite its enormous practical potential, only had mixed success. To date, there does not appear to be an accepted method of representing the permanent strain behaviour of granular bases under repeated load. Most relationships are, by and large, empirical and based on phenomenological description of observed behaviours. Nonetheless, a number of important parameters are now known to affect the permanent strain response of granular bases. A review of these parameters follows.

2.2.1 Stress Level

Maree et al (1982b) carried out tests using the Heavy Vehicle Simulator to determine the effect of wheel loading on the permanent deformation of a light unbound pavement. The results of their tests which involved three levels of dual wheel load, showed that the permanent vertical deformation during the tests was roughly linearly proportional to the wheel load for the two cases involving wheel loads of 40 and 80 kN. However, the permanent deformation from a wheel load of 100 kN was more than twice that from a 80 kN load. The result indicated the susceptibility of the material to large permanent deformation when high wheel load was used.

Many researchers who carried out repeated load triaxial tests found that the permanent strain behaviour is governed by some form of shear stress ratio.

Barksdale (1972) related permanent axial strain to the ratio of repeated deviator to confining stress, q_r/σ_3, using a complicated hyperbolic stress-strain law. This approach seems to be appropriate in the light of the results from the wheel tracking tests mentioned above. Brown (1974) found that the permanent axial strain was directly related to q_{max}/σ_3 where q_{max} is the maximum deviator stress. Pappin (1979) noted that the permanent shear strain he obtained could be expressed as a function of the length of the stress path in p-q space and the stress ratio $(q/p)_{max}$. Others found that permanent strain was determined by how close the applied stress was from the failure stress. As a result, the stress ratio $q_{max}/q_{failure}$ was found to be appropriate for the results of the tests performed by both Barrett and Smith (1976) and Raymond and Williams (1978). Thom (1988), on the other hand, found that the permanent shear strain he obtained was better related to the stress ratio $(q_{failure}-q_{max})/q_{max}$.

Another approach was to relate, indirectly, the resilient strain, which in turn was controlled by the applied stress, to the permanent strain. Shenton (1974) performed a large number of tests on railway ballast under repeated loading and found that the permanent axial strain could be predicted by means of the strain obtained after the first load cycle. Descornet (1977) also adopted this approach for a wide range of granular materials but found that an additional ratio of resilient axial strain to confining pressure, ε_r/σ_3, was needed to characterise the permanent strain behaviour.

2.2.2 Principal Stress Rotation

The effects of principal stress rotation and anisotropy on soil strength have attracted a great deal of attention among geotechnical engineers (Youd [1972], Arthur et al [1977], Symes et al [1984]). However, the number of studies on the effect of principal stress rotation on permanent strain behaviour of granular material under repeated load is

comparatively small. Most of these studies were targeted towards the understanding of the liquefaction potential of saturated sand during earthquakes (Peacock and Seed [1968], Silver and Seed [1971]) or involved tests with rather severe stress conditions (Wong and Arthur, [1986]). As a result, the strains induced on the granular materials were generally rather large when compared with those occurring in granular bases under traffic loading.

Youd (1972) found that with principal stress rotation, a large increase in density of his sand samples tested in a cyclic shear box resulted. For the purpose of analysing pavement responses, Ansell and Brown (1978) used a cyclic simple shear apparatus to produce shear reversal conditions during tests on a single sized sand. They concluded that the reversed shear stresses which caused principal plane rotation had a significant effect on the volumetric strains in granular materials and suggested this be taken into consideration when designing new compaction equipment. In recent years, repeated load tests were carried out using hollow cylinder apparatus. Using such a device to perform tests on a 4mm down crushed rock, Thom and Dawson (1989) also concluded that the rotating stress planes had considerable effect on the permanent strain behaviour of granular materials. However, their limited number of tests involved a range of specimen densities and stress paths. Hence, the effect due to principal stress rotation might not have been completely isolated.

2.2.3 Load Repetitions

In general, if the wheel load or stress ratio used in tests on granular layers or laboratory specimens was below a particular threshold, the resulting permanent strain would eventually reach an equilibrium condition. Under this condition, most researchers found that permanent strains obtained either from repeated load triaxial tests

(Barksdale, 1972, Pappin 1979, Thom, 1988) or large scale wheel tracking tests (Brown et al, 1980) increased approximately linearly with the logarithm of the number of cycles of applied stress. At high levels of shear stress close to the static strength of the material, permanent strains are likely to increase rapidly under repeated load as a result of dilation. The permanent strain-log number of cycles relationship, in this situation, is more likely to follow a hyperbolic rather than linear function.

2.2.4 Stress History

The permanent deformation behaviour of a granular material at any instant is dependent on its stress history. In soil, the stress history may be quantified in terms of an overconsolidated ratio. However, in granular material, such quantification is not appropriate. The stress history effect occurs as a result of material stiffening or change in structure under repetitive loads, hence causing a decrease in the proportion of plastic to elastic strain during subsequent loading. The effect has been recognised and carefully avoided during laboratory tests. However, very little direct research has been carried out on the study of this effect.

2.2.5 Physical and Environmental Factors

Density and grading have a large influence on the permanent deformation behaviour of granular materials. Barksdale (1972) found that, in general, low density and high fines content would lead to an increase in permanent strain. Thom and Brown (1988) reached similar conclusions and further commented that broadly graded materials would have higher permanent deformation resistance than uniformly graded materials when both were well compacted.

Aggregate shape, angularity, surface roughness and roundness can have an important influence on the permanent strain behaviour of granular material. A study by Barksdale and Itari (1989) indicated that a blade-shaped material appeared to be more susceptible to rutting as it tended to have a larger initial void for the same compactive effort. Particles with cubic shape and smooth surfaces were also found to deform more under cyclic load because they usually had the lowest particle packing.

The influence on the permanent strain behaviour due to the degree of saturation can be linked to the existence of pore pressures generated during repeated loading. As saturation is approached, positive pore pressure can be generated more easily. With effective stress decreasing, the sample will be subjected to more strain. This phenomenon has been observed by many researchers in both field and laboratory conditions. Conversely, the development of suction in partially saturated material may effectively increase strength and resistance to repeated load.

2.3 PERMANENT DEFORMATION CHARACTERISTICS OF GEOSYNTHETICS-REINFORCED GRANULAR BASES

The permanent deformation characteristics of granular bases are influenced by the inclusion of geosynthetics in several ways. When placed at the boundary between a granular layer and a soft subgrade, geosynthetics, especially geotextiles, can prevent the penetration of the base material into the underlying layer. This separation effect can in turn prevent the progressive reduction in the thickness of the granular layer. If the latter is allowed to happen, the layer's structural value will effectively reduce (Black and Lister, 1979) and hence, may result in larger or more rapid build-up of permanent deformation. Another indirect benefit which granular layers may gain from

geosynthetic inclusion is the prevention of the upward migration of water-borne fines from the subgrade into the aggregate matrix. This will result in a reduction in permeability of the layer and render it more susceptible to permanent deformation. A detailed discussion of the role of geotextiles in controlling sub-base contamination was presented by Dawson (1986).

The most important benefit which the granular base can receive from geosynthetics is probably due to their reinforcing action. A detailed description of the possible mechanisms of the reinforcement effect, as shown in Figure 2.1, was presented by Lai and Robnett (1981) and Robnett et al (1982). In principle, the effect is due to rutting-induced tension developing in the geosynthetic and the geosynthetic's ability to hinder lateral spreading of the materials by surface friction. Milligan et al (1989) noted that the contribution of the tensioned membrane was usually very small, except at unacceptably large rut depths and could not be applied to the case where vehicles could wander over the reinforced area or the case where wrinkled geotextile was found to have a reinforcing effect (Ruddock et al, 1982). The results of his research programme tended to favour a mechanism which is similar to the subgrade/aggregate restraint effect and is independent of the stiffness of geosynthetic at small rut depths.

The benefits of including geosynthetics below unpaved roads over soft ground are well documented (Chaddock, 1985, Ruddock et al ,1982, Lai et al, 1981, Potter and Currer, 1981 and Webster and Watkins, 1977). Most indicated an improvement of the permanent deformation resistance of the granular layer. However, very little research has been performed on the reinforced granular layers of flexible paved roads. Pappin (1975) reported an experiment carried out in New South Wales where a relatively low stiffness geogrid was placed under a thinly paved aggregate road. The road was found to experience much reduced surface deformation. However, both Brown et al (1982)

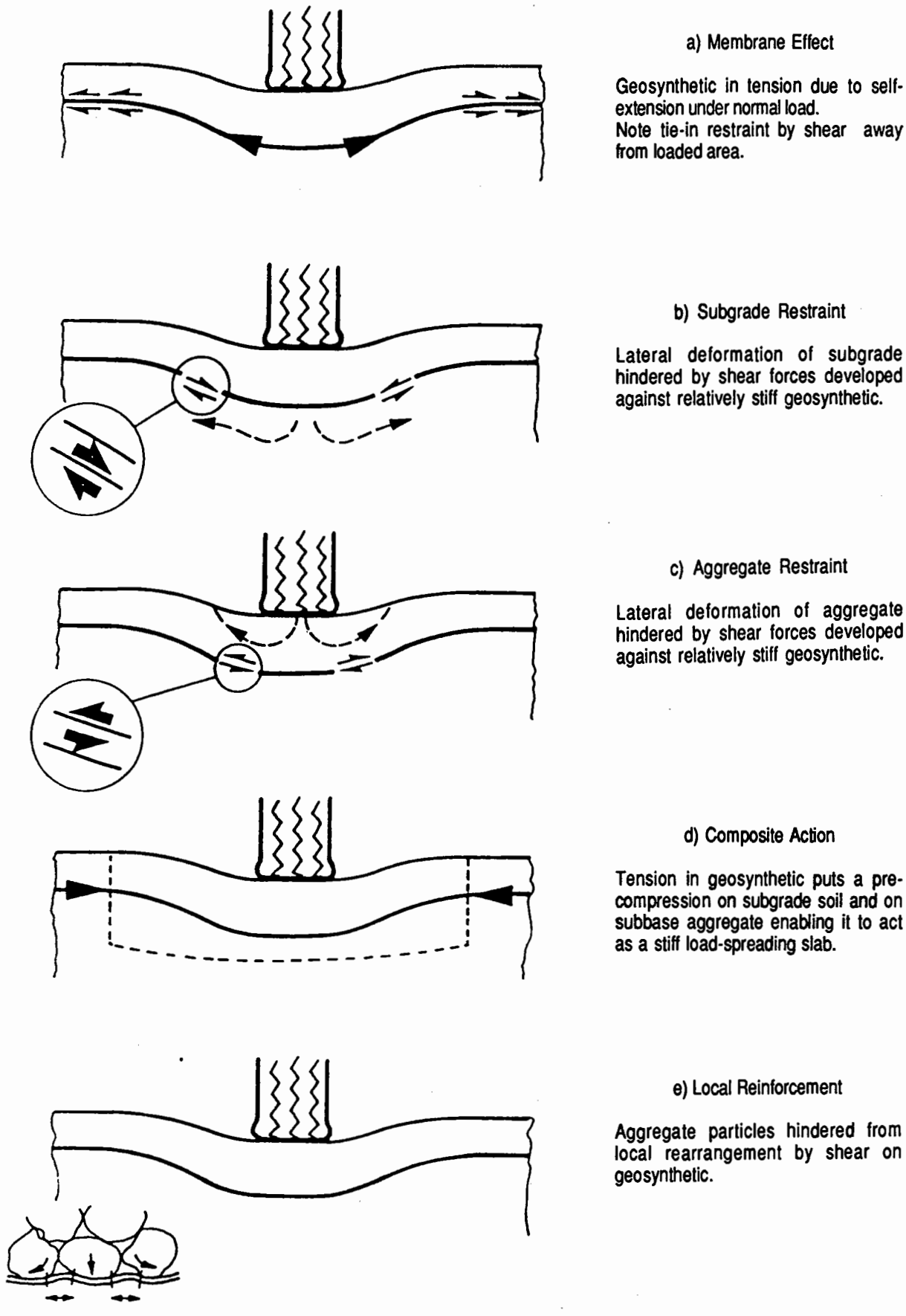

Figure 2.1 Mechanisms of Geosynthetics Reinforcement (after Lai and Robnett, 1981)

and Ruddock et al (1982) showed that slightly greater or, at best, no greater permanent deformation occurred when a stitched geotextile was installed.

Beneath paved roads where low strains are usually encountered, the use of prestressed geosynthetics in the granular base may be beneficial. Prestress can be introduced by either prerutting of the granular base (by means of heavy construction traffic) prior to the construction of the bound layer or by a deliberate prestressing process. Barvashov et al (1977) has shown, experimentally that deflections of their unpaved roads can be reduced by geosynthetic prestressing. Raad (1982), who uses a finite element approach, has shown similar benefit.

PART A

A STUDY OF METHODS OF IMPROVING PERMANENT DEFORMATION RESISTANCE OF GRANULAR BASES BY MEANS OF GEOSYNTHETICS

CHAPTER THREE

EXPERIMENTS IN THE NOTTINGHAM PAVEMENT TEST FACILITY

3.1 INTRODUCTION

As part of a joint-effort to investigate the potential benefits of using geosynthetics as reinforcement for granular bases in flexible pavements, four series of full scale experiments were conducted in the Notttingham Pavement Test Facility (PTF). The work was sponsored by the American Association of State Highway and Transportation Officials, in co-operation with the Federal Highway Administration, and was conducted in the United States National Co-operative Highway Research Programme.

The main objective of the experiments carried out in Nottingham was to investigate the conditions under which permanent deformation resistance of the granular bases could be improved. In addition, the experiments would provide feedback and verification, based on the measured pavement responses, for the analytical model used in a parallel theoretical study. This latter study was carried out at Georgia Institute of Technology in the United States where a comprehensive finite element program, GAPPS7, had been developed (Zeevaert, 1980) and was used.

The analytical work was mainly related to the elastic response of the pavement structure and, as a result, was able to investigate the influence on performance and design of a large number of variables. The emphasis of the full scale experiments, however, was placed on the study of a limited number of pertinent factors which were difficult to model theoretically. These included the build-up of permanent strains, particularly in

the granular layer, as well as the effect of prerutting and prestressing of the geosynthetics.

Since the scope of this thesis is primarily concerned with the development of permanent strain and permanent deformation resistance of granular materials, details of the programme and results of the theoretical study carried out at Georgia Institute of Technology will not be included. The report by Barksdale et al (1989) should, instead, be referred to.

3.2 SCOPE OF THE EXPERIMENTS

The number of potentially important variables is quite large in a study of the performance of flexible pavements incorporating granular bases reinforced with geosynthetics. In the experiments, consideration was given to pavement strength which was basically controlled by the quality of the granular layer. The type and stiffness of geosynthetic which was placed either at the middle or bottom of the granular base were also investigated. Furthermore, two special techniques which had high potential for improving the performance of the reinforced granular layer were considered. They were:

1. Prestressing of geosynthetic and
2. Prerutting of the granular layer both with and without reinforcement.

A full factorial study of the variables mentioned above would be prohibitive in the light of the limited resources and time available. As a result, their combinations were selectively studied by means of four series of main tests, each consisting of three different pavement sections. These sections were arranged in parallel to allow

simultaneous loading by each pass of wheel load. A summary of these sections and their designations are given in Table 3.1.

Table 3.1

Summary of Test Sections in Laboratory Experiment

Test Series	*Proposed Geometry*	*Section Designation*	*Details of Geosynthetic and Section Specification*
1	25mm H.R.A. 150mm sand & Gravel	PR-GX-B	Geotextile placed at bottom of Base; Subgrade prerutted by 18mm.
		CONTROL	Control Section; no geosynthetics and no prerutting.
		GX-B	Same as PR-GX-B; no prerutting.
2	25mm A.C. 200mm Crushed Limestone	PR-GD-B	Geogrid placed at bottom of Base; Subgrade prerutted by 10mm.
		CONTROL	Control Section
		GD-B	Same as PR-GD-B; no prerutting.
3	25mm A.C. 200mm Crushed Limestone	GX-B	Geotextile placed at bottom of Base.
		CONTROL	Control Section;
		GX-M	Geotextile placed at middle of Base
4	25mm A.C. 200mm Crushed Limestone	GX-M	Same as GX-M (Series 3);
		GD-M	Same as GX-M but use geogrid.
		PS-GD-M	Prestressed Geogrid placed at middle of Base.

Notes for section designation:

PR= Prerutted
GX= Geotextile
B= Bottom of Base
PS= Prestressed
GD= Geogrid
M= Middle of Base

A section name is normally preceded by the letters PR (prerutted) or PS (prestressed) if prerutting or prestressing is involved, then followed by the letters GX (geotextile) or GD (geogrid) indicating the type of geosynthetic used. The location of the geosynthetic which follows, is represented by either M (middle of base) or B (bottom of base). Therefore the section PR-GD-B would mean that it is the Prerutted section with Geogrid located at the Bottom of the granular base.

In order to create extra opportunities for comparison of pavement performance, three additional series of supplementary tests were also performed on the pavement area which was not disturbed by the main tests carried out during the second to fourth test series. A summary of the test sections involved in the supplementary tests is presented in Table 3.2.

3.3 NOTTINGHAM PAVEMENT TEST FACILITY

The Nottingham Pavement Test Facility (PTF), as shown in Figure 3.1, was described in detail by Brown and Brodrick (1981). In brief, it consists of a 560mm diameter and 150mm wide loading wheel fitted to a carriage, which runs on bearings between two beams spanning the long side of a rectangular laboratory. The beams are in turn mounted on end bogies which allow the whole assembly to traverse across the pavement. Lifting and lowering of the wheel, which determines the magnitude of the applied load, is controlled via two ultra low friction rams by a servo-hydraulic system. A load feedback mechanism is incorporated to maintain constant load. The maximum load that can be achieved by the PTF is about 15 kN with a speed range of up to 16 km/hr. The whole assembly is housed in an insulated area where temperature could be

Table 3.2

Details of Test Sections of the Supplementary Tests

Test Series	*Section Geometry*	*Section Designation*	*Details of Geosynthetic and Section Specification*
2	200mm Crushed Limestone	GD-B	Geogrid at bottom of Base
		CONTROL	Control Section
		GD-B	Same as the 1st GD-B
3	25mm A.C. 200mm Crushed Limestone	GX-B	Geotextile at bottom of Base
		PR-CONTROL	Control section; base pre-rutted by 50mm
		GX-M	Geotextile at middle of Base
4	25mm A.C. 200mm Crushed Limestone	PR-GX-M	Same as GX-M; base pre-rutted by 50mm
		PR-GD-M	Same as PR-GX-M; use geogrid
		PS-GD-M	Pre-Stressed Geogrid at middle of non-pre-rutted base

controlled via heaters or cooling fans. Maximum dimensions of the pavement section that can be constructed are 4.8m long, 2.4m wide and 1.3m deep.

3.4 PAVEMENT MATERIALS

Each pavement section included a thin asphaltic layer, a granular base layer with or without geosynthetic inclusion and a subgrade layer. In all, two types each of the

asphaltic, granular and geosynthetic materials were used. The subgrade material remained the same throughout the four series of tests.

3.4.1 Granular Base

In order to enhance the benefit of geosynthetic inclusion in the granular base, a weak granular material was used during the first series of tests. It consisted of partially crushed sand and gravel with rather smooth surfaces. The maximum particle size of this material was about 20mm and about 3% of it passed the 75 micron sieve. The grading of the granular material, as shown in Figure 3.2, conformed with the British Standard Type 2 sub-base specification (DTp 1976). According to the ranking system established by Thom (1988), this material had a fair to poor elastic performance (i.e. low elastic stiffness), very poor resistance to permanent deformation and very poor shear strength. Subsequent laboratory tests carried out on this material during the project confirmed these findings (see Figure A1.1, Appendix A).

As a result of the very early failure of pavement sections incorporating the sand and gravel base, the material was used only once. In subsequent series, a crushed dolomitic limestone was used. This material had a maximum particle size of 37.5 mm and about 7% passing the 75 micron sieve. The material was slightly angular and was considered non-flaky according to the results of the BS812 (1985) index tests. The grading, as shown in Figure 3.2, lay within the British Standard Type 1 sub-base specification. This latter type of granular material is widely used in British highway construction.

Both granular materials were compacted at optimum moisture content. For the sand and gravel, 100% maximum dry density (ASTM D-1557-78 test method [1987]) was generally achieved during construction of the base layer, whilst for the crushed

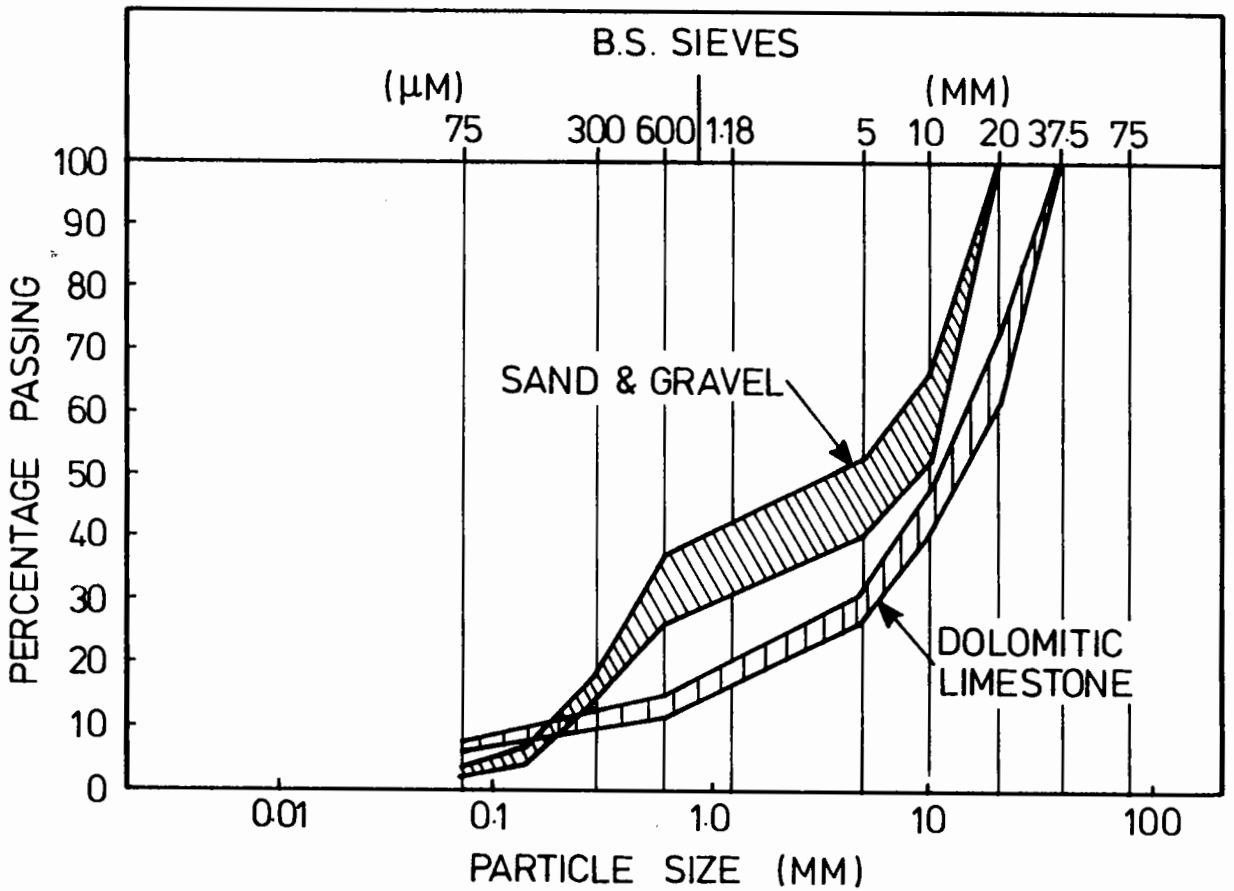

Figure 3.2 Grading Envelopes of Granular Base.

In laboratory testing, the most commonly used device has been the repeated load triaxial test apparatus. In it, a cylinder of material is subjected to two stress components - a confining stress through a surrounding compressed medium and a vertical stress. Despite its relative simplicity, the limitations of stress conditions that can be applied to the cylindrical specimen are rather severe. Figure 1.1 shows the stress conditions imposed on a vertically orientated element of granular material by a moving wheel load. It indicates that for each passage of the wheel, there is a corresponding reversal in the direction of the shear stress on the vertical and horizontal planes. Opposite sense of shear reversal will occur if the wheel travels in the opposite direction. The combination of the vertical and horizontal stress can be reproduced in the repeated load triaxial test when both the deviator and confining stresses are cycled. However, the reversal of shear stress requires an apparatus which can apply this mode of stress directly to the boundaries of the specimen. Various devices, such as the Cyclic Simple Shear Apparatus (Ansell and Brown, 1978) and the Directional Shear Cell (Arthur et al, 1977) emerged over the years. None the less, one of the most promising methods is believed to be the Hollow Cylinder Apparatus (HCA). With it, a repeated torsion can be applied to a hollow thin-walled cylinder. If the hollow cylinder is at the same time subjected to an axial stress and a lateral stress over both the inner and outer cylinder face, then the stress conditions imposed on an element of material along the wall of the cylinder will be similar to those shown in Figure 1.1.

Because of the added ability to apply the reversed shear stress, an HCA can allow tests to be carried out within a much wider and more flexible stress regime. More importantly, it can simulate the insitu stress conditions. Hence, it will provide much stronger support for the longer term objective of modelling the permanent deformation behaviour of granular material with respect to its response to wheel loading in a pavement.

dolomitic limestone, the dry density varied between 96 and 100% maximum dry density (BS 5835 test method [1980]).

3.4.2 Asphaltic Material

During the first series of tests, a gap graded Hot Rolled Asphalt (HRA) mix was used in accordance with the British Standard 594 (1973). For the remaining three series of tests, a continuously graded asphaltic concrete mix was used, having been designed by the Marshall method (ASTM Standard 1987). The specifications of both mixes are shown in Table 3.3.

3.4.3 Subgrade

The subgrade used in this project was an inorganic, low plasticity silty clay known as Keuper Marl. The material was obtained in the form of unfired wet bricks from a local quarry. 450 mm of this fresh and soft material with an average California Bearing Ratio (CBR) of 2.6% and a moisture content of 18% was placed over an existing 1.07 m thick layer of drier and stiffer subgrade material from the same source. The CBR value of this stiffer material was found to be about 8 to 10%.

Table 3.3

Specifications for Asphaltic Mixes

Specification	*Hot Rolled Asphalt*	*Asphaltic Concrete*
% Passing		
20mm Sieve	100	100
10mm	96	73
5mm	70	51
600μm	64	21
300μm	40	13
75μm	7	5
Binder Penetration	100	50
Binder Content (% by weight)	8	6.5
Delivery Temperature	110° C	160° C
Rolling Temperature	80° C	120° C

3.4.4 Geosynthetic Material

Two types of geosynthetic were used in this study:

1. A stiff, woven geotextile (stiffness at 5% strain, Sg=750 kN/m) and
2. a geogrid of lower stiffness (Sg=280 kN/m) which still classifies as being stiff following the system of Barksdale et al (1989).

Both geosynthetic materials were made from polypropylene and their characteristics are summarized in Table 3.4.

Table 3.4

Properties of Geosynthetics Used.

Geosynthetic Property	*Geotextile*	*Geogrid*
Polymer Composition	Polypropylene	Polypropylene
Weight / Area (g/m^2)	966	203
Tensile Strength (kN/m)	155	20.8
Stiffness at 5% strain (kN/m)	753	280
% Open Area	2 - 8	n/a
Grid Size (mmXmm)	n/a	31X40

Note: n/a means "not appropriate".

3.4.5 Material Properties

For the purpose of quality control, some of the readily measurable material properties were constantly monitored and evaluated during and after the construction of the test sections. The insitu testing devices used on the granular material included the Nuclear Density Meter, Clegg Impact Hammer and the Dynamic Cone Penetrometer. On the subgrade, a static cone penetrometer which could enable a correlated CBR value to be obtained was used. Descriptions of these device have been presented elsewhere (Chan et al 1989). A summary of the in-situ properties of the pavement materials is shown in Table 3.5. In addition to the insitu tests, the properties of the above-mentioned pavement materials were thoroughly examined under an extensive laboratory testing programme. Details of the programme and results are described in Appendix A.

Table 3.5 Summary of Quality Control Tests in Laboratory Experiment.

Pavement Layer	*Type of Quality Control Test*		*Test Series*			
			1	*2*	*3*	*4*
Asphaltic	Binder Content (%)		8	6.5	6.5	6.5
	Max. Aggregate Size (mm)		14	14	14	14
	Ave. Compacted Density (kg/m^3)	Before	2115	2259	2259	2307
		After(1)	2307	2323	2387	2387
	Ave. Air Void (2)(%)	Before	8.8	6.4	7.0	4.4
Granular	Material type		Sand & Gravel	Crushed Limestone	Crushed Limestone	Crushed Limestone
	Max. Aggregate Size (mm)		20	37.5	37.5	37.5
	% Finer than 0.075mm		3	7	7	7
	Ave.Dry Density (kg/m^3)	Before	2115	2259	2179	2211
		After(3)	1986	2243	2131	2179
	Ave. Moisture Content (%)	Before	8.3	6.0	8.0	7.0
		After	4.8	4.5	4.4	5.5
	Ave. Clegg Hammer Reading	Before	14	46	32	40
		After	23	78	75	70
	Ave. Dynamic Cone Reading	Before	10	40	35	40
	(No. of blows/10cm penetration)	After	8	100	80	85
Subgrade	Ave. Dry Density (kg/m^3)	Before	1794	1778	1778	1778
		After	1778	1778	1778	1810
	Ave. Moisture Content (%)	Before	17.3	17.9	17.8	17.2
		After	18.7	18.4	18.4	17.3
	Ave. Static Cone Reading(4)	Before	286	262	282	330
		After	204	288	319	384
	Ave. CBR (ASTM D4429)	Before	2.9	/	/	/

Notes:
1. Measured from core samples.
2. Based on the average initial density and binder content.
3. Values may be too low because a lot of fine sand had to be used to provide a flat surface for the nuclear density meter to operate on.
4. CBR value can be obtained approximately by dividing the reading by 110.

3.5 PAVEMENT CONSTRUCTION

3.5.1 General

The subgrade was installed as 7 layers of wet bricks. Each layer was compacted by pneumatic tampers (Figure 3.3 and 3.4) which had enough energy to destroy the brick and provide a level surface. The granular base materials were moisture conditioned prior to placing and compacting. The sand and gravel base used in the first series of tests was compacted in three 50mm layers. A heavy vibrating plate (Figure 3.5), with a working area of 475x508mm, weight of 1.25 kN and maximum centrifugal force of 10 kN was used. For the crushed dolomitic limestone, compaction of the two 100mm thick layers were carried out by a pedestrian operated single drum vibrating roller (Figure 3.6). The roller weighed 4 kN and could generate a total centrifugal force of 22 kN.

The geotextile was stretched tight during installation by hand-pulling at the edges while the granular base material was being placed. For the geogrid, small U-shaped steel anchors were used to hold the geosynthetic in place.

Three times the amount of asphaltic mixes required for the construction was delivered for each series of tests. The excess material prevented rapid loss of heat during transportation. Compaction of the single layer was performed using the same vibrating roller used for the granular base.

3.5.2 Prerutting

Prerutting was carried out in every series of tests prior to the construction of the asphaltic layer. The intended purposes of prerutting were:

1. To eliminate any slack left in the geosynthetic during placement and
2. If the rut was large enough, to induce a tensile force in the geosynthetic, thereby possibly increasing its reinforcing potential.

To carry out prerutting, channelized traffic provided by a moving wheel load from the PTF was applied directly onto the surface of the granular base layer of the pavement section. This simulates the traffic condition that exists during construction when heavy lorries operate on the granular base. The prerutting load varied from 5 kN for the sand and gravel to 9 kN for the crushed dolomitic limestone. Prerutting was continued until either a surface rut of 50mm had developed or in the case where instrumentation in the subgrade was available, a targeted subgrade rut was achieved. On completion of prerutting, the rut at the surface of the granular layer was refilled and compacted with new material at the appropriate moisture content.

3.5.3 Prestressing of Geosynthetics

One means of introducing a tensile force into the geosynthetic is the straight forward prestressing of the material. This was carried out during the last series of tests on the geogrid. A schematic diagram showing the prestressing arrangement is given in Figure 3.7. After the first layer of granular material was placed and compacted, the geogrid was clamped to the side wall of the test pit using the clamping system detailed in Figure 3.7. The geogrid then went through a set of rollers and was connected, via a load transfer steel bar and steel cable, to a hydraulic jack. By jacking against a steel column which was firmly bolted to the concrete floor, a tensile force was generated and transferred to the geogrid. The initial prestress force, which was measured by a load

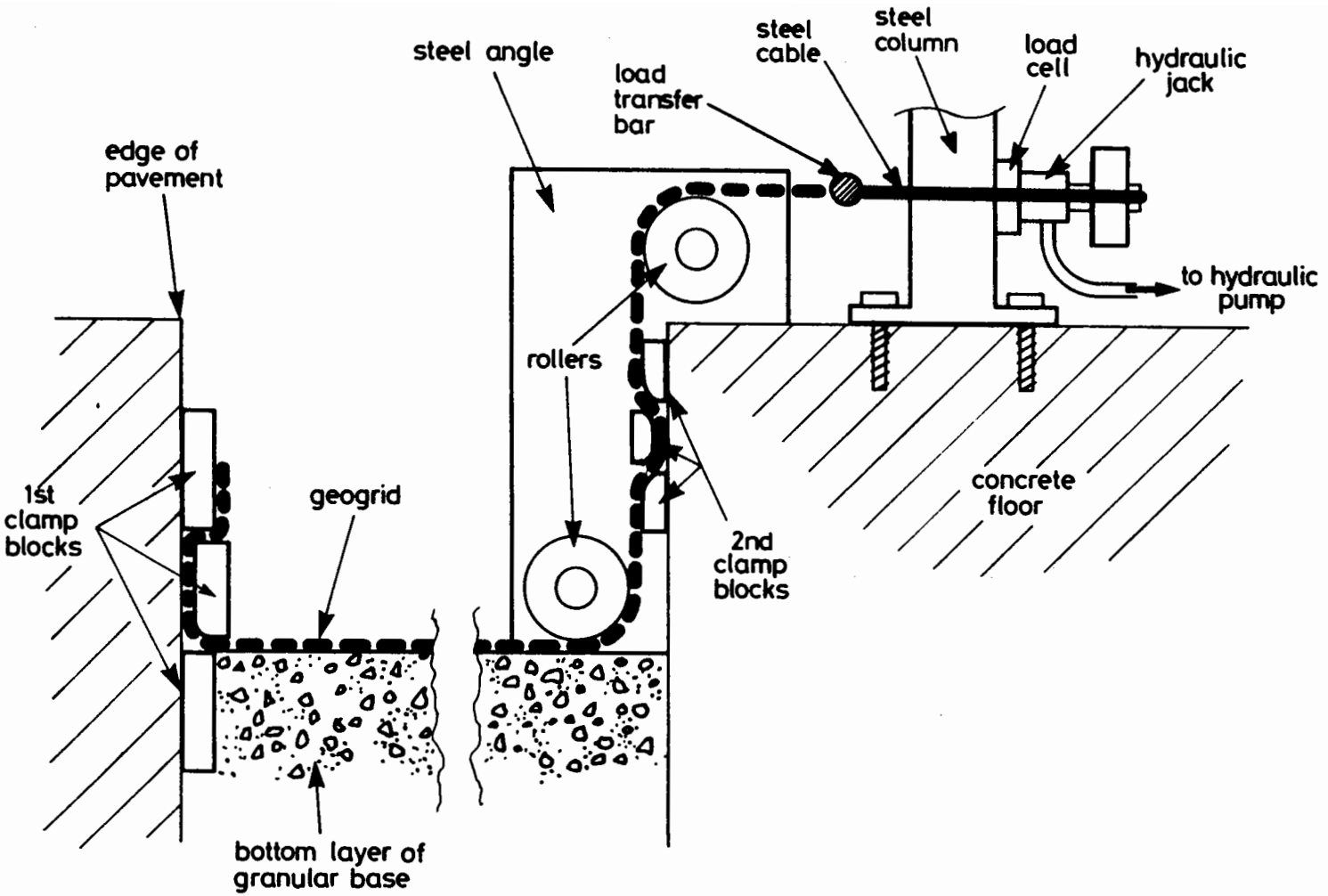

Figure 3.7 A Schematic Diagram for the Prestressing Arrangement.

cell located behind the steel column, was 7 kN/m. This represented about 34% of the tensile strength of the geosynthetic. After this stress level was achieved, a pair of clamps were used to lock the geogrid in its prestressed condition. This helped to reduce the chance of slippage during construction of the upper granular layer. The load from the hydraulic jack and the second clamp block (see Figure 3.7) was released after the top layer of granular base was placed and compacted. The total period of prestressing during which the hydraulic jack was in action was about one hour.

3.5.4 Finished Profile of Sections

Despite care during construction, thicknesses of the finished pavement were not exactly as specified. This was probably due to difficulties in judging the quantity of material required for a specified compacted thickness. However, variations between sections within one series of tests were considered to be slight, generally less than 10%. The finished profiles for all 12 sections are summarized in Table 3.6. The thicknesses of individual layers were obtained by various techniques including: (1) Core samples of the asphaltic mix, (2) Instrumentation installed in the pavement materials, (3) Measurements from a reference beam to points on each layer surface and (4) Cross sections during trench excavation at the end of the test series.

3.6 INSTRUMENTATION

All the sections were instrumented using diaphragm pressure cells developed at Nottingham, Bison inductance strain coils and copper- constantan thermocouples.

Table 3.6

Layer Thickness of Pavement Sections and Depth of Geosynthetics from Pavement Surface

Test Series	*Pavement Section*	*Thickness of Layer (mm)*			*Depth of Geosynthetic from Surface (mm)*
		A.C.	*Base*	*Soft Subgrade*	
1	PR-GX-B	30	160	445	191
	CONTROL	34	147	455	n/a
	GX-B	33	155	447	188
2	PR-GD-B	30	216	389	246
	CONTROL	30	211	394	n/a
	GD-B	28	206	401	234
3	GX-B	30	206	399	236
	CONTROL	30	211	394	n/a
	GX-M	33	196	406	130
4	GX-M	38	211	386	137
	GD-M	34	216	386	142
	PS-GD-M	41	218	376	147

Details of instrument calibration were reported by Brown and Brodrick (1977). The arrangement of instruments installed in each pavement section was similar. Details of one particular section are shown in Figure 3.8. The instruments were installed mainly to measure the stresses and strains in the pavement materials. All the instruments were installed directly underneath the centre line of each test section in the direction of wheel travel.

Pressure cells and strain coils in the subgrade were placed in holes which were cut with special tools designed to ensure minimum disturbance around the instruments.

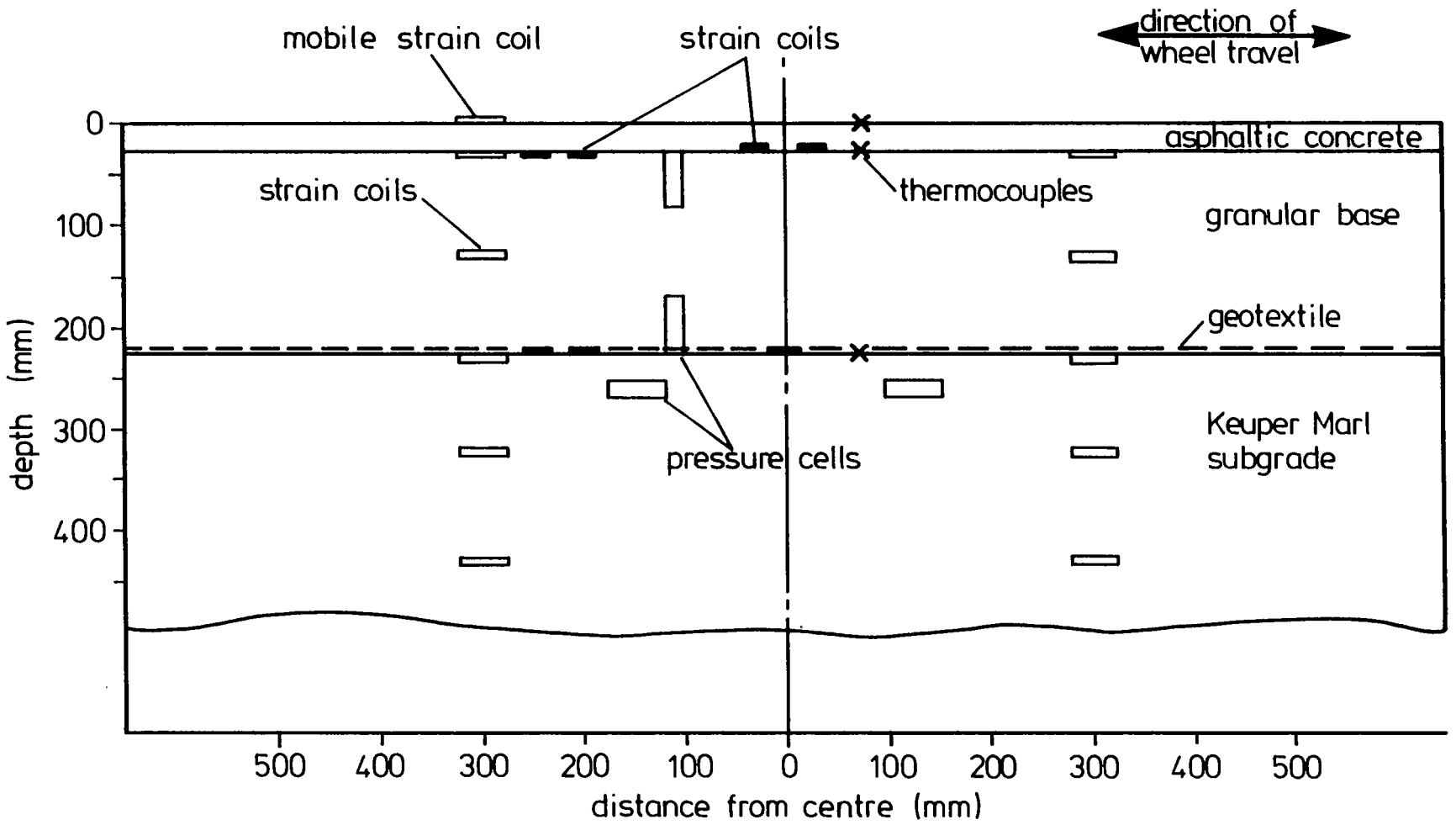

Figure 3.8 Side View of Typical Layout of Instrumentation.

Excavated soil was tamped in layers around the instruments and the holes and layer surfaces were scarified as installation proceeded.

To install pressure cells and strain coils in the granular base, holes were excavated after compaction of the layer was completed. In order to prevent large aggregate particles from damaging or influencing the output of the instruments, fine dust, passing the 212 micron sieve was placed and tamped around the instruments. For pressure cells located vertically, the cells were placed in a prepacked condition with fine material held in position over the diaphragm with thin plastic film. This installation procedure is compatible with that used during calibration in a large triaxial specimen.

The strain coils in the geotextile were attached to their underside by means of a set of plastic nuts and bolts which passed between the filaments of the geotextile (Figure 3.9). For the geogrid, a very small hole was drilled through the thick junction of the grid before the coil was attached using the plastic nut and bolt (Figure 3.10). In order to prevent the strain coils from interlocking with the surrounding soil or granular material, they were covered, on the underside by a small piece of geotextile.

In addition to the instrumentation installed within the pavement materials, a profilometer (Figure 3.11), consisting of a linear potentiometer mounted on a roller carriage, was used. It was connected to an X-Y plotter which provided hard copies of the measured surface profile.

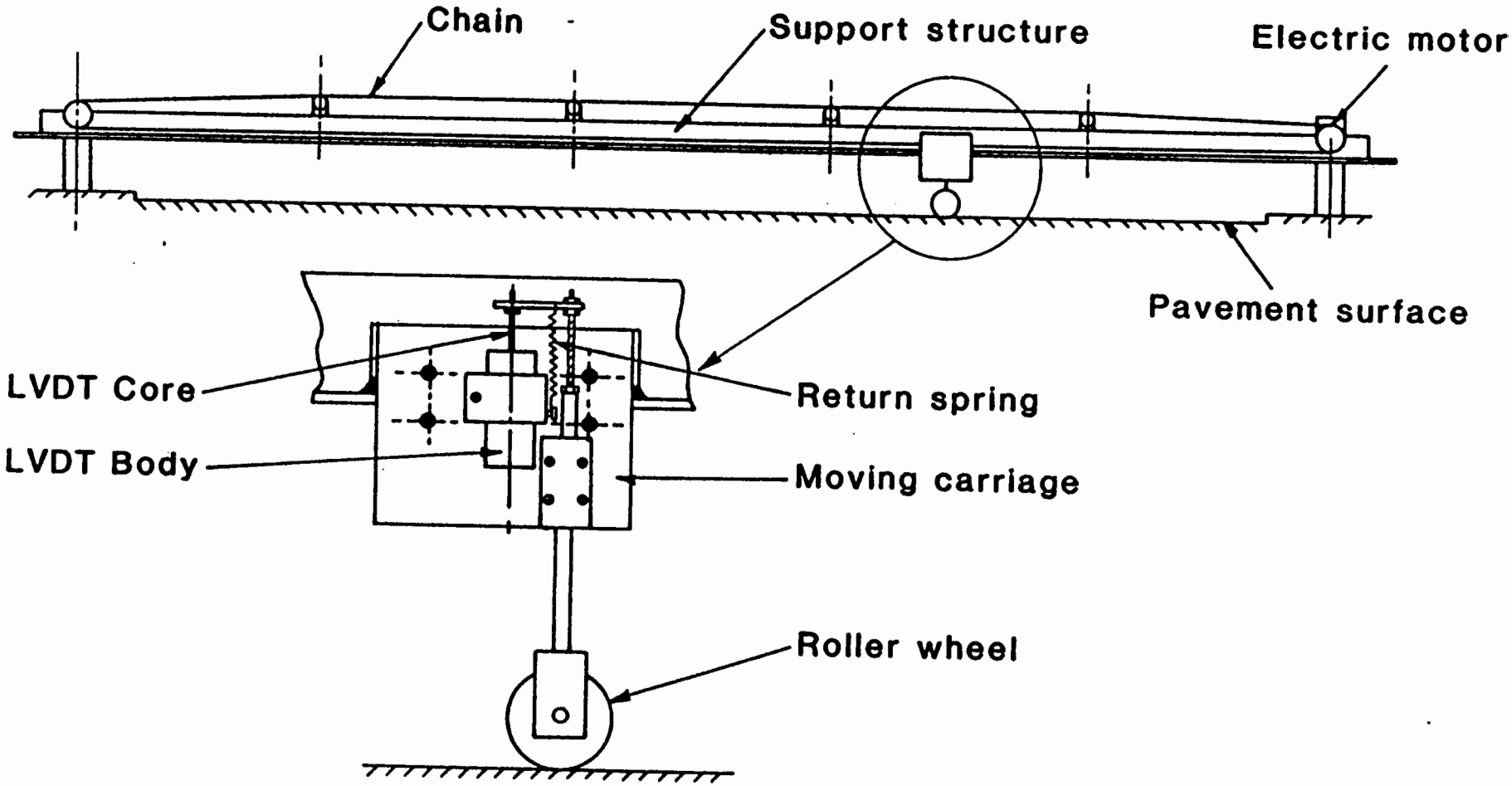

Figure 3.11 Profilometer used for Measurement of Transverse Profile of Pavement Sections.

3.7 PAVEMENT TEST PROCEDURE

3.7.1 Multiple Track Test

To simulate traffic wander, the moving wheel in the PTF can be programmed to traverse, in a random sequence, across the pavement to nine specified positions (four on each side of the centre line) where it can carry out a preset number of wheel passes. Spacing between these positions is set at a constant step of 75mm. Table 3.7 summarizes the loading programme adopted for the last three series of tests. It consisted of a 250-pass cycle, starting with 55 passes along the centre of the section (position 5), followed by 15 passes at position 8, then 7 passes at 9 and so on until it finished back at the centre line where the cycle was repeated. During the scheduled recording of output from the instruments, the centre line track was given an additional 100 passes of wheel load before actual recording began. This procedure ensured that consistent and compatible outputs were recorded from the instruments installed directly below the centre line of the pavement. The total number of passes in the multiple track tests for the second to fourth series of tests were 69,690, 100,070 and 106,300 respectively. The distribution of these passes across each loading position is shown in Figure 3.12.

In the first series of tests, because of the rapid deterioration and very early failure of the pavement sections, the loading programme mentioned above could not be executed. The total number of wheel load passes for this test series was 1,690 and their distribution is shown in Figure 3.12a.

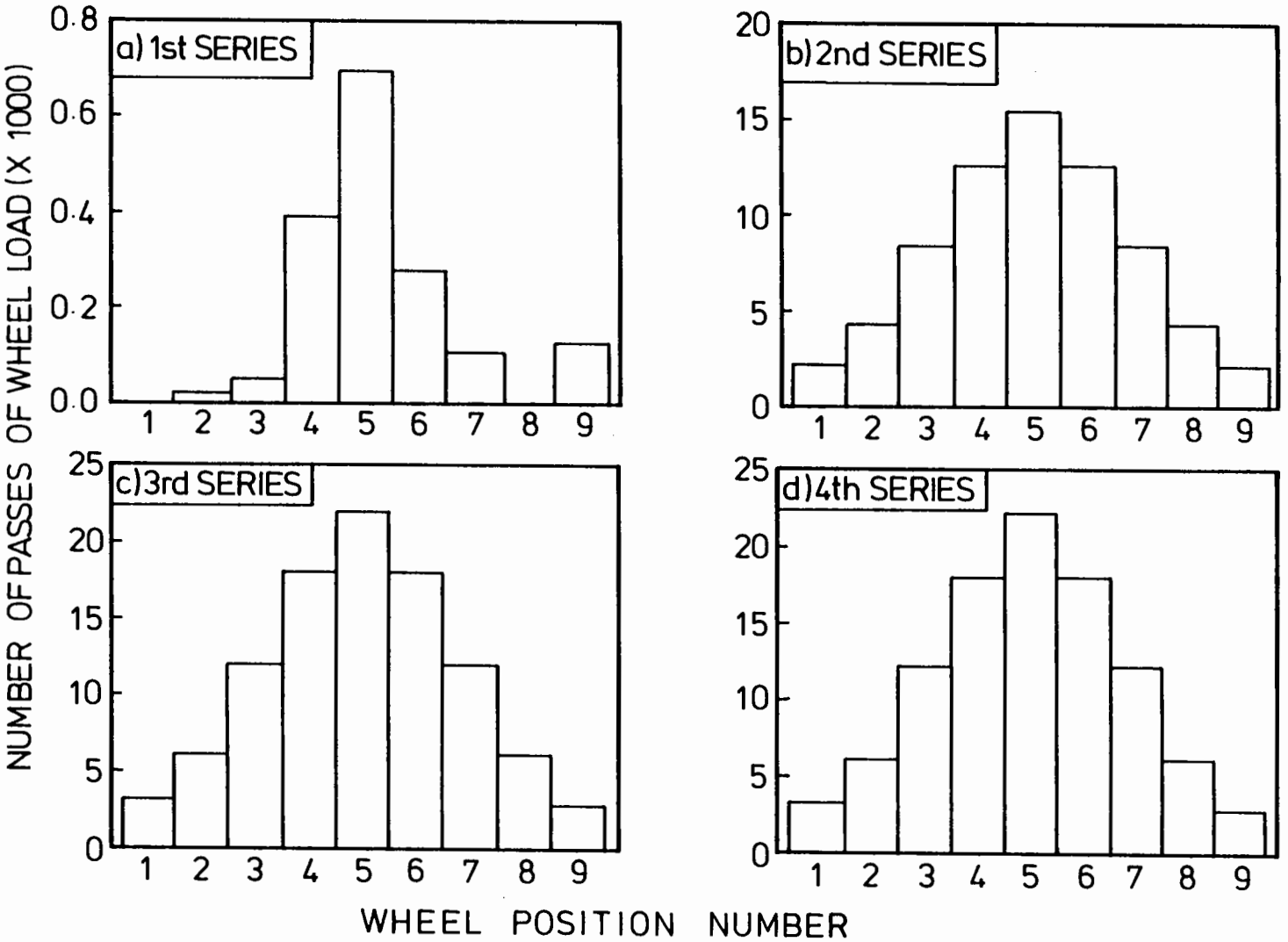

Figure 3.12 Distribution of the Number of Passes of Wheel Load in Multiple Track Tests for all four Test Series.

Table 3.7

Details of Traverse Program Used in Multiple Track Tests

Sequence No.	1	2	3	4	5	6	7	8	9
Track Position No.	5	8	9	7	6	4	1	2	3
Distance of Track from Centre Line (mm)	0	225	300	150	75	75	300	225	150
No. of Passes	55	15	7	30	45	45	8	15	30

3.7.2 Single Track Tests

On completion of the main multi-track tests, single track tests were carried out on one or both sides of the main test area where the pavement was not disturbed. These tests normally involved the use of a much higher wheel load, so that the deterioration of the pavement structure might be further accelerated. Since there were no instruments at the single track test locations, stress and strain data were not available. Only the loading conditions and the rut depth were measured during these tests. Nonetheless, the tests helped to confirm trends in the development of permanent deformation during the multi-track tests. They also created extra opportunities for comparison of performance of pavement sections tested under different conditions. The three additional series of tests summarized in Table 3.2 belong to this category of test.

3.7.3 Data Recording Procedure

The transverse profile and permanent strain readings from the granular and subgrade layers were taken at appropriate intervals during testing of all pavement sections in order to establish their deformation characteristics under loading. In addition, elevations of all the reference points at the surface of the sections along the centre line were measured and checked. During the actual loading, resilient strains and transient stresses were recorded on an Ultra Violet Oscillograph which also recorded information relating to wheel load, position and speed. The outputs from the thermocouples, which measured temperature at various depths in the pavement structure, were monitored regularly by means of a readout device. Air temperature of the PTF was obtained from a thermometer placed inside the facility.

3.8 TEST CONDITIONS

The load exerted by the rolling wheel on the pavement during the multi-track tests was 6.6 kN. Bidirectional loading was used in all tests. Minor variations, generally less than 10% of the average value were encountered. The variation was caused by the unevenness in the longitudinal profile of the pavement. In single track tests, loads of 8 and 9 kN were used for the first and the subsequent series of tests respectively. With the exception of the test carried out during the first series, all single track tests used bidirectional loading.

The tyre pressure used for all series of tests was 550 kPa. Based on a previous investigation into the effect of wheel tread, tyre wall strength, tyre pressure and load, the contact pressures acting on the pavement from a 6.6 and 9 kN wheel load were

estimated to be 460 and 500 kPa respectively. These gave radii of contact areas, assuming them to be circular, of 68 and 76 mm respectively.

The wheel moved at a speed of about 3 to 5 km/hr with slight variations between forward and reverse direction. Towards the end of the test when the pavement surface became uneven, a slower speed was sometimes necessary in order to maintain constant loading.

The temperature inside the PTF was kept at 20 ± 2 °C throughout the testing. Temperatures at the asphalt surface and within the granular material and the subgrade were found to be about 1 to 2 °C lower than that of the air.

CHAPTER FOUR

RESULTS OF EXPERIMENTS IN THE PAVEMENT TEST FACILITY

4.1 INTRODUCTION

Results of the four series of tests can be divided into 3 categories as discussed in detail below. A summary of the key pavement response data recorded close to the end of each test series is given in Table 4.1. Unless specified, all the results presented in this chapter were obtained from multi-track tests. Most of the results show either variation of test data with time (i.e. number of load cycles) or with depth in the pavement structure at a particular time. The presentation of results emphasizes comparisons within each series. However, it is possible to compare results across series after adjustments are made, based on the response of the control section of the particular series. When duplicate readings were recorded, an average is reported. However, obviously erroneous data were discarded and excluded from the averaging process.

4.2 PERMANENT VERTICAL DEFORMATION

In this study, the permanent vertical deformation of the pavement was taken as the principal parameter for characterizing performance. It is defined as the vertical distance between the surface of the deformed and the untrafficked pavement layers along the centre-line of the wheel track. Therefore, it is different from rut depth which also considers the possible heaving of the pavement materials away from the centre of the wheel track.

Table 4.1

Summary of Key Pavement Response Data Close to the End of Wheel Tracking Tests

Test Series	*Section Designation*[1]	*Section Geometry*[2]	*No. of Passes*	*Permanent Deformation (mm)*			*Subgrade* σ_v *(kPa)*[3]	*Asphalt* ε_t *(με)*[4]
				Total	*Base*	*Subgrade*		
1	PR-GX-B	30/160	1262	16.0	15	1.0	44.8	/
	CONTROL	34/147		23.9	17.5	6.4	70.3	3929
	GX-B	33/155		14.0	8.9	5.1	80.0	/
2	PR-GD-B	30/216	70000	14.2	11.4	0.8	55.2	2676
	CONTROL	30/211		39.4	27.2	9.4	59.3	2941
	GD-B	28/206		34.5	27.9	3.80	41.4	3788
3	GX-B	30/206	70000	24.9	19.6	3.3	43.4	4090**
	CONTROL	30/211		22.9	15.7	3.3	40.7	/
	GX-M	33/196		17.8	13.0	3.8	44.8	2917**
4	GX-M	38/211	70000	17.3	11.7	1.8	53.4	2850
	GD-M	34/216		10.7	6.4	1.8	58.6	/
	PS-GD-M	41/218		6.6	4.3	0.8	53.8	2700

Notes: (1) For explanation of key see footnote to Table 3.1.
(2) Thickness of asphaltic/granular base layer in mm.
(3) Vertical transient stress at the top of subgrade.
(4) Longitudinal resilient strain at the bottom of the asphaltic layer.
** measured at 10,000 passes of wheel load.
/ data not available.

4.2.1 Results from the Main Tests

Based on the average result from the 12 pavement sections, about 73% of the total permanent deformation took place in the granular base. This compares with 16% in the

subgrade and 11% in the asphaltic surfacing. This statistical finding clearly identifies the permanent deformation resistance of the granular base as a dominant property of the pavement sections tested.

The surface conditions of the pavement sections at the end of each test series are shown in Figure 4.1 and the section profiles measured by the profilometer are shown in Figure 4.2. Based on these profiles, rut depth of the pavement sections as shown in Figure 4.3 could be obtained. The permanent vertical deformations in the granular and subgrade layer were calculated from the changes in distance between the pairs of installed strain coils. The results thus obtained are shown in Figures 4.4 and 4.5 respectively.

Figure 4.4a indicates that the pavement sections in the first series of tests were generally very weak, with large deformations developing in less than 2000 passes of wheel load. However, it shows conclusively that the inclusion of geotextile at the bottom of the very weak sand and gravel material used in that particular series of tests did help to reduce the permanent deformation of the base layer. When compared with the control section, reduction of 50% was achieved after 1262 passes of wheel load. Furthermore, Figure 4.4a indicates that prerutting of the reinforced granular base does not appear to significantly improve the performance of the pavement layer. The reduction in permanent deformation obtained under this condition was only 29% of that from the non-prerutted-reinforced section at the same number of passes mentioned above.

Because of the use of a higher quality granular material and thicker pavement layer, the life for the pavement sections of the other three series of tests were very much longer. As a result, comparisons on the performance of the granular layer were made after 70,000 passes of wheel load.

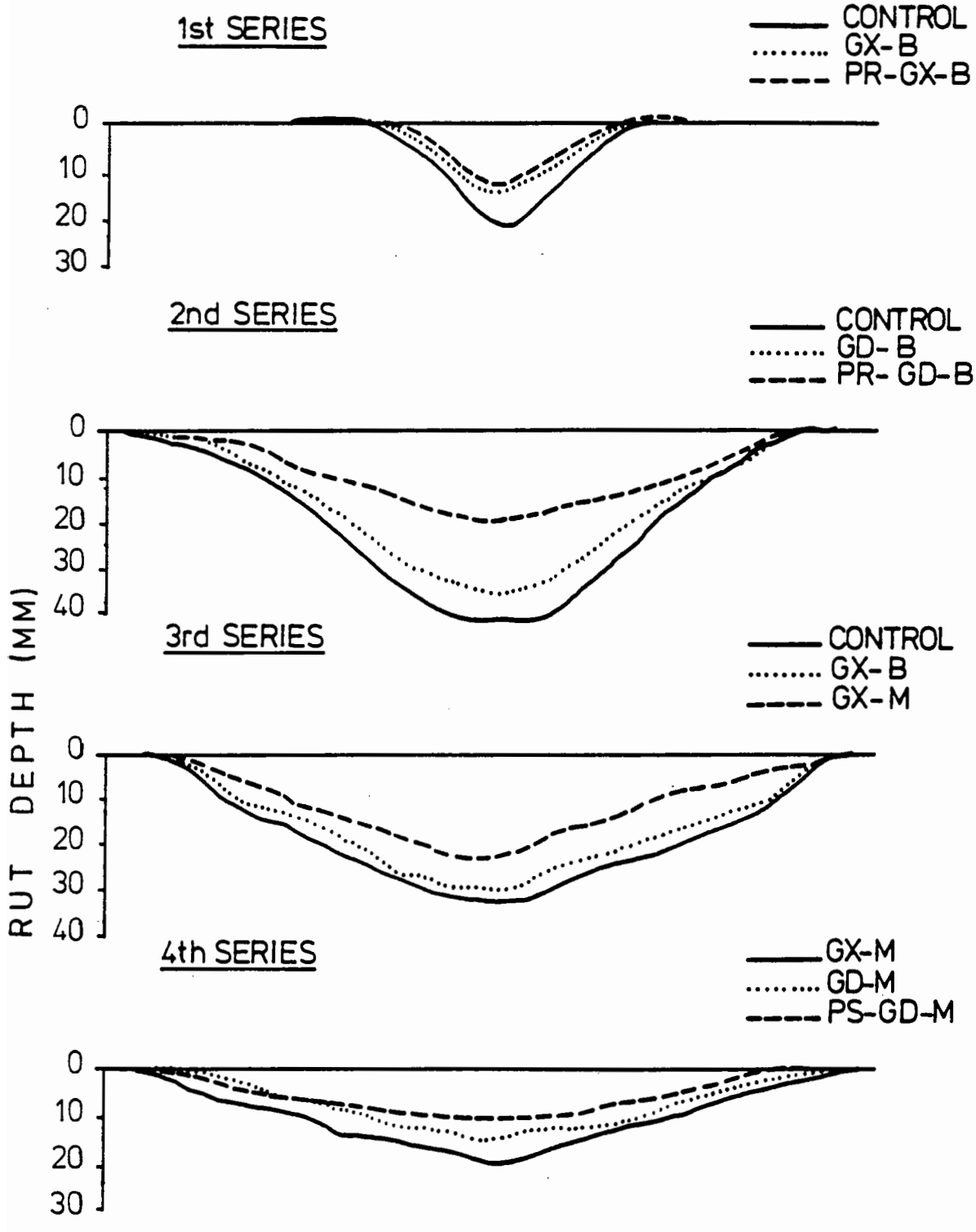

Figure 4.2 Section Profiles meausred by Profilometer at End of Tests for all four Test Series. For Explanation of Keys see footnote to Table 3.1.

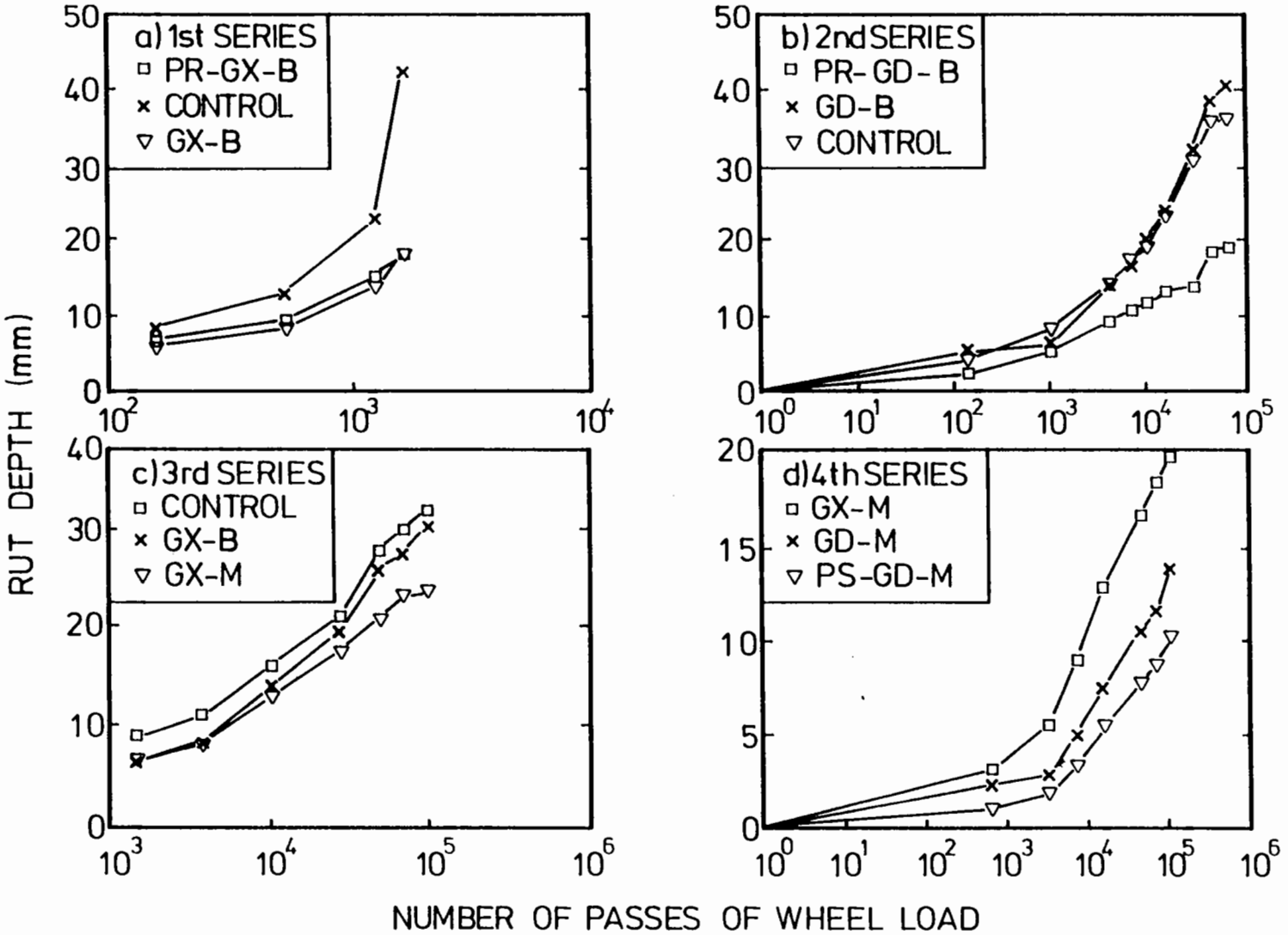

Figure 4.3 Variation of Rut Depths measured by Profilometer with Number of Passes of 6.6kN Wheel Load for all four Test Series. For Explanation of Keys see footnote to Table 3.1.

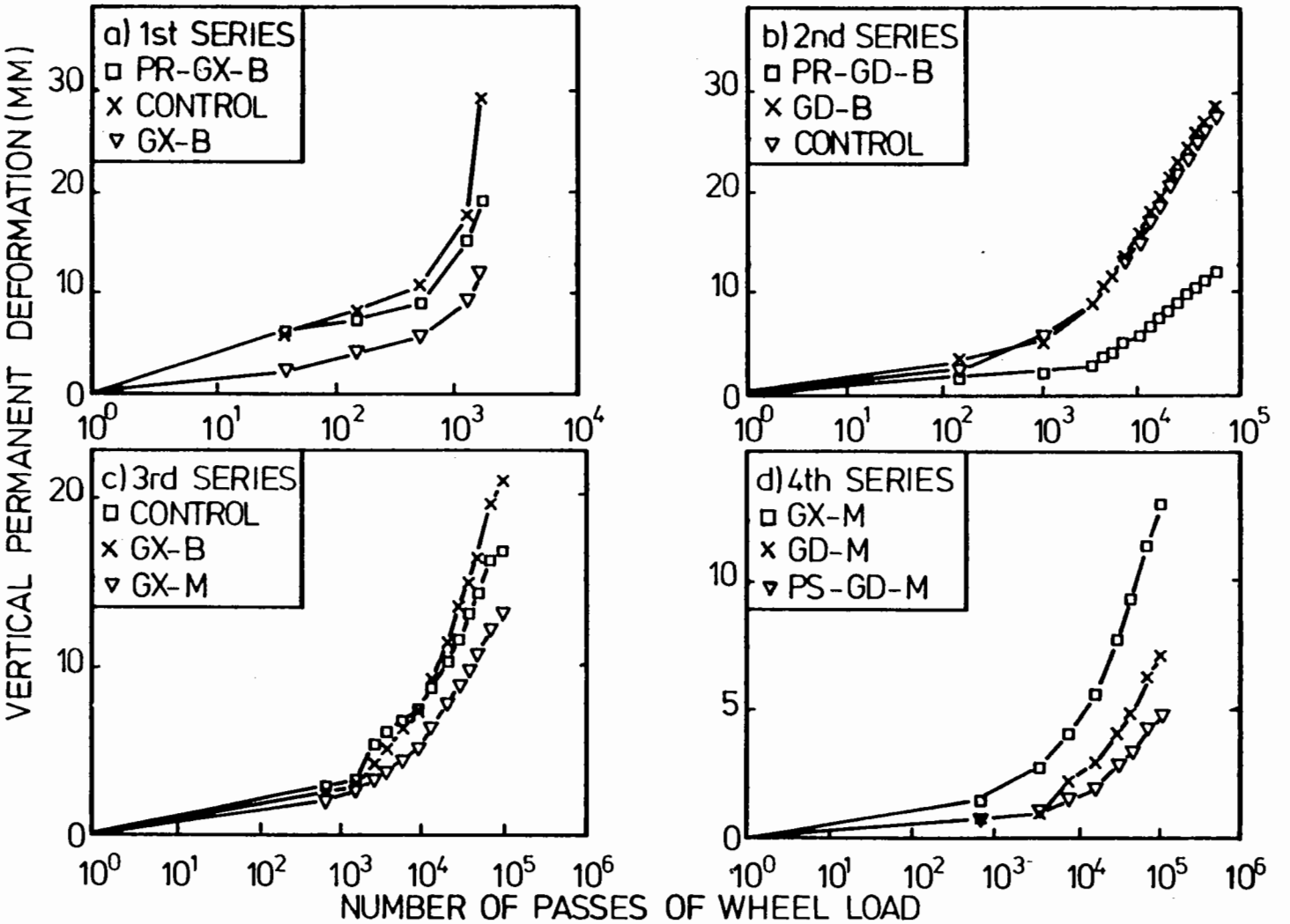

Figure 4.4 Variation of Vertical Permanent Deformation in the Granular Base with Number of Passes of 6.6kN Wheel Load for all four Test Series. For Explanation of Keys see footnote to Table 3.1.

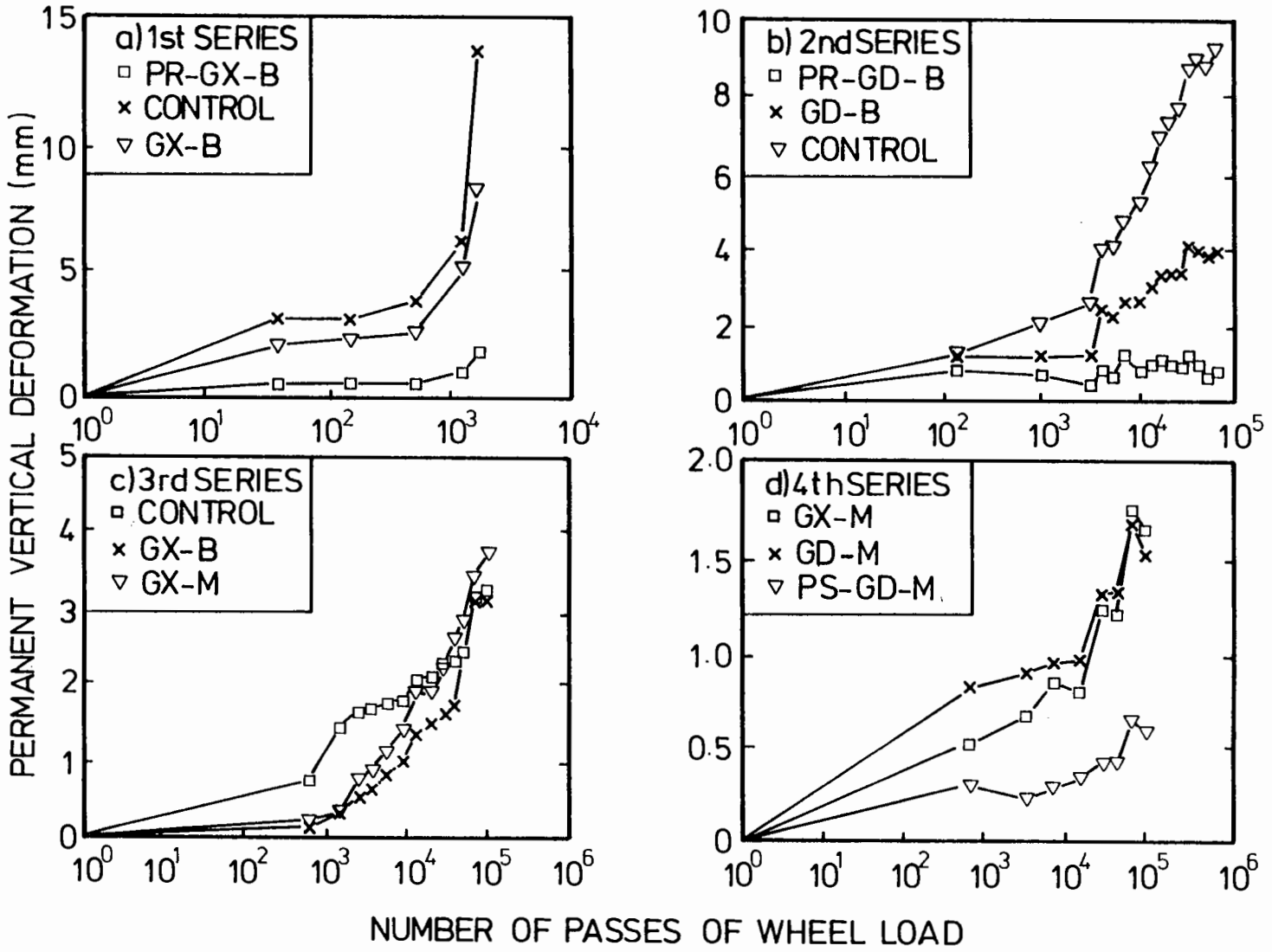

Figure 4.5 Variation of Vertical Permanent Deformation in the Subgrade with Number of Passes of 6.6kN Wheel Load for all four Test Series. For Explanation of Keys see footnote to Table 3.1.

Contrary to the results of the first test series, the prerutted-reinforced section in the second series performed best with 58% reduction in permanent deformation when compared with the control section. The inclusion of the low stiffness geogrid at the bottom of the granular base was also found to produce no improvement in the performance of the layer, as shown in Figure 4.4b. The same "ineffectiveness" of the inclusion of a stiff geotextile at the bottom of the granular base was observed in the third series of tests. In fact, 24% higher permanent deformation were obtained in the base layer. However, with the location of the geotextile raised to the middle of the granular base, some improvement (about 18% reduction) in performance began to emerge (see Figure 4.4c). Results from the last series of tests indicated that after an initial 3000 passes of wheel load, prestressing of the geogrid appeared to improve performance when compared with the non-prestressed section using the same geosynthetic. Permanent deformation in the prestressed section was only 68% of that in the non-prestressed section. The result also indicated that the inclusion of a geogrid, despite its lower stiffness, resulted in 46% less permanent deformation than that with geotextile inclusion when both geosynthetics were placed at the middle of the granular layer (see Figure 4.4d).

Permanent vertical deformation in the subgrade was generally small, particularly so for the prerutted sections which had little further development during the main tests. Reduction in deformation was evident when a geosynthetic was placed directly on top of the subgrade, as shown in Figures 4.5a to 4.5c. Results from the fourth series of test also indicated that prestressing of the geogrid resulted in less permanent deformation in the subgrade.

The trend in the development of total permanent vertical deformation in all 12 sections of the four test series under the multitrack loading was generally confirmed by the

single track tests. The results of these tests are shown in Figure 4.6. Two points are worth noting:

1. The prerutted sections in the first and second series of tests were actually not prerutted at the single track position. Therefore, as expected, their performance were similar to that of the non-prerutted sections.

2. The sections with geotextile placed at the middle of the granular base showed a marked improvement in performance when under the more severe loading conditions used in the single track tests. Results from the fourth series of tests indicated that it performed as well as the geogrid (Figure 4.6d).

4.2.2 Results of the Supplementary Single Track Test

Results of the three series of supplementary single track tests as detailed in Table 3.2 are shown in Figure 4.7. Based on these results, the following observations were made:

1. In the second series of experiments when tests were carried out on an unsurfaced pavement in order to create even more severe stress and strain conditions, the inclusion of a geogrid at the bottom of the granular base still did not have any influence on the pavement performance . This behaviour was confirmed by the results from two identical reinforced sections, as shown in Figure 4.7a.

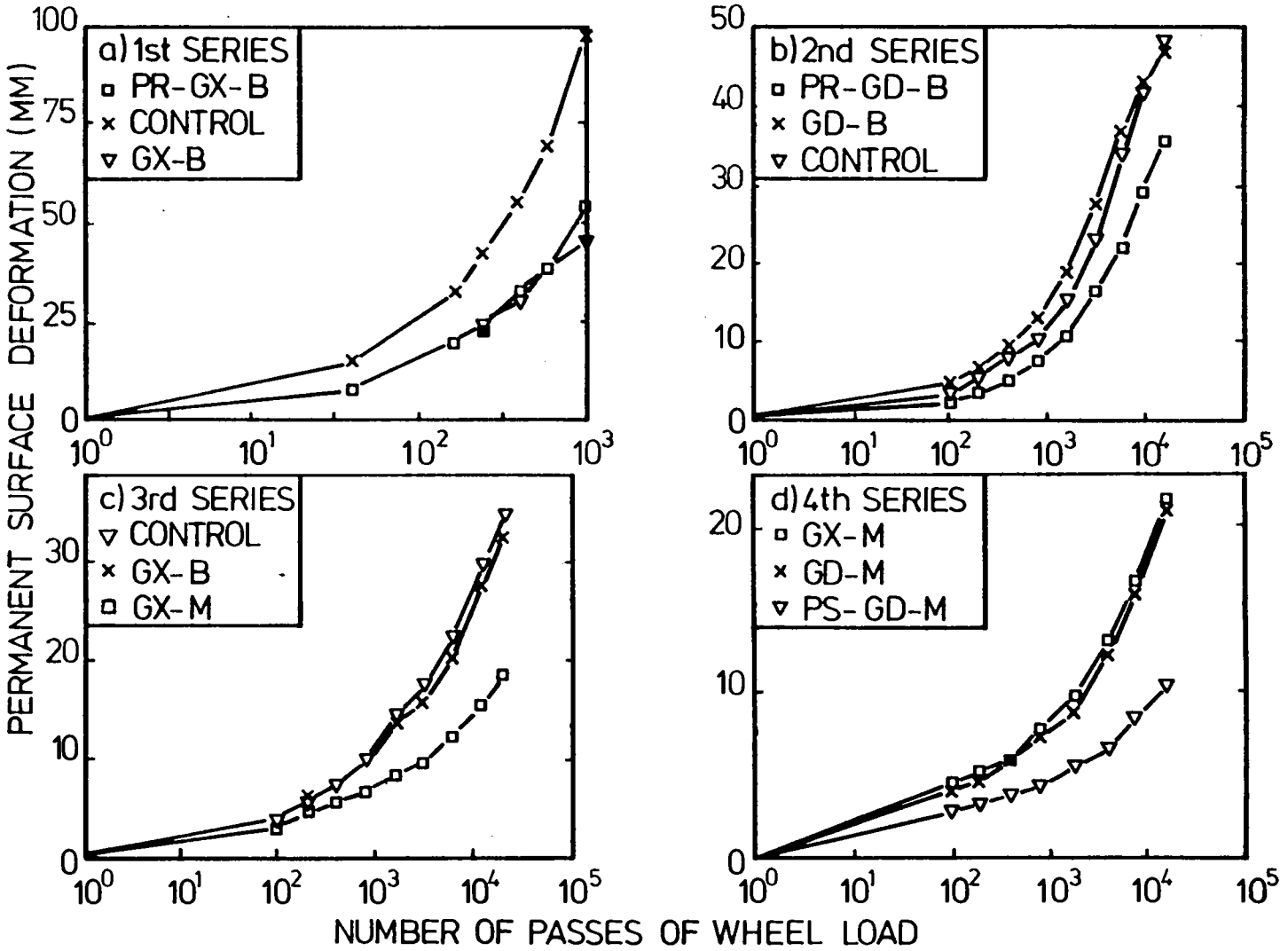

Figure 4.6 Variation of Permanent Vertical Surface Deformation with Number of Passes of 9 kN Wheel Load in Single Track Tests for all four Test Series. For Explanation of Keys see footnote to Table 3.1.

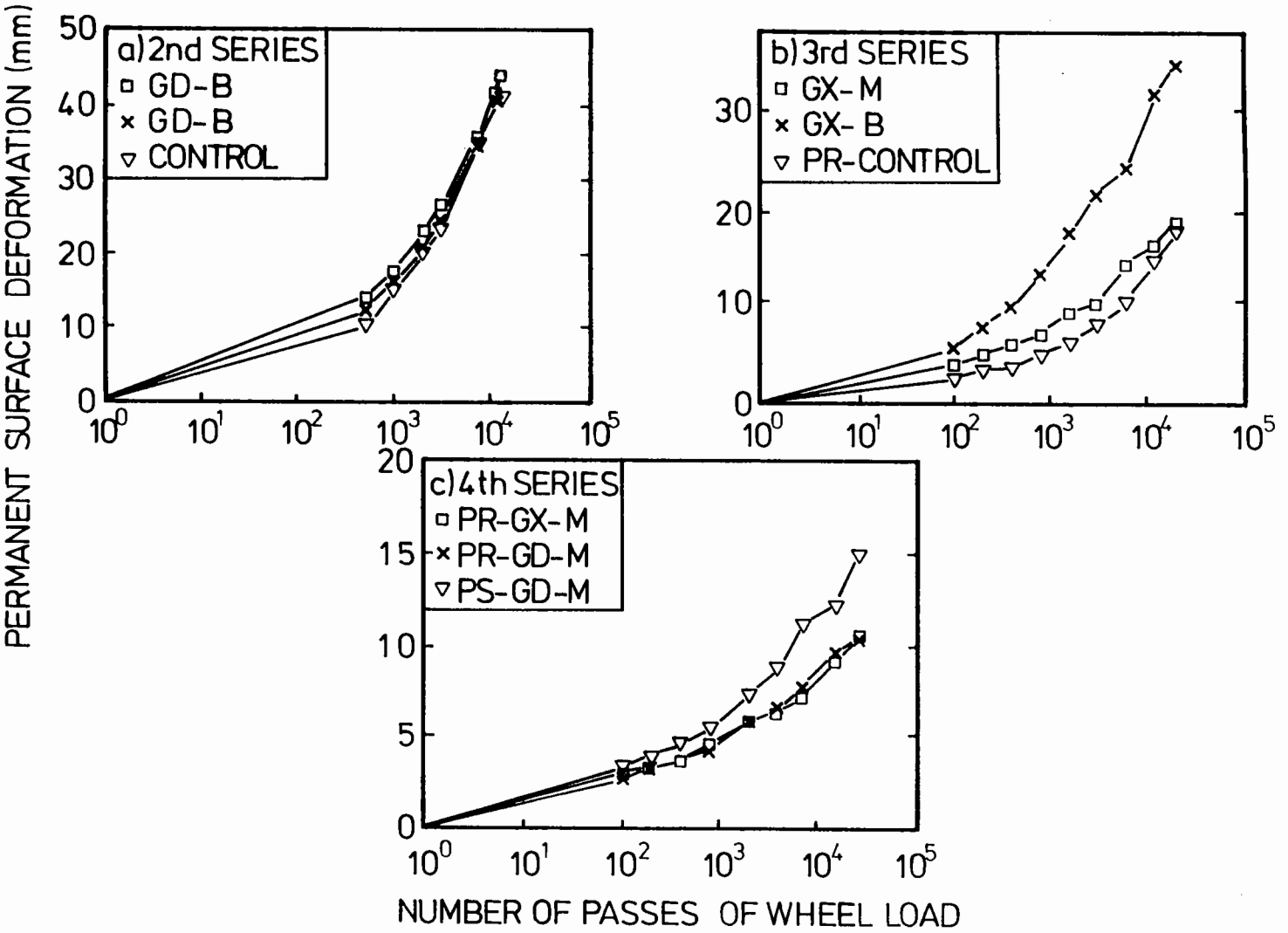

Figure 4.7 Variation of Permanent Vertical Surface Deformation with Number of Passes of 9 kN Wheel Load in Supplementary Single Track Tests. For Explanation of Keys see footnote to Table 3.1.

2. In the third series, when the section which was prerutted but not reinforced with geosynthetic was tested, it was found to perform better than the section with geotextile placed at the middle of the granular layer (see Figure 4.7b). This occurred despite the fact that the latter section had been found to have an improved performance during the main tests.

3. The improvement in performance due to a combination of prerutting and inclusion of geosynthetics at the middle of the granular layer was found to outweigh that of using a prestressed geogrid placed at the same location within the granular base but not prerutted (see Figure 4.7c).

4.3 PERMANENT VERTICAL STRAIN

The variation of permanent vertical strain with depth for all the sections at the end of testing are shown in Figure 4.8. The values are plotted at the mid-distance between the two strain coils which measure the corresponding vertical movement. In general, the pattern of results is very similar for all test series, with large permanent strain at the top of the granular base, decreasing rapidly with depth towards the subgrade. However, a closer look at the results revealed the following differences between each pavement section:

1. When comparing results from the "reinforced" and control sections, it becomes evident that redistribution of strain occurs due to the presence of the geosynthetic. For sections with geosynthetic placed at the bottom of the granular base, a decrease of strain near the surface of the subgrade is generally observed but at the same time, an increase in strain

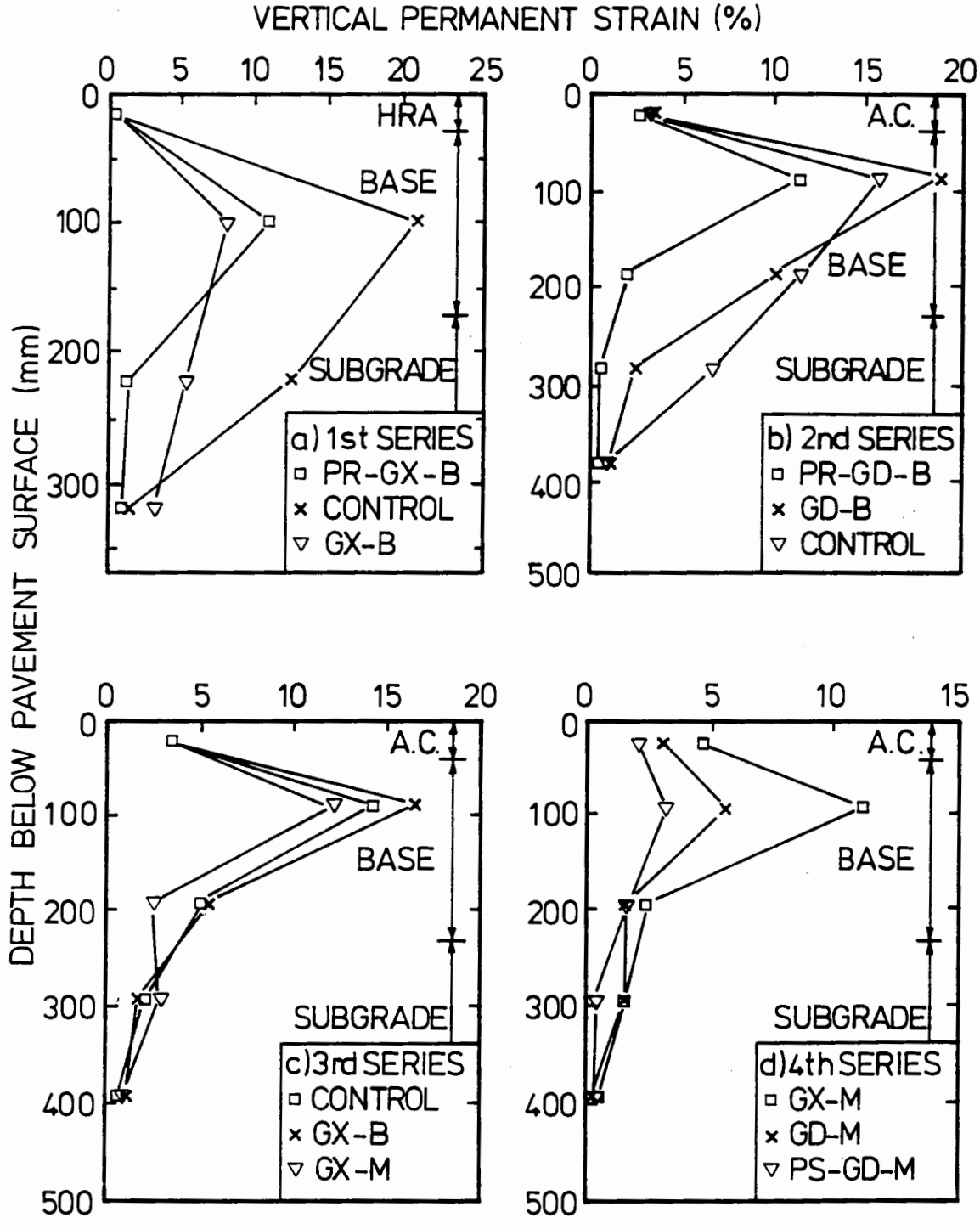

Figure 4.8 Variation of Vertical Permanent Strain with Depth of Pavement for all four Test Series. For Explanation of Keys see footnote to Table 3.1.

at the top half of the granular base occurs. This behaviour could not be monitored for the sections in the first series because of the absence of instruments at the middle of the granular layer.

2. Figure 4.8c indicates that, as a result of placing a geotextile at the middle of the granular base, a substantial decrease in permanent vertical strain immediately below the geotextile occurred. At the same time, strain at the top of the subgrade increased when compared with that from the control section. This pattern was repeated for the two similar sections used in the fourth series of tests, as shown in Figure 4.8d.

3. The vertical permanent strains in both the granular base and subgrade for the two prerutted sections are smaller than those in the non-prerutted section, as shown in Figs. 4.8a and 4.8b. The only exception is the permanent strain developed within the prerutted sand and gravel which shows a greater value than its non-prerutted counterparts.

4. Prestressing of the geogrid appears to reduce the development of permanent vertical strain in all the pavement layers. The biggest improvement, however, was observed at the top half of the granular layer.

4.4 TRANSIENT STRESSES AND RESILIENT VERTICAL STRAIN

The transient subgrade stress, as shown in Figure 4.9, for the last three series remained sensibly constant throughout with magnitudes varying around 42 to 63 kPa. For the first series of tests, however, the subgrade stress increased as the pavement deformed

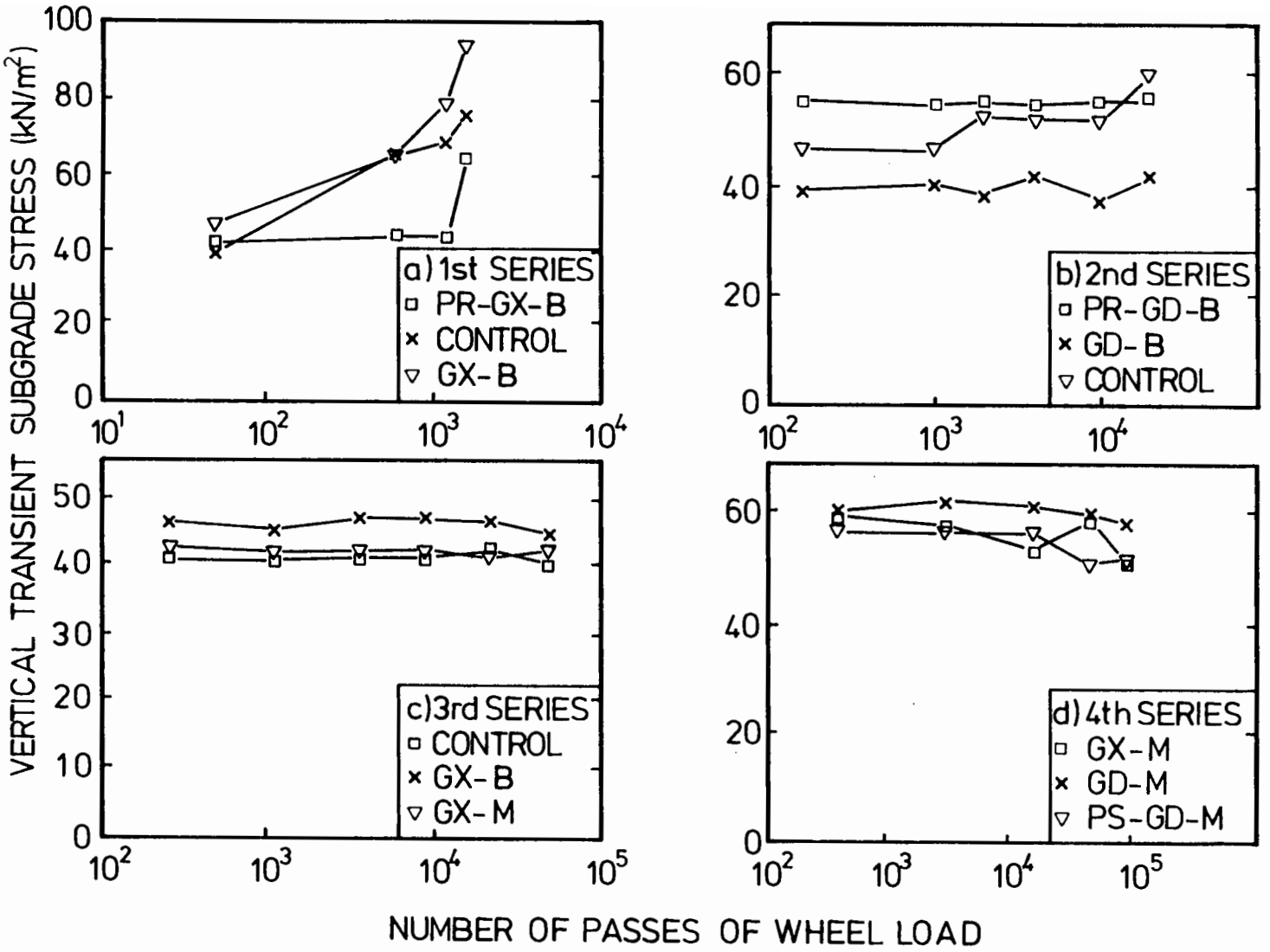

Figure 4.9 Variation of Transient Vertical Stress at the Top of Subgrade with Number of Passes of 6.6kN Wheel Load for all four Test Series. For Explanation of Keys see footnote to Table 3.1.

rapidly. No consistent influence on subgrade stress due to the presence of geosynthetics was noted for any of the test series. Longitudinal horizontal transient stresses (in the direction of wheel traffic) at both the top and bottom of the granular layer were measured in the third and fourth test series. The results, as shown in Figure 4.10, indicate that the stress at the top of the granular layer generally increases during the test. Figure 4.10a also suggests that the inclusion of a geosynthetic at the middle of the granular layer may result in a slower rate of increase in horizontal stress at the top of the same layer. The horizontal stress at the bottom of the granular layer, on the other hand, did not seem to be influenced by the progress of the test, nor by the presence of the geosynthetics above.

The variations of vertical resilient strain with depth for all the pavement sections are shown in Figure 4.11. In general, large strains were obtained at the top of both granular base and subgrade. The overall resilient response of the granular layer used in these experiments did not seem to be significantly influenced by the geosynthetic, regardless of its location within the pavement structure. However, in the fourth series, much larger resilient strain were obtained at the top half of the granular layer reinforced with a geotextile. Furthermore, neither prestressing nor prerutting appeared to affect the measured resilient vertical strain in the granular base.

Results of the resilient vertical strain in the subgrade were less consistent, especially for those obtained at the bottom half of the the layer. However, both prerutting and prestressing were found to contribute to a significant reduction in strain at the top of the subgrade.

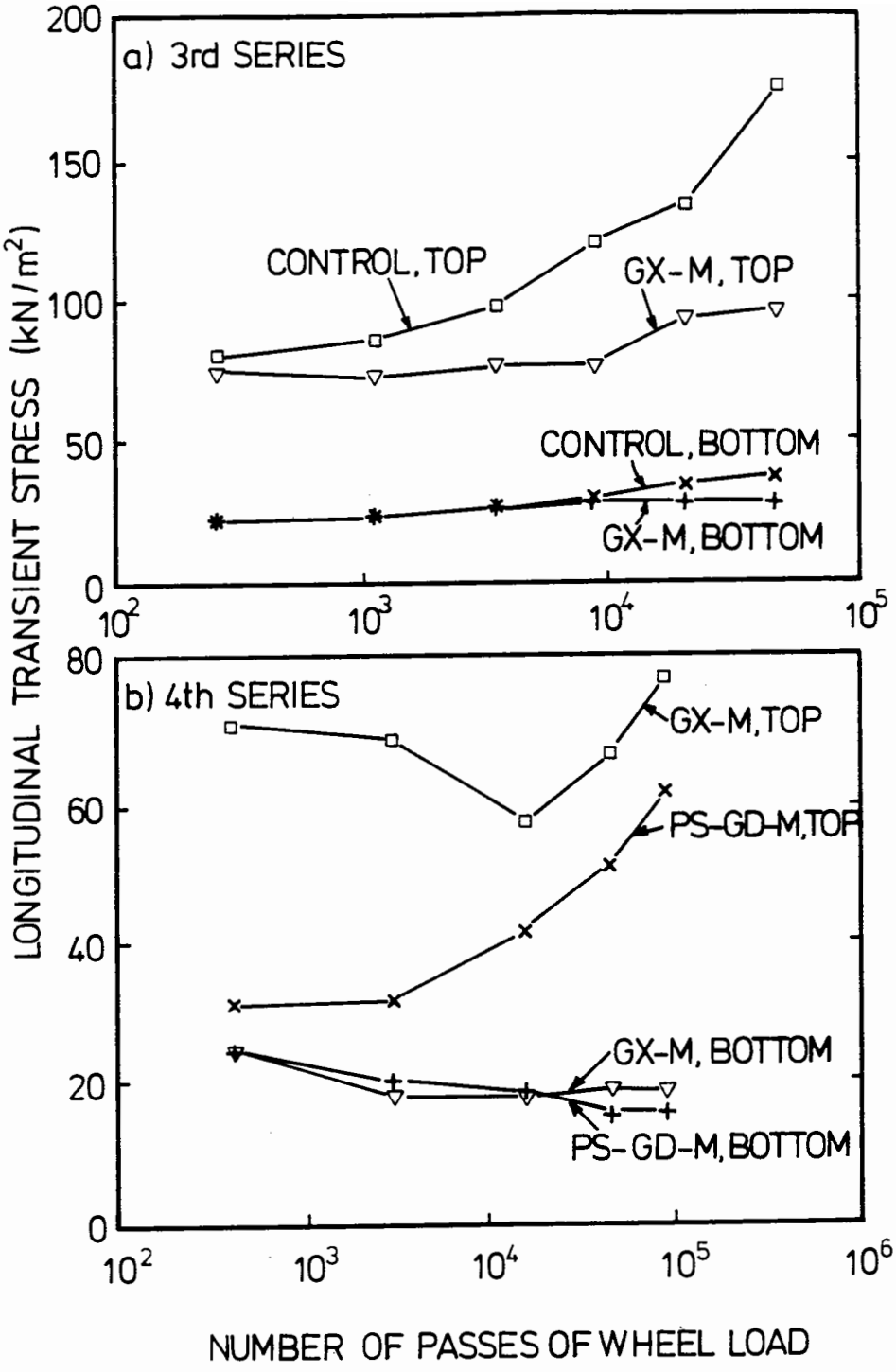

Figure 4.10 Variation of Transient Longitudinal Stress at Top and Bottom of Granular Base with Number of Passes of 6.6kN Wheel Load for the third and fourth Test Series. For Explanation of Keys see footnote to Table 3.1.

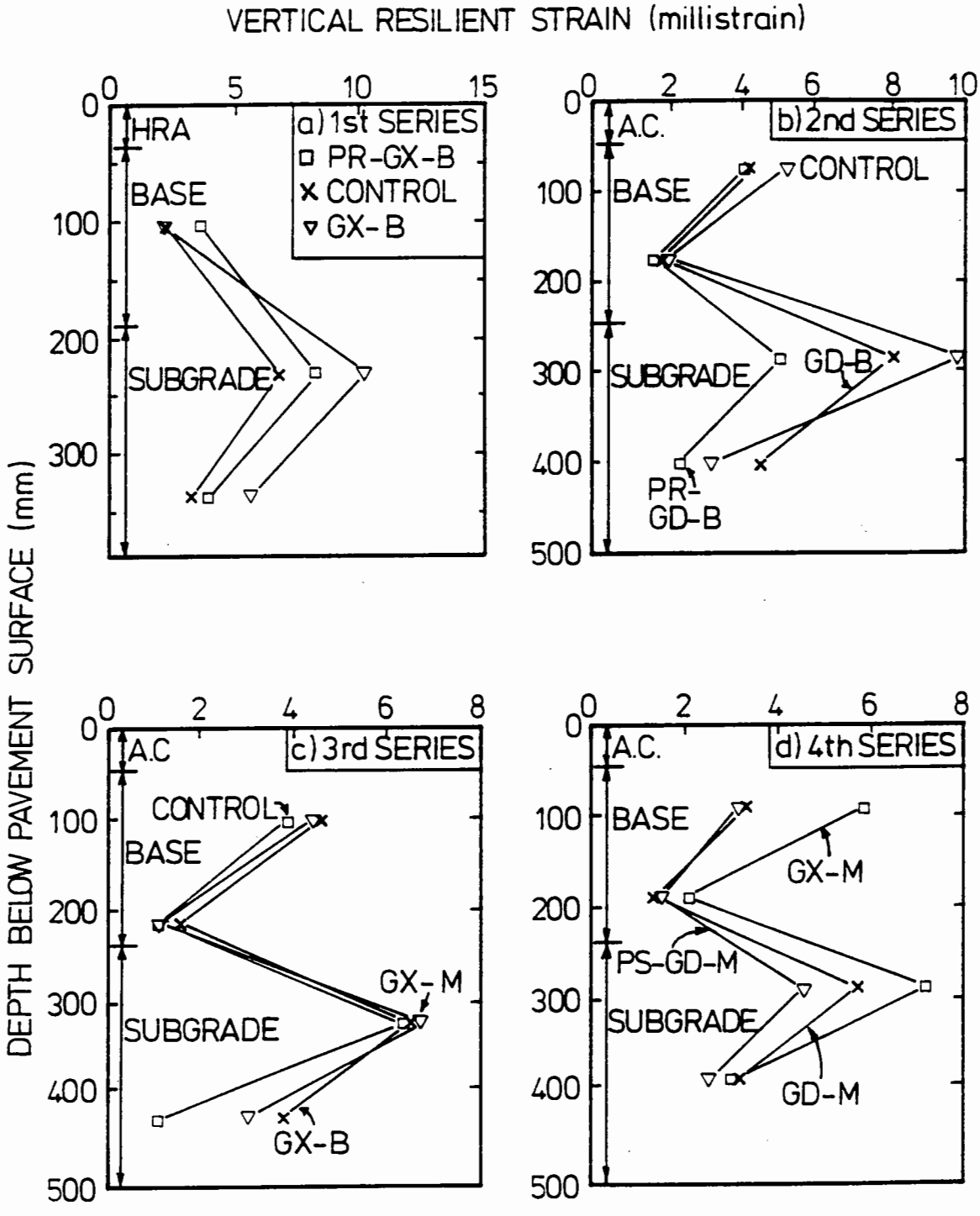

Figure 4.11 Variation of Vertical Resilient Strain with Depth of Pavement for all four Test Series. For Explanation of Keys see footnote to Table 3.1.

4.5 DISCUSSION OF RESULTS

The improvement in permanent deformation resistance of the granular bases in the current experiments were due primarily to the reinforcement function of the geosynthetics. Other functions such as separation, filtration and in-plane drainage, the benefits of which are sometimes difficult to separate from those of reinforcement, were either non-existent or considered to be unimportant under the particular laboratory conditions used.

In order to summarise the results of the experiment, two charts, one for the sections with the low quality sand and gravel base and the other with the better quality dolomitic limestone base, as shown in Figure 4.12 and 4.13 respectively, were prepared. In these figures, the rut potential for the pavement sections, defined as the rut depth expressed as a percentage of that of the corresponding unreinforced and non-prerutted control section, are ranked. In general, improvement in performance, when compared with the control section, was achieved by most reinforced sections. However, a large range of level of improvement, from an insignificant 8% to an encouraging 82% reduction in overall rut depth was obtained. A discussion of the various parameters investigated, their influences on pavement performance and the possible performance mechanism involved in the improvement are presented as follows.

4.5.1 Quality of Granular Base

There is no doubt that the permanent deformation resistance of the sand and gravel base under wheel loading is substantially lower than that of the dolomitic limestone. In the absence of any geosynthetic inclusion, the two resistances can be directly compared by means of the permanent deformation that took place within the layer. However, when

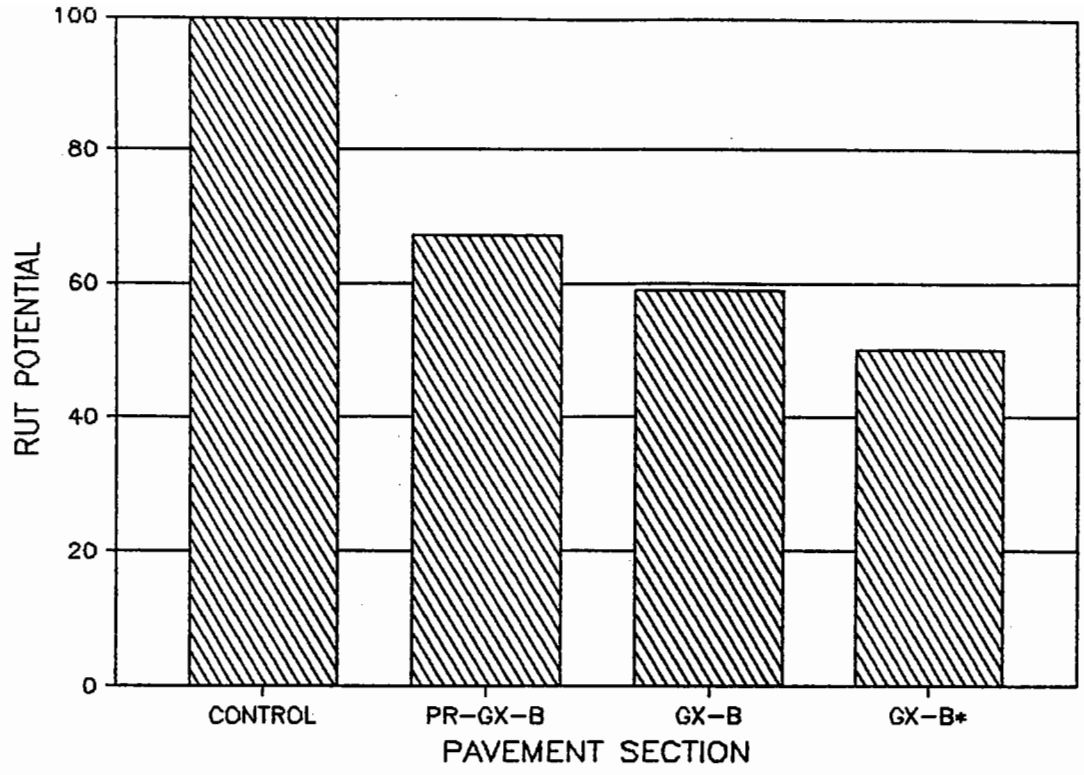

Figure 4.12 Rankings of Performance for Pavement Sections with Sand and Gravel Base by means of Rut Potentials. For Explanation of Keys see footnote to Table 3.1 (Sections with "*" were under higher and concentrated wheel load).

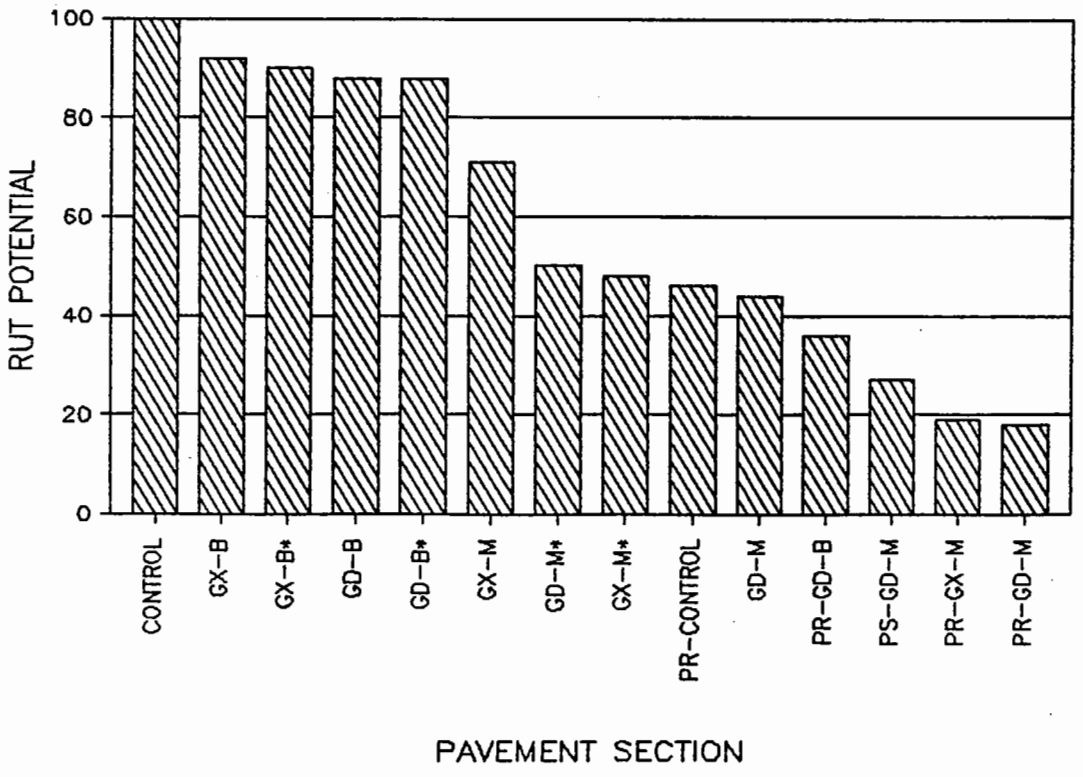

Figure 4.13 Rankings of Performance for Pavement Sections with Dolomitic Limestone Base by means of Rut Potentials. For Explanation of Keys see footnote to Table 3.1 (Sections with "*" were under higher and concentrated wheel load).

geosynthetics were placed at the bottom of both granular bases, the relative performance of the reinforced sections (when compared with that of their control sections) is found to be significantly influenced by the load spreading capability of the granular material.

In the reinforced sections with sand and gravel base, which has got a lower elastic stiffness, the vertical as well as horizontal stresses throughout the layer would be high. Under these conditions, the most likely mechanism which contributes to the observed improved performance is probably the combination of both the aggregate and subgrade restraint effect and the membrane-type support. The latter mechanism became more evident when much higher and channelised loading was used. This resulted in much higher wheel-path rutting which, in turn, led to development of higher tensile stresses in the stiff geotextile.

In the reinforced sections with higher thicknesses of better quality dolomitic limestone, the stresses transmitted down to the reinforcement location were probably small with possibly negligible differences between those of the control section. Under these conditions, the performance was dominated by the permanent deformation at the upper part of the granular layer. Therefore, the mechanisms described above would not be applicable although a small amount of subgrade restraint could still be found. As a result, only small improvement was observed.

4.5.2 Location of Geosynthetics

Results of the current project have clearly indicated the importance of the location of the geosynthetic within the granular base in order to improve its permanent deformation resistance. The limited number of tests did not allow the development of a discrete

mathematical solution to determine the optimum depth. However, in the tests performed, the advantage of placing the geosynthetic as high up in the granular layer as practical was evident since reduction in permanent deformation in the granular material immediately beneath the geosynthetic was observed in all the sections where the geosynthetics were located at the middle of the layer. Furthermore, the results appeared to suggest that under the circumstances investigated, the position of the geosynthetic had a greater influence than the geosynthetic type or stiffness. This is especially true when the overall deformation is small hence eliminating the possible membrane effect.

4.5.3 Stiffness and Type of Geosynthetics

The geogrid generally led to better performance than the geotextile despite its much lower stiffness. This result shows that the conventional concept which accredits the reinforcement effect to a curved tensioned membrane is not applicable. Since otherwise, the stiffer geotextile should have provided more support. The better performance of the geogrid under the relatively small wheel load could be due to better interlocking between the geosynthetic and the granular base.

Nevertheless, if large shear forces are needed to hinder the lateral deformation of aggregate at small rut depths (and therefore small strains), the stiffness of the reinforcement may be important. This point was highlighted by the fact that whilst the performance of the GX-M section improved during the more severe conditions of the single track test, no similar improvement was observed for the GD-M section (see Figure 4.13). In fact, comparative results indicate that the geogrid performed better under the multi-track test than the single track test.

4.5.4 Prerutting

The tensile forces that prerutting induced on the geosynthetics used in these experiments were probably small. Otherwise, they should have been reflected by the performance of the PR-GX-M and PR-GD-M sections in which geosynthetics with large difference in stiffness and hence, induced tensile forces, were used. However, prerutting is generally beneficial because of the additional compactive effect applied to the granular base, similar to that from a pneumatic-tyred roller. This normally resulted in the formation of a denser and stiffer zone at the top of the granular layer. As a result, improved resistance to permanent deformation and less rutting were achieved. This effect alone was shown to have equal, if not more benefit than placing a stiff geotextile at an effective location (see Figure 4.7b). Furthermore, in this experiment, the use of a combination of prerutting and geosynthetic reinforcement was found to have more benefit than using a prestressed geogrid.

Despite the above-mentioned benefits of prerutting, it may not be entirely advantageous to perform prerutting on weak granular materials as the reinforced system may fail in shear rather than densify under the severe stress conditions. The formation of a shear plane or weakened zone within the granular layer as a result of prerutting may have a detrimental effect on the pavement performance, as indicated by high permanent strain in the granular base of the prerutted section in the first test series (Figure 4.8a).

4.5.5 Prestressing of Geosynthetic

The benefit of prestressing was clearly indicated by the results of the fourth test series (Figure 4.4d). When the prestress force on the geogrid was released, a proportion of it was transmitted to the granular material as a horizontal compressive force. As a result,

both the stiffness and the resistance to permanent deformation of the granular material increased.

The good performance of the prestressed section used in this experiment may, to a large extent, have been due to the use of relatively high prestress levels and the provision of good anchors. The latter substantially reduced the chances of slippage and, hence, helped to maintain the prestressed condition within the geogrid during the construction of the upper granular layer.

PART B

AN INVESTIGATION OF THE PERMANENT STRAIN BEHAVIOUR OF GRANULAR MATERIAL

CHAPTER FIVE
LARGE SCALE RUTTING TESTS

5.1 INTRODUCTION

As shown in Figure 1.1 of Chapter one, the stress conditions imposed on an element of granular material by a moving wheel load are extremely complex. For each passage of the wheel, principal plane rotation occurs as a result of the reversed shear stresses. At the present time, there are very few pieces of equipment capable of simultaneously applying the stress patterns shown in Figure 1.1 onto a test specimen. Although large amounts of data were obtained from the repeated load triaxial tests (Barksdale, 1972, Brown, 1974, Pappin,1979 and Thom, 1988), the latter only correctly simulates the in-situ stress conditions underneath a circular plate which is repeatedly loaded vertically. Examination of this mode of loading in large scale, which does not involve the application of reversed shear stresses is needed in order to establish the difference in behaviour, particularly in the development of permanent strains, compared with that due to wheel loading.

Examination of the difference in the permanent deformation behaviour of granular material due to uni-directional and bi-directional wheel loading also appears to be desirable. In practice, all traffic travels in the same direction over the pavement (i.e. uni-directional). However, bi-directional loading is usually adopted for wheel tracking experiments in order to bring about failure of the test pavement in a reasonable period of time. Since the shear stress reversal conditions differ, an understanding of the different response of the material is needed.

This chapter describes an investigation which is aimed at highlighting the effect of reversed shear stresses on permanent deformation of granular materials. To tackle the

problem caused by the difference between repeated vertical and moving wheel loading, the Nottingham Slab Test Facility (STF) was used. Details of this facility are described later in this chapter. For the problem involving uni- and bi-directional wheel loading, the Nottingham PTF was, again, employed.

5.2 TEST MATERIALS

The same dolomitic limestone used for the tests in Part A of the project was used in both the tests carried out in the STF and PTF. Two gradings of this material were considered. Apart from the grading for the British Standard Type 1 sub-base material, a high density grading which was developed during a different investigation (Chan and Brown, 1989) was used. The latter grading is identified as "Optimum" in this thesis. A third material, consisting of an open-graded carboniferous limestone was also used in the PTF tests. The grading envelopes of these materials are shown in Figure 5.1. The three materials enabled a range of compacted densities to be achieved.

5.3 TEST FACILITIES AND EXPERIMENT PROGRAMME

5.3.1 Slab Test Facility

The Nottingham STF was originally used to evaluate the deformation resistance of a slab of bituminous material. However, by confining a layer of compacted granular material in a mould, the facility can also be used to study the same characteristic of this material.

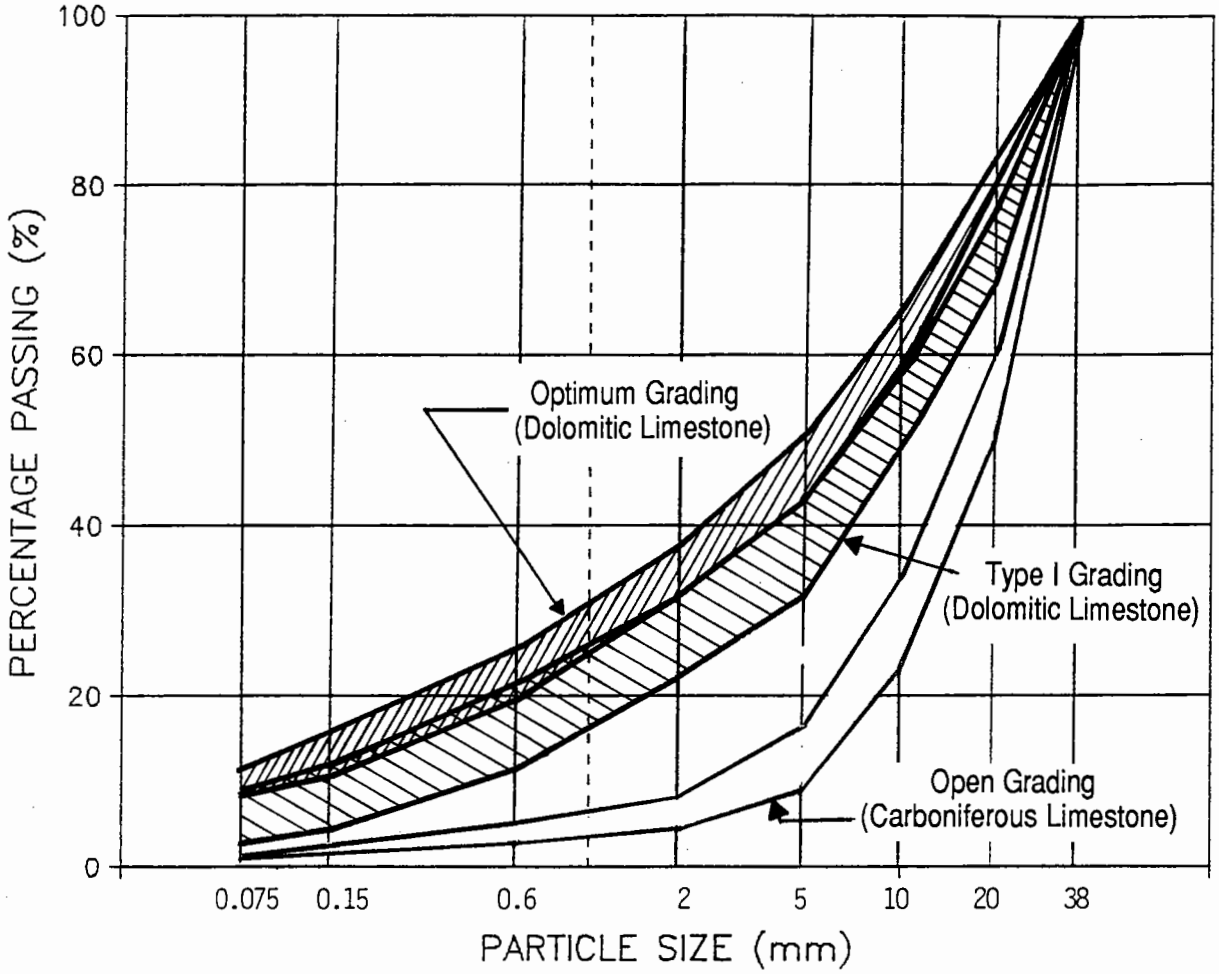

Figure 5.1 Grading Envelopes of Granular Materials used in Large Scale Rutting Tests.

A side view of the STF is shown in Figure 5.2. The carriage is mounted onto a pair of beams and is driven by means of a wire rope tensioned around a drum which is axially coupled to the motor. Loading is provided via a hydraulic actuator located at one end of the facility. A feedback mechanism involving the use of four load cells located under the corners of the steel pallet is used. Constant wheel load over the slab can only be achieved by applying an increasing actuator load of the correct gradient as the wheel approaches the actuator. Alternatively, the wheel can be fixed at a position directly above the compacted granular material. Repeated vertical loading, which is regulated by means of a signal generator can then be applied via the hydraulic actuator onto the specimen.

A 75mm wide hard rubber tyre was used in both the repeated vertical and wheel loading conditions to ensure that the same contact area was achieved. A sinusoidal waveform with frequency of 0.5 Hz (or one cycle of load every two seconds) was used for the repeated vertical loading condition. For the travelling wheel load, an average speed of approximately 2 km/hr was used. Loading in this case was bi-directional. An element of granular material loaded under the moving wheel had a rest period of approximately two seconds while that for the repeated vertical load was zero.

The samples tested in the STF were compacted in a specially manufactured steel mould as shown in Figure 5.3. The thickness of the granular layer was 180mm. A 60mm thick concrete slab with a rough surface was placed at the bottom of the steel mould in order to provide a rigid foundation for compaction. The entire mould was then placed on top of a piece of 25mm thick soft rubber which simulated a medium-stiff subgrade condition. The rubber, in turn, was located on top of a steel platform with cross bracing at the bottom face to provide additional reinforcement. The weight of granular material used per sample was about 325 kg. Total weight of the assembly shown in Figure 5.3 was about 750 kg .

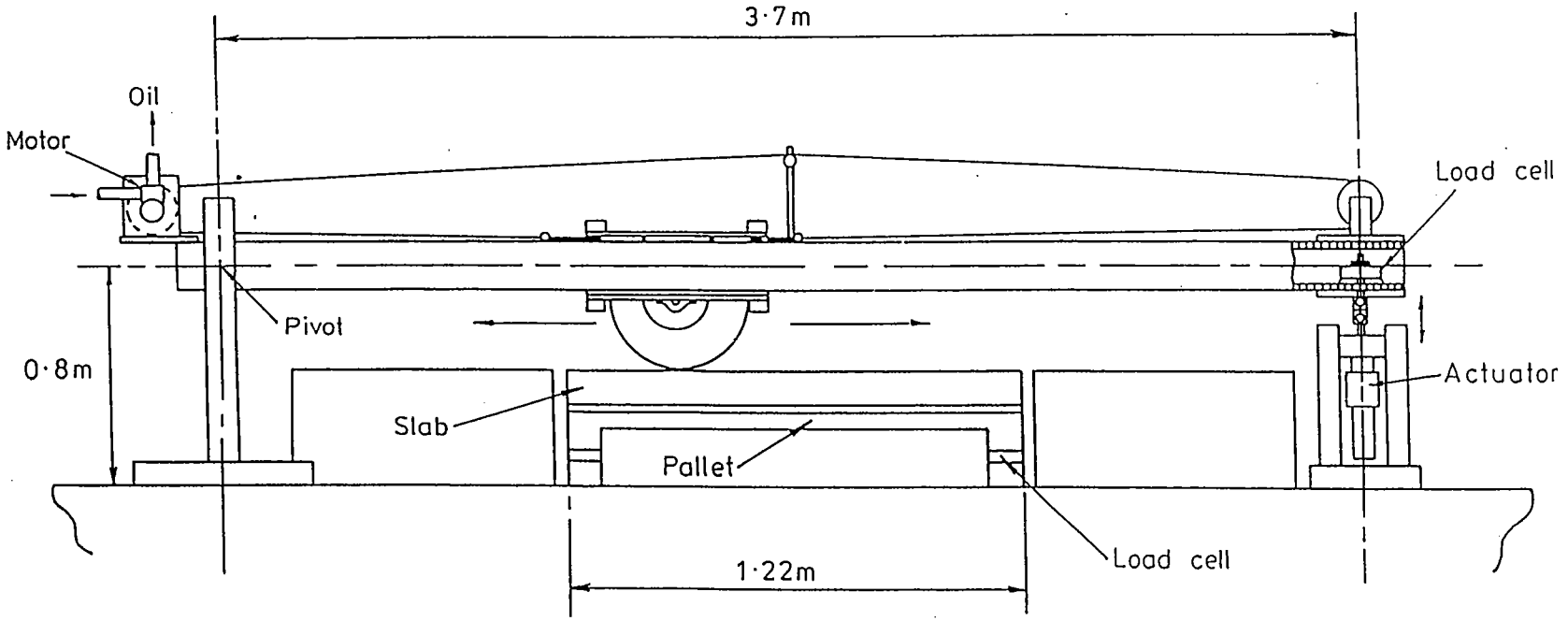

Figure 5.2 Side View of the Nottingham Slab Test Facility.

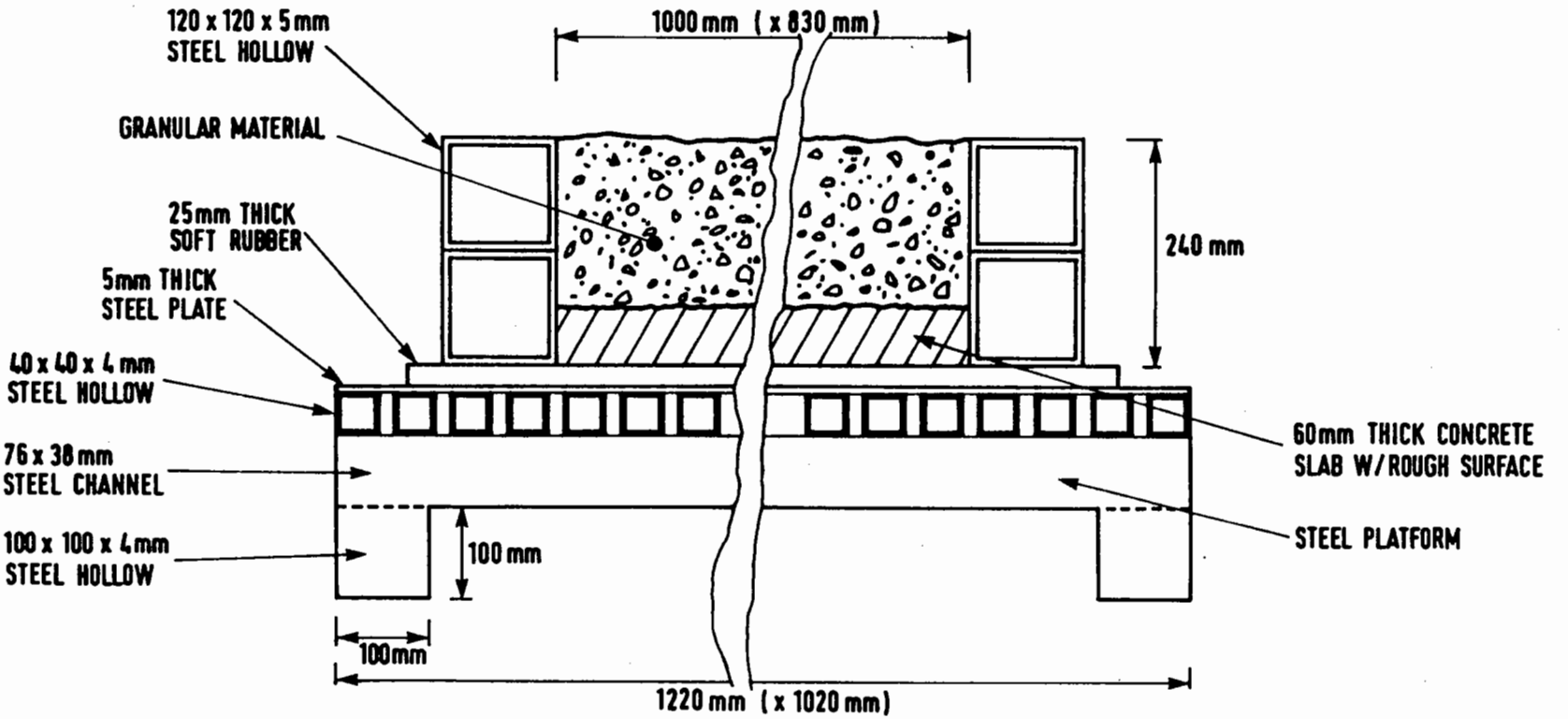

Figure 5.3 Details of Large Steel Mould used in Tests carried out in the Slab Test Facility.

Compaction of the material was carried out by the heavy vibrating plate described in Part A (Figure 3.5) for the compaction of the sand and gravel base. Compaction was carried out in two layers with a thickness of 60mm for the bottom and 120mm for the top layer. Compaction was continued until refusal or no increase in density was detected in successive density measurements. In order to avoid segregation, the finest fraction, (5mm nominal size) was placed last and allowed to fill the void of the matrix formed by the larger size materials during compaction.

A 10mm thick sand sheet asphalt mix with 10% by weight of a grade 100 pen bitumen was added to provide a smooth surface for the wheel. No instrumentation was installed in the sample because of great disturbance which could be caused by the necessary excavation and recompaction of the relatively small sample. Therefore, only the wheel load, the surface profile and the permanent vertical deformation of the granular layer underneath the centre-line of the wheel were monitored.

Details of the test programme and some material properties of the granular materials are shown in Table 5.1. A total of seven tests were carried out. These tests involved two levels of contact stress, (750 and 1100 kPa), two gradings and two types of loading (a moving wheel load and a repeated vertical load).

5.3.2 Pavement Test Facility

Description of the Nottingham PTF has already been presented in Chapter three. A cross-section of the pavement structure used for this experiment is shown in Figure 5.4. The thickness of the granular layer was 240mm. The subgrade at the time of the tests consisted of an inorganic low plasticity silty clay . The CBR at the surface of the

Table 5.1

Details of Rutting Tests carried out in the Slab Test Facility

Test No.	*Grading*	*Means of Loading*	*Contact Pressure (kPa)*	*Dry Density (kg/m^3)*	*Average In-situ Properties*		
					CBR (%)	*CIV*	*DCP (cm/blow)*
1	Type I	Plate	750	2182	62	46	0.25
2	Type I	Wheel	750	2180	-	46	-
3	Optimum	Plate	750	2225	52	35	0.20
4	Optimum	Plate	1100	2200	-	44	-
5	Optimum	Wheel	750	2220	-	40	-
6	Type I	Plate	1100	2160	39	37	0.22
7	Type I	Wheel	1100	2131	-	36	-

Note: "-" means no tests were performed.

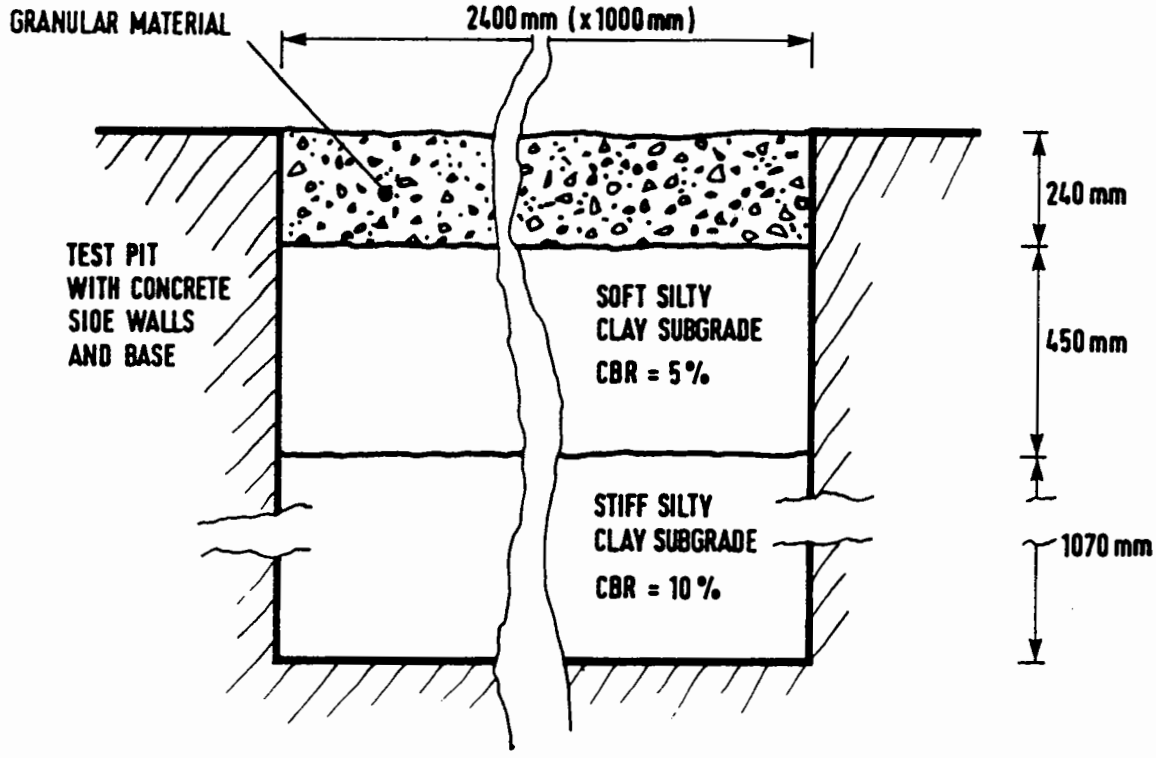

Figure 5.4 Cross-section of Pavement Structure used in Tests carried out in the Pavement Test Facility.

top 450mm of material was found to be about 5%. Underneath this layer the material became much drier and stiffer with CBR of about 10%. The compaction of the granular materials was provided by the same pedestrian operated single drum vibrating roller used in the Part A experiments (Figure 3.6). Compaction was carried out in two layers, each 120mm in thickness and until refusal. A 10mm thick sand sheet surface (as used in the STF tests) was again used.

For this part of the project, two wheel tracks, each running across the three pavement sections consisting of the three different granular materials were used. In one track, a uni-directional wheel load was applied and in the other, the loading was bi-directional.The movement of the wheel was channelized, hence allowing accelerated deformation of the sections to occur. Details of the sections and the material properties are shown in Table 5.2. A 150mm wide wheel, with tyre pressure of 550 kPa and contact stress of about 500 kPa was used. Speed of the wheel was about 3 km/hr. The temperature inside the PTF during the tests was 24 to 27°C.

5.4 RESULTS OF RUTTING TESTS

5.4.1 Slab Test Facility Experiments

Figure 5.5 shows the profiles of the various sections at the end of the tests carried out in the STF and Figure 5.6 shows the variation of permanent vertical deformation with the number of load applications for all the tests.

Table 5.2

Details of Rutting Tests carried out in the Pavement Test Facility

Section No.	*Grading*	*Material*	*Direction of Loading*	*Average Section Properties*							
				Granular Base					*Subgrade*		
				Dry Density (kg/m^3)	*Moisture Content (%)*	*CBR (%)*	*CIV*	*DCP (cm/blow)*	*Moisture Content (%)*	*CBR (%)*	*DCP (cm/blow)*
1	Type I	Dolomitic Limestone	Uni-directional	2050	3.3	32	32	0.30	15.2	4.7	1.22
2	Optimum	Dolomitic Limestone	Uni-directional	2105	4.0	38	37	0.22	14.8	4.9	1.15
3	Open	Carboniferous Limestone	Uni-directional	1995	3.6	28	46	0.22	15.5	4.2	1.31
4	Type I	Dolomitic Limestone	Bi-directional	2011	4.2	-	29	-	15.2	4.5	-
5	Optimum	Dolomitic Limestone	Bi-directional	2056	3.2	-	32	-	15.6	4.7	-
6	Open	Carboniferous Limestone	Bi-directional	1966	3.5	-	40	-	15.0	5.0	-

Note: "-" means no tests were performed.

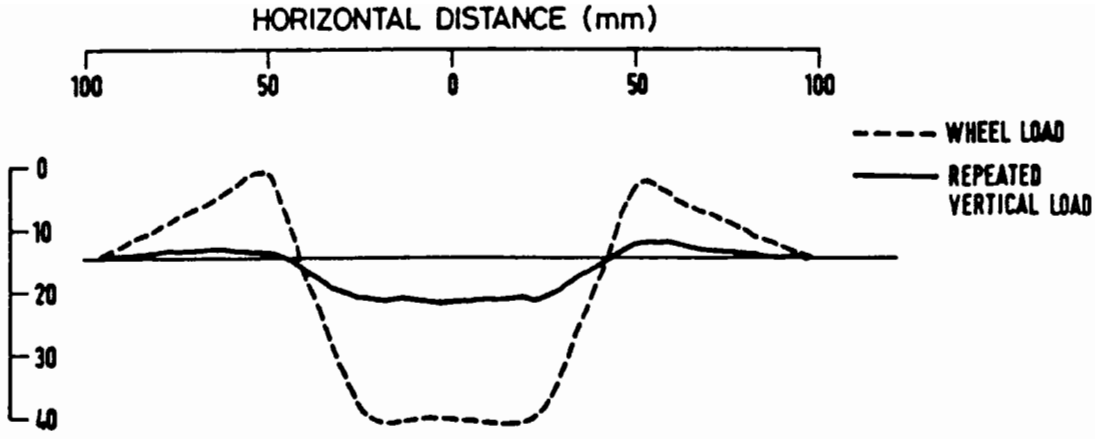

a. Type I Grading; Contact Pressure = 750 kPa.

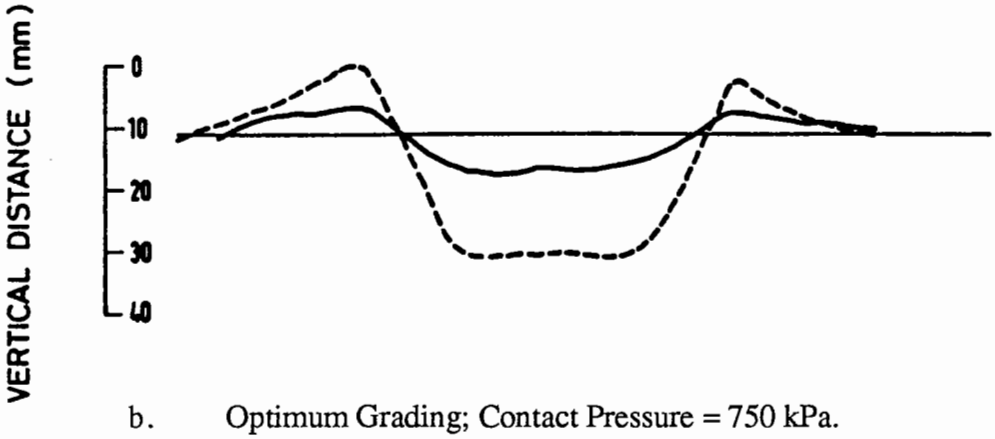

b. Optimum Grading; Contact Pressure = 750 kPa.

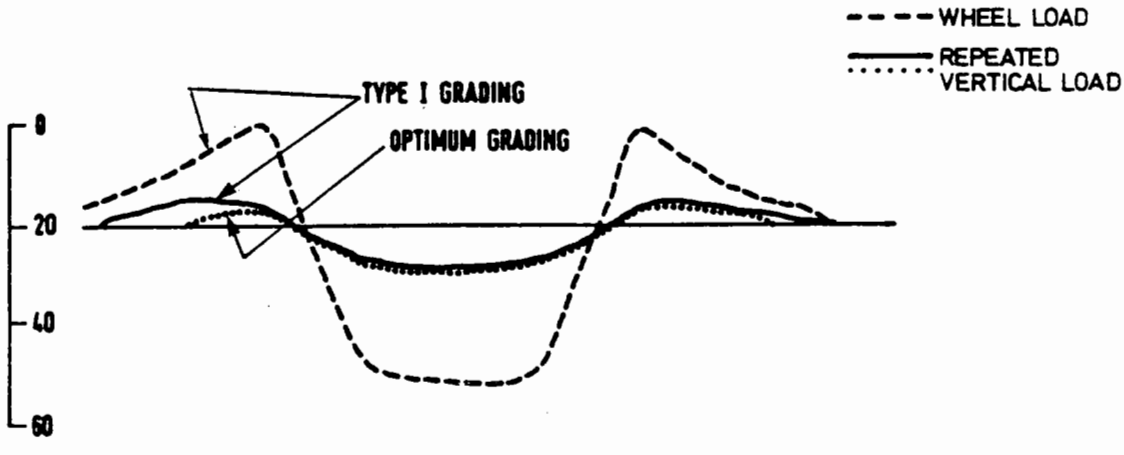

c. Contact Pressure = 1100 kPa.

Figure 5.5 Section Profiles at the End of the Rutting Tests carried out in the Slab Test Facility.

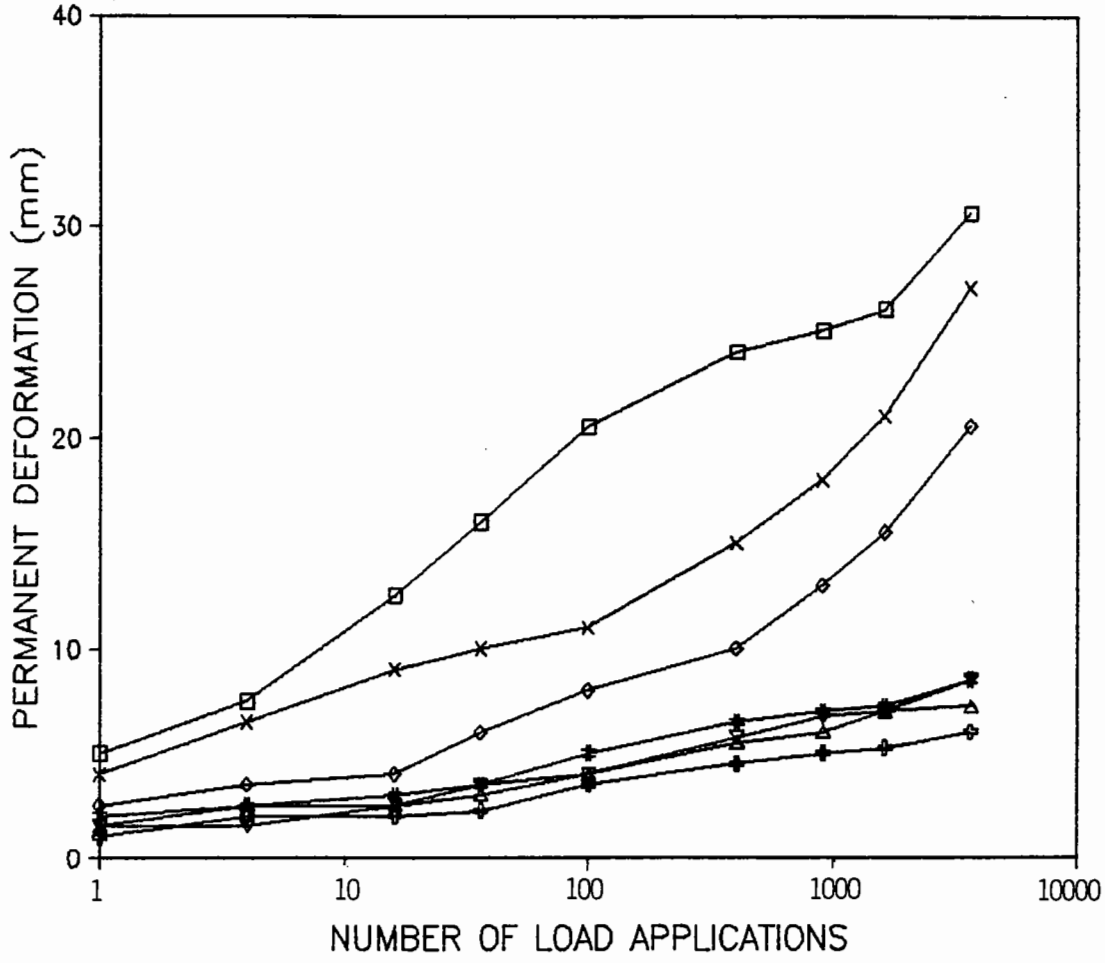

Symbol	Grading of Granular Base	Type of Loading	Contact Pressure (kPa)
✕	Type I	Wheel	750
△	Type I	Repeated Plate	750
□	Type I	Wheel	1100
#	Type I	Repeated Plate	1100
◇	Optimum	Wheel	750
+	Optimum	Repeated Plate	750
▽	Optimum	Repeated Plate	1100

Figure 5.6 Variation of Permanent Vertical Deformation with Number of Load Applications for the Rutting Tests carried out in the Slab Test Facility.

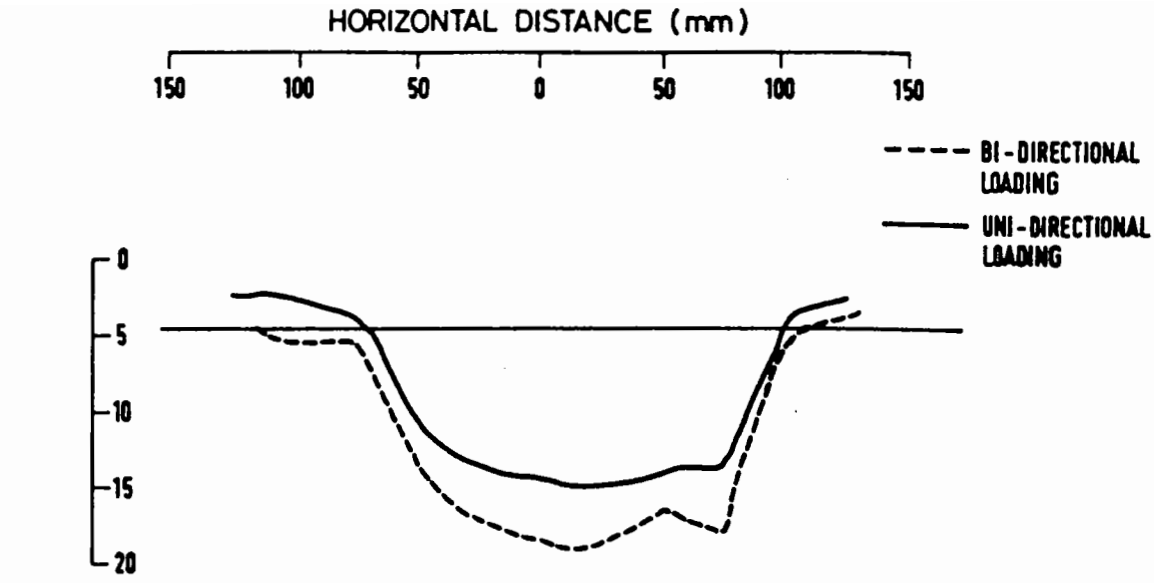

a. Type I Grading; Dolomitic Limestone.

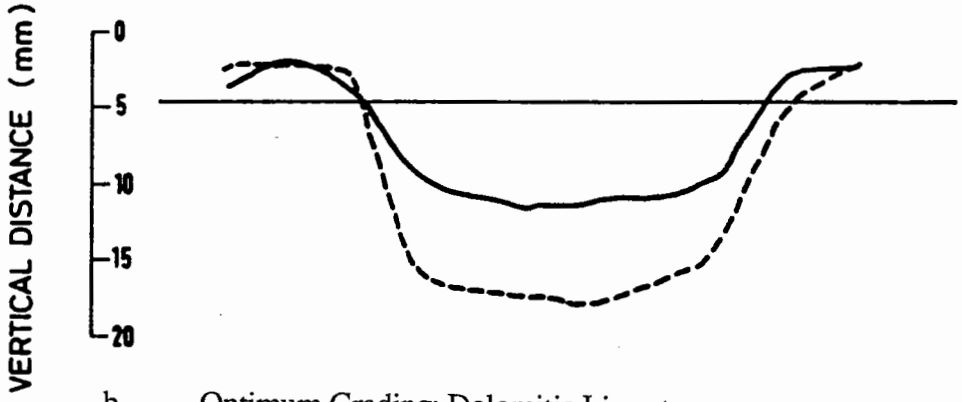

b. Optimum Grading; Dolomitic Limestone.

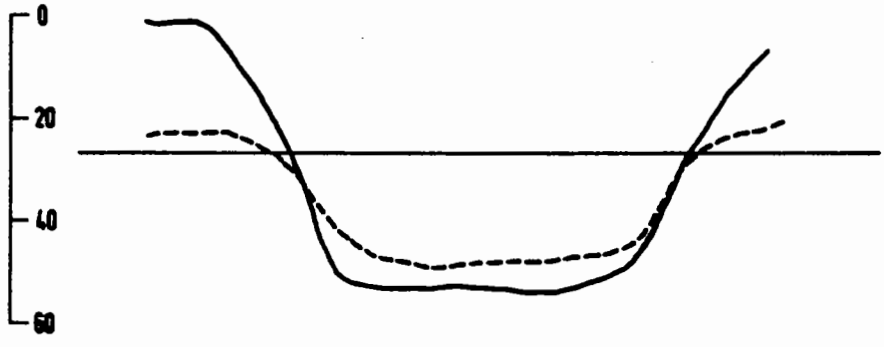

c. Open Grading; Carboniferous Limestone.

Figure 5.7 Section Profiles at the End of the Rutting Tests carried out in Pavement Test Facility.

Figure 5.5 indicates that a significant amount of heaving took place along the shoulder of the rut for those sections subjected to a moving wheel load. This occurred as a result of lateral spreading of the granular material. For these sections, the permanent vertical deformations were found to be at least three times higher than those subjected to a repeated vertical load. Whilst the increase in stress level caused a great deal of increase in permanent deformation in the wheel loading case, the permanent deformation due to repeated vertical load was not significantly affected by this factor. As far as rate of deformation is concerned, Figure 5.6 indicates that most deformation occurs within the first 1000 cycles of load. For sections subjected to wheel loading, deformation does not stabilise even after 6000 cycles of load. However, for sections subjected to repeated vertical load, very little additional deformation was observed after about 2000 cycles. Furthermore, the results show that sections with the "optimum" grading have less permanent deformation under both the moving wheel and repeated vertical loads.

The results of the tests performed in the Slab Test Facility indicated that, under the particular test conditions, far more permanent deformation was caused by a moving wheel load than a repeated vertical load. The primary reasons for the results are probably due to the additional reversed shear stresses caused by the moving wheel and the lack of confining pressure at the surface of the granular material. The combined effect caused the material immediately in front of the wheel to dilate and weaken, and when the wheel moved over the weakened material, large deformation occurred. In the case of the repeated vertical load, the wheel is in contact with the pavement over a fixed area, hence effectively providing the confining pressure required for higher strength. This may account for the observation that the permanent deformation was not sensitive to the applied stress level.

5.4.2 Pavement Test Facility Experiments

Figures 5.7 and 5.8 shows the results of the two series of tests carried out in the PTF. The profiles shown in Figure 5.7 indicate that in the two sections where dolomitic limestone was used, bi-directional loading caused 18 and 60% higher rut than those under uni-directional loading. However, the opposite effect was obtained for the section with an open graded carboniferous limestone where much higher deformation developed under both types of loading. The overall high deformation in these sections, which were generally less well compacted, might have the effect of overriding any trend in the development of permanent deformation caused by the different modes of loading.

If the results from the carboniferous limestone sections can be discarded, then the tests from the PTF indicate that higher permanent deformation may be obtained from bi-directional than uni-directional wheel loading. The results apparently agreed with those obtained by Brown (Brown et al, 1982) who observed an increase of rut depth of 19 to 40% due to bi-directional loading. It is thought that in bi-directional loading, the structure of the granular material, which is basically formed by the interparticle contacts, is subjected to more disruption due to the two opposite senses of reversed shear stress. As a results, the structure will be weakened and more deformation will occur.

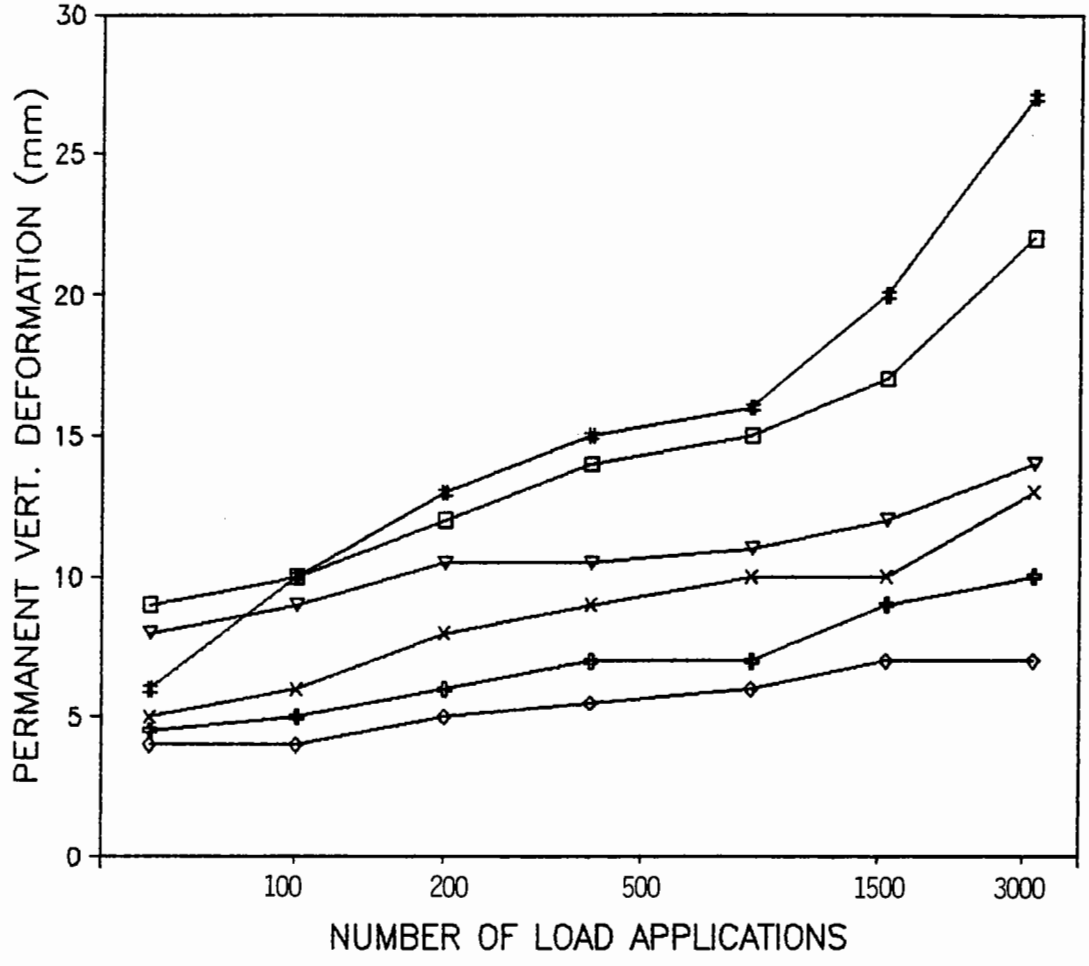

Symbol	Type of Granular Base	Grading of Granular Base	Type of Loading
	Dolomitic Limestone	Type I	Uni-directional
	Dolomitic Limestone	Type I	Bi-directional
	Dolomitic Limestone	Optimum	Uni-directional
	Dolomitic Limestone	Optimum	Bi-directional
	Carboniferous Limestone	Open	Uni-directional
	Carboniferous Limestone	Open	Bi-directional

Figure 5.8 Variation of Permanent Vertical Deformation with Number of Passes of Wheel Load for the Rutting Tests carried out in Pavement Test Facility.

CHAPTER SIX

REPEATED LOAD HOLLOW CYLINDER TESTS

6.1 INTRODUCTION

The last three chapters have shown that full scale pavement testing is an essential component of road pavement research. However, because of the large amount of raw materials, instrumentation and human effort involved in each test, this type of experiment may only be cost-effective for the investigation or validation of an idea which has been shown to have potential. For background research or study of more fundamental principles, smaller scale accelerated testing on elements of material is clearly more desirable. In the study of the permanent deformation behaviour of granular material, the repeated load hollow cylinder test apparatus (HCA) appears to be a promising device. Its capability to apply reversed shear stresses to the test specimen has meant that realistic in-situ stress conditions caused by a moving wheel loading can be simulated. The importance of close and correct simulation of this condition has already been highlighted by the results presented in Chapter five. Furthermore, the study of material anisotropy, principal stress rotation effects and the influence due to different intermediate principal stresses are all made possible using the HCA.

6.2 NOTTINGHAM REPEATED LOAD HOLLOW CYLINDER TEST APPARATUS

The Nottingham HCA was first constructed in 1985 and the history of its development was reported by O'Reilly (1985). Since then, some modifications have been performed.The basic configuration of the HCA is shown in Figure 6.1. For this project, further improvement modifications were made. These included:

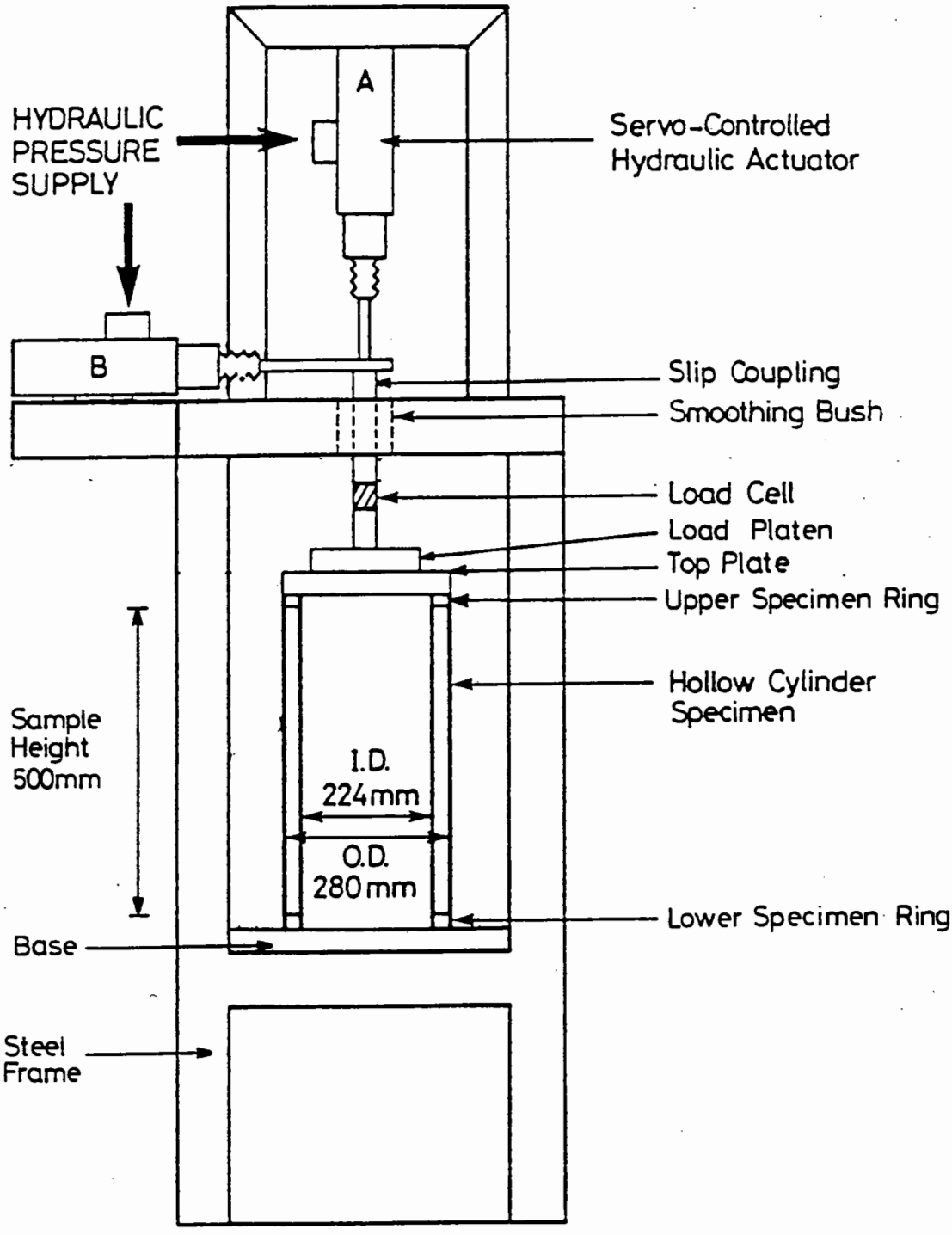

Figure 6.1 Basic Configuration of the Nottingham Repeated Load Hollow Cylinder Apparatus.

1. Addition of an external pressure chamber and the associated pressurising system.

2. Redesign of the top cap and base to accommodate the new pressure chamber.

3. Upgrading of the electronic controls for the loading system.

4. Addition of a new data acquisition system.

A photograph of the laboratory set-up of the modified apparatus is shown in Figure 6.2 and a flow diagram showing the inter-connection between the various components of the system is presented in Figure 6.3.

6.2.1 Size of Test Apparatus and Specimen

The designed dimensions of the repeated load HCA are mainly influenced by the size of the test specimen. One of the main inherent disadvantages of using a hollow cylinder specimen is the non-uniformity of stress and strain across the specimen wall due to curvature. Furthermore, because of the need to transfer shear stresses from the loading system to the specimen, a more severe end restraint effect normally results when compared with the triaxial tests. In order to reduce stress non-uniformity caused by specimen curvature, it is necessary to increase the external diameter and reduce the wall thickness of the specimen. As a result of these considerations, an external diameter of 280mm and a wall thickness of 28mm were adopted for the Nottingham hollow cylinder specimen. This produces a ratio of external diameter to wall thickness of 10, a value which finite element calculations (Hight et al ,1983) showed to be satisfactory.

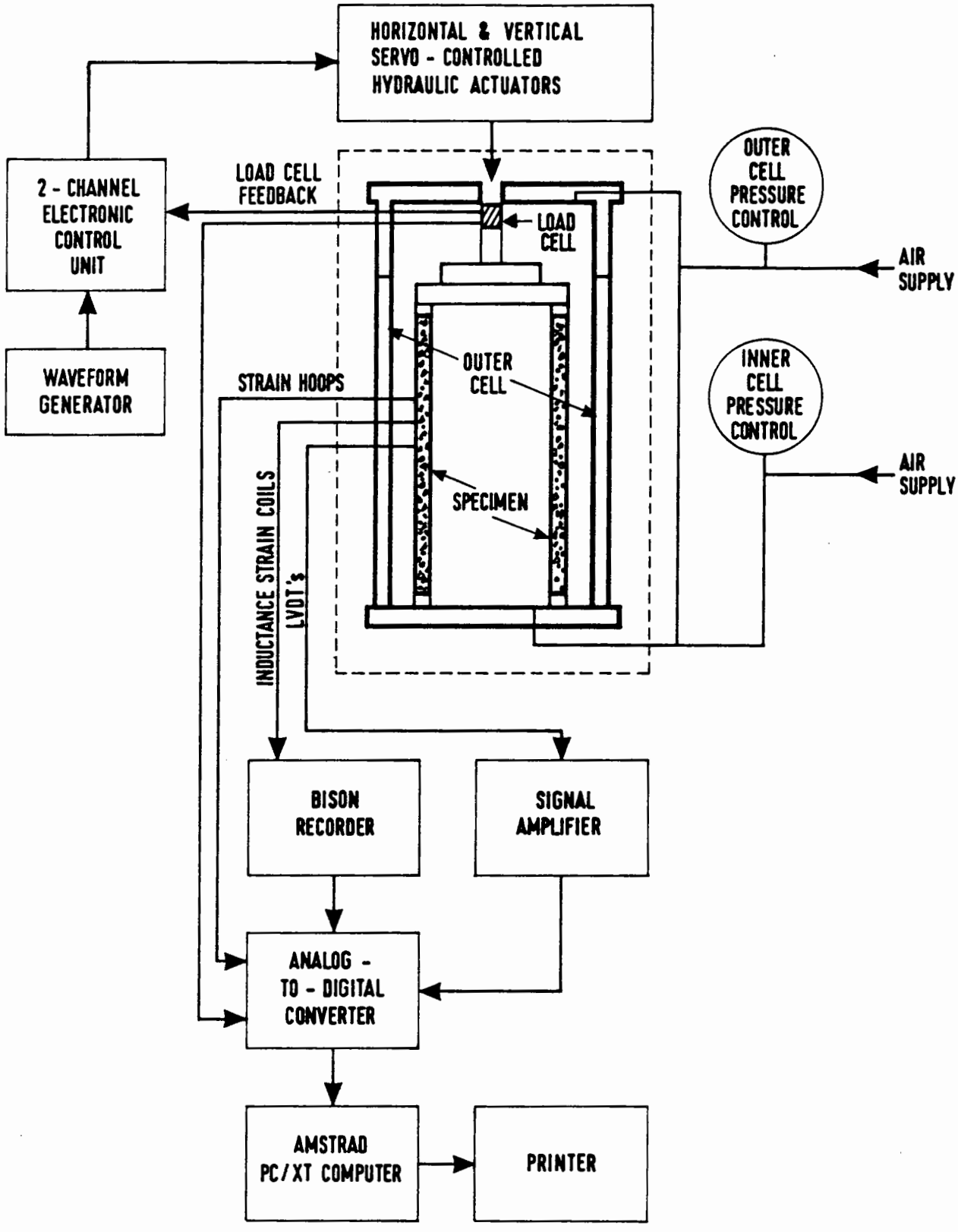

Figure 6.3 Inter-Relationship Between Different Components of the Repeated Load Hollow Cylinder Test Apparatus.

In determining the height of the specimen, both the presence of end restraints and the need to provide a sufficiently long gauge length for deformation measurements were considered. A study carried out by Wright et al (1978) proposed that the height of the specimen should satisfy the following equation:-

$$H \geq 5.44 \sqrt{(b^2 - a^2)} \qquad (6.1)$$

Where H is the height of hollow cylinder specimen

b is the external radius

a is the internal radius

Equation 6.1 ensures that a control zone, free from end effects, is equal to or greater than the zone affected by the end platens. Using this equation a minimum height of 457mm is required. Based on this criterion and other practical considerations such as weight of the specimen and the dimensions of the loading frame, a height for the Nottingham hollow cylinder specimen of 500mm was used.

6.2.2 Loading System

Both the vertical and torsional loads are applied by servo-controlled hydraulic actuators as shown in Figure 6.4. The vertically mounted actuator can provide a maximum load on the specimen of 20 kN with a 150mm stroke. The horizontally mounted actuator, with its stroke of 100mm, can provide a torsional moment of up to 4.6 kNm to the centre shaft through the 230mm long torque arm. A slip coupling device allows both the axial load and torque to be applied down the same shaft. It also enables both loads to be measured by a simple purpose-made, combined strain gauged load cell (Figure 6.5) which is located immediately above the specimen. The axial load is transferred to

the specimen via the top platen and the upper specimen ring. For the transfer of shear load, six shear vanes located at the bottom of the upper specimen ring and 16 interlocking castellations at the lower specimen ring (Figure 6.6) were used.

In order to carry out repeated loading, a waveform generator, capable of providing sinusoidal, square or triangular waveforms at frequencies between 0.001 and 100 Hz for two channels at variable phase angles shift was used. The command signal from the waveform generator is fed into the electronic control unit where it is compared with the feedback signal obtained from the load cell. An error signal is then sent to the two servo valves so that they may make the necessary adjustments. The time required by this feedback closed loop control is generally very short, in the order of milliseconds, and can be adjusted by means of the gain setting to suit different test materials.

Confining pressure can be applied through the medium of silicone oil or compressed air in both the inner and outer cell chambers. The former medium is more desirable in repeated loading situations (due to the quicker response caused by the incompressibility of the fluid) while for constant pressures, the use of compressed air is found to be satisfactory. Maximum pressure of up to 400 kPa can be achieved for both the inner and outer cells. Both pressures can be controlled simultaneously by a single valve, hence allowing an isotropic condition during the pressure build up. Alternatively, pressures for the inner and outer cell can be controlled individually to allow pressure differences across the specimen wall. These pressures are monitored by pressure gauges located outside the HCA.

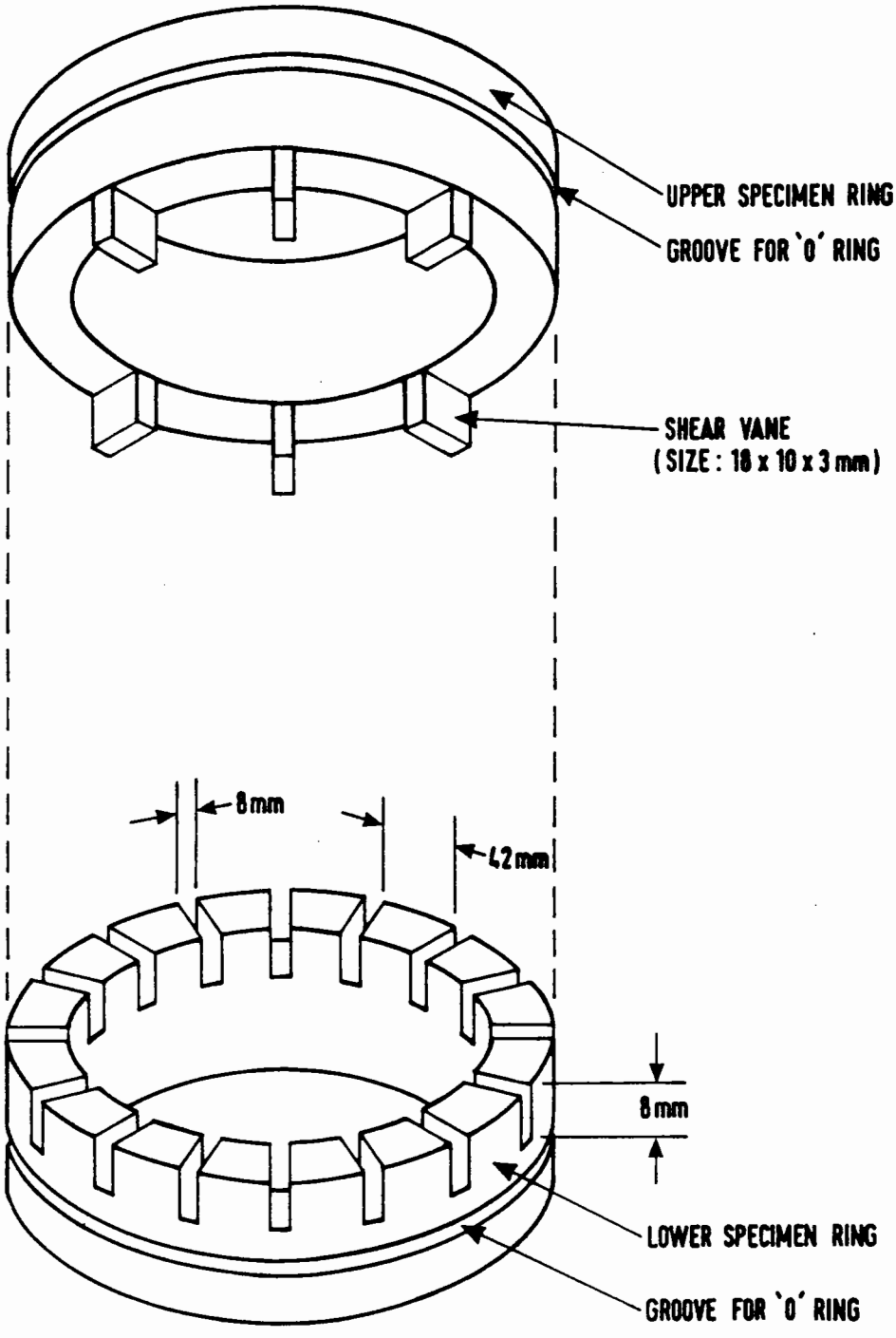

Figure 6.6 Details of Upper and Lower Specimen Rings for the Repeated Load Hollow Cylinder Test Apparatus.

6.2.3 Sealing System

In order to maintain a good hollow cylindrical shape for the specimen of granular material during sample preparation and testing, a tight seal condition must be achieved. Furthermore, if different inner and outer cell pressures are to be used, a good sealing system becomes even more essential.

A section of the HCA with the specimen showing all the major sealing units is presented in Figure 6.7. The hollow cylinder specimen is basically enclosed by two 0.635mm thick cylindrical latex membranes with different diameters (280 and 224mm) and two pairs of specimen rings (upper and lower). The lower inner specimen ring, with its built-in rubber "O" ring is fastened to the base with six 3mm diameter Allen head bolts. After the inner membrane is placed over this ring, the lower outer ring on which the specimen is made, slides in , trapping the inner membrane between the two tapered surfaces of the rings. The lower outer specimen ring is then fastened onto the base by six 8mm Allen head bolts from the bottom of the base upward. A further "O" ring located at the bottom of this specimen ring provides a seal between the inner and outer pressure chambers. The outer membrane is simply secured by another "O" ring along the outside of the specimen ring.

A similar sealing method is adopted at the top of the specimen where the inner membrane is trapped between the tapered surfaces of the upper specimen rings. However, in order to tighten the two rings together, three membrane holder blocks with 3mm Allen head bolts are used. After the outer membrane is secured by an "O" ring the top platen is placed and fastened with 8mm Allen head bolts to the upper outer specimen ring which contains an "O" ring around the edge of its top face.

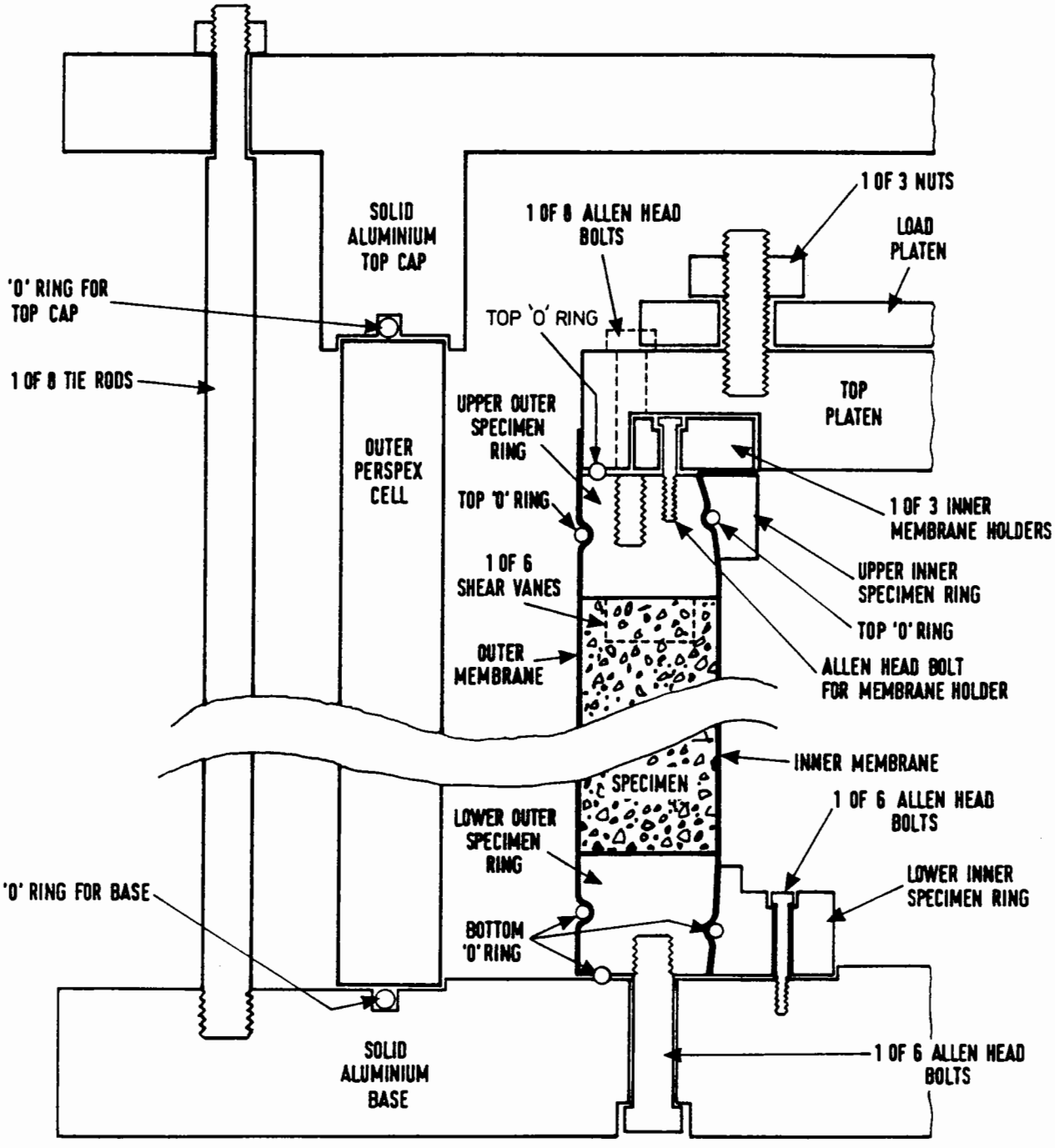

Figure 6.7 Details of Major Sealing Units for the Repeated Load Hollow Cylinder Test Apparatus.

The outside pressure chamber consists of a hollow cylindrical perspex cell with 385mm outside diameter and a wall thickness of 20mm, a top cap and a base cast out of hard anodized aluminium. The three units are held together by eight 15mm diameter tie rods. A thick rubber "O" ring is provided at each of the joints between the cell, cap and base. Two rubber seals are provided at the centre hole of the cap through which the driving shaft transfers the loads from the servo-rams to the specimen. Outside electrical, vacuum and pressure connections are made through holes provided in the cap and base. Each of these holes within the pressurised chamber are individually sealed with expansion "O" rings.

6.2.4 Deformation Measurements

Four independent deformation measurements are required to determine the complete strain pattern. These are the change in specimen wall thickness, the overall change in sample diameter, the axial deformation and the torsional deformation.

To measure the change in specimen wall thickness or the radial deformation, two pairs of 25mm inductance coils attached to opposite sides of the specimen wall are used. A known alternating current flows in one coil and the current induced in the other, which is a function of their distance of separation, is recorded. Changes in specimen diameter are measured using two strain gauged epoxy hoops attached to the inner chamber of the hollow cylinder specimen using embedded studs. These devices, as shown in Figure 6.8, have been used extensively at Nottingham (Boyce and Brown [1976]).

Axial deformation is measured by two LVDTs mounted vertically on the specimen by means of embedded studs. Deformation in a direction at 45 degrees to the vertical is also measured by means of LVDTs. This latter measurement, together with those from

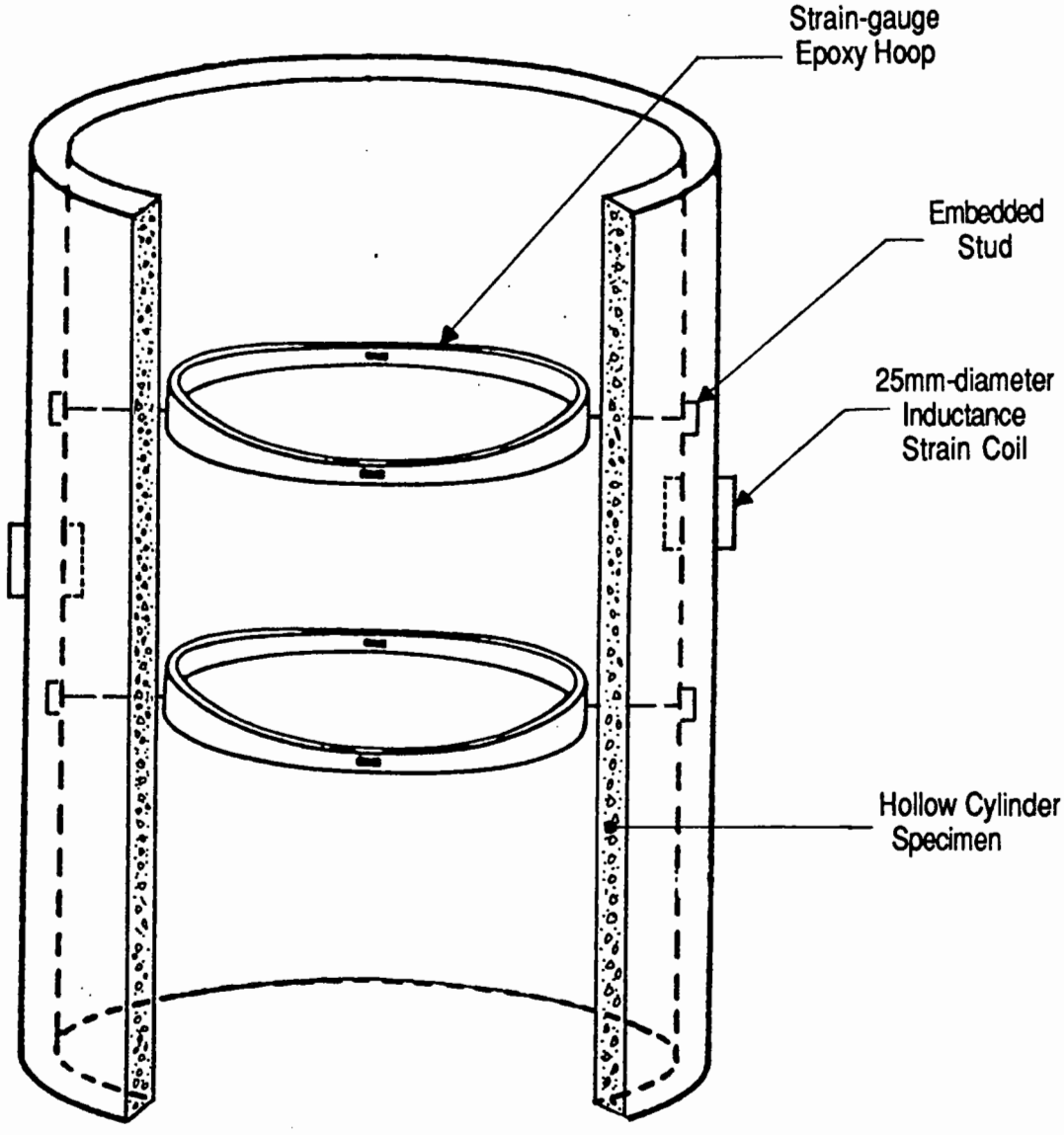

Figure 6.8 Strain -gauged Epoxy Hoops and 25mm-diameter Inductance Strain Coils mounted on the Hollow Cylinder Apparatus.

the axial and circumferential directions are used in the following equation to calculate the torsional deformation. A photograph of the arrangement of the instruments is shown in Figure 6.9.

$$\gamma = 2\varepsilon_{45} - \varepsilon_z - \varepsilon_\theta \qquad (6.2)$$

Where γ = engineering shear strain

ε_{45} = normal strain at 45 degrees to vertical direction

ε_z = axial strain

ε_θ = circumferential strain

All the instrumentations were located at the middle one third of the specimen to minimize the end effects. Calibrations of the instrumentation were carried out regularly during the project. A description of the calibration methods, procedure used and results obtained are presented in Appendix B.

6.2.5 Data Acquisition System

The data acquisition system for this project consists basically of the following four components:-

1. A micro computer with a single disk drive, a 20 Mb hard disk, an expanded 640 kb RAM (Random Access Memory), a colour monitor and option slots that support feature cards for additional devices.

2. An analogue-to-digital convertor with eight differential input channels, four output channels and four relays. The A/D conversion time is

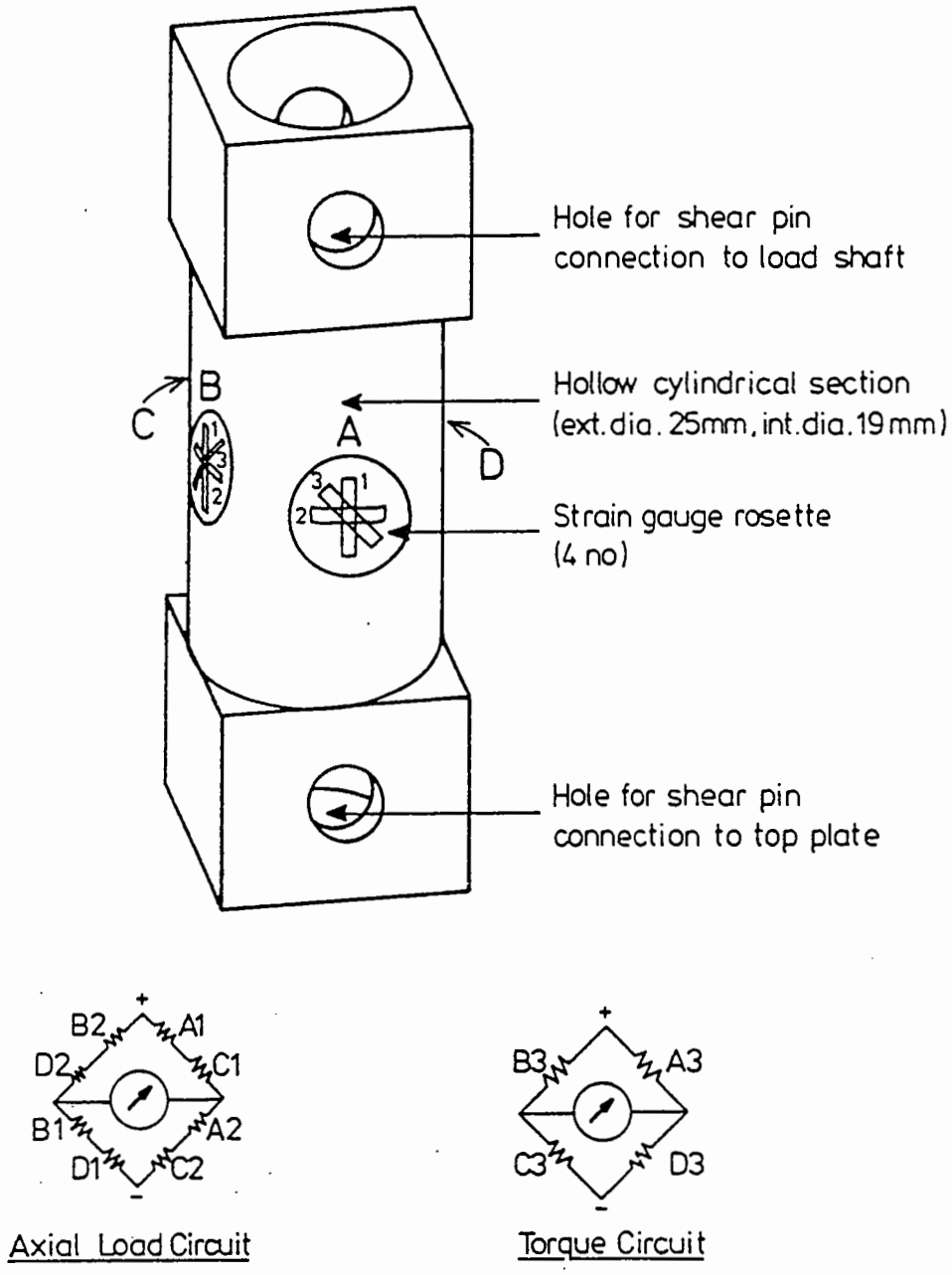

Figure 6.5 Combined Axial and Torsional Load Cell for the Repeated Load Hollow Cylinder Test Apparatus.

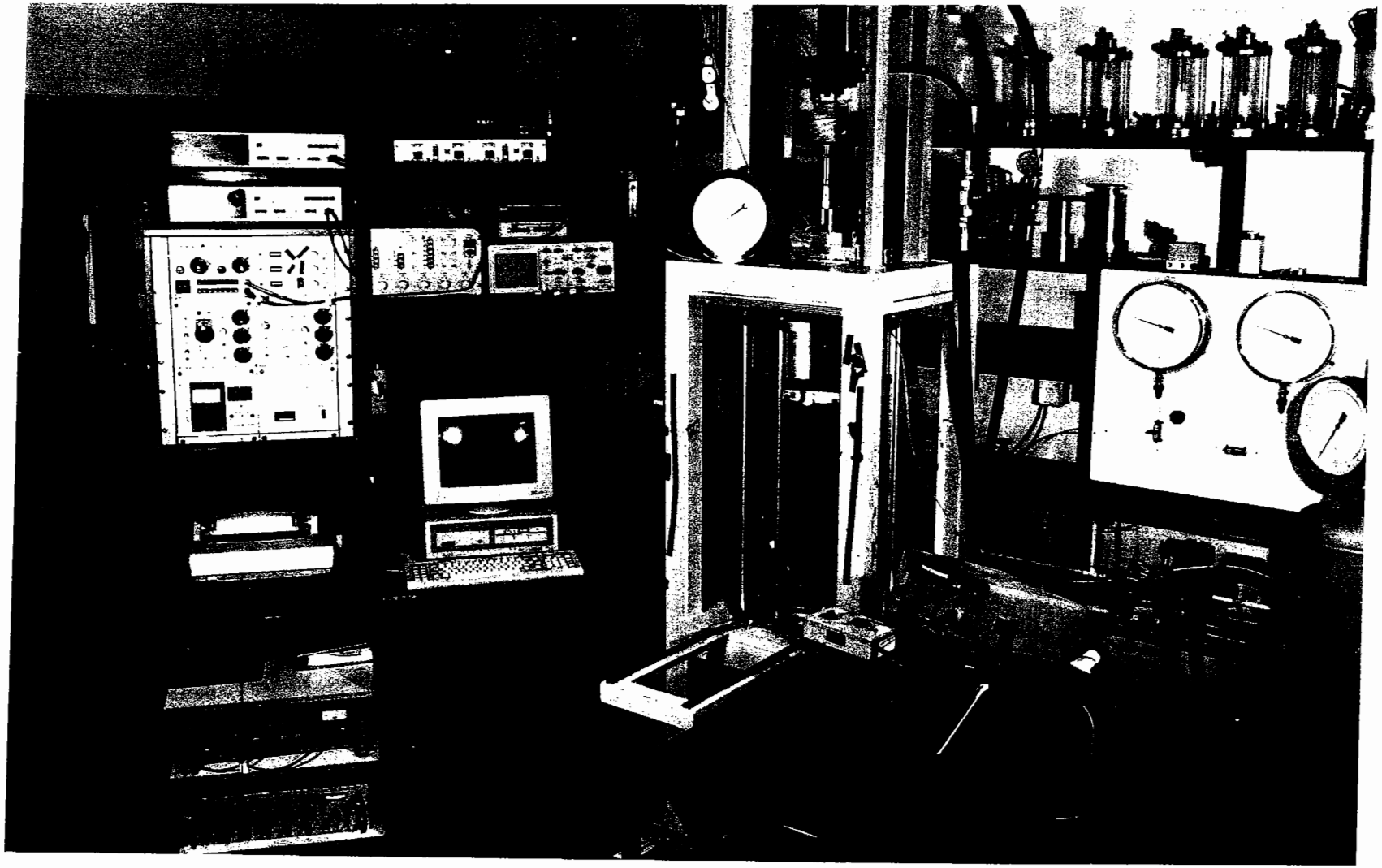

Figure 6.2 Laboratory Set-up of the Modified Nottingham Repeated Load Hollow Cylinder Apparatus

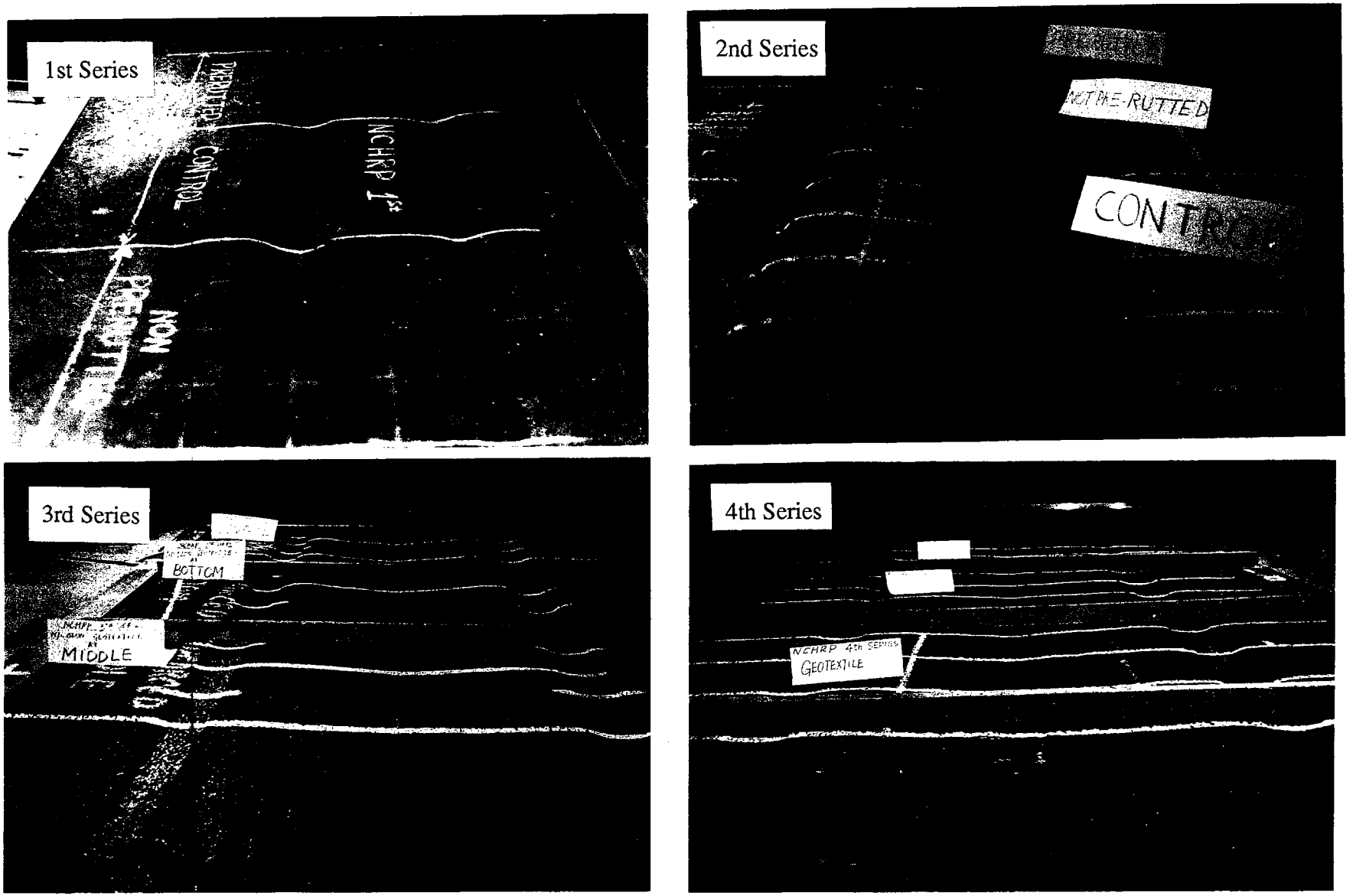

Figure 4.1 Pavement Surface Conditions at the End of Multiple-Track Tests for all four Test Series

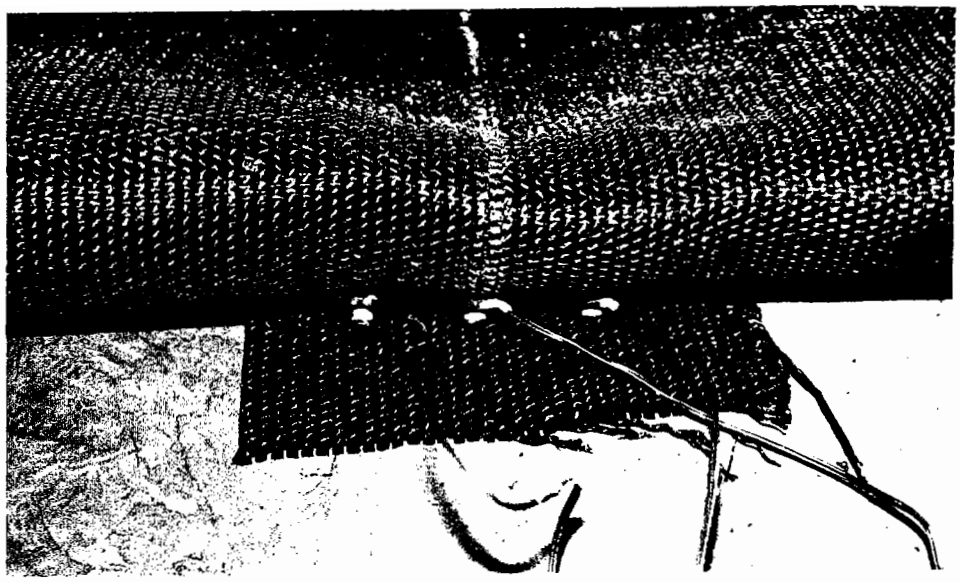

Figure 3.9 Woven Geotextile with 25mm-diameter Inductance Strain Coils

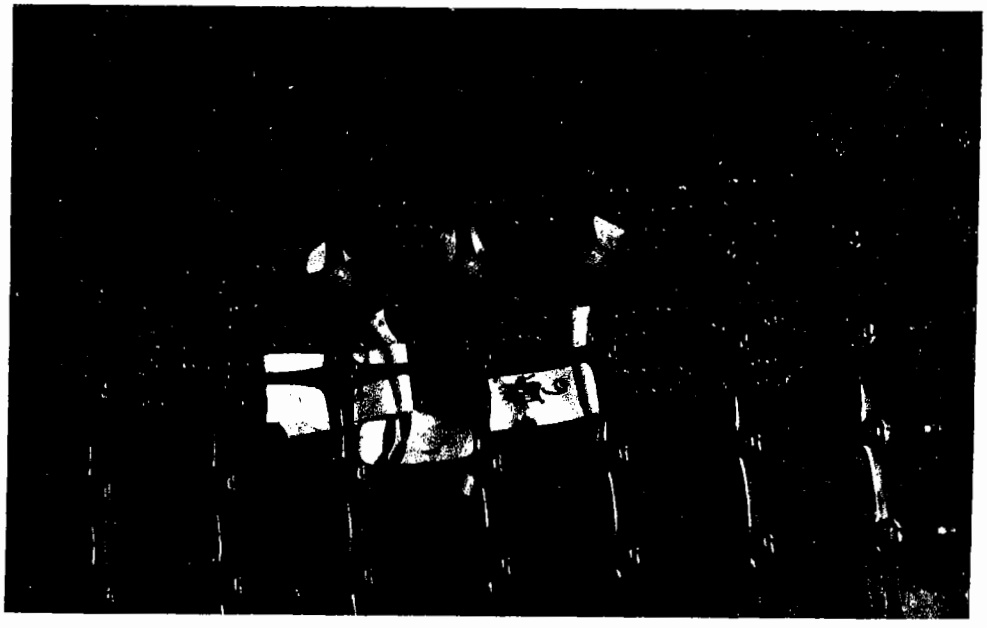

Figure 3.10 Geogrid with 25mm-diameter Inductance Strain Coils

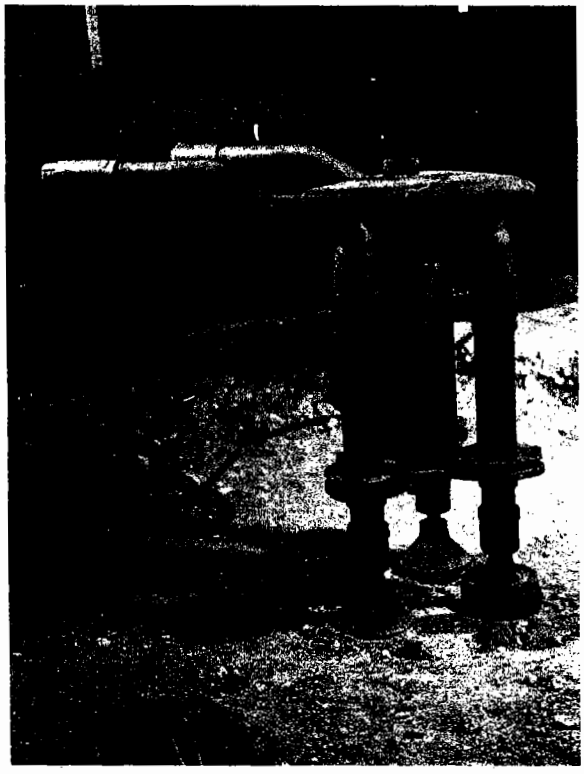

Figure 3.3 Triple legged Pneumatic Tamper used on Subgrade

Figure 3.4 Single legged Pneumatic Tamper used on Subgrade

Figure 3.5 Vibrating Plate Compactor used on Sand & Gravel

Figure 3.6 Vibrating Roller used on Limestone & Asphaltic Mix

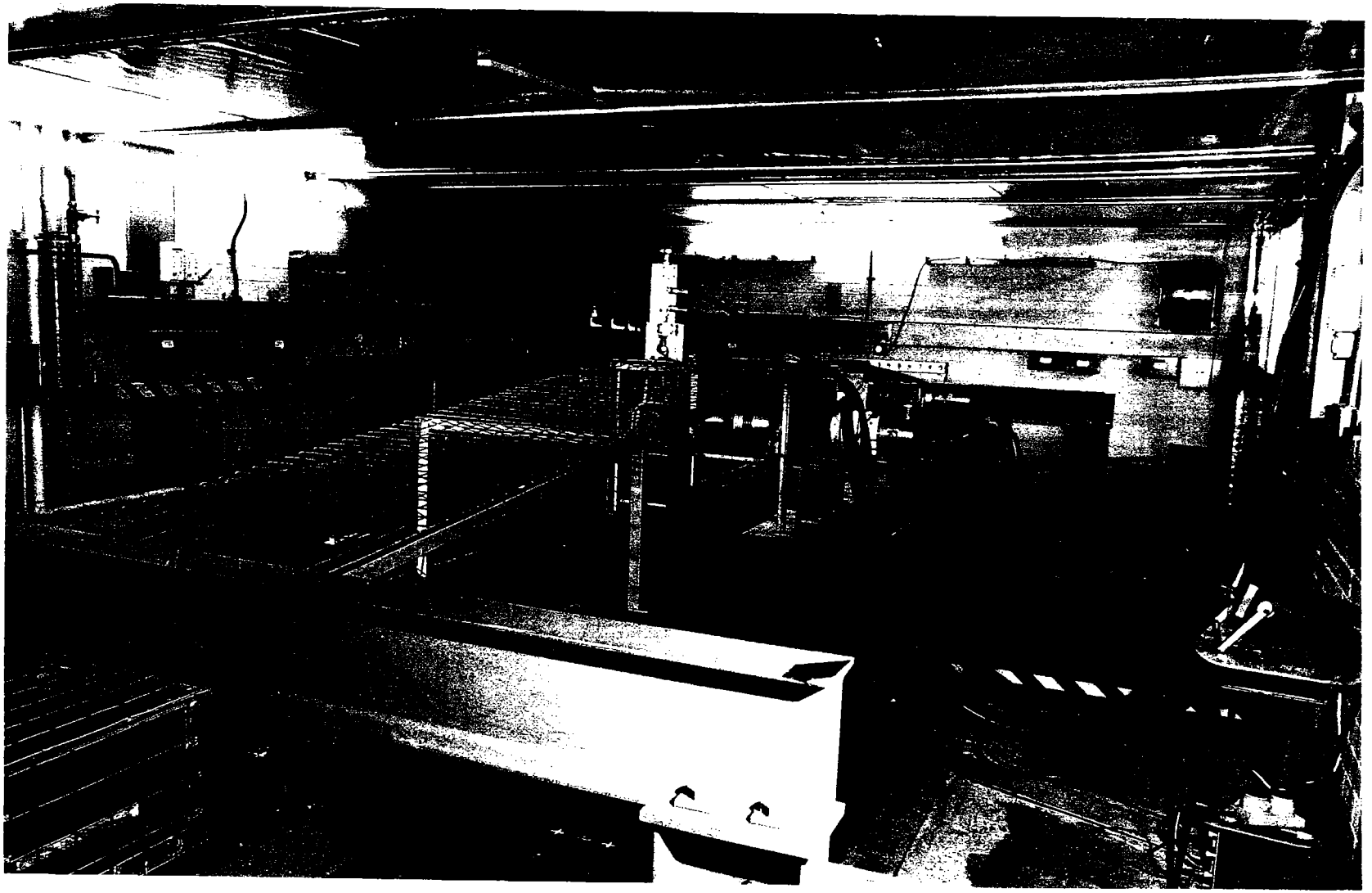

Figure 3.1 Nottingham Pavement Test Facility

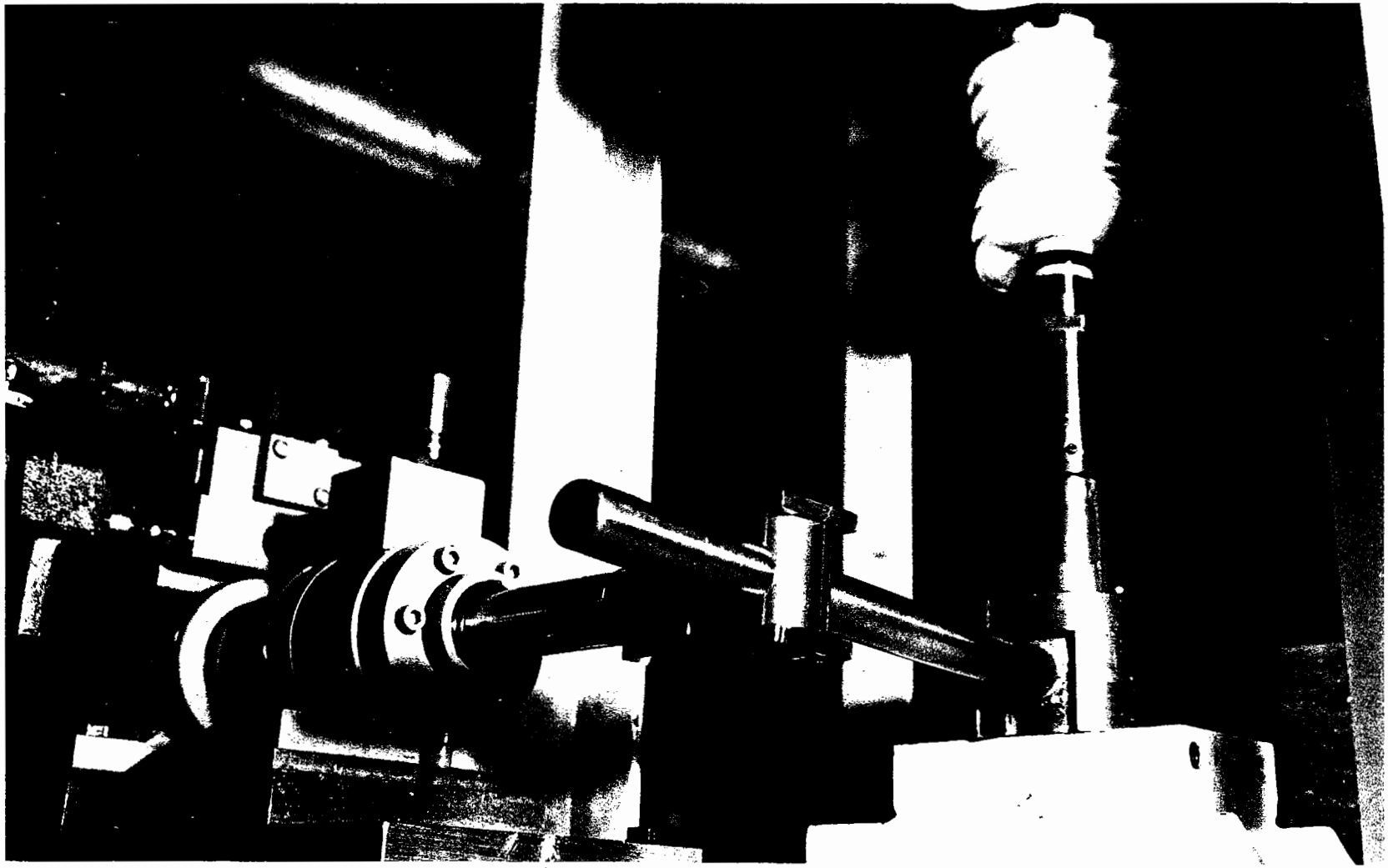

Figure 6.4 Vertical and Horizontal Servo-controlled Hydraulic Actuators and Slip Coupling of the Repeated Load Hollow Cylinder Test Apparatus

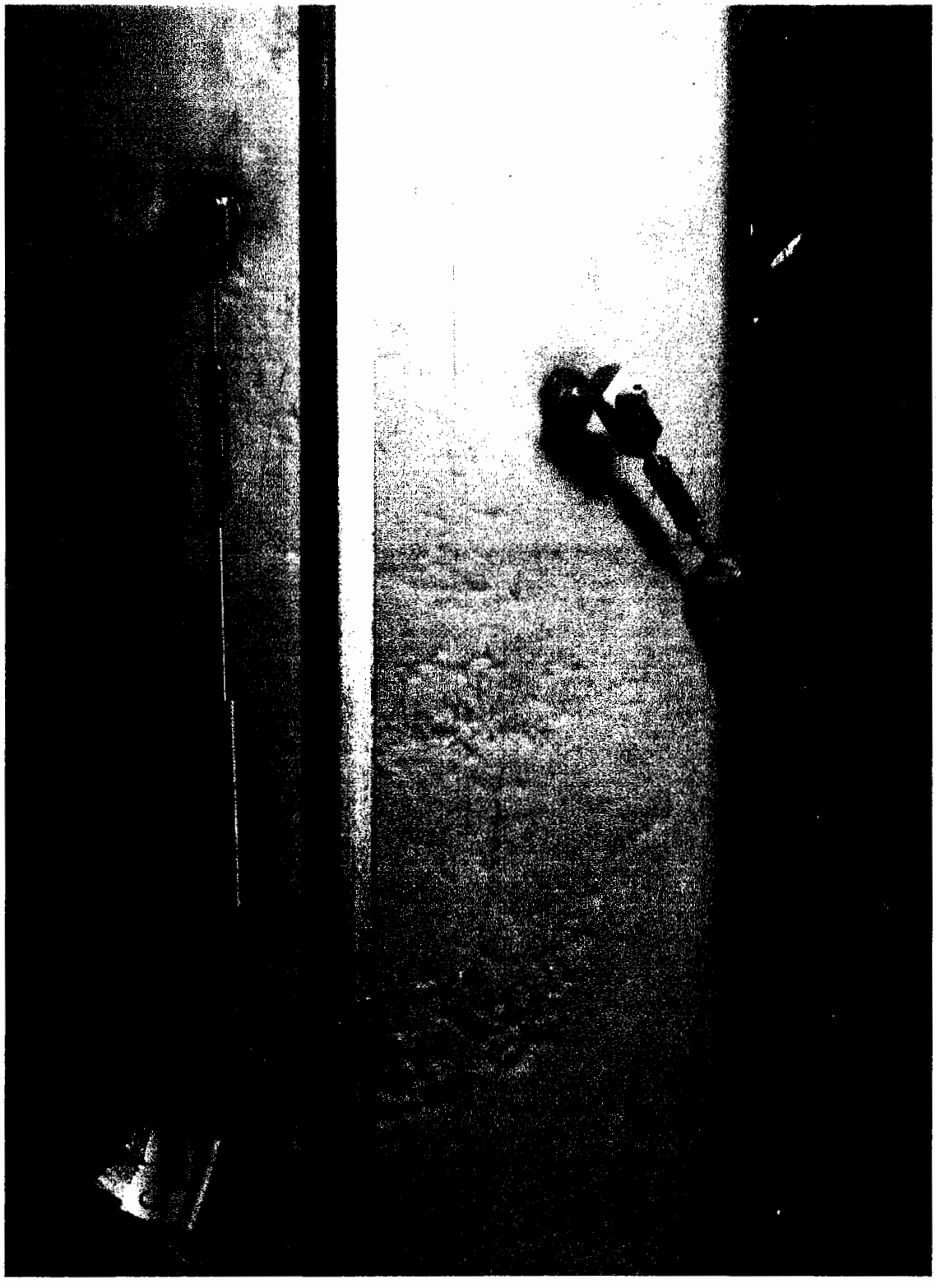

Figure 6.9 Arrangement of Vertical and 45-degree oriented LVDTs

approximately 1.8 ms and up to 2048 readings can be stored at each execution.

3. An IEEE 488 interface card which organises and manages information flow between 1 and 2.

4. A line printer which provides hard copies of graphics and text.

In order to retrieve, store and analyse the data from the load cells, strain gauged hoops, inductance strain coils and LVDTs, several software programs have been developed. Some of these programs make use of existing commercially available packages for plotting and managing of data. The main program for the data acquisition of the repeated load HCA tests is called HCA. Details of this program, written in BASIC language is shown in Appendix C. In order to test out the program and to establish the appropriate test procedure, a series of preliminary tests on a specially manufactured rubber hollow cylinder specimen was carried out.

6.3 STRESS CONDITIONS IN A HOLLOW CYLINDER

Figure 6.10 shows a hollow cylinder sample under the action of axial load W, torque M_T, internal pressure p_i and external pressure p_o. Despite the use of a high ratio of external diameter to wall thickness and a tall specimen, stress non-uniformity cannot be completely eliminated. Therefore, it is necessary to assume that the stresses are uniform and hence allowing their average values to be defined. The stresses acting on an element of material along the wall of the hollow cylinder, shown in Figure 6.10, are defined as follows:-

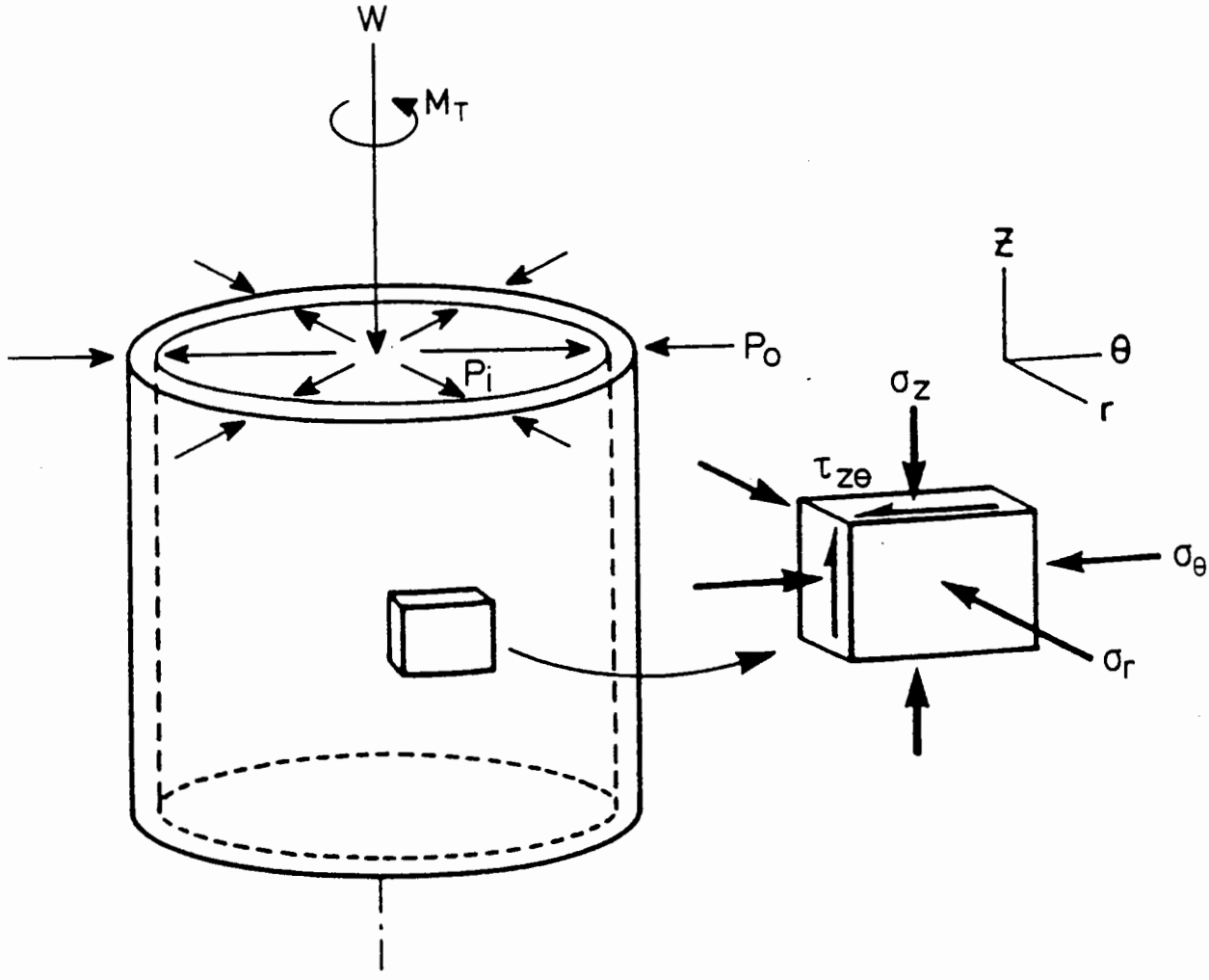

Figure 6.10 Loads and Stresses on a Hollow Cylinder.

$$\sigma_z = \frac{W}{\pi\,(b^2 - a^2)} + \frac{(p_o b^2 - p_i a^2)}{(b^2 - a^2)} \tag{6.3}$$

$$\sigma_r = \frac{(p_o b + p_i a)}{(b + a)} \tag{6.4}$$

$$\sigma_\theta = \frac{(p_o b - p_i a)}{(b - a)} \tag{6.5}$$

$$\tau_{\theta z} = \frac{3M_T}{2\pi\,(b^3 - a^3)} \tag{6.6}$$

Where σ_z = average vertical stress

σ_r = average radial stress

σ_θ = average circumferential stress

$\tau_{\theta z}$ = average shear stress in the θ-z plane

a, b = internal and external radius of the specimen

Since there are no shear stresses acting in the radial direction of the hollow cylinder specimen, σ_r and the plane on which it acts (Figure 6.10) must be a principal stress and a principal plane respectively. It follows that the directions on which the other two principal stresses act must be normal to that of σ_r (ie. in the z-θ plane). The exact directions of these latter principal stresses which, again, must be normal to each other depend on the magnitude of the shear stresses acting on the z-θ plane and can be easily obtained by means of the Mohr's circle for stress (Atkinson and Bransby, 1978).

Figure 6.11 illustrates the construction of a Mohr circle based on the condition that $\sigma_z > \sigma_\theta$ and $\tau_{\theta z}$ is positive and shows that the same condition can be represented by the two principal stresses and an angle of rotation α. Based on Figure 6.11, the following

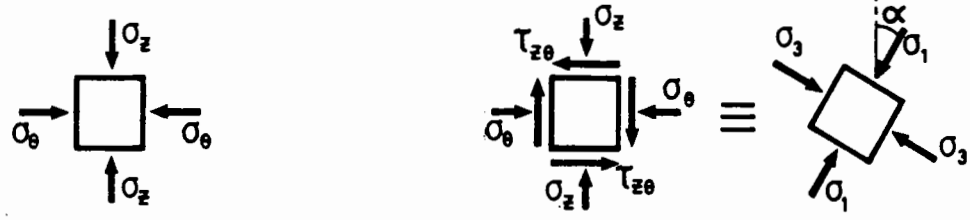

a. Condition with No Shear.

b. Condition with Shear.

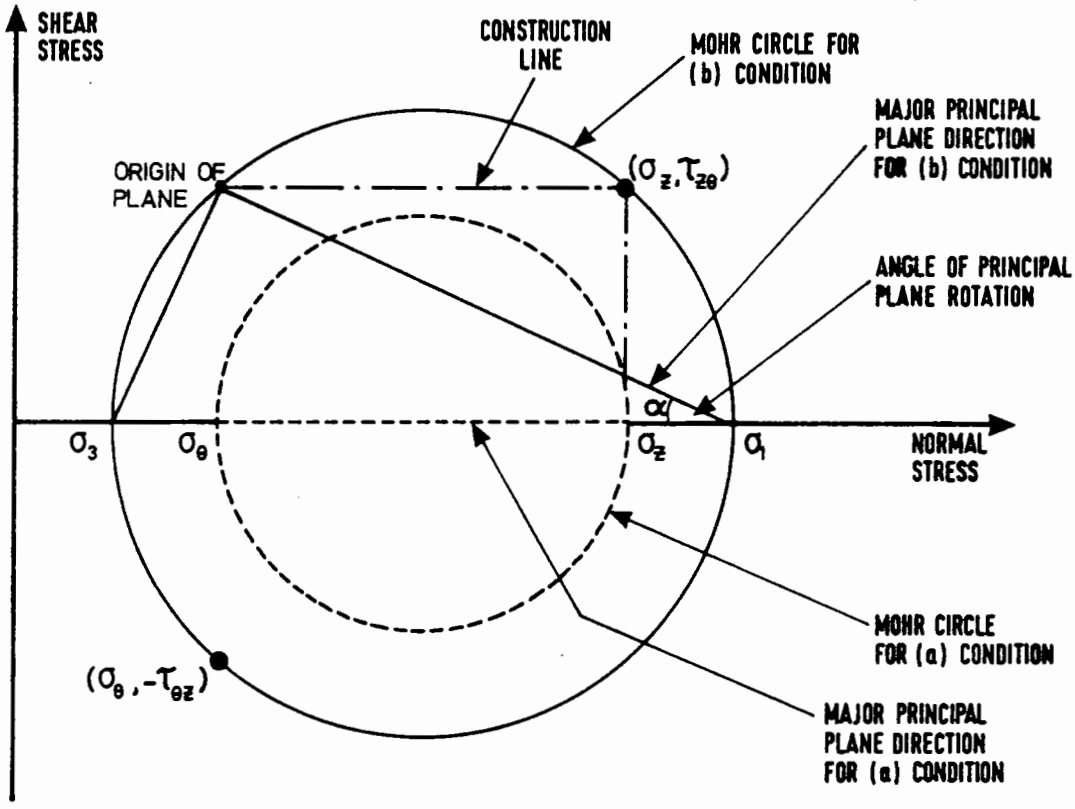

c. Mohr Circle showing Principal Plane Rotation.

Figure 6.11 Mohr Circle for Stress.

equations for the principal stresses and the angle of principal stress rotation can be established:-

$$\sigma_1 = \frac{\sigma_z + \sigma_\theta}{2} + \sqrt{\left(\frac{\sigma_z - \sigma_\theta}{2}\right)^2 + \tau_{\theta z}^2} \qquad (6.7)$$

$$\sigma_2 = \sigma_r \qquad (6.8)$$

$$\sigma_3 = \frac{\sigma_z + \sigma_\theta}{2} - \sqrt{\left(\frac{\sigma_z - \sigma_\theta}{2}\right)^2 + \tau_{\theta z}^2} \qquad (6.9)$$

$$\alpha = \tan^{-1}\left(\frac{\tau_{\theta z}}{(\sigma_1 - \sigma_\theta)}\right) \qquad (6.10)$$

Note that equations (6.7) to (6.10) are only true under the following conditions:-

1. $p_i \geq p_o$ (6.11)

2. $p_i - p_o \leq \frac{W}{\pi ab}$ (6.12)

Where W, P_i, P_o, a and b are as defined earlier.

The stress conditions in a hollow cylinder sample can also be expressed in the form of stress invariants such as the octahedral normal and octahedral shear stress. In terms of principal stresses, they are defined by:-

$$\sigma_{oct} = \frac{1}{3}(\sigma_1 + \sigma_2 + \sigma_3) \qquad (6.13)$$

$$q_{oct} = \frac{1}{\sqrt{2}} \left[(\sigma_1 - \sigma_2)^2 + (\sigma_2 - \sigma_3)^2 + (\sigma_3 - \sigma_1)^2 \right]^{1/2} \qquad (6.14)$$

Note that

$$p = \sigma_{oct} \qquad (6.15)$$

According to Figure 6.11 and Equations 6.7 to 6.10, the rotation of principal planes in the hollow cylinder specimen can only occur within the σ_1 and σ_3 planes. Therefore, it appears to be possible to use the shear invariant q whenever shear stresses in the σ_1-σ_3 plane are considered. q is defined by:-

$$q = (\sigma_1 - \sigma_3) \qquad (6.16)$$

However, in order to investigate the influence due to the intermediate principal stress, σ_2, it is also necessary to use the parameter, b, which is defined as:-

$$b = \frac{(\sigma_2 - \sigma_3)}{(\sigma_1 - \sigma_3)} \qquad (6.17)$$

The parameter b can only be either 0 or 1 in triaxial test conditions. However, in a hollow cylinder test, this parameter can be varied continuously from 0 to 1.

6.4 STRAIN IN A HOLLOW CYLINDER

For the same reasons discussed for stress in a hollow cylinder, assumptions about the uniformity of strains have to be made. The average strains for a hollow cylinder are defined as follows:-

$$\varepsilon_z = \frac{\delta l}{L} \tag{6.18}$$

$$\varepsilon_\theta = \frac{\delta d}{(a + b)} \tag{6.19}$$

$$\varepsilon_r = \frac{\delta t}{(b - a)} \tag{6.20}$$

Where ε_z, ε_θ and ε_r are the average axial, circumferential and radial strains respectively

δl = change in vertical displacement over the gauge length L

δd = Change in specimen diameter

δt = Change in thickness of specimen wall

a, b = interior and exterior radius of the specimen respectively

The shear strains in the z-θ plane can be deduced from the Mohr circle for strain if ε_z, ε_θ and the normal strain at a known direction within the plane can be obtained. A convenient method is to measure the strain at 45 degrees to the vertical axis. The Mohr circle to determine the shear strains is shown in Figure 6.12. It can be graphically shown that:-

$$\varepsilon_{z\theta} = \varepsilon_{45} - \frac{1}{2}(\varepsilon_\theta + \varepsilon_z) \tag{6.21}$$

Where $\varepsilon_{z\theta}$ is the pure shear strain on the plane at an angle α_ε from the vertical

ε_{45} is the normal strain at 45 degrees to the vertical and

α_ε is the rotation of the major principal strain plane

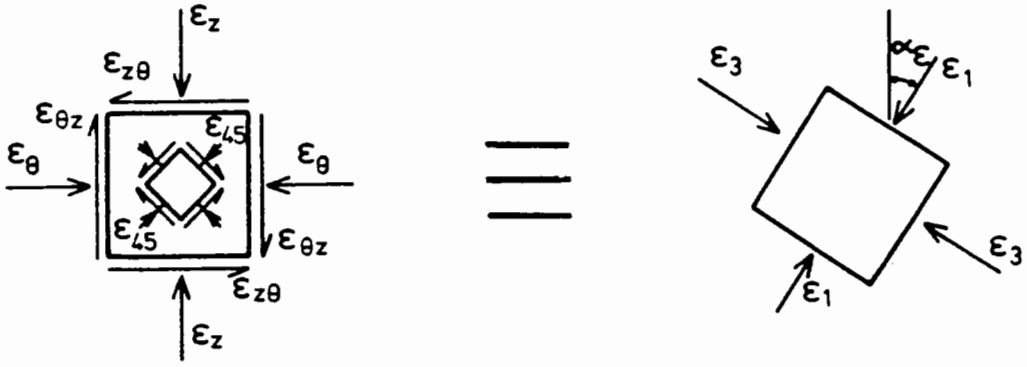

a. General Strains.

b. Principal Strains and Angle of Rotation.

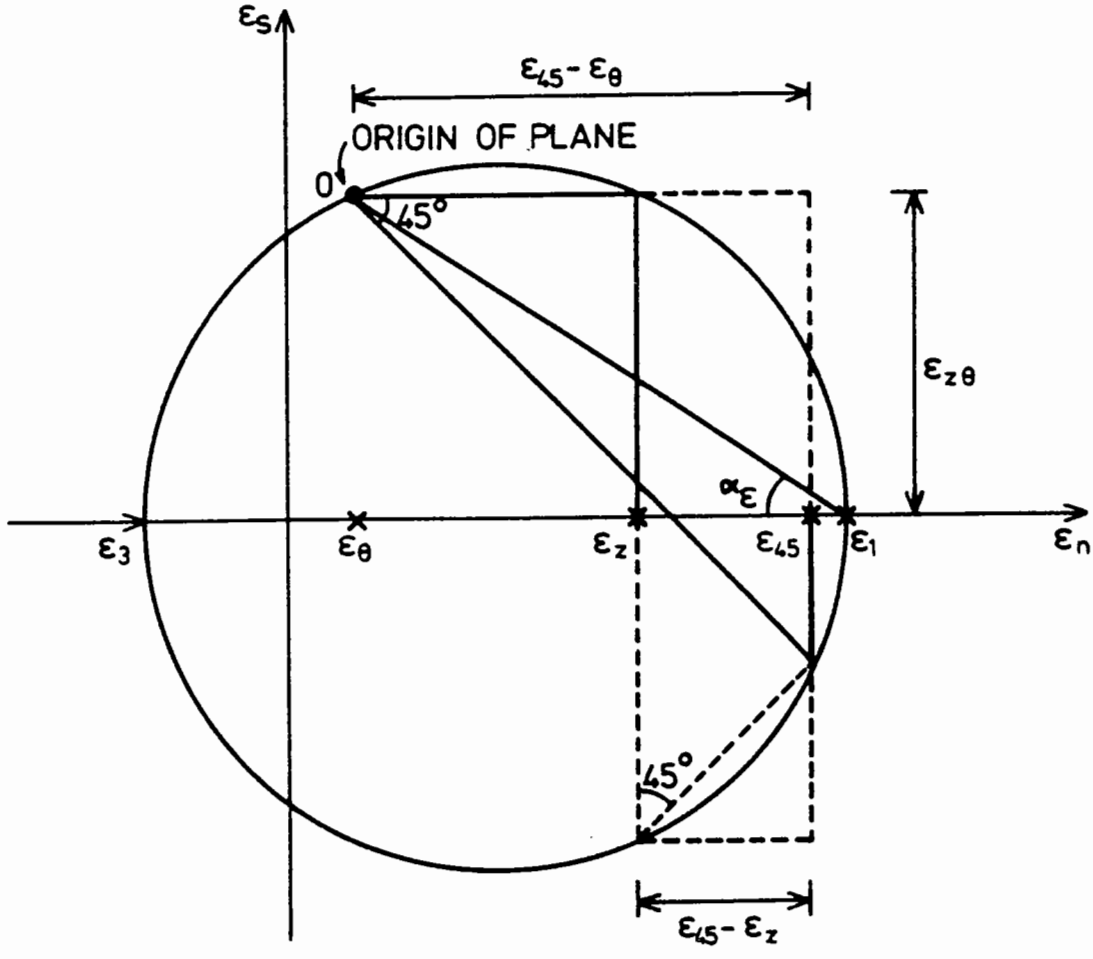

c. Mohr Circle Construction for Strain.

Figure 6.12 Mohr Circle for Strain

Figure 6.12 also shows that:-

$$\varepsilon_1 = \frac{\varepsilon_z + \varepsilon_\theta}{2} + \sqrt{\left(\frac{(\varepsilon_z - \varepsilon_\theta)}{2}\right)^2 + \varepsilon_{z\theta}^2} \qquad (6.22)$$

$$\varepsilon_3 = \frac{\varepsilon_z + \varepsilon_\theta}{2} - \sqrt{\left(\frac{(\varepsilon_z - \varepsilon_\theta)}{2}\right)^2 + \varepsilon_{z\theta}^2} \qquad (6.23)$$

$$\alpha_\varepsilon = \tan^{-1}\left(\frac{\varepsilon_{z\theta}}{\varepsilon_1 - \varepsilon_\theta}\right) \qquad (6.24)$$

Where ε_1 and ε_3 are the major and minor principal strains in the θ-z plane respectively.

Because there is no shear stress acting on the z-r and r-θ directions, it can be assumed that the shear strains ε_{rz} and $\varepsilon_{r\theta}$ are zero. Hence ε_r becomes the third principal strain and in theory:-

$$\varepsilon_r = \varepsilon_2 \qquad (6.25)$$

The maximum shear strain in the z-θ plane is defined as ε_{max} where:-

$$\varepsilon_{max} = \frac{1}{2}(\varepsilon_1 - \varepsilon_3) \qquad (6.26)$$

The state of strain in the specimen can also be represented by strain invariants. However, the invariants should be selected such that they correspond to those used for stresses. The strain invariant for q (Equation 6.16) is ε_{max} defined in equation 6.26. The invariants for p and q_{oct} (Equation 6.14) are ε_v and ε_s respectively and they are defined as:-

$$\varepsilon_v = \varepsilon_1 + \varepsilon_2 + \varepsilon_3 \tag{6.27}$$

$$\varepsilon_s = \frac{\sqrt{2}}{3} [(\varepsilon_1 - \varepsilon_2)^2 + (\varepsilon_2 - \varepsilon_3)^2 + (\varepsilon_3 - \varepsilon_1)^2]^{1/2} \tag{6.28}$$

6.5 SPECIMEN PREPARATION

When carrying out destructive tests, such as those for the investigation of permanent deformation characteristics of granular material, the importance of using "identical" specimens is overwhelming. Therefore, a specimen preparation technique which is repeatable and capable of producing specimens with the same properties is needed. For the repeated load hollow cylinder tests, a new method, based on the British Standard vibrating hammer test (BS5835) was developed. A sketch showing the basic principal of the method is presented in Figure 6.13.

To make a hollow cylindrical specimen, an inner and an outer mould are required. The inner mould consists of three articulated sections which can be extended and locked in its cylindrical shape by two internal connections. The outer mould is essentially a thin walled cylinder which is divided into three equal sections and held together by three Jubilee clips. Both moulds rest under their own weight on top of the base which is placed on top of a vibrating table. Three spacers are used at the top of the mould to ensure that the required uniform wall thickness is achieved.

Two pieces of membranes are also required. The inner membrane fits the outside of the inner mould tightly, thereby forming the required cylindrical shape. For the outer

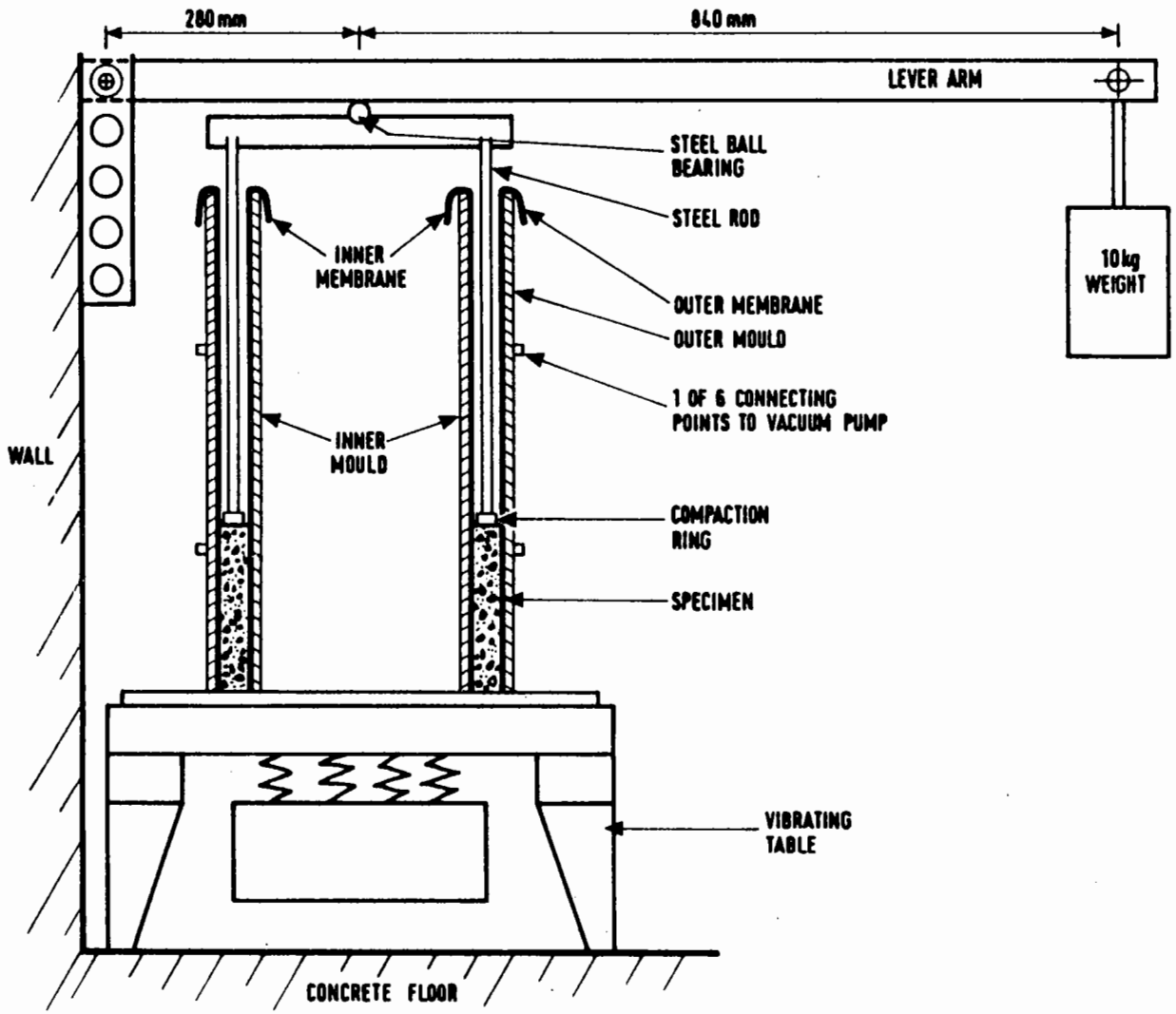

Figure 6.13 Details of Compaction Device for Hollow Cylinder Specimen.

membrane, the use of vacuum at six locations is need to hold it firmly against the inside of the outer mould.

The sample was built up in approximately seven layers each consisting of three kilograms of dry material. After the material had been poured and evenly spread, an aluminium compaction ring was placed on top. A surcharge load of approximately 40 kg was imposed on the ring through a lever system. While the surcharge is acting, 120 seconds of vibration, at 50 Hz frequency was applied. The amplitude of vibration was allowed to decrease gradually from its maximum value to 0 during the last 30 seconds.

After each layer had been compacted, the vertical distance between the surface of the compacted material to the top of the mould was measured at eight locations. These measurements allowed the average thickness, and hence density, of each layer to be calculated.

After the specimen was completely built and sealed (see Figure 6.7) an internal vacuum was applied prior to release of the moulds. The inner mould was folded inward and removed while the outer mould was released simply by unfastening the Jubilee clips. A plan view of these moulds during and after specimen construction is shown in Figure 6.14. Installation of the instrumentation then followed before the outer pressure chamber was placed and the top cap was fastened.

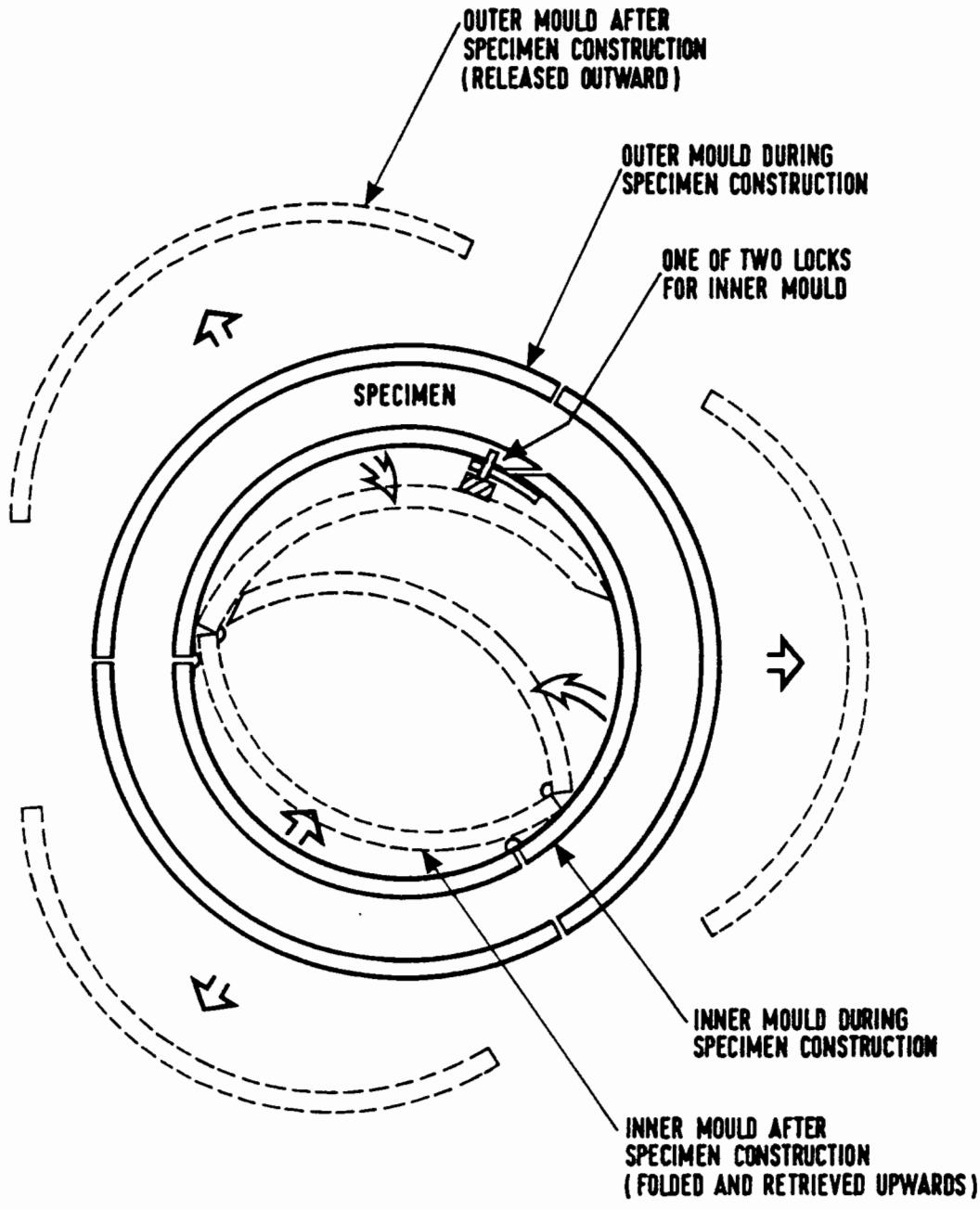

Figure 6.14 Plan View of Compaction Moulds for Hollow Cylinder Specimen during and after Compaction.

CHAPTER SEVEN

TEST PROGRAMME FOR REPEATED LOAD HOLLOW CYLINDER TESTS

7.1 INTRODUCTION

The main objective of carrying out repeated load hollow cylinder tests for this project was to study the effect of reversed shear stresses on the permanent deformation behaviour of granular material. For this part of the study, emphasis was placed on the difference between the with-shear and without-shear (or simply the triaxial) conditions. The tests also examined the difference in behaviour under the laboratory simulated condition involving uni-directional and bi-directional shear reversal.

The test programme also included, to a lesser extent, tests to determine the resilient stress-strain behaviour of the granular material concerned. An understanding of this behaviour under the new stress regime available from the HCA is also essential as the stiffness of the material will affect the load spreading capability of the granular material and, hence, the permanent strain which may develop.

Comparison between the behaviour of granular material tested in the repeated load HCA under triaxial conditions and that tested in the repeated load triaxial test apparatus is also warranted. This comparison can be viewed as a means to "calibrate" both test devices, thereby, possibly enabling new interpretations to be made of the large amount of existing results from the repeated load triaxial tests. Details of the repeated load triaxial test apparatus used in this project was reported by Brown et al (1989). A brief description of it is presented in Appendix D.

7.2 THE TEST MATERIAL

The material used for the repeated load hollow cylinder tests was a crushed dolomitic limestone. Because of the small thickness of the specimen wall, the maximum particle size was limited to about 5mm, giving a ratio of specimen thickness to maximum particle size of approximately 1:6. A representative grading envelope for the uncompacted "virgin" material is shown in Figure 7.1. The envelope indicates that the material was continuously graded with 95 and 18% of the material passing the 5mm and 75μm sieve respectively. A series of standard vibrating hammer tests (BS5835) was carried out on the dry materials. The maximum dry density obtained from the test was 2216 kg/m^3 . The specific gravity of the material contained between the 5mm and 2mm sieves was found to be 2.7 according to the BS812 test method. The shape of the aggregate particles for this group of materials, when examined under a microscope, could be considered as flaky. Because there were no pore pressure or suction measuring devices available in the HCA, the material was tested dry. This ensured that all the stresses used and measured were effective stresses.

The method of specimen preparation described in the last chapter was found to be satisfactory and capable of producing relatively high density, despite the large height of the specimen. Segregation was found to be acceptable as shown also in Figure 7.1 by the average gradings of the materials retrieved from the top, middle and bottom of the tested specimen. Except for the last layer, the variation of density of the compacted material between different specimens was found to be small, as shown in Figure 7.2 for all the specimens prepared. Furthermore, if consideration was given only to the middle section of the specimen where deformations were measured, the difference became insignificant.

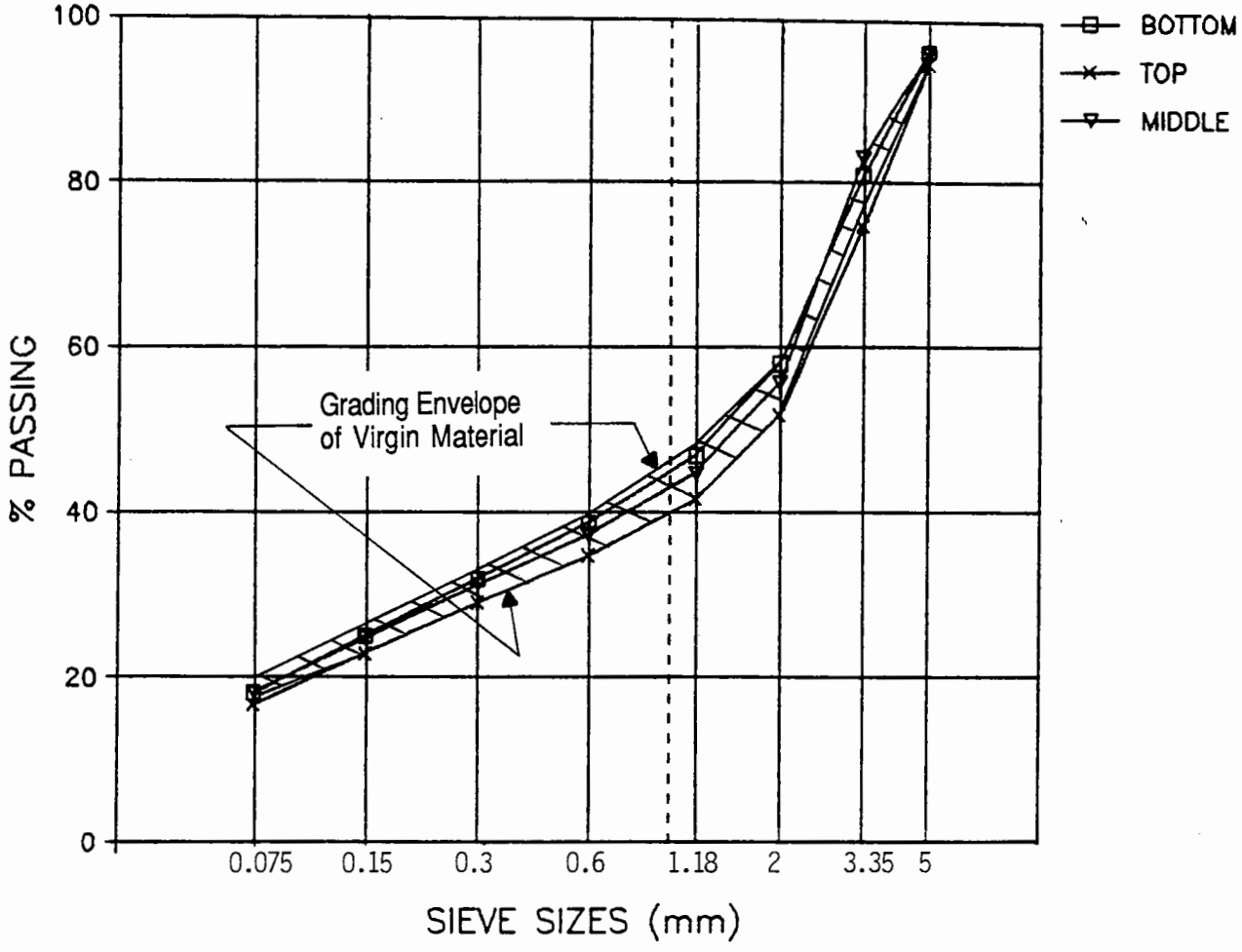

Figure 7.1 Grading Envelope of the Virgin Material and the Average Gradings of Samples obtained from Top, Middle and Bottom of tested Hollow Cylinder Specimens.

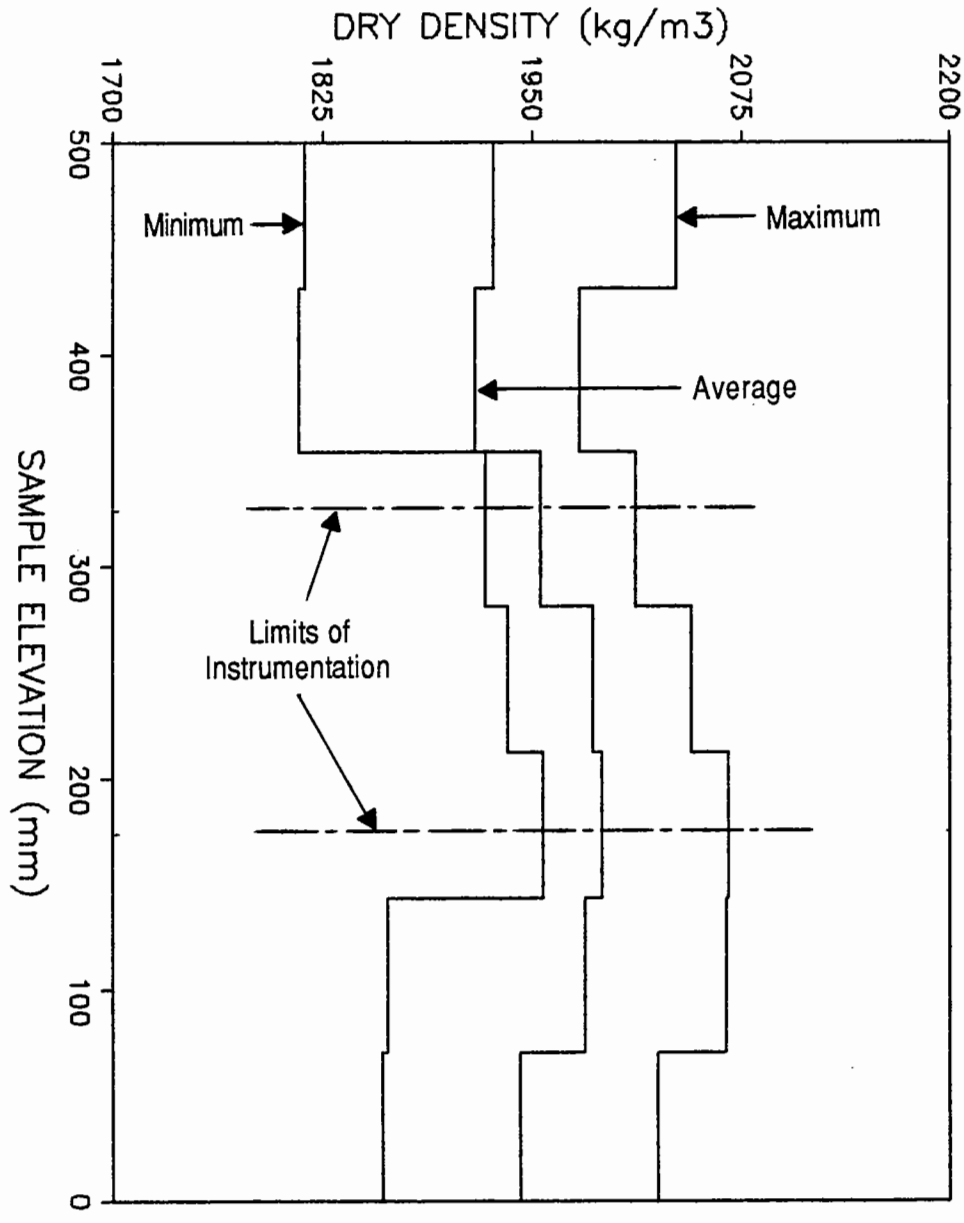

Figure 7.2 Variation of Dry Density with Depth of Hollow Cylinder Specimens

7.3 PERMANENT STRAIN TESTS

A permanent strain test consisted of applying many cycles of the same stress conditions to a specimen and monitoring its permanent, non-recoverable deformation at regular time intervals. Because the permanent strain behaviour of granular material is dependent on its stress and strain history (i.e. the stresses and strains it has previously been subjected to), only one particular set of stress conditions could be used for each specimen.

A total of 9 tests belonging to this category, each involving at least 10,000 cycles of repeated loading, were carried out. These tests were divided into three series of three tests each as detailed in Table 7.1. The magnitude of the stresses chosen were based on the stress measurements obtained from the granular base in a full scale test carried out in the Nottingham PTF (Brown et al, 1982). Although the granular materials involved were different, it was believed that the stresses adopted here were realistic. In all nine tests, both the internal and external cell pressures were kept constant at 100kPa.

The three specimens involved in each series were subjected to the same repeated vertical stress which varied sinusoidally at a frequency of 0.5 Hz. The only difference was the applied shear stress. The variations of shear stress in each test within one series were designed to allow comparison of results for the following three conditions:

1. Triaxial Condition

   In this case, no shear stress was applied. This provided the basis for comparison of results with those which involved shear stress reversals. It also allowed results obtained from the repeated load triaxial test apparatus to be compared.

Table 7.1

Details of Permanent Strain Tests carried out with the Repeated Load Hollow Cylinder Test Apparatus

Test Series	*Test Number*	*Vertical Stress (kPa)*	*Torsional Shear Stress (kPa)*	*Phase Angle between Vertical & Torsional Stresses*
1	1	0-150	0	0
	2	0-150	-20-+20	-90
	3	0-150	-20-+20	+90/-90
2	4	0-200	0	0
	5	0-200	-20-+20	-90
	6	0-200	-20-+20	+90/-90
3	7	0-200	0	0
	8	0-200	-30-+30	-90
	9	0-200	-30-+30	+90/-90

2. Condition under a wheel load moving in one direction (uni-directional shear reversal)

To simulate the stresses under this condition, the phase angle between the vertical and the shear stress (which also varied sinusoidally at the same frequency) waveforms was adjusted to 90 degrees, as shown in Figure 7.3. As a result, the variation of angle of principal plane rotation with time shown in Figure 7.4 was obtained. Because the HCA was not able to generate a variable cell pressure, the variation of horizontal stress (as shown in Figure 1.1, Chapter one) could not be simulated. Instead, a constant pressure was used.

3. Condition under a wheel load moving in both directions (bi-directional shear reversal)

This condition , as represented in Figures 7.5 and 7.6, was basically the same as that for the uni-directional shear reversal. The exception was that at regular pre-set interval during the test, the phase angle between the vertical and shear stress was switched from +90 to -90 degrees or visa versa. For the purpose of simulating laboratory bi-directional loading, it would be ideal if the switching of the phase angle were carried out in successive cycles. However, since the switching process was manually controlled, it became impractical, if not impossible for it to happen. Therefore a compromise for the sequence of changes of phase angle as shown in Figure 7.7 was adopted for this test.

The stress paths for the three series of tests are shown, in q-p stress space, in Figure 7.8. The paths for the two conditions with reversed shear stresses are practically identical and slightly curved. For the triaxial condition, a straight stress path is apparent. Despite this difference, the end points of the paths are identical for each series of tests.

7.4 50-CYCLE TESTS

When the stress path used in a permanent deformation test approaches the static failure condition, both the magnitude and the rate of development of permanent strain will increase. As the resulting deformations are generally large, the effect due to stress or strain history will be very much reduced. Using this assumption, a series of permanent strain tests involving several stress paths, each of increasing severity, can be carried out

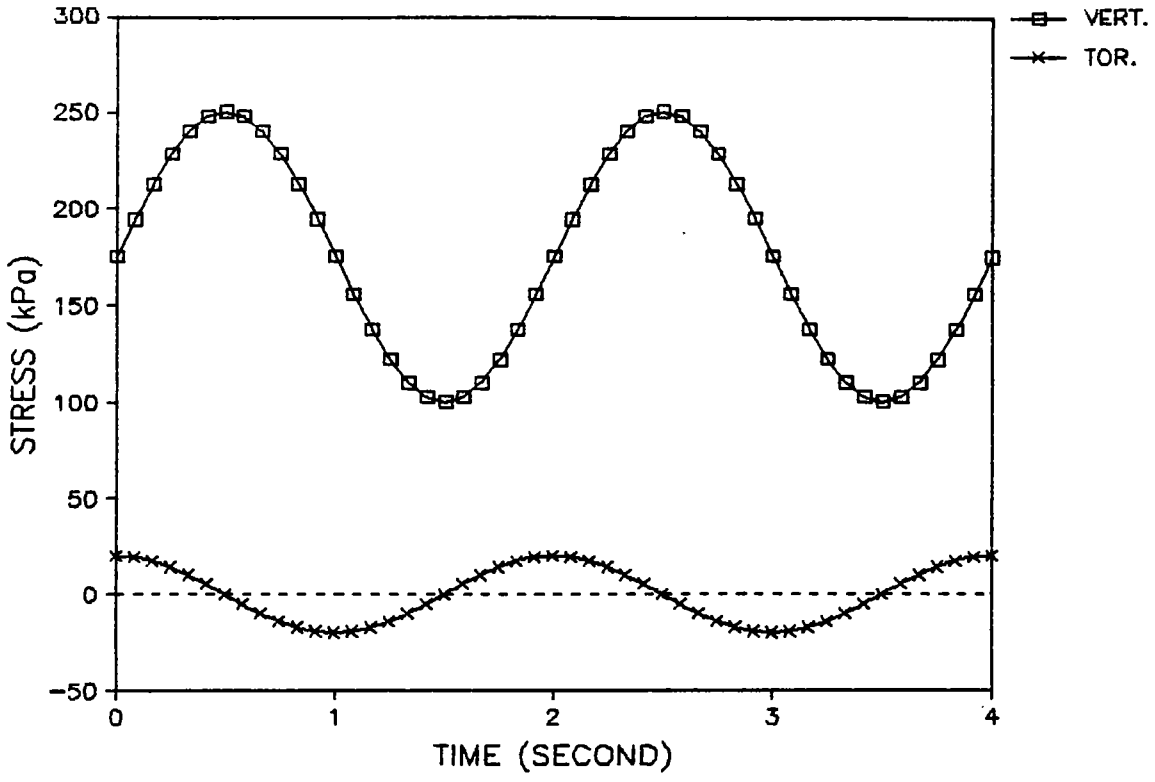

Figure 7.3 Waveforms for Vertical and Torsional Stresses in Tests with Uni-directional Shear Reversal.

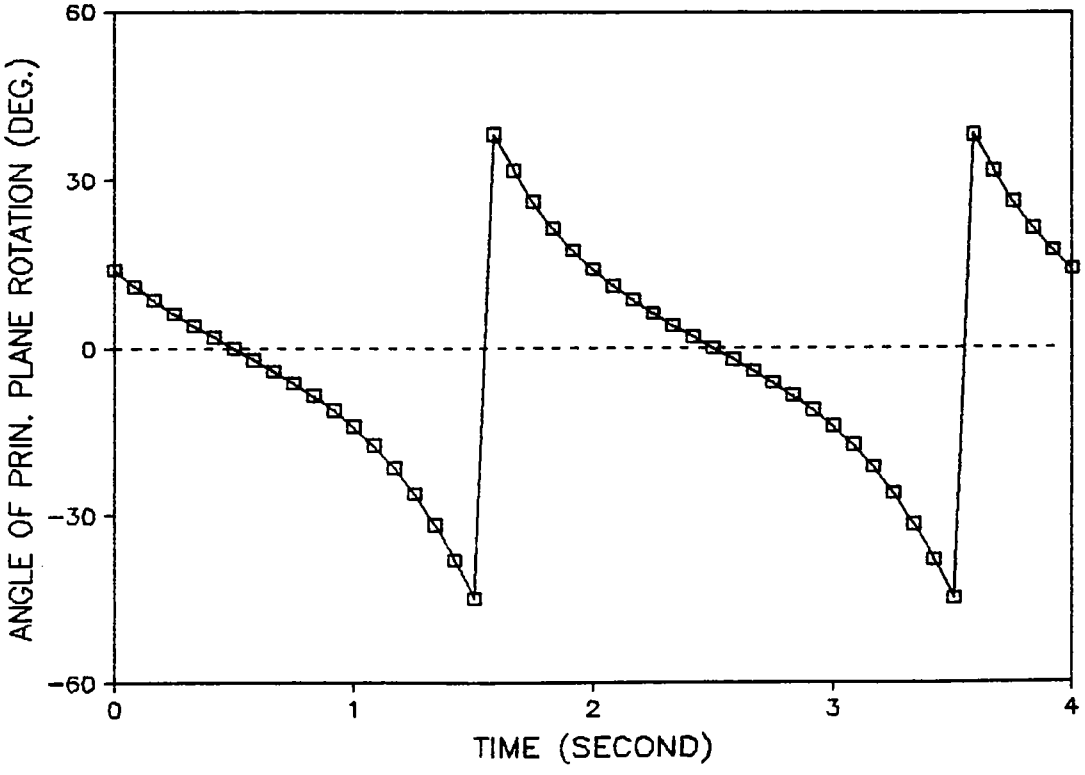

Figure 7.4 Variation of Angle of Principal Plane Rotation with Time in Tests with Uni-directional Shear Reversal.

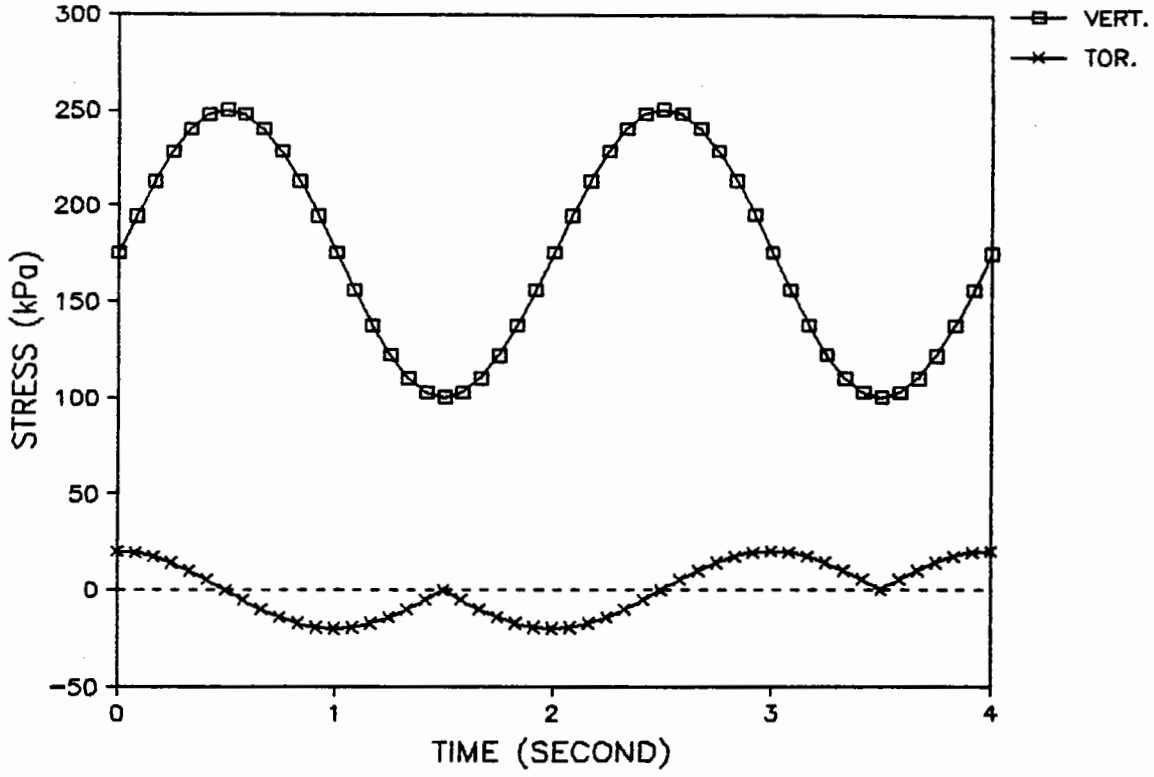

Figure 7.5 Waveforms for Vertical and Torsional Stresses in Tests with Bi-directional Shear Reversal.

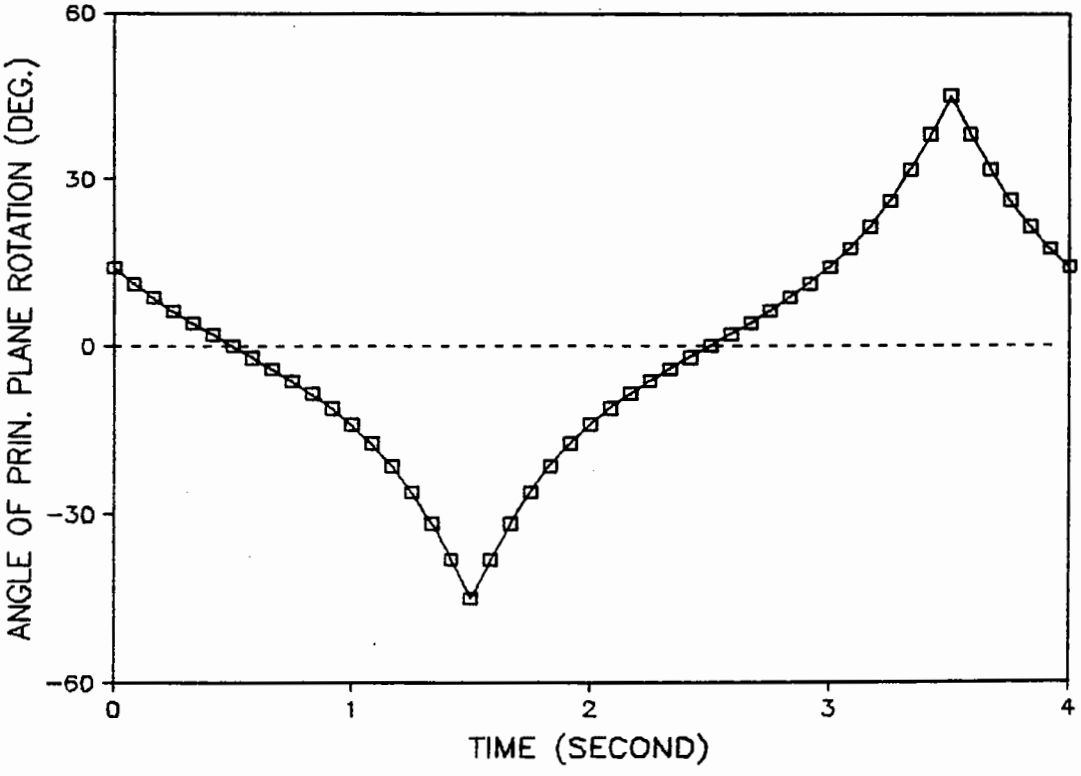

Figure 7.6 Variation of Angle of Principal Plane Rotation with Time in Tests with Bi-directional Shear Reversal.

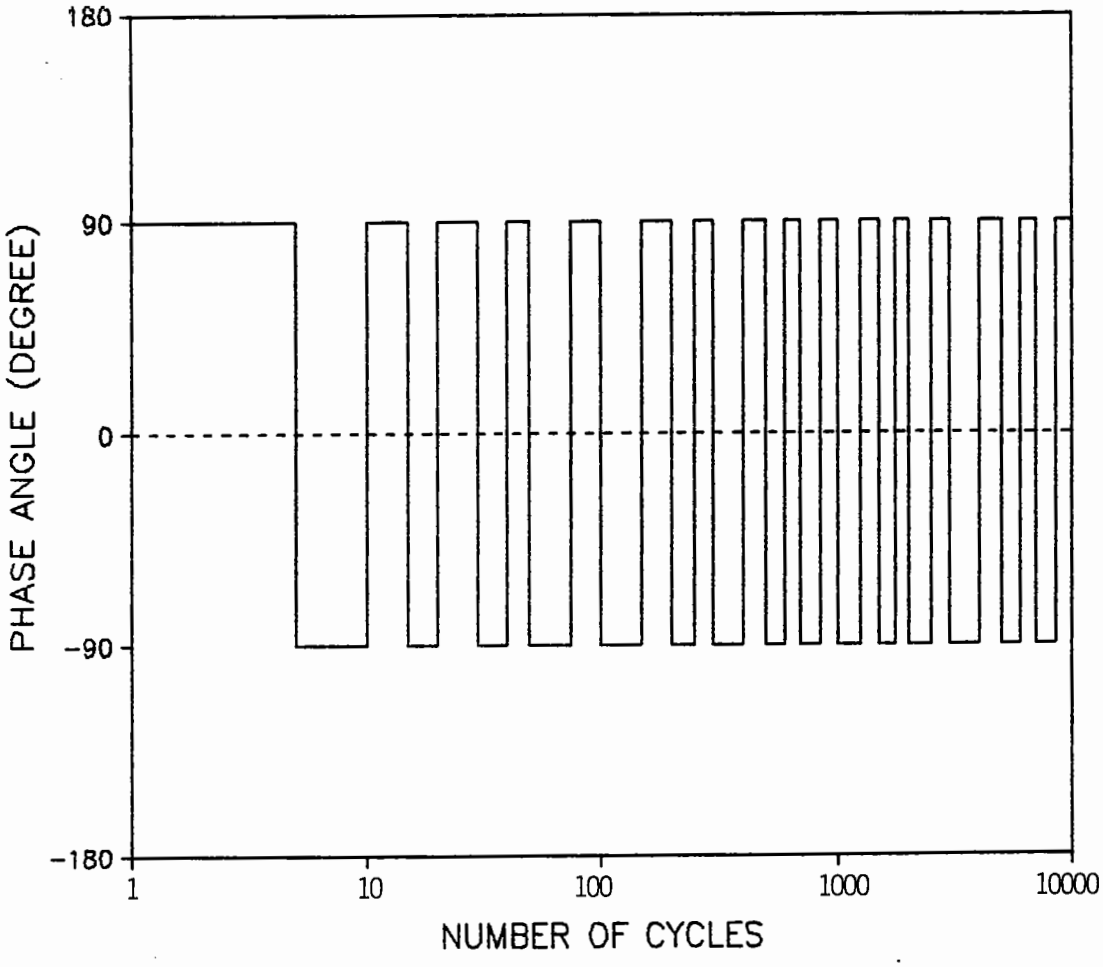

Figure 7.7 Variation of Phase Angle Shift between the Vertical and Torsional Stress Waveforms during Tests with Bi-directional Shear Reversal.

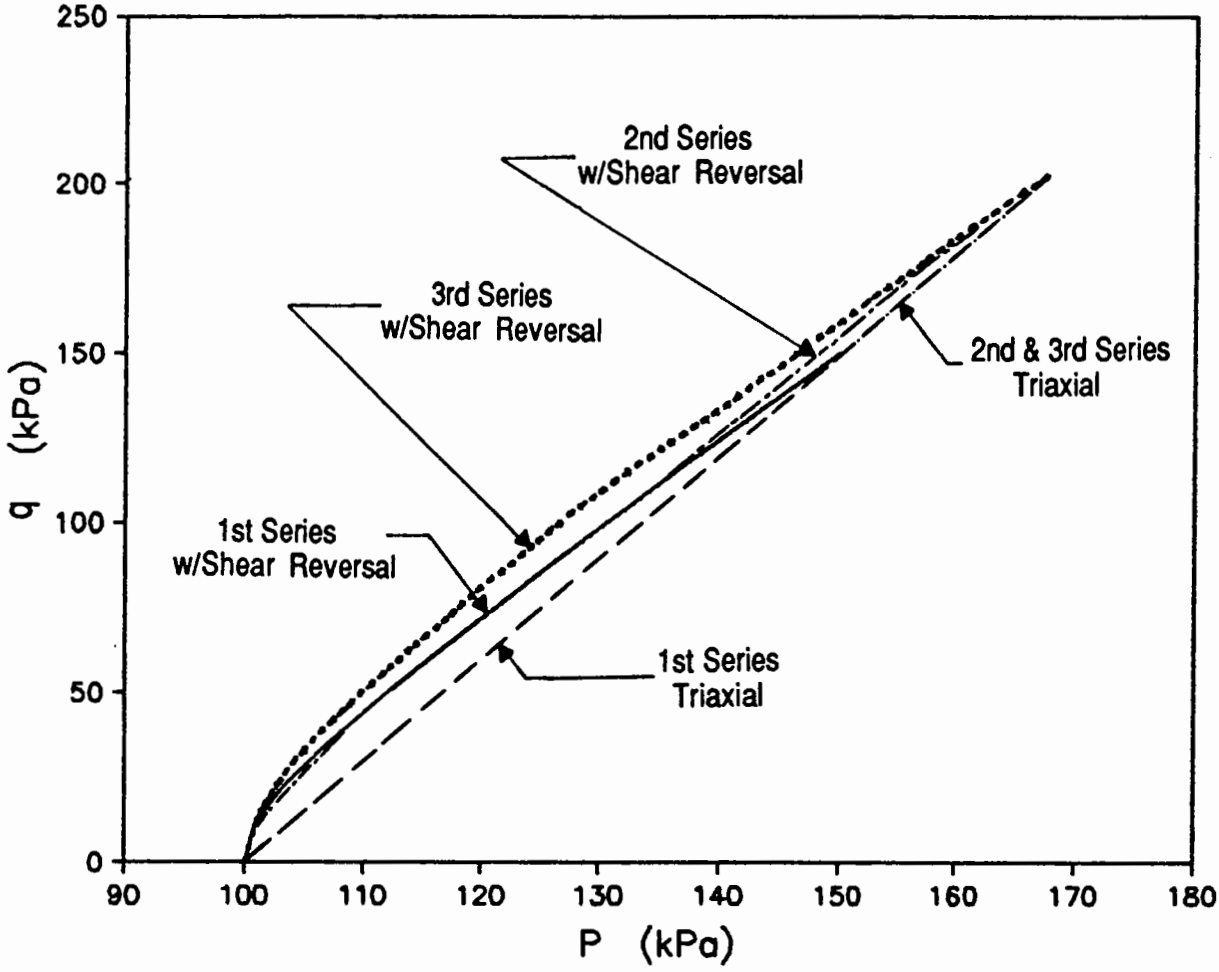

Figure 7.8 Stress Paths in q-p Space used in Permanent Strain Tests.

on a single specimen of granular material. Because of the rapid build-up of permanent strain, only a limited number of cycles of each repeated stress condition could be allowed before the specimen was totally damaged.

In this project, the number of cycles used for each stress path was approximately 50, hence the name "50-cycle test". The main objective of the "50-cycle" test was to make use of a less time-consuming method to examine the effect of the reversed shear stresses on the rate of development of permanent strains. In order to achieve this, each test was divided into two parts, each part consisting of 25 cycles of the same stress condition. In one part, only the vertical stress was cycled while, in the other, an additional uni-directional reversed shear stress was applied. An example of the variation of the stress conditions recorded during a 50-cycle test is shown in Figure 7.9. In some tests, the "without-shear" condition was allowed to precede the "with-shear" (or triaxial) condition in order to counteract the possible strain history effect caused during the initial 25 cycles of stresses. All components of strain, both recoverable and the non-recoverable (permanent), were monitored continuously during the 50 cycles of stress, hence allowing their variations during the two parts of test to be compared.

Seven 50-cycle tests were carried out on one hollow cylinder specimen. Details of the stress conditions used are shown in Table 7.2. The stress paths in q-p stress space are shown in Figure 7.10. The solid lines represent the paths with reversed shear stresses. In order to allow more time to implement the stress changes (from "with-shear" to "without-shear"), a slower frequency of 0.4 Hz was used for the repeated stress waves.

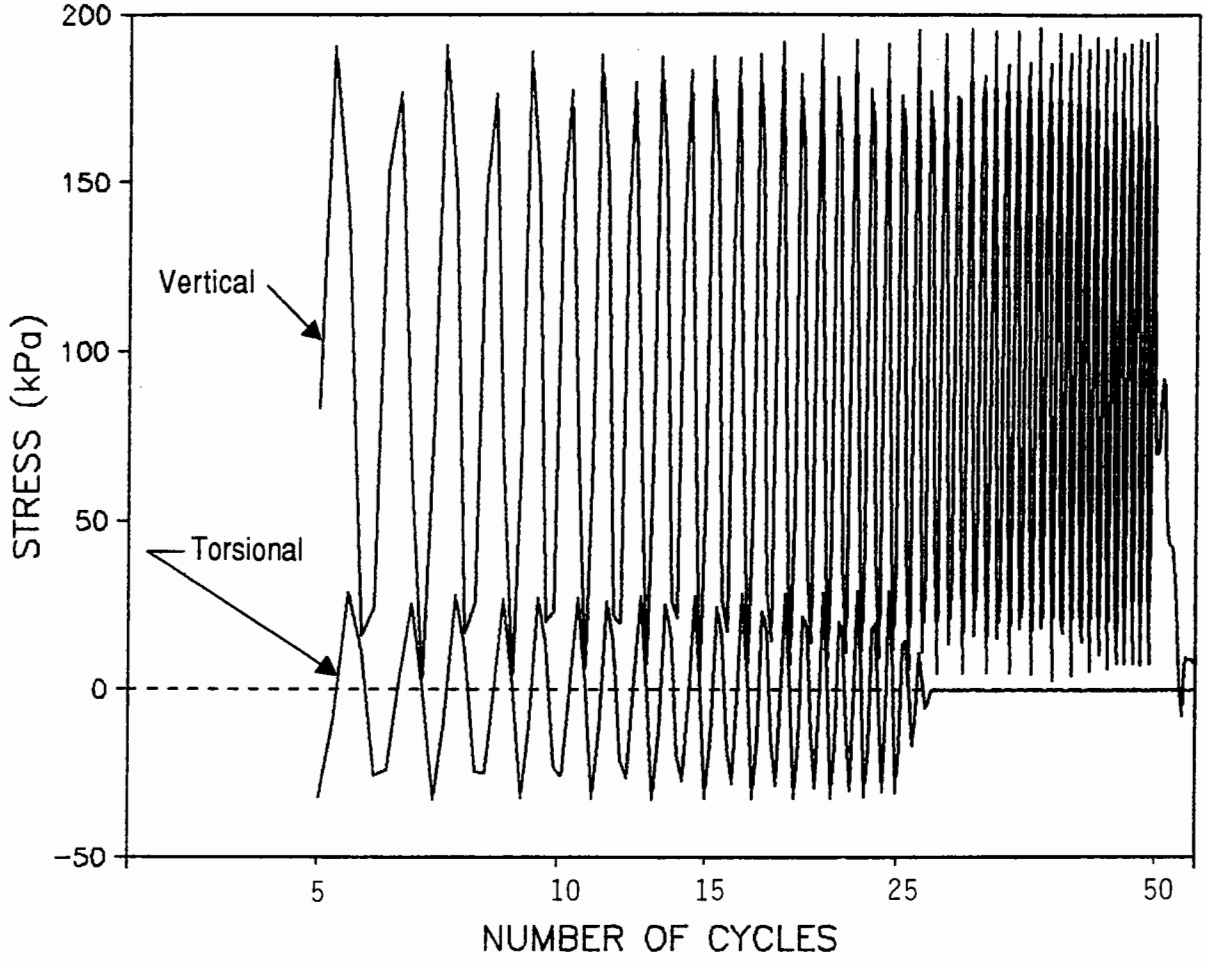

Figure 7.9 Variation of Stresses with Time in a 50-Cycle Test.

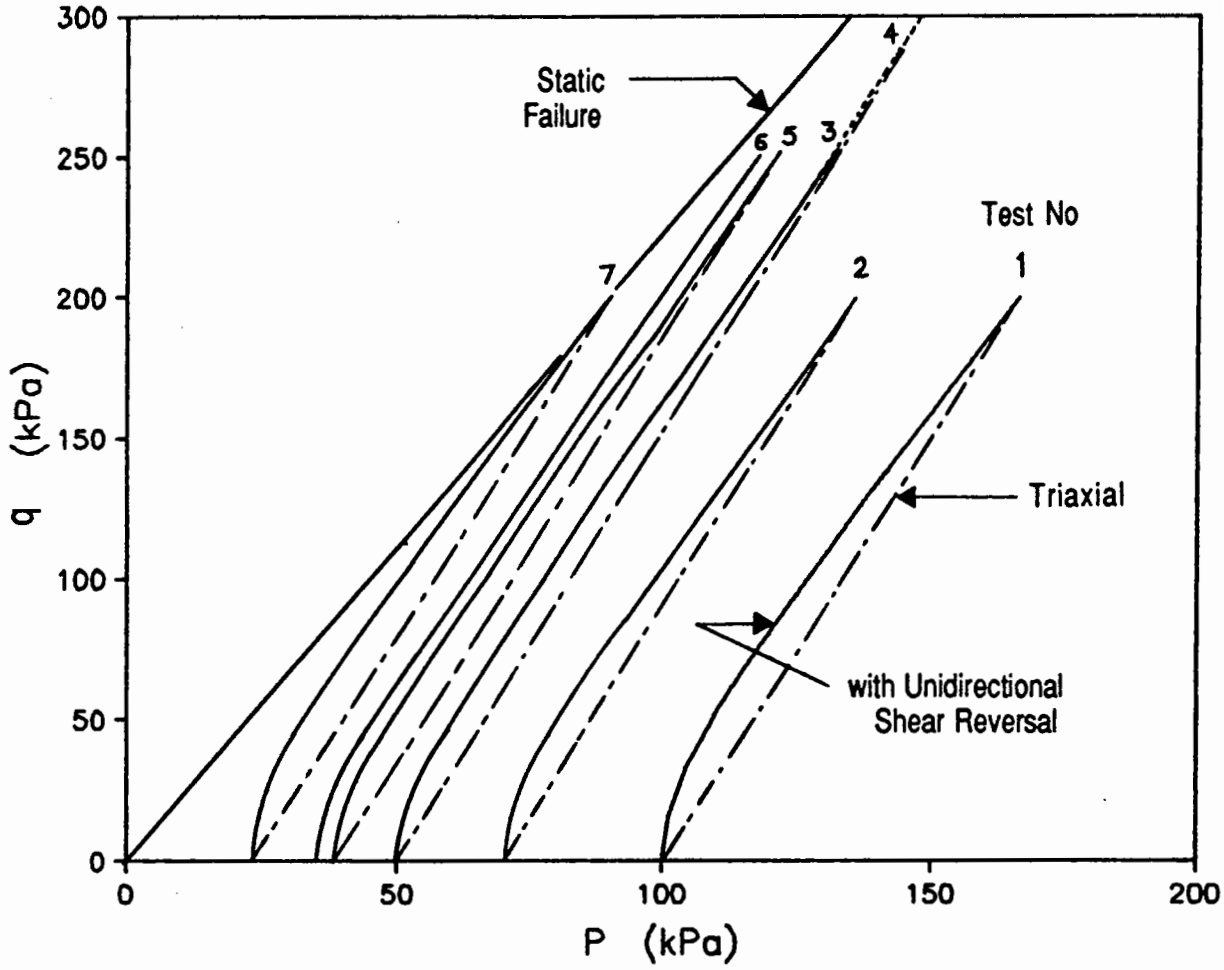

Figure 7.10 Stress Paths in q-p Space used in 50-Cycle Tests.

Table 7.2

Details of 50 Cycles Tests

Test Number	*Vertical Stress (kPa)*	*Torsional Shear Stress (kPa)*	*Cell[1] Pressure (kPa)*	*Maximum (q/p) Ratio*	*Test[2] Sequence*
1	0-200	-30-+30	100	1.20	1
2	0-200	-30-+30	70	1.46	2
3	0-250	-30-+30	50	1.88	1
4	0-300	-30-+30	50	2.00	1
5	0-250	-30-+30	38	2.06	2
6	0-250	-30-+30	35	2.11	1
7	0-200	-30-+30	23	2.23	2

Note: 1. The pressure is for both the inner and outer cell chamber.
2. "1" means that the "without-shear" condition precedes the "with-shear" condition. "2" means the reverse.
3. Phase angle between the vertical and torsional stresses is 90 degree for all tests

7.5 RESILIENT STRAIN TESTS

In a resilient strain test, the stress paths used are well away from the failure condition. As a result, it can be assumed that the specimen responds elastically and all the strain components essentially recover during unloading.

The resilient behaviour of the specimen used in the permanent strain tests was regularly monitored during the tests. However, the resilient stress paths involved were only limited to the one used for that particular permanent strain test. This cautious procedure

was adopted in order to minimize the risk of causing a stress or strain history effect on the result of the permanent strain tests which were the main object of investigation for this project. A new specimen, therefore, was constructed in order to allow a more thorough study of the resilient behaviour of the granular material used. The specimen was subjected to a much wider range of stress conditions as detailed in Appendix E. The test programme aimed at covering a range of intermediate principal stress and angle of principal plane rotation.

However, "Jump" rotation of 90 degrees can occur between the circumferential plane (on which σ_θ acts) and the axial (on which σ_z acts) or radial (on which σ_r acts) plane during repeated loading when σ_r becomes larger than σ_z and σ_θ or when σ_θ becomes larger than σ_r. In these cases, principal plane rotation will occur in both the z-r or θ-r directions. Therefore, in order to avoid complications caused by the three dimensional rotation, the conditions stated in equations 6.11 and 6.12 were followed at all times during the resilient tests. This ensured that σ_r was always the intermediate principal stress and rotation of principal stress plane was restricted to the θ-z plane. The frequency of the repeated stress wave used in these tests was 0.5 Hz.

7.6 REPEATED LOAD TRIAXIAL TESTS

The repeated load HCA is undoubtedly a complicated testing device which will remain as a research tool for some time. At the moment, results of tests from this device are scarce and, therefore, cannot be used immediately with confidence. As a result, it appears to be advantageous to make comparisons between the performance of the HCA and that of the more widely used repeated load triaxial test apparatus.

Two cylindrical specimens of the same granular material used in the HCA tests, with diameters of 150mm and heights of 300mm were tested in a repeated load triaxial test apparatus. In the first test, a series of resilient stress paths, as detailed in Appendix E, were applied. After the resilient tests were completed, a permanent strain test, which used the same stress path as that for test number 4 and 7 of the HCA test programme, was carried out on the same specimen. For the second specimen, only the permanent strain test was performed. The permanent strain test involved at least 10,000 cycles of repeated load at a frequency of 0.5 Hz.

The triaxial specimens were manufactured using the same vibrating table and surcharge as for the HCA specimens. As a result, the densities obtained for the triaxial specimens TX1 and TX2, which were 1950 and 1909 kg/m^3 respectively, were similar to those of the hollow cylinder specimens.

CHAPTER EIGHT

RESULTS FROM REPEATED LOAD HOLLOW CYLINDER TESTS

8.1 INTRODUCTION

The results of the tests described in Chapter seven are presented in the following sections. A total of eleven hollow cylinder and two triaxial specimens were tested for this part of the investigation. In the permanent strain tests, because the number of specimens was limited, it was not possible to perform replicate tests for each stress path. However, for the resilient strain tests, duplicate tests were carried out. The emphasis of the presentation of the results from the permanent strain tests is placed mainly on the trend of permanent strain development rather than the absolute values of strains. This approach is considered to be applicable, particularly for programmes involving small numbers of tests. In general, more information was available from resilient strain tests, despite the use of much fewer specimens. As a result, a more detailed analysis of the results was possible.

8.2 PERMANENT STRAIN TESTS

In a permanent strain test, the electronic signals from all the instrumentation were monitored without interruption during the first 30 cycles. Typical plots of the relationship between stresses and one of the strain components with time are shown in Figures 8.1 and 8.2 respectively. It is worth noting that a few cycles of time are normally required at the start of the test for the stresses to reach their target values. The average number of data points captured per cycle during the first 30 cycles was about

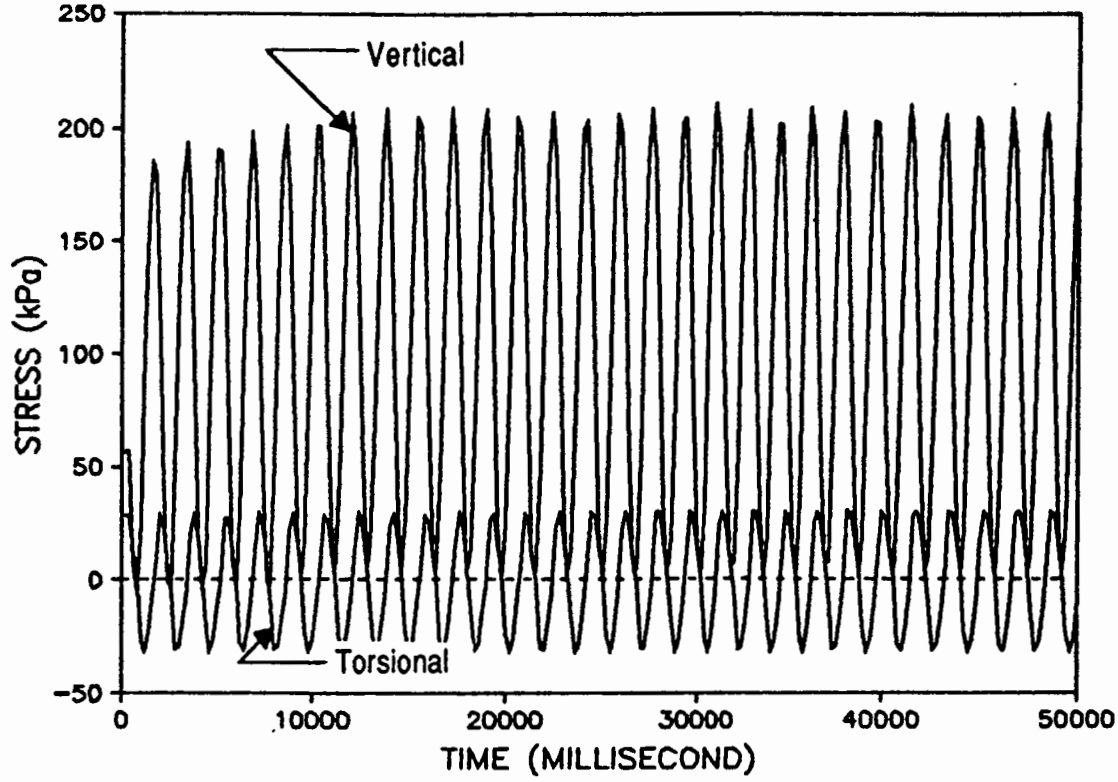

Figure 8.1 Variation of Stresses with Time during the first 30 Cycles of a Permanent Strain Test.

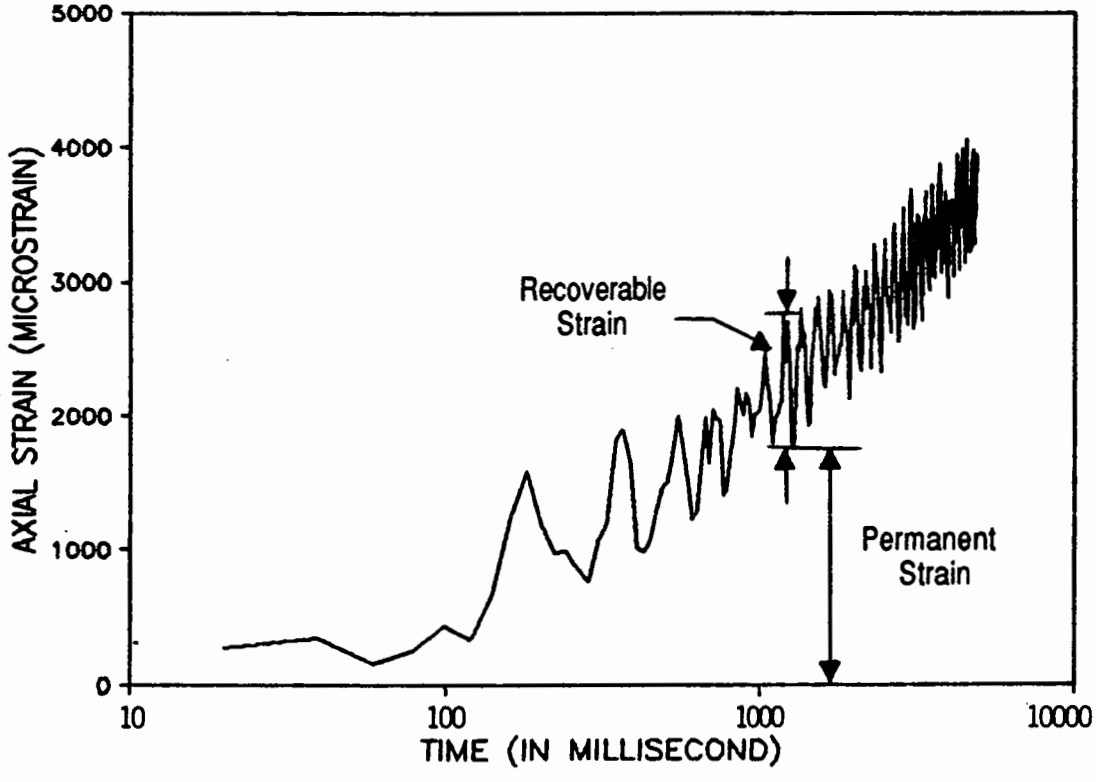

Figure 8.2 Variation of Axial Strain with Time during the first 30 cycles of a Permanent Strain Test.

eight. To collect data for subsequent numbers of cycle, the test was stopped and the non-recoverable or permanent strain components were then individually recorded.

8.2.1 Comparison between Triaxial, Uni- and Bi-directional Shear Reversal Conditions

The variations of permanent strain with number of stress cycles, for the nine specimens used in the three series of repeated load HCA tests, are shown in Figures 8.3 to 8.6. Four types of strains were included for comparison. They were the permanent axial strain, $(\varepsilon_a)_p$ (Figure 8.3), the permanent horizontal strain, $(\varepsilon_h)_p$ (Figure 8.4), defined here as the sum of the radial and circumferential strains , the permanent volumetric strain, $(\varepsilon_v)_p$ (Figure 8.5) and the permanent maximum shear strain in the θ-z plane, $(\varepsilon_{max})_p$, as defined in equation 6.26 (Figure 8.6).

The use of the sum of the radial and circumferential instead of their individual values was justifiable as they both had broadly the same magnitude and sign and varied in similar manner with the number of cycles.

Figures 8.3 to 8.6 are largely self-explanatory. However, some description may be required to highlight the important features:

1. In the first series of tests, while the skill of operating the newly modified test apparatus was still being perfected, the stresses which were applied to the specimens during the first 10 cycles were rather variable. As a result, it was decided that the permanent strains occurring during this early period should be discarded. Hence, zero permanent strains were assumed at cycle 10 for all the tests in this series. In subsequent test series, all strains were presented from the first cycle.

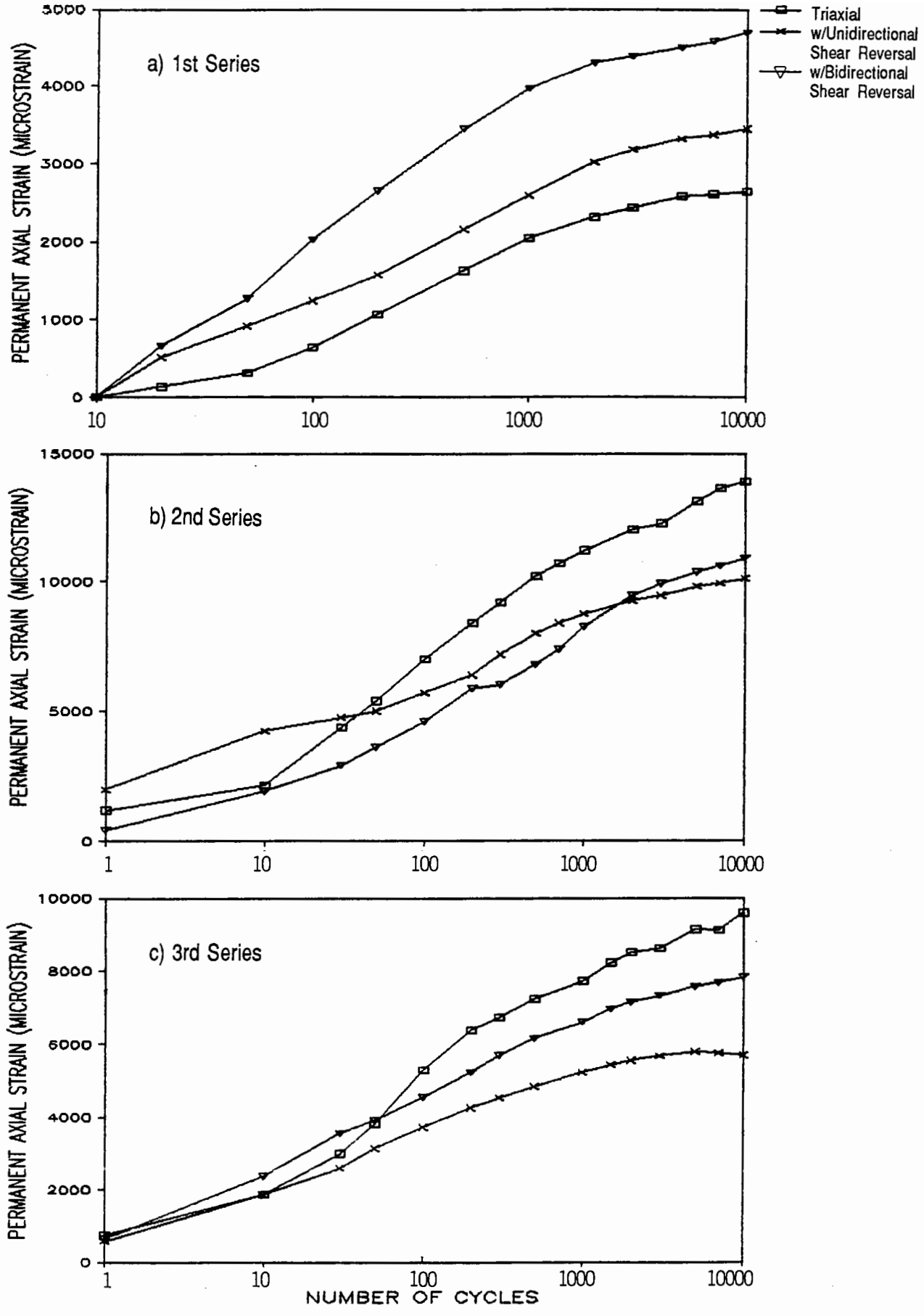

Figure 8.3 Variation of Permanent Axial Strains with Number of Stress Cycles for all Series of Permanent Strain Tests.

2. The magnitude of all strain components is quite small, even after 10,000 cycles of stress. In the first test series, the maximum strain remained less than 0.5%. With the shear stress ratio, $(q/p)_{max}$ increased from 1 (in the first test series) to 1.2, the maximum strain in the second and third series reached about 1.5%. In general, $(\varepsilon_v)_p$ is about 2 times $(\varepsilon_{max})_p$. In all tests, $(\varepsilon_a)_p$ are positive (compressive) while most $(\varepsilon_h)_p$ values are negative (dilatant). However, because of the predominantly high magnitude of the axial strains, the resulting volumetric strains are all positive, indicating contraction. The permanent maximum shear strains, on the other hand, are all positive by definition.

3. Most components of strains, with the exception of $(\varepsilon_h)_p$, increase gradually and, broadly linearly, with the logarithm of the number of cycles. In the first test series, after about 2000 cycles, the permanent strains tended to stabilize. In subsequent series, signs of stabilization of strain were observed for some but not all tests.

4. The most obvious difference in permanent strain behaviour among the three investigated stress conditions is found in the development of permanent horizontal strain (Figure 8.4). Under triaxial condition, $(\varepsilon_h)_p$ was dilatant and remained so throughout the test. It also tended to stabilize rather rapidly at a terminal value. However, when reversed shear stresses were applied, the initial permanent strain was dilatant but then after 100 to 300 cycles of stress, it started to move towards the compressive end. In the two cases with uni-directional shear reversal in Series 1 and 2, the change from negative to positive permanent strain occurred rather rapidly and tended to accelerate towards the end of the tests.

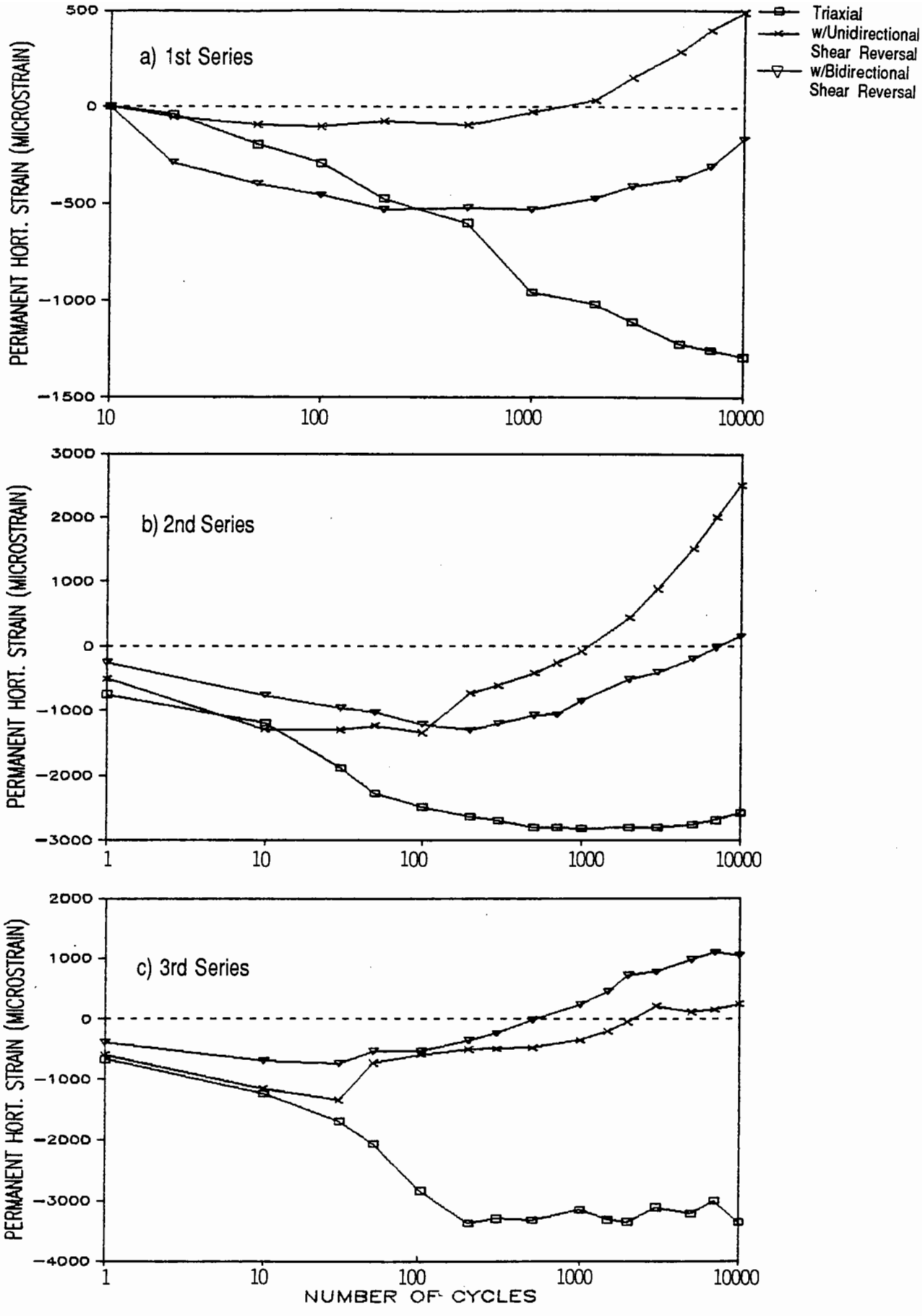

Figure 8.4 Variation of Permanent Horizontal (Sum of Radial and Circumferential) Strains with Number of Stress Cycles for all Series of Permanent Strain Tests.

5. It appears to be evident that higher permanent contractive volumetric strains occurred when reversed shear stresses were applied (see Figure 8.5). In the first test series, $(\varepsilon_v)_p$ under triaxial stress conditions was only one third to one fourth of that with shear reversal. However, with the ratio of the torsional shear to vertical stress reduced, there seemed to be less difference between the strains for the three conditions. Figure 8.5 may also suggest that when the stress ratio mentioned above is high, conditions with bi-directional shear reversal are likely to result in more permanent volumetric strain.

6. The behaviour of $(\varepsilon_a)_p$ and $(\varepsilon_{max})_p$ is very similar. In the first test series, the specimen under triaxial stress conditions (which incidentally was the very first specimen to be tested in the test programme) developed the smallest permanent strain. However, in both subsequent test series, specimens under triaxial stress conditions were found to develop the highest strains. The results from these latter test series led to the belief that the first specimen may have suffered from some disturbance or strain history during the "set-up" of the test. This may also explain the much smaller permanent volumetric strains which occurred in this specimen.

7. Taking into account of the possible error mentioned in item 6 above and based on Figure 8.6b and 8.6c, it appears that when reversed shear stresses are applied, a reduction in the build-up of permanent maximum shear strain is likely to occur. Figure 8.6 also indicates consistently that higher $(\varepsilon_{max})_p$ occurs under the bi-directional than uni-directional shear stress reversal.

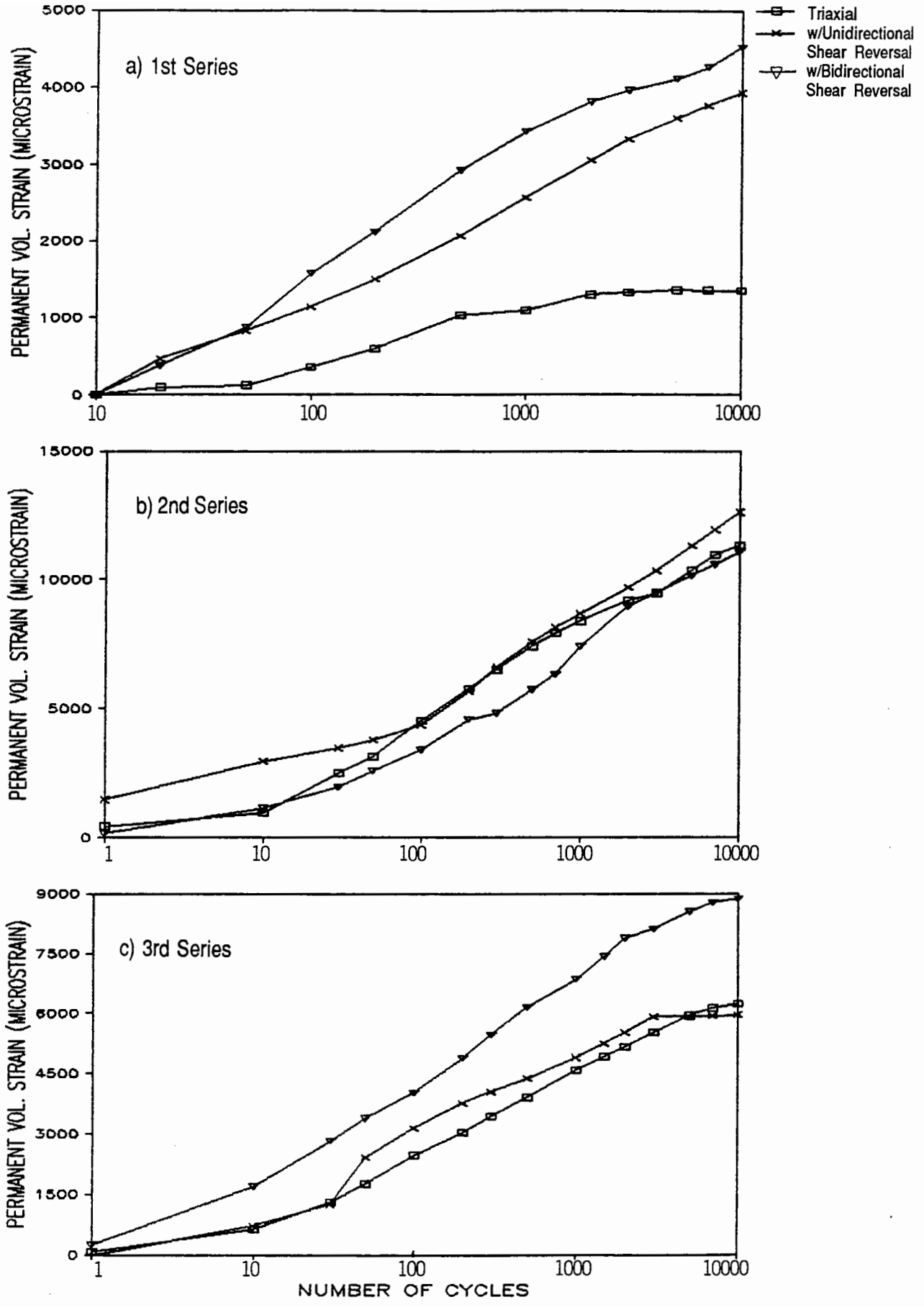

Figure 8.5 Variation of Permanent Volumetric Strains with Number of Stress Cycles for all Series of Permanent Strain Tests.

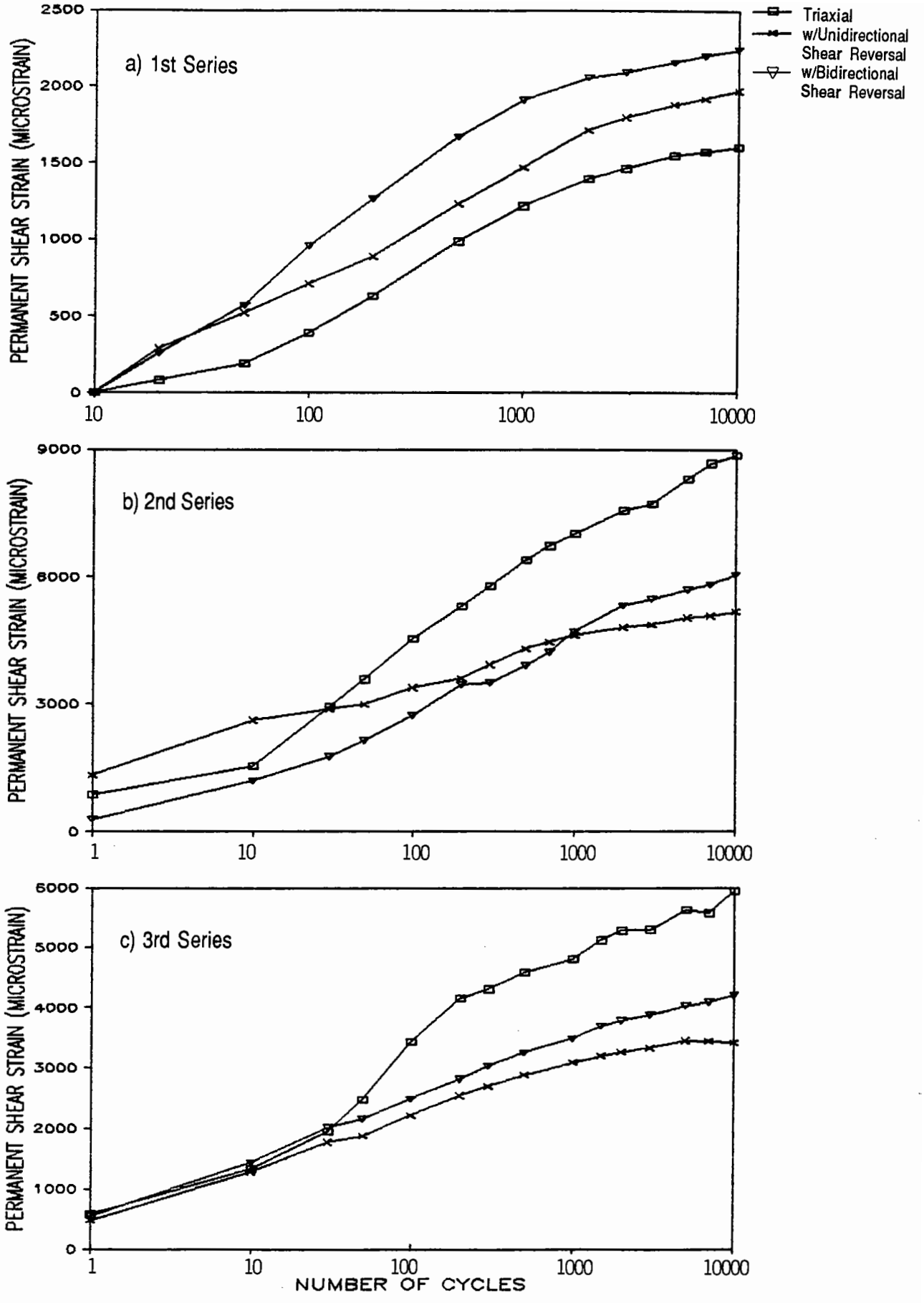

Figure 8.6 Variation of Permanent Maximum Shear Strains with Number of Stress Cycles for all Series of Permanent Strain Tests.

8.2.2 Comparison between Results from Tests carried out in Repeated Load HCA and Triaxial Apparatus

A comparison of the permanent strains from the HCA tests number 4 and 7 under triaxial stress conditions and the two tests carried out in the repeated load triaxial test apparatus involving the use of an identical set of stresses are shown in Figures 8.7 to 8.10.

The scatter of results shown in the figures were considered acceptable when compared with others (Pappin, 1979) which involved up to 5 replicate tests using one piece of test apparatus. More consistent results were obtained for permanent axial strain than for horizontal strain which, for tests carried out in the triaxial test apparatus, is defined as twice the permanent radial strain. For the latter strain, although the pattern of strain development in tests carried out in both apparatus was very much the same, the strain magnitudes obtained from the HCA were found to be much higher.

A comparison of $(\varepsilon_v)_p$ and $(\varepsilon_{max})_p$ from the HCA tests number 5 and 8 and the two tests performed with the repeated load triaxial test apparatus are shown in Figure 8.11 and 8.12 respectively. Both the HCA tests were performed under the condition with uni-directional shear reversal and both repeated load triaxial tests involved an identical $(q/p)_{max}$ value as those used in the HCA tests.The comparison indicates that the permanent strain behaviour of the granular material under the condition simulated by the HCA with the particular magnitude of reversed shear stresses is, by and large, similar to that obtained by the repeated load triaxial test apparatus.

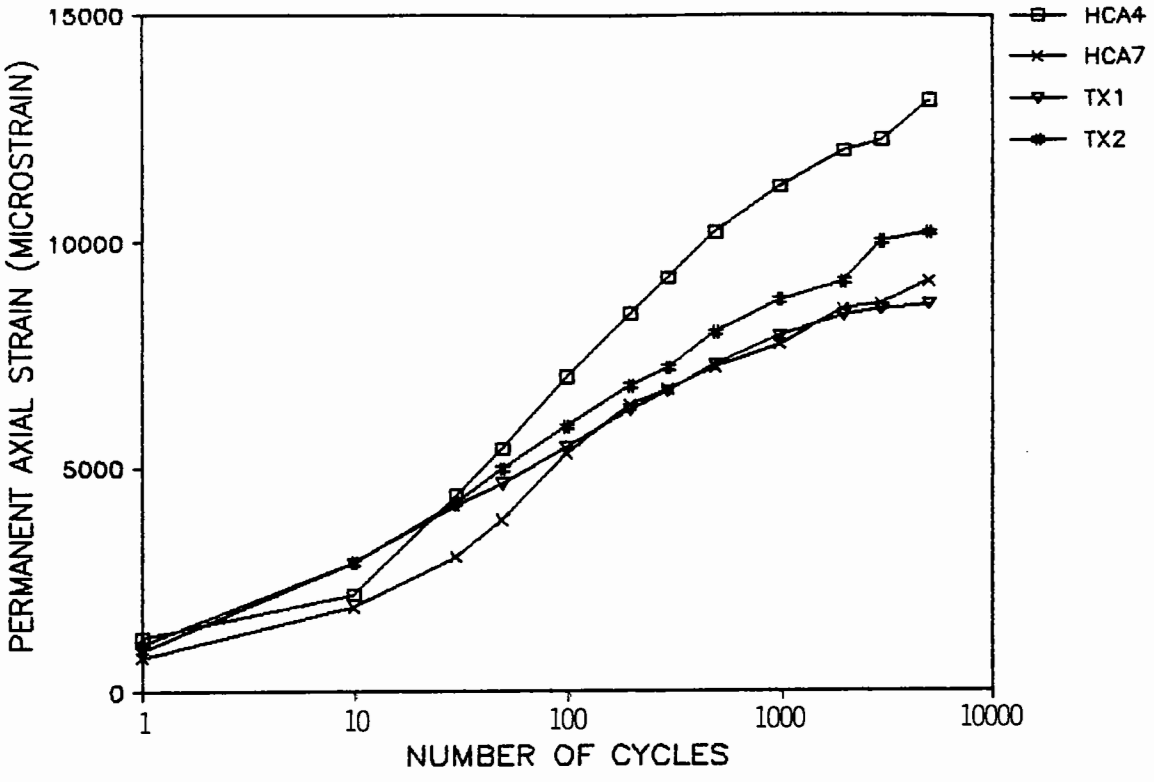

Figure 8.7 Comparison between Permanent Axial Strains obtained under identical Stress Conditions from the Repeated Load Triaxial and Hollow Cylinder Test Apparatus.

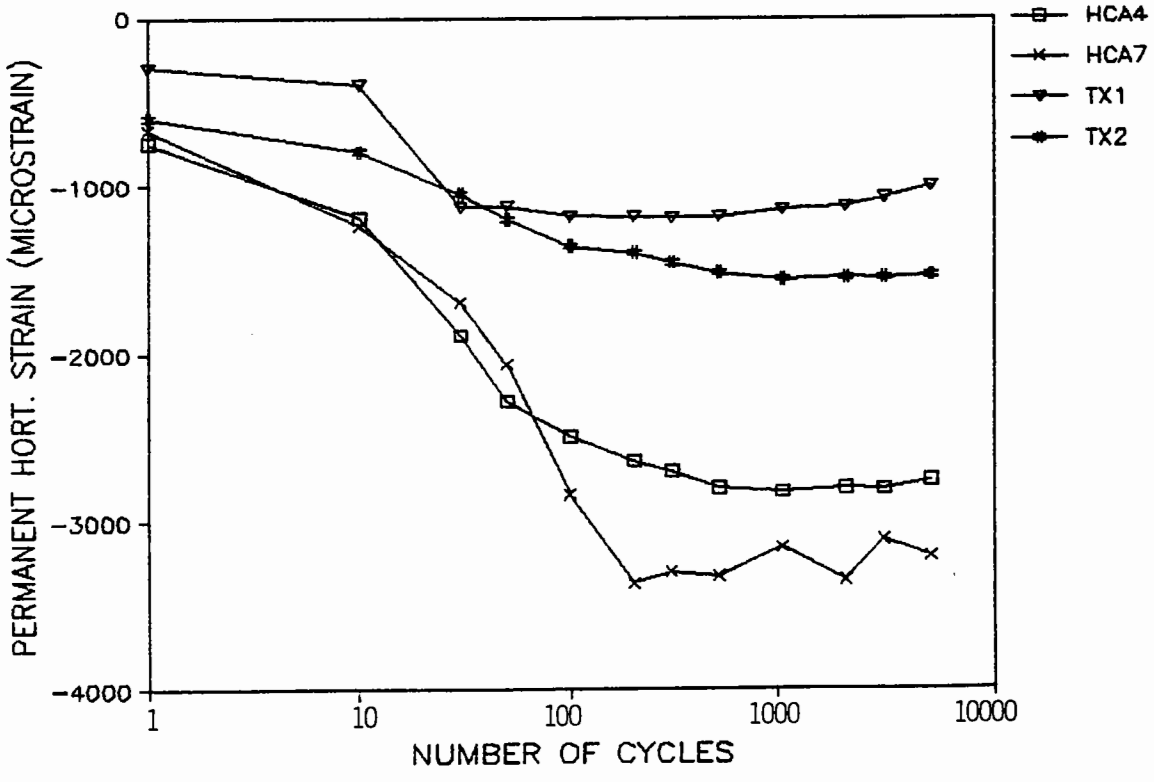

Figure 8.8 Comparison between Permanent Horizontal (Sum of Radial and Circumferential) Strains obtained under identical Stress Conditions from the Repeated Load Triaxial and Hollow Cylinder Test Apparatus.

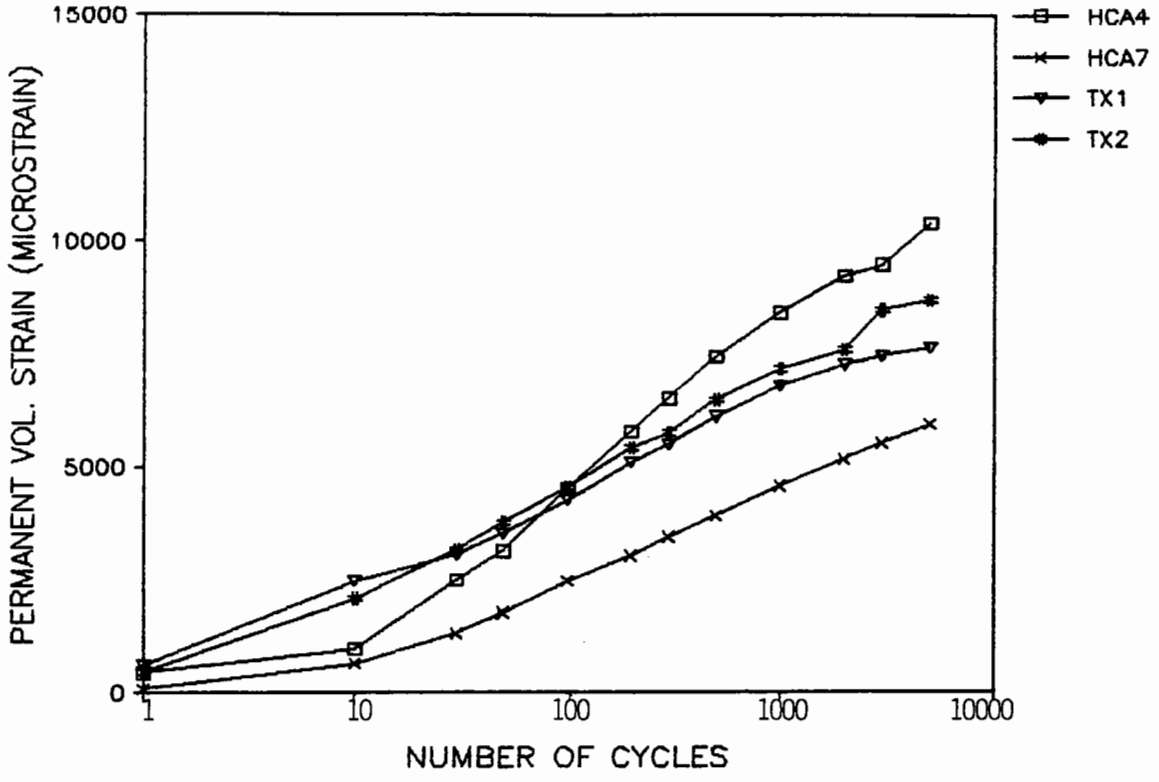

Figure 8.9 Comparison between Permanent Volumetric Strains obtained under the identical Conditions from the Repeated Load Triaxial and Hollow Cylinder Test Apparatus.

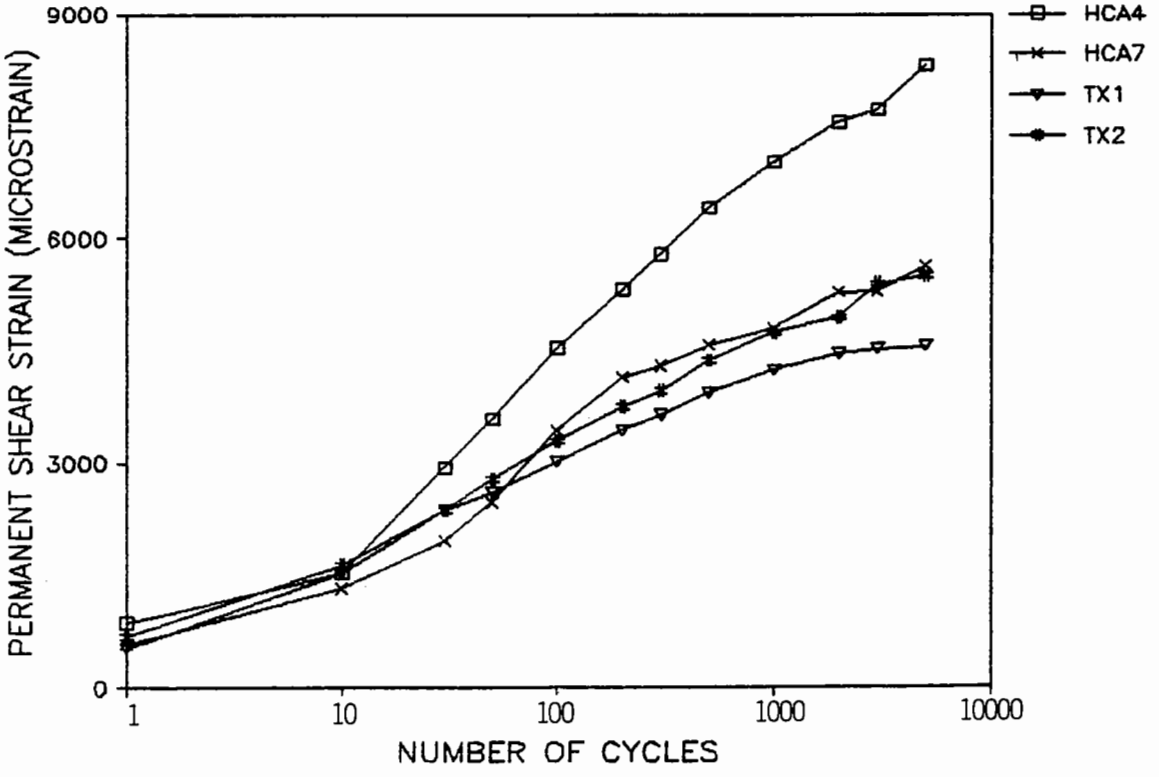

Figure 8.10 Comparison between Permanent Shear Strains obtained under identical Stress Conditions from the Repeated Load Triaxial and Hollow Cylinder Test Apparatus.

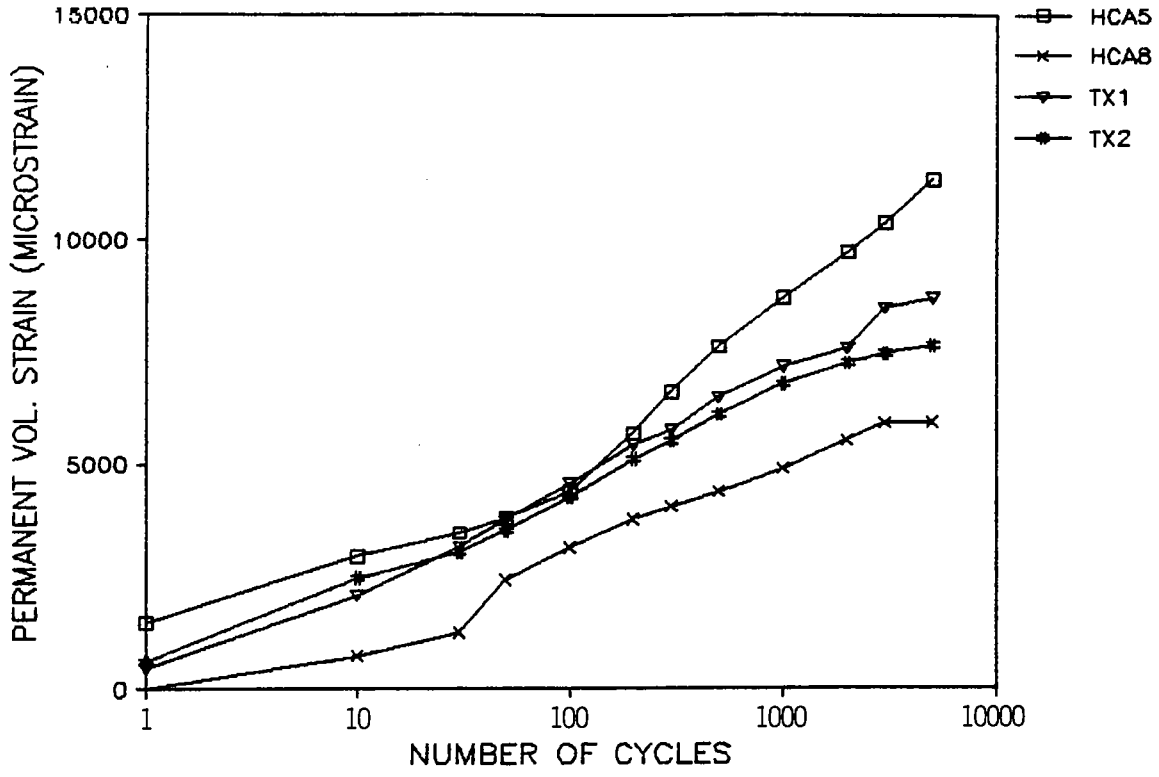

Figure 8.11 Comparison between Permanent Volumetric Strains obtained under identical $(q/p)_{max}$ from Repeated Load Triaxial Tests and Repeated Load Hollow Cylinder Tests with Uni-directional Shear Reversal.

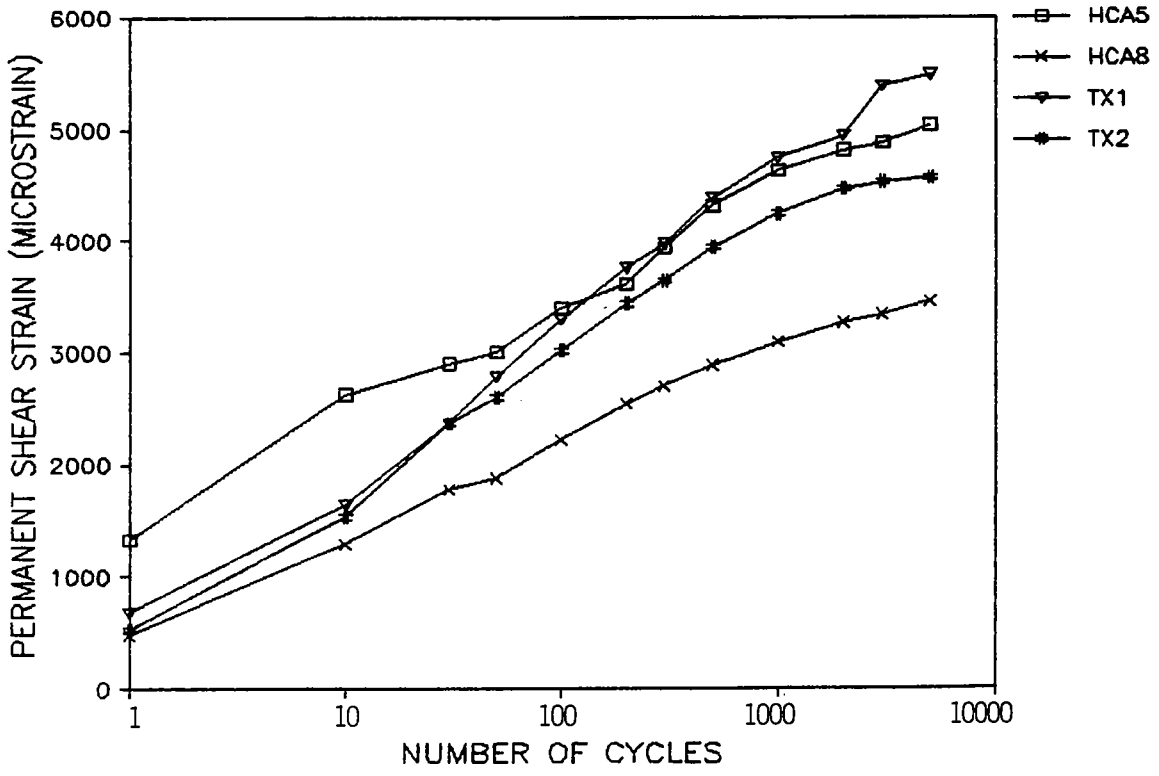

Figure 8.12 Comparison between Permanent Shear Strains obtained under identical $(q/p)_{max}$ from Repeated Load Triaxial Tests and Repeated Load Hollow Cylinder Tests with Uni-directional Shear Reversal.

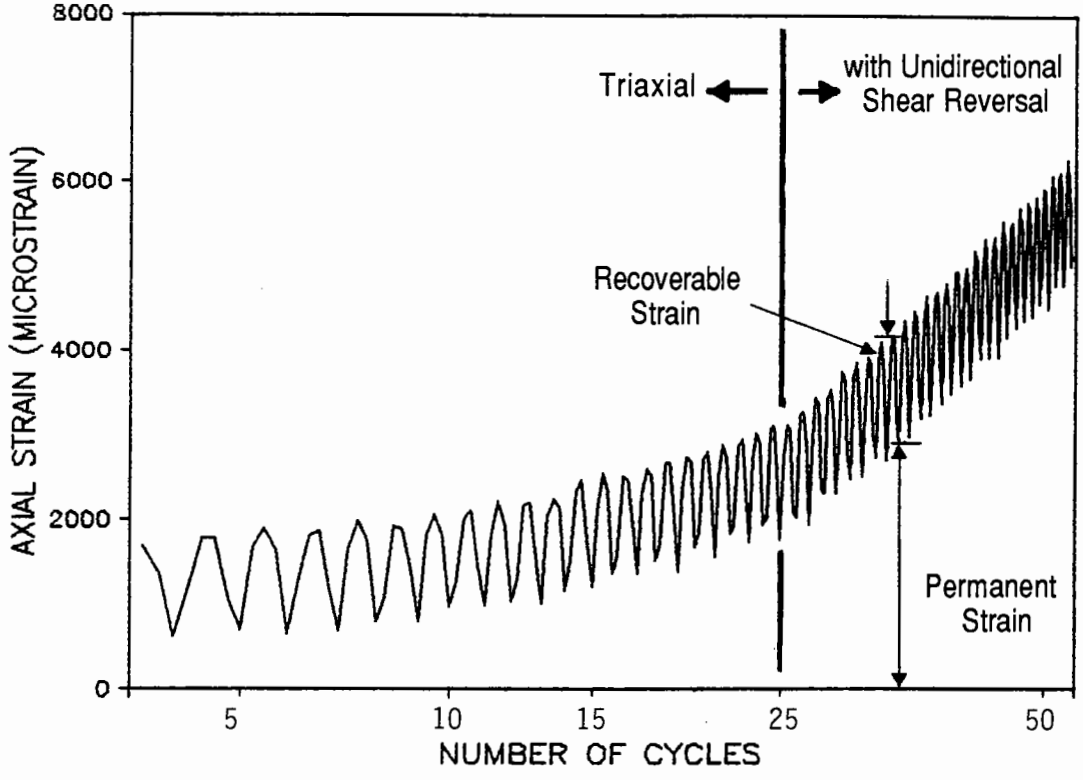

Figure 8.13 Variation of Axial Strain with Number of Stress Cycles in a 50-Cycle Test with Reversed Shear Stresses applied at the 25th Cycle.

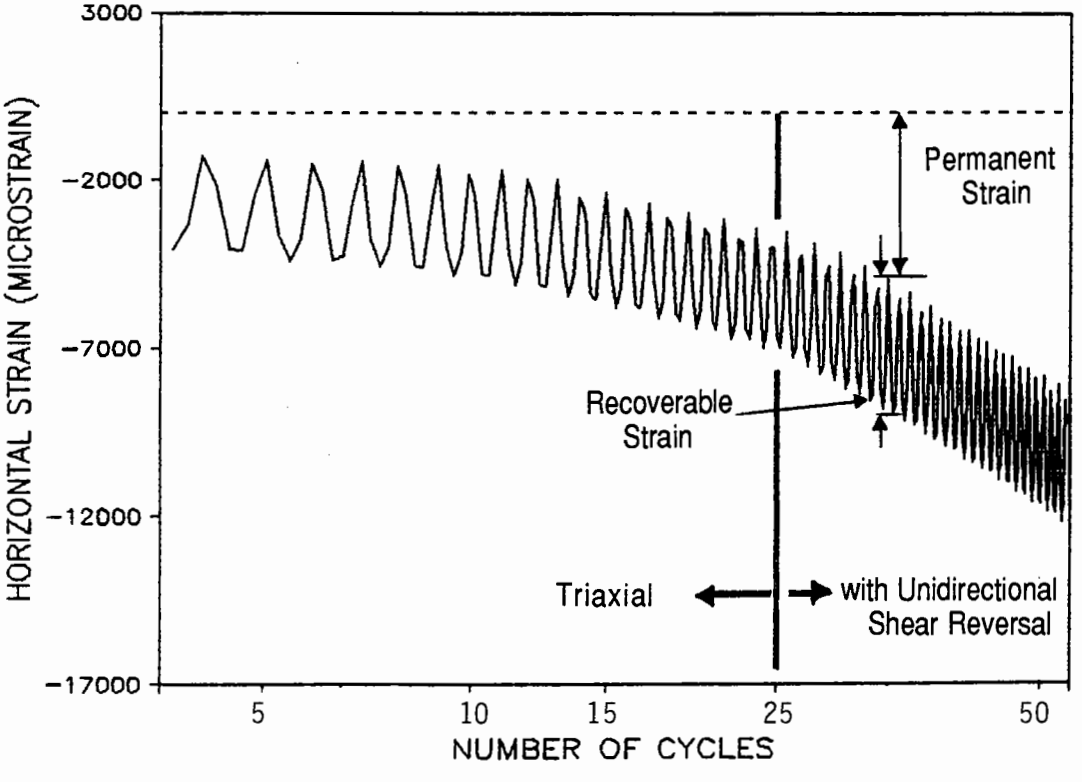

Figure 8.14 Variation of Horizontal (Sum of Radial and Circumferential) Strain with Number of Stress Cycles in a 50-Cycle Test with Reversed Shear Stresses applied at the 25th Cycle.

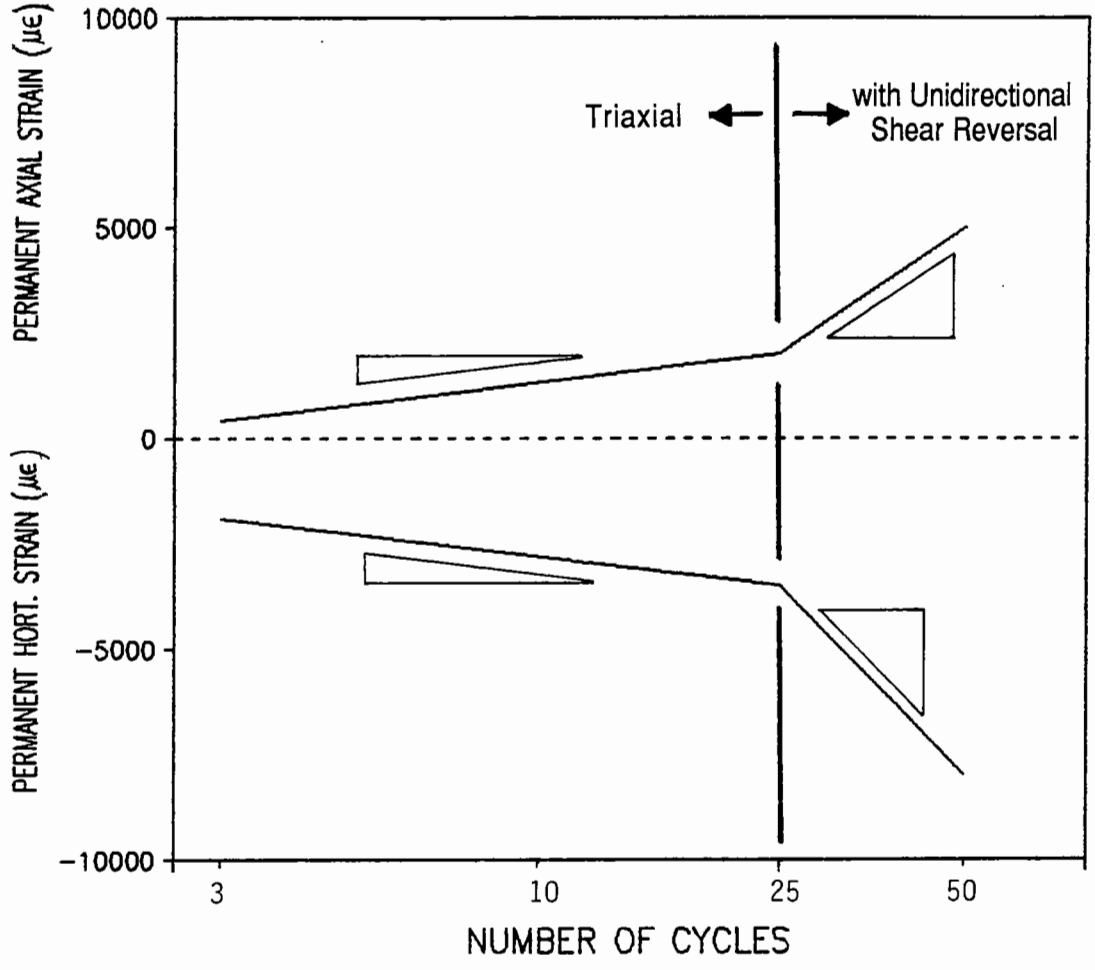

Figure 8.15 Simplified Plot of Variation of Permanent Strains with Number of Cycles showing the corresponding Strain Rates.

8.3 50 - CYCLE TESTS

Since the stress-strain behaviour of the hollow cylinder specimen was continuously monitored during the 50-cycle tests, the average number of data points recorded per cycle was reduced to five. As a result, some peaks and troughs of the stress and strain waveforms could not be captured. However, it was believed that the overall rate of permanent strain development during the two parts of each test was satisfactorily obtained for comparison purpose.

Figures 8.13 and 8.14 illustrates one of the results obtained from a 50-cycle test. In these figures, the variation of strain, including both the recoverable and non-recoverable components, with the logarithm of the number of cycles for the two parts of the test is shown. Figure 8.13 indicates that the accumulated permanent axial strain varies approximately linearly with the logarithm of the number of cycles within both parts of the test but at different rates under the two different stress conditions. This behaviour was also observed for the permanent horizontal strain, as shown in Figure 8.14, although the behaviour was generally dilatant. Simplified plots to illustrate these results are shown in Figure 8.15 in which the vertical axis represents only permanent strain and the slopes for the two parts of the test are highlighted. Similarly, the slopes for the permanent volumetric and maximum shear strain could be calculated.

A summary of these slopes, or rate of permanent strain development for the seven 50-cycle tests is shown in Table 8.1. All positive rate values represent a tendency to develop compressive strain while the negative ones indicate dilatancy. When these results were analyzed, emphasis was placed on the comparison of strain rates obtained within one test. The use of an individual strain rate for general comparison purposes may be misleading because of the likely strain history effect on the particular rate value. Examples can be found from the results for test numbers 2 and 6. The strain rates

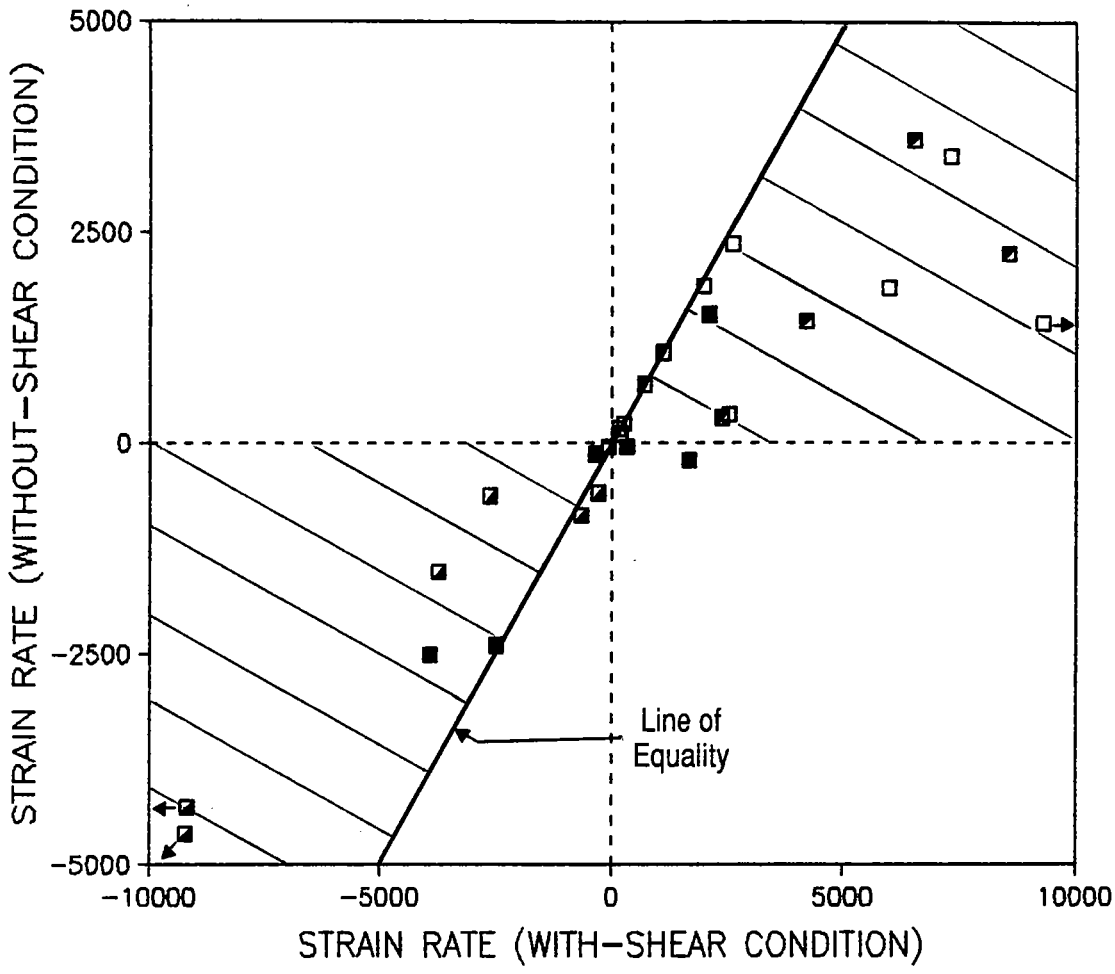

Symbol	Component of Strain
□	Axial
◪	Horizontal
■	Volumetric
◪	Maximum Shear
▨	Region where (strain rate) $_{\text{with shear}}$ > (strain rate)$_{\text{without shear}}$

Figure 8.16 Comparison of Rates of Permanent Strain.

Table 8.1

Summary of Permanent Strain Rates in 50 Cycle Tests

Test Number	*Axial Strain*		*Horizontal Strain*		*Volumetric Strain*		*Shear Strain*	
	w/Shear	*No/Shear*	*w/Shear*	*No/Shear*	*w/Shear*	*No/Shear*	*w/Shear*	*No/Shear*
1	2600	2352	-300	-600	2100	1520	1100	1071
2	264	220	-76	-50	190	100	150	165
3	2530	334	-2616	-630	-346	-134	2375	289
4	5964	1832	-3737	-1532	1667	-209	4198	1443
5	10740	1471	-15226	-4712	-3924	-2513	8537	2242
6	1975	1859	-667	-860	325	-50	715	689
7	7291	3388	-14176	-9956	-2480	-2400	6501	3580

obtained in these tests were generally very low despite an increased stress ratio $(q/p)_{max}$ (see Table 7.2).

A plot of the permanent strain rates obtained from stress conditions with uni-directional shear reversal against those from triaxial (no shear) conditions is shown in Figure 8.16. The plot contains values from the four strain components.

Figure 8.16 indicates that most data points lie well within the region where the absolute value of the permanent strain rate obtained under the condition with shear reversal is higher than that under triaxial condition. Note that the data points include results involving the two test sequences described in Table 7.2. Therefore, any possible strain history caused by the first 25 cycles of stress are considered in the comparison.

In Figure 8.16, the horizontal distance between the data points and the line of equality represents the difference between the two strain rates. It can be seen that, generally, large differences were obtained for both the permanent axial and horizontal strain rates. The change in strain rate for the permanent shear strain is somewhat smaller. The least difference in strain rate between the "with-" and "without-" reversed shear condition was that for the permanent volumetric strain. This is due largely to the fact that the signs for the permanent axial and horizontal strains are opposite. Hence, when their summation was performed to obtain the permanent volumetric strain, the effect due to the reversed shear stresses was significantly reduced. None the less, it is worth noting that in tests number 4 and 6, the permanent volumetric strain changed from dilatant when under triaxial condition to compressive when reversed shear stresses were applied (see Table 8.1).

8.4 RESILIENT STRAIN TESTS

8.4.1 Resilient Behaviour during Permanent Strain Tests

The resilient behaviour of the granular material during the permanent strain tests was continuously monitored. Comparisons of the resilient volumetric and maximum shear strains obtained during the nine tests are shown in Figures 8.17 and 8.18 respectively. All the strains were caused by the same stress conditions which were used for the particular permanent strain test. The comparisons generally indicate that the application of a reversed shear stress, either uni- or bi-directional, does not result in significant changes in the resilient behaviour of the material. The only exception occurred, again, in the resilient volumetric strain of the first specimen of the first series (Figure 8.17a)

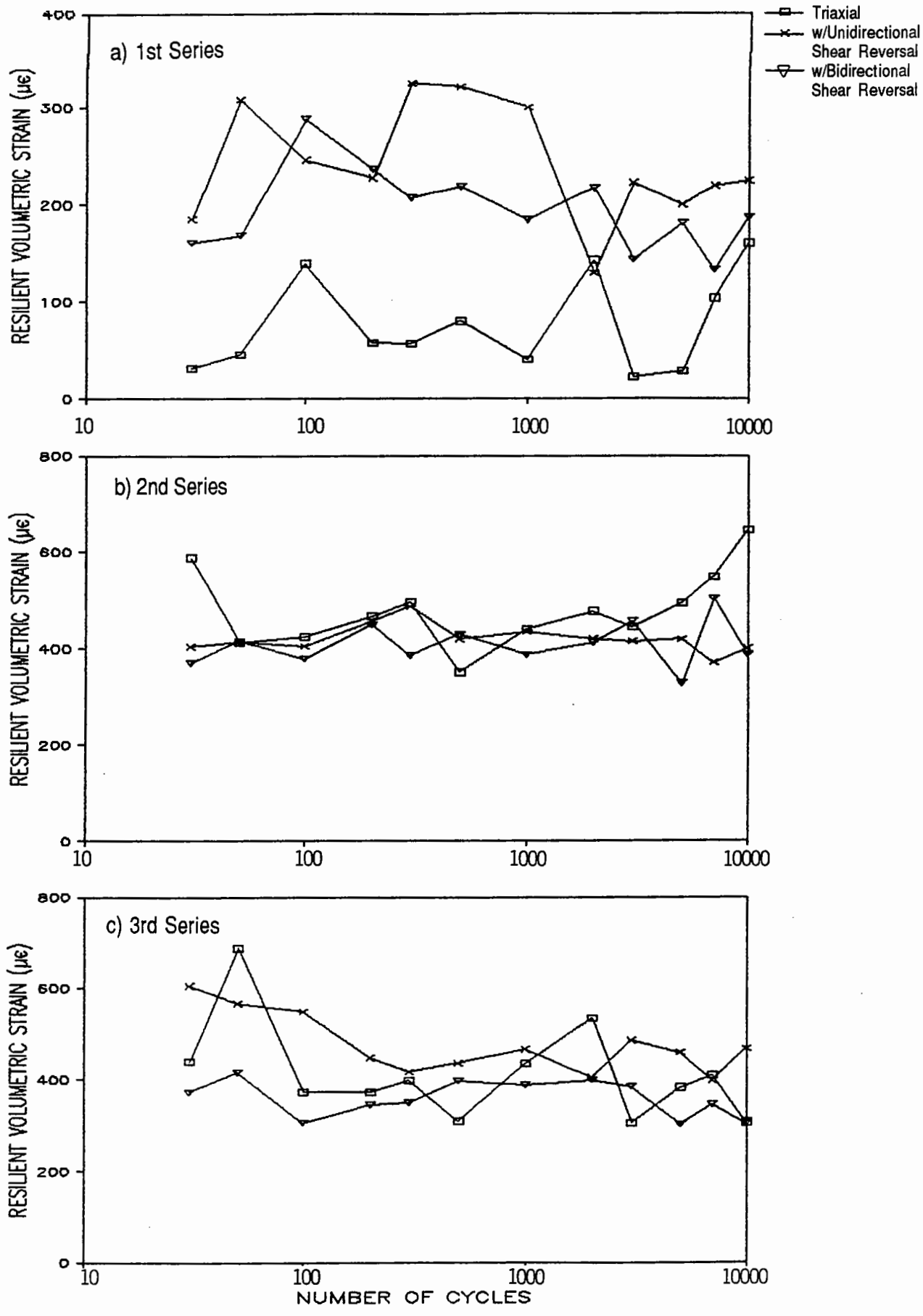

Figure 8.17 Variation of Resilient Volumetric Strains with Number of Stress Cycles in all Series of Permanent Strain Tests.

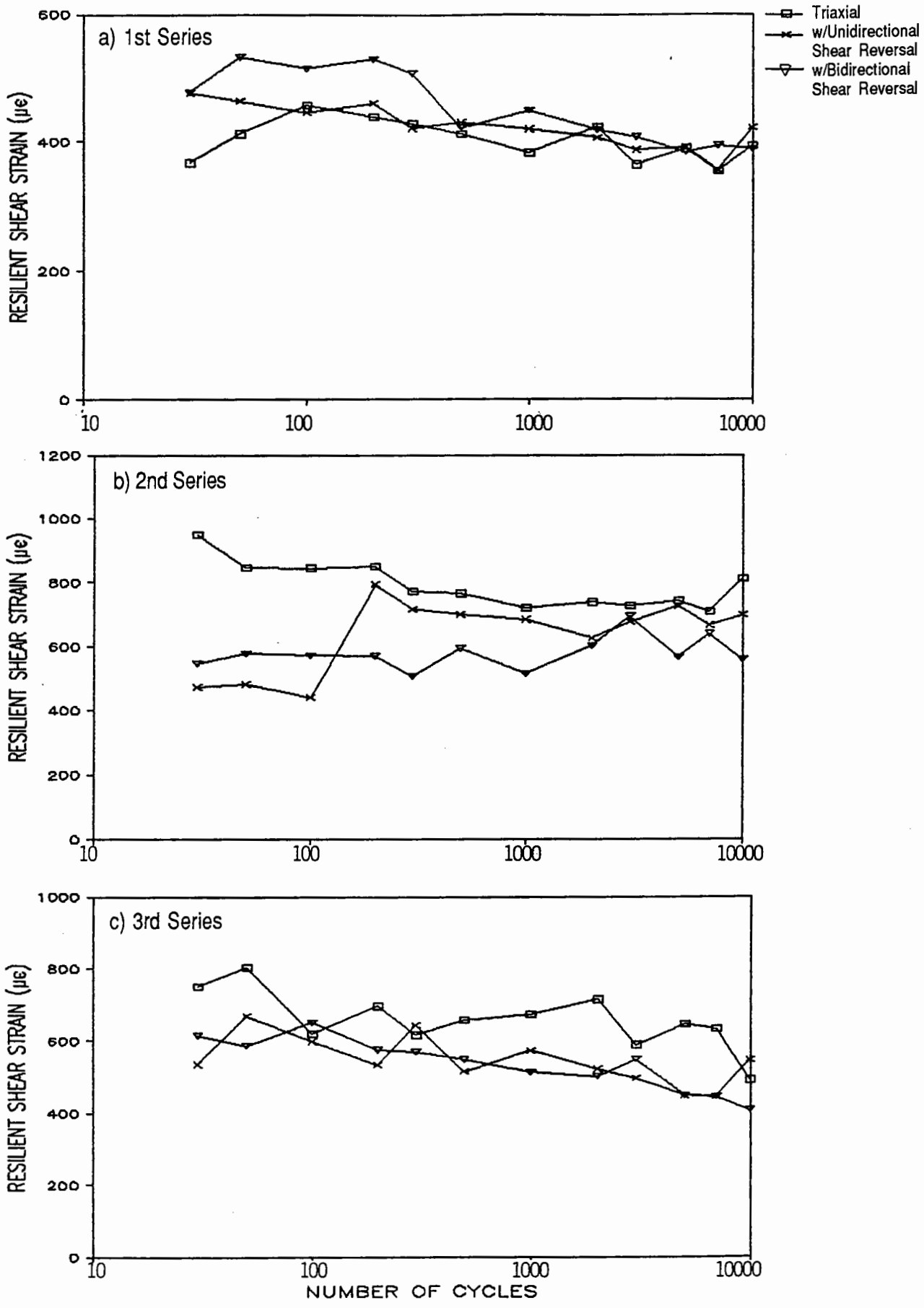

Figure 8.18 Variation of Resilient Maximum Shear Strains with Number of Stress Cycles in all Series of Permanent Strain Tests.

which may have undergone some degree of strengthening due to previous straining. However, the overall results also indicate a gradual decrease in resilient strains as permanent strains build up.

8.4.2 Resilient Behaviour under Wide Range of Stress Conditions

While Figures 8.17 and 8.18 only show the influence due to reversed shear stresses, more results were obtained from resilient strain tests performed on a separate hollow cylinder and one triaxial specimen. These tests covered a large number of stress paths which included variations in the angle of principle plane rotation and the intermediate principal stress. A summary of the results of these tests are presented in Appendix E.

For each stress path used in a resilient strain test, at least 50 cycles of stress were applied before the first set of strain responses was recorded. A duplicate set of results was taken after another 20 to 30 cycles (time required for the first set of data to be processed). The average of the two sets of results was then used for analysis. Since only one cycle of stresses and strains was normally recorded for each stress path used in a resilient strain test, it was possible to record 50 data points for each component of stress and strain.

8.4.2.1 Results of Tests carried out in the Repeated Load Triaxial Test Apparatus

Both the average resilient axial and radial strains were measured during the tests which involved the use of 19 stress paths. However, strains are more appropriately expressed

in terms of the shear and volumetric invariants, $(\varepsilon_s)_r$ and $(\varepsilon_v)_r$, which in triaxial conditions are defined as:-

$$(\varepsilon_s)_r = \frac{2}{3}(\varepsilon_1 - \varepsilon_3) \tag{8.1}$$

$$(\varepsilon_v)_r = \varepsilon_1 + 2\varepsilon_3 \tag{8.2}$$

where ε_1 and ε_3 are resilient principal strains.

In order to summarise the stress-strain relationships of the granular materials tested, the mathematical contour model proposed by Pappin (1980) and modified by Jouve et al (1987) was used. The model involves use of the following equations:-

$$G = \frac{q}{3(\varepsilon_s)_r} \tag{8.3}$$

$$G = G_1 p^{(1-m)} \tag{8.4}$$

$$K = \frac{p}{(\varepsilon_v)_r} \tag{8.5}$$

$$K = \frac{K_1 p^{(1-n)}}{\left\{1 - \beta \left(\frac{q}{p}\right)^2\right\}} \tag{8.6}$$

where q, p, $(\varepsilon_s)_r$ and $(\varepsilon_v)_r$ are as defined earlier.
G is the resilient shear modulus
G_1 and m are the shear strain coefficients
K is the resilient bulk modulus
K_1, n and β are the volumetric strain coefficients

A multiple regression analysis was carried out to determine the coefficients used in equations 8.4 and 8.6. The best fit values thus obtained are shown as follows:

G1= 1282 m= 0.20

K1= 1596 n= 0.33 β= 0.08

where G1 and K1 are in kPa and the strains calculated are in fractions.

Plots of the resilient volumetric and shear strains calculated using the above coefficients against their measured values are shown in Figures 8.19 and 8.20 respectively. For the resilient shear strain, a correlation coefficient, R^2, of 0.96 was obtained. For the resilient volumetric strain, R^2, was 0.95. The overall high R^2 values confirmed that the contour model was able to predict the resilient behaviour of the granular material tested by the repeated load triaxial apparatus.

8.4.2.2 Results of Repeated Load Hollow Cylinder Tests

Triaxial Stress Paths

Prior to the analysis of the cases involving principal plane rotation, it appeared to be appropriate to consider the stress-strain behaviour of the hollow cylinder specimens tested under triaxial stress conditions. To do this, the same contour model described in the last section (8.4.2.1) was used. In order to allow direct comparison of the coefficients which governed the resilient shear modulus, the shear strain as defined in equation 8.1 was used. The principal values involved in the equation were in turn calculated using equations 6.22 and 6.23. For the evaluation of bulk modulus, the volumetric strain as defined in equation 6.27 was used.

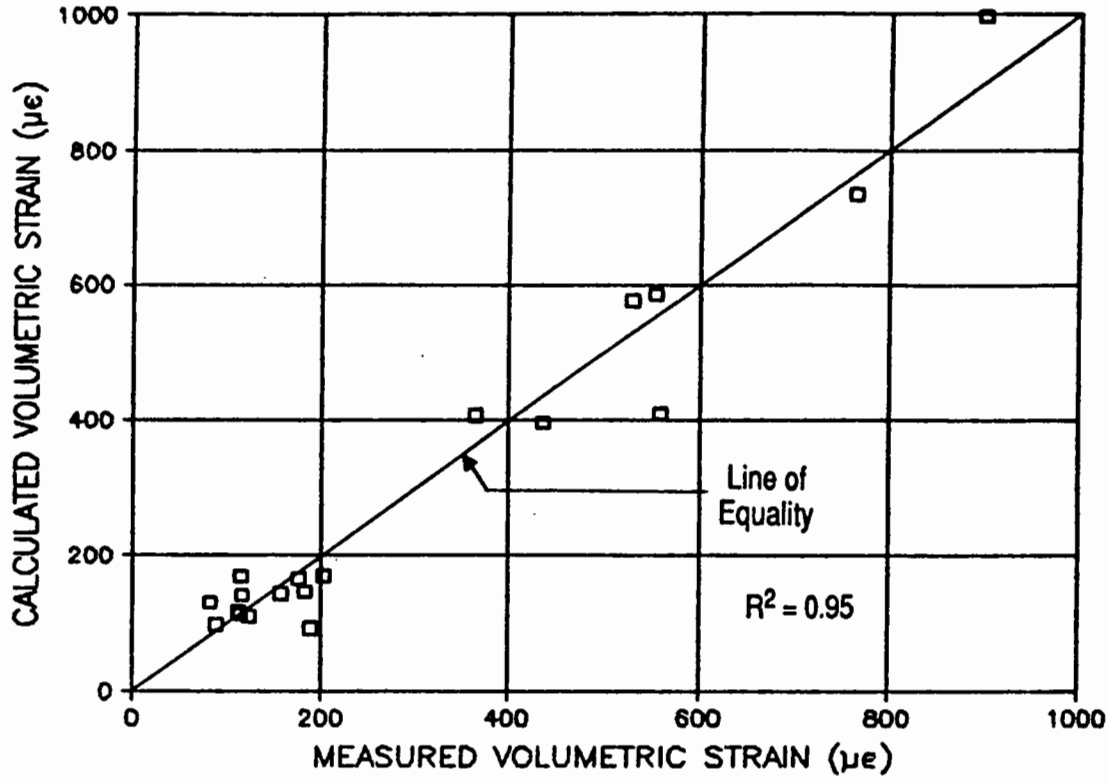

Figure 8.19 Comparison of Predicted and Measured Resilient Volumetric Strain from Repeated Load Triaxial Tests.

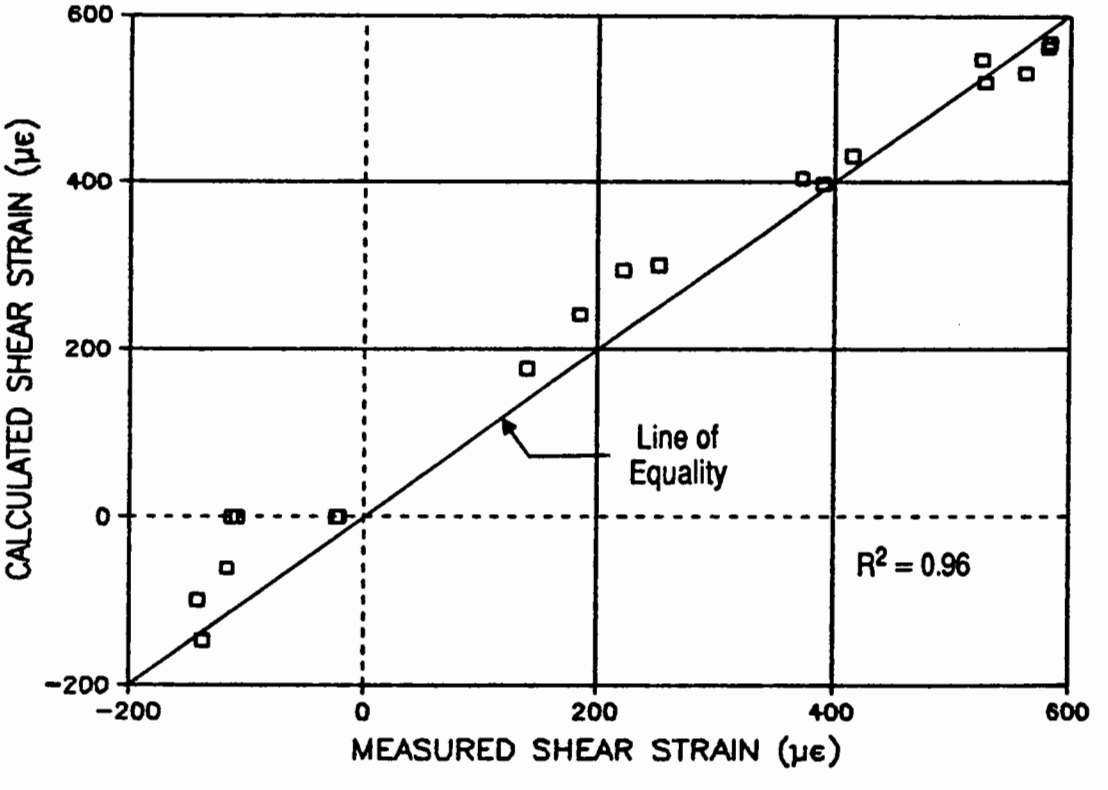

Figure 8.20 Comparison of Predicted and Measured Resilient Shear Strain from Repeated Load Triaxial Tests.

A total of 23 triaxial stress paths were used in the resilient strain tests performed by means of the HCA. A multiple regression analysis performed on the results of these tests yielded the following results:

G1 = 994	m = 0.20	
K1 = 809	n = 0.33	$\beta = 0.08$

where G1 and K1 are in kPa and the strains calculated are in fraction.

Plot of the calculated resilient volumetric and shear strains against their measured values are shown in Figure 8.21 and 8.22 respectively. The R^2 value for the resilient shear strain is again very high but that for the volumetric strain is very much reduced. However, it is worth noting that the best fit values for the coefficients m,n and β which were obtained independently by means of the multiple regression analysis are all the same as those obtained from tests using the repeated load triaxial apparatus. This indicates that both pieces of laboratory devices are consistent in determining the non-linear and stress-dependent components of the behaviour model used. However, for the remaining constants, K1 and G1, they were found to be respectively 97% and 29% less than their counterparts obtained from the triaxial test apparatus.

Stress Paths involving Principle Plane Rotation

In order to model the behaviour of granular material under rotating principal stresses, it is vital to know the directions of the strain change. In traditional material science

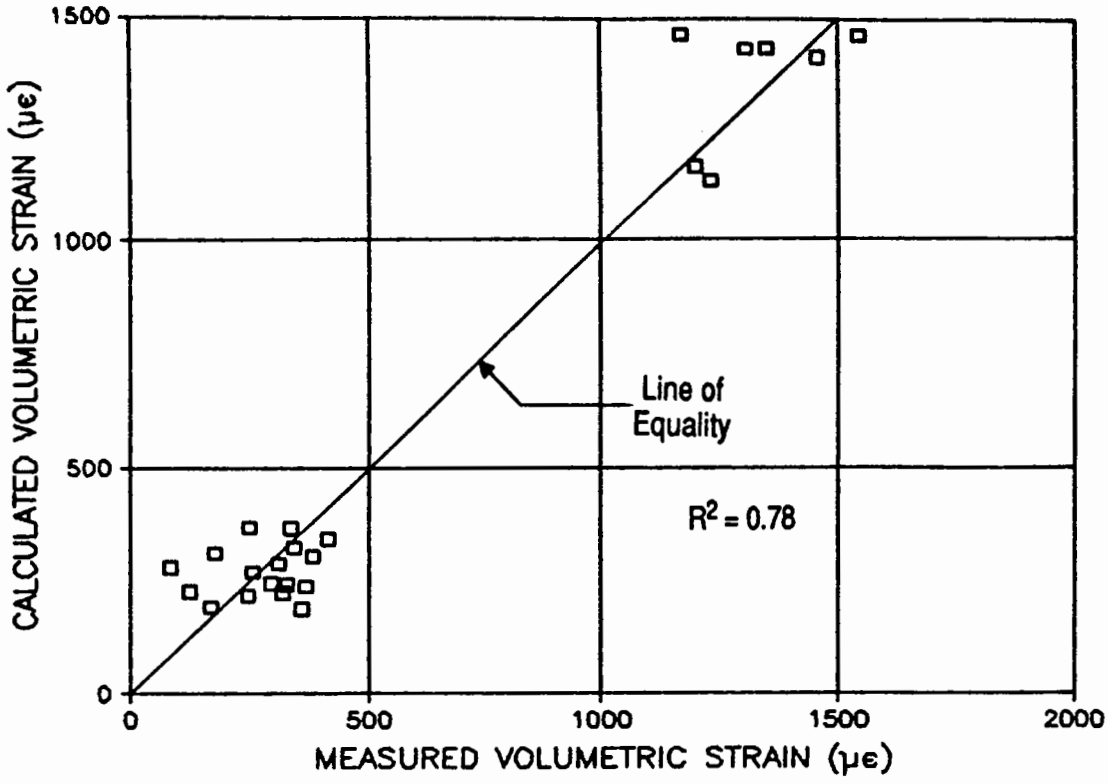

Figure 8.21 Comparison of Predicted and Measured Resilient Volumetric Strain from Repeated Load Hollow Cylinder Tests under Triaxial Stress Conditions.

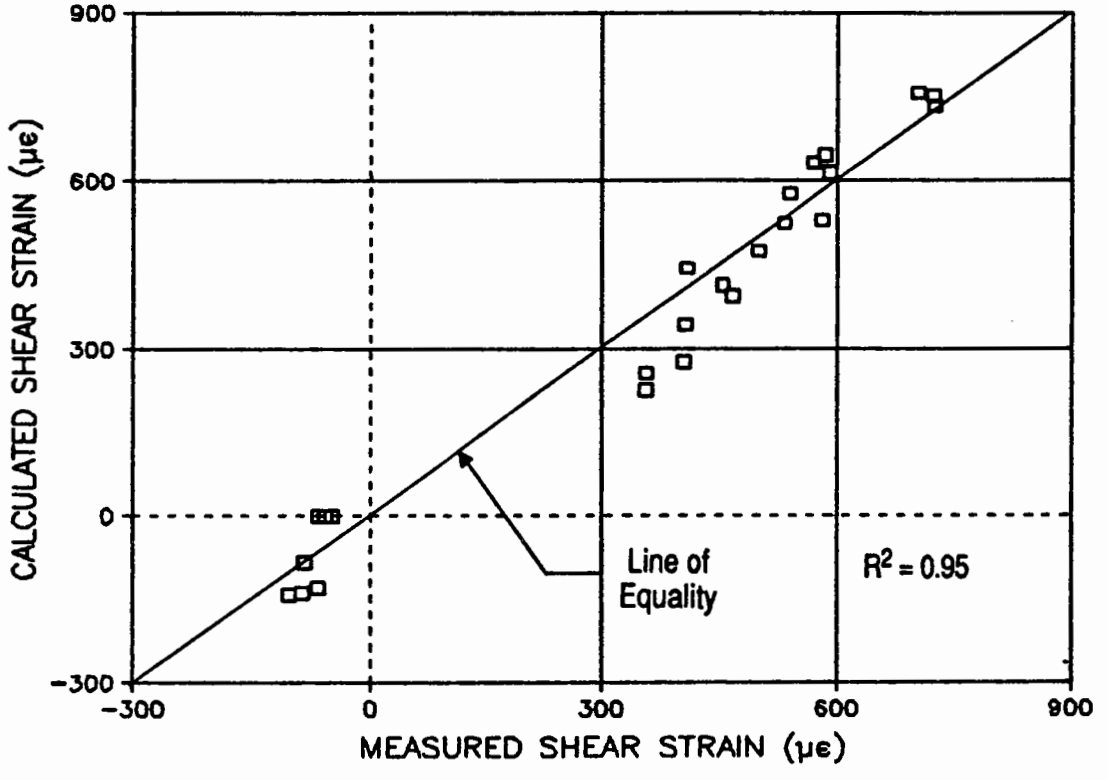

Figure 8.22 Comparison of Predicted and Measured Resilient Shear Strain from Repeated Load Hollow Cylinder Tests under Triaxial Stress Conditions.

theories, the general assumption is that during elastic behaviour, the directions of principal stress and strain coincide. In this project, this assumption was examined first.

Figures 8.23 to 8.26 show the variation in the angles of major principal stress and strain (from the vertical direction) with time during one cycle of loading. The figures embrace the results from four different stress paths involving different modes of stress and strain rotation. The data shown in the figures were calculated from measured responses which were not electronically or mathematically filtered. As a result, they are subjected to errors due to electrical "noise" and other interference in the measuring system. Despite this, they indicate that the rotations of major principal stress and strain are generally coincident.

This finding is particularly encouraging as it suggests that there is no need for a stress-strain model to consider the additional relationship between the direction of stress and strain. As a result, the use of an invariant approach, such as the contour model, to represent the general stress and strain conditions may still be considered appropriate. However, in doing so, the angle of principal plane rotation, α and possibly, the b-value which is used to characterize the intermediate principal stress, may need to be included.

The development of a resilient stress-strain models under general stress conditions is beyond the scope of this project. Therefore, the investigation performed here is only limited. The analysis consisted of using the contour model and the coefficients established earlier for the triaxial conditions to predict the resilient strains under the new and more complex stress conditions which involved principal plane rotation. In the prediction calculation, only principal stresses and strains were used. The applicability of the model was then evaluated by determining how well strains could be predicted.

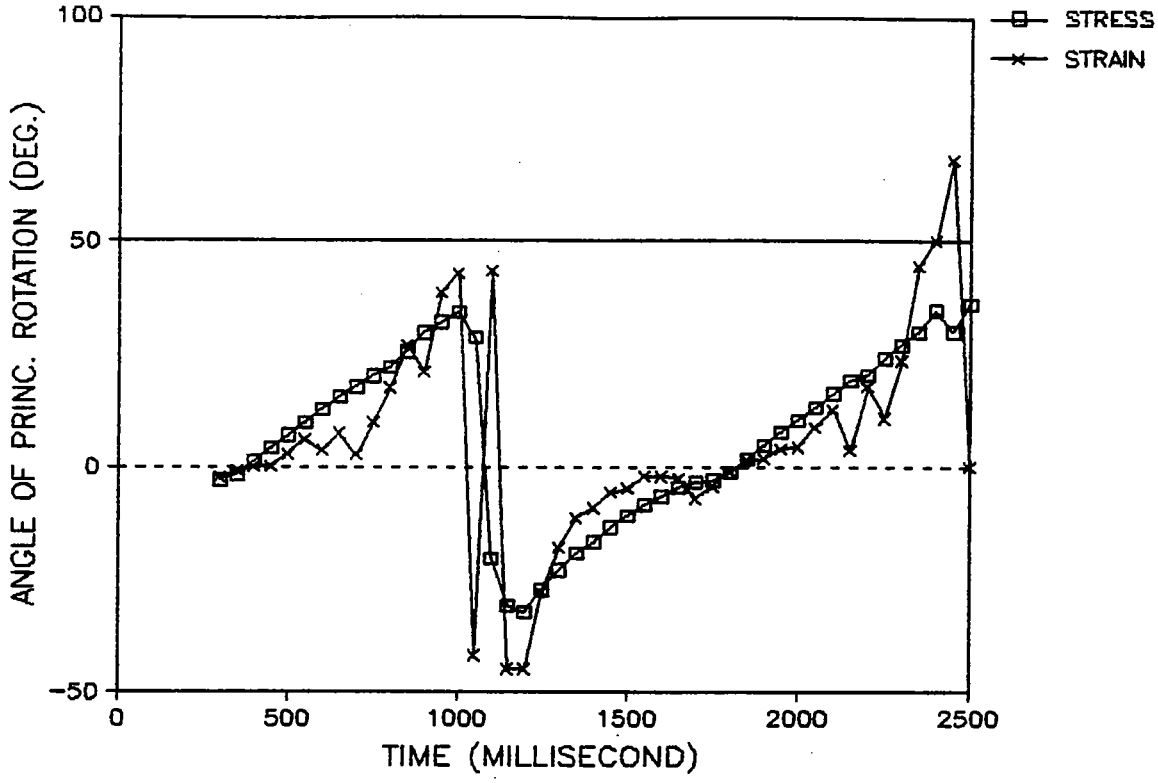

Figure 8.23 Relationship between Rotation of Principal Stress and Strain Planes (when Pi =Po= 100 kPa; σ_z varies from 100 to 250 kPa; $\tau_{z\theta}$ varies from -22 to 22 kPa and the phase angle shift between σ_z and $\tau_{z\theta}$ is +90°).

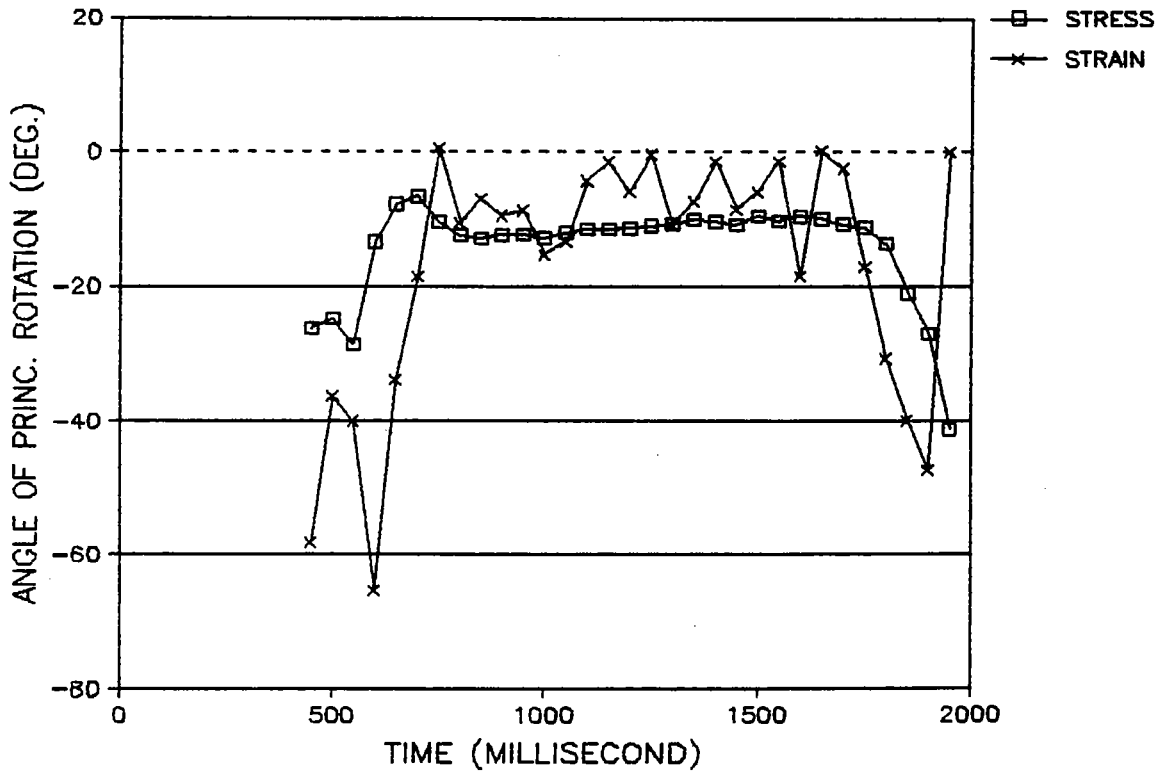

Figure 8.24 Relationship between Rotation of Principal Stress and Strain Planes (when Pi =Po= 100 kPa; σ_z varies from 100 to 200 kPa; $\tau_{z\theta}$ varies from 0 to 20 kPa and the phase angle shift between σ_z and $\tau_{z\theta}$ is 0°).

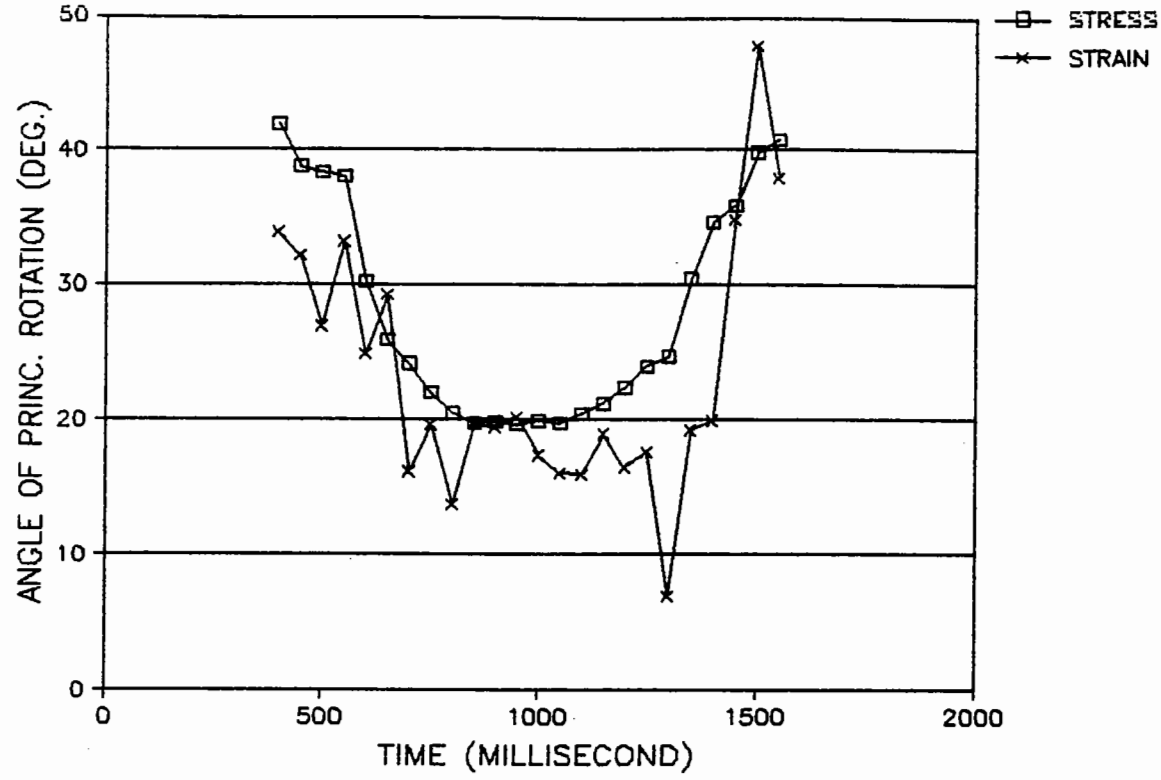

Figure 8.25 Relationship between Rotation of Principal Stress and Strain Planes(when Pi =Po= 100 kPa; σ_z varies from 100 to 150 kPa; $\tau_{z\theta}$ = 20 kPa)

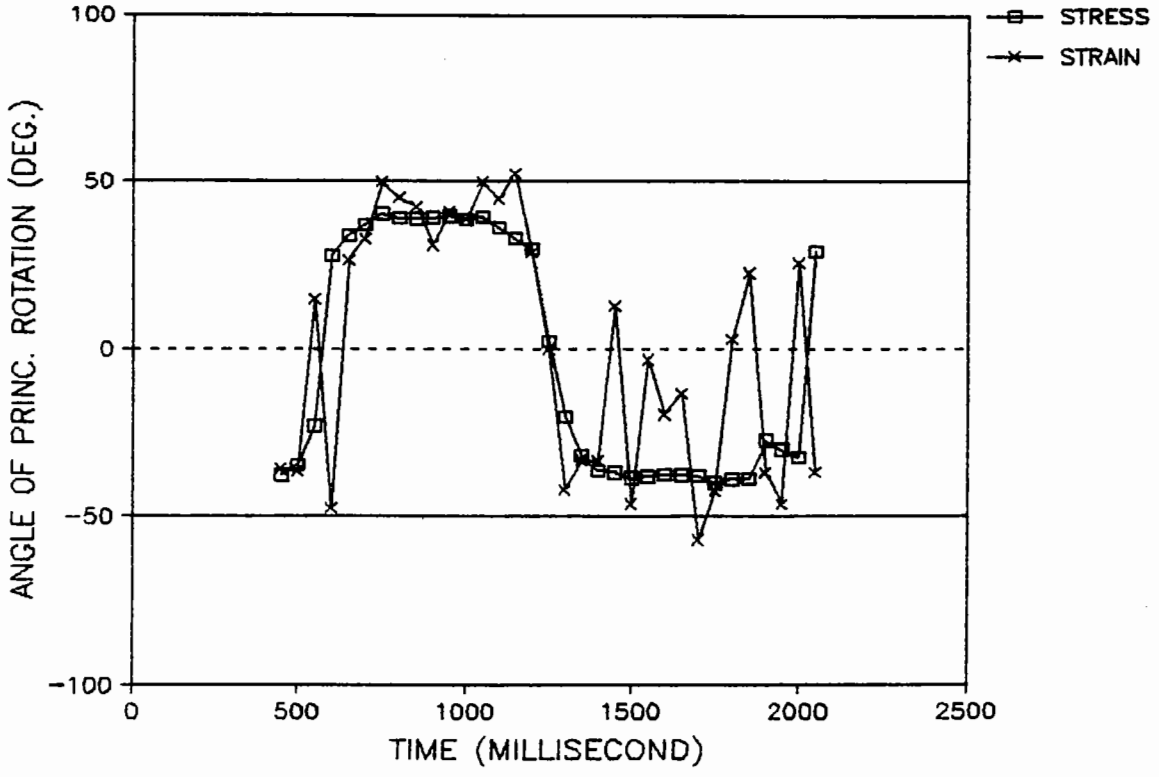

Figure 8.26 Relationship between Rotation of Principal Stress and Strain Planes(when Pi =Po= 100 kPa; σ_z =100 kPa; $\tau_{z\theta}$ varies from +20 to -20 kPa)

As shown in Figure 8.27, the correlation between the predicted and measured resilient shear strains for the 133 stress paths which were used is generally very good with R^2 equal to 0.93. This indicates that principal plane rotation, which is not represented in the stress-strain model does not have much influence on the shear behaviour. The results also show that, for the stress conditions analyzed which cover a wide range of b values (see Figure E1.2,Appendix E), the effect of the intermediate principal stress, σ_2, can be satisfactorily represented by the stress invariant p. It is worth noting that better correlation is generally obtained when the strain is positive than negative.

To calculate resilient volumetric strain, the invariant for shear stress, q in equation 8.6 was replaced, more appropriately, by the octahedral value, q_{oct}. This also necessitates the correction of the β value in the equation. A plot of the calculated and measured strains is shown in Figure 8.28. Although a general trend towards equality was observed, considerable scatter of results and a marked drop in the degree of correlation were obtained. In order to investigate the discrepancy, the value, $\delta\varepsilon_v$ defined as:

$$\delta\varepsilon_v = \varepsilon_{v_{(measured)}} - \varepsilon_{v_{(predicted)}} \qquad (8.7)$$

was singled out for further analysis.

Figure 8.29 shows a plot of $\delta\varepsilon_v$ against $\delta\tau/p_m$ which represents the change of torsional shear stress normalized by the mean p value, p_m. A similar plot of $\delta\varepsilon_v$ against $\delta b/\eta_m$ which represents the change in b value normalized by the mean shear stress ratio, $(q_{oct})_m/p_m$, is shown in Figure 8.30. These normalized parameters were chosen simply because they fulfilled the vital requirement of being dimensionless and were able to represent respectively, the effect of principal plane rotation and the variation in intermediate principal stress. Furthermore, both parameters include the mean normal stress value, p and shear stresses, in the form of either τ or q_{oct}, which are of fundamental importance in the strain behaviour of granular materials. Hence, they both

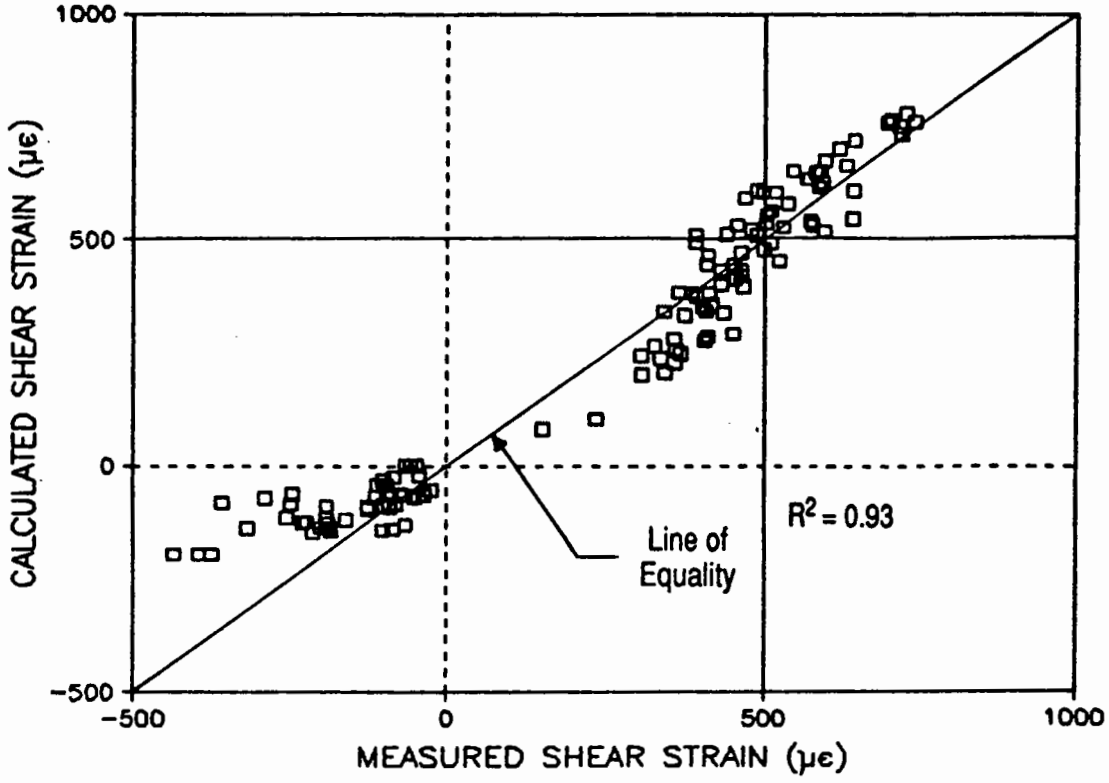

Figure 8.27 Comparison of Predicted and Measured Resilient Shear Strain from Repeated Load Hollow Cylinder Tests under General Stress Conditions.

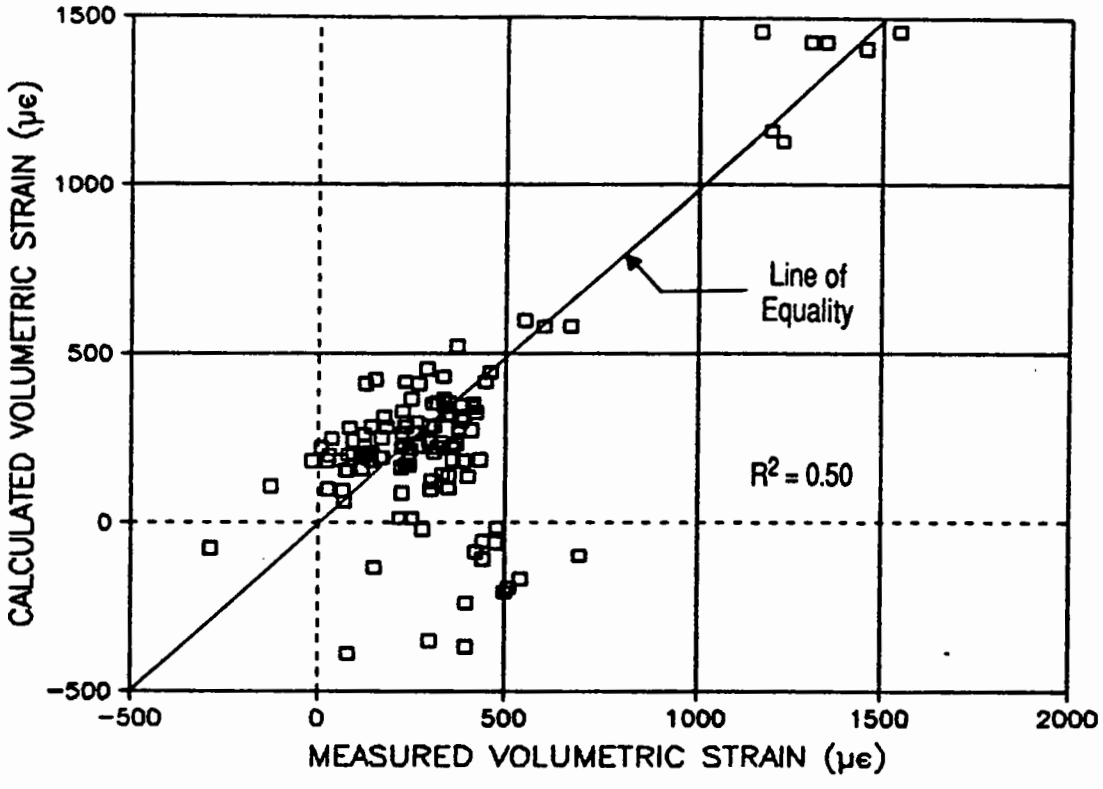

Figure 8.28 Comparison of Predicted and Measured Resilient Volumetric Strain from Repeated Load Hollow Cylinder Tests under General Stress Conditions.

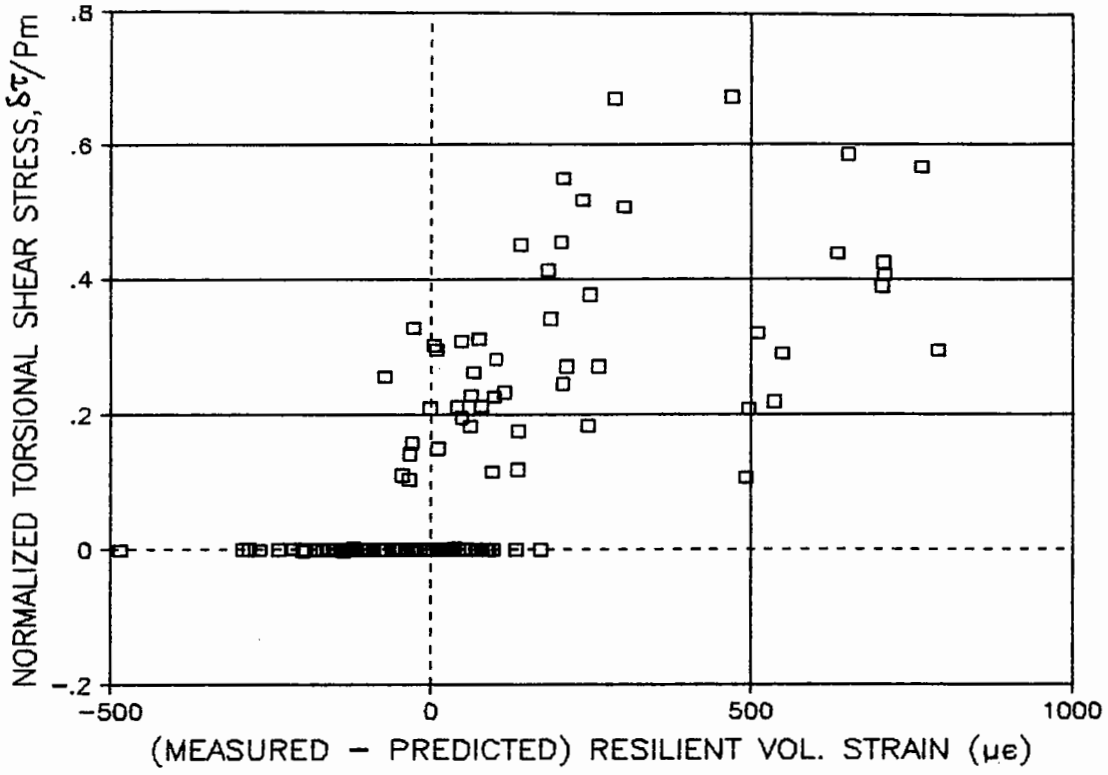

Figure 8.29 Variation of Normalized Torsional Shear Stress with Errors in Predicted Resilient Volumetric Strains in Repeated Load Hollow Cylinder Tests.

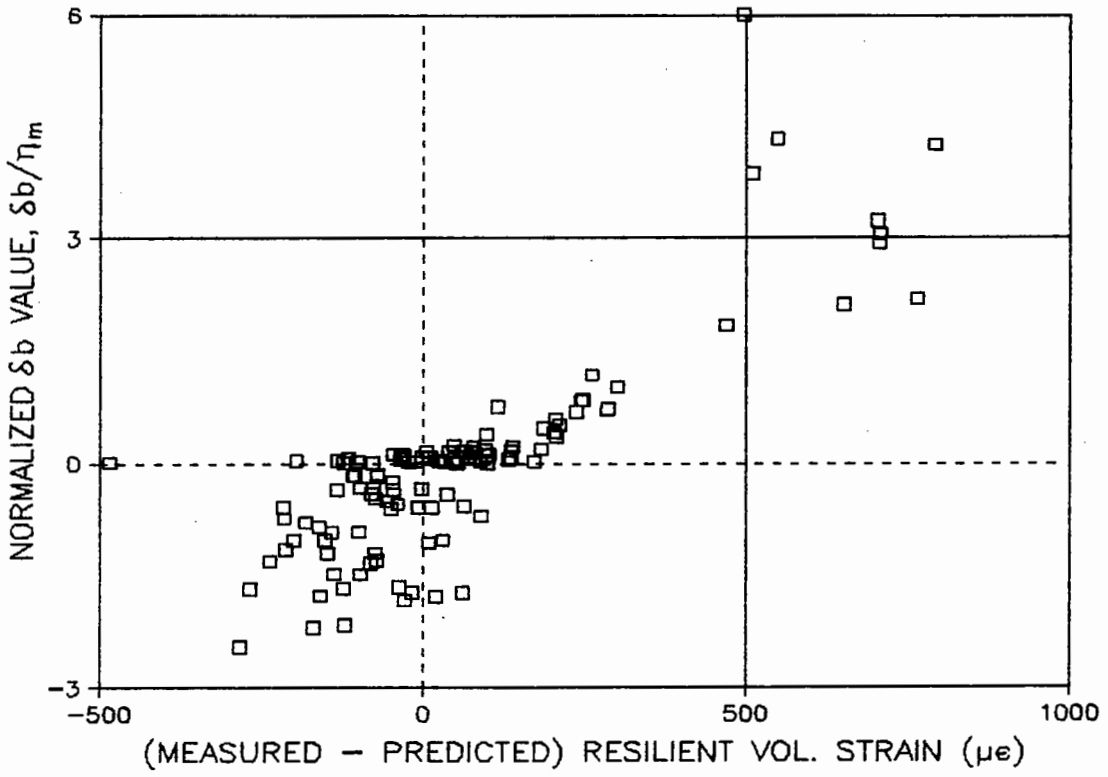

Figure 8.30 Variation of Normalized δb-value with Errors in Predicted Resilient Volumetric Strains in Repeated Load Hollow Cylinder Tests.

have good potential to be included in the development of an improved stress-strain model.

Despite the widespread scatter of results in both figures, it can be observed from Figure 8.29 that there is a tendency for higher change of torsional shear stress to cause more compressive volumetric strain than predicted. This finding is in apparent agreement with those of the permanent strain tests regarding the effect of the torsional shear stresses.

In Figure 8.30, the results suggest that for those stress paths which involved a decrease of b-value (i.e. $+\delta b$), the contour model tends to underpredict the compressive volumetric strain. However, when δb is negative, higher strain is predicted. Very little work appears to have been done to consider the effect of the b-value on resilient behaviour of granular material. One set of test results which has close relevance to the data presented here is from the triaxial extention-compression tests performed by Pappin (1979). In those tests, b changed from 1 during extention to 0 when under compression. Hence δb equal to +1. He found that most of his calculated resilient volumetric strains were also underpredicted.

8.5 DISCUSSION OF RESULTS

8.5.1. Permanent Strain Behaviour

From the results of the hollow cylinder tests, it is clear that the permanent strain behaviour of granular material is affected by the reversed shear stresses. However, because of the limited number of tests and stress conditions involved, it is difficult to

draw any definite conclusion about their influence. The tests revealed that when stress conditions were approaching failure, the rate of development of permanent strain may be significantly increased due to the additional reversed shear stresses. In conditions where $(q/p)_{max}$ is low and when the magnitude of the reversed shear stress is small compared with other normal stresses, the difference between the strain response under the "with-shear" and triaxial conditions may be small. Under these low stress conditions, results of tests performed by the less complicated repeated load triaxial test apparatus were found to be sufficiently accurate.

Results of the permanent strain tests consistently suggest that higher permanent strains, both volumetric and maximum shear, are obtained due to bi-directional reversed shear stresses. This finding appears to conform with the results of the large scale rutting tests carried out in the Pavement Test Facility.

8.5.2 Resilient Strain Behaviour

Although the scale of effort invested in the study of the resilient strain behaviour was not as large as that for the permanent strain, a few interesting findings were obtained. One which may be considered important is the observation that rotation of principal stress and strain planes were coincident during resilient tests. This provides support for the continuing use of a relatively simple invariant approach to model the resilient behaviour even under the more complex stress conditions. The investigation showed that the resilient shear strain in the plane where the torsional shear stress was acting was independent of the rotation of the principal plane caused by the shear stress. It further indicated that the contour model and its coefficients which were obtained from tests under triaxial conditions could be used to provide reasonably good predictions of the shear strain under a much wider range of complex stress conditions.

The volumetric behaviour, however, was found to be difficult to model correctly. None the less, an indication of behaviour relating to the applied torsional shear stress and the variation of the intermediate principal stresses was obtained. This should provide some insight for future improvement of models for resilient volumetric strain.

Tests carried out in the repeated load triaxial apparatus and the HCA were found to yield similar coefficients for the contour model. However, under identical stress conditions, the volumetric strains obtained from the HCA were found to be higher. One possible reason for the discrepancies could be due to the small gauge length in the radial direction of the hollow cylinder specimen. Compared with that in the circumferential direction of the same specimen and the radial direction of a triaxial specimen, it was respectively 8 and 5.4 times less. As a result, any possible error will be magnified by the same order. As the calculation of the resilient maximum shear strain in the hollow cylinder is independent of the radial strain, the discrepancy between the results obtained from the two pieces of apparatus was found to be very much reduced.

END OF

PART B

CHAPTER NINE

CONCLUSIONS

Research has been carried out to improve knowledge about the permanent deformation resistance of granular bases. The work has made use of various laboratory equipment which are uniquely available at the University of Nottingham. These include:

1. A large scale Pavement Test Facility which is able to provide uni-directional and bi-directional wheel loading in single-track or multiple-track tests.

2. A modified Slab Test Facility which is able to provide repeated vertical plate loading or bi-directional wheel loading onto a granular specimen contained in a large steel box.

3. A substantially improved repeated load Hollow Cylinder Test Apparatus which can provide both repeated axial and torsional shear loads with individually controlled inner and outer chamber pressures on a hollow cylindrical specimen with 280mm external diameter, 28mm wall thickness and 500mm height.

4. A repeated load triaxial test apparatus which can test cylindrical specimens with a diameter of 150mm.

The combined capability of the equipment has allowed a wide range of test programmes to be carried out. These vary, in this project, from the practical experiments which compared the performance of pavement sections with geosynthetic-reinforced granular bases to fundamental studies which determined the influence of reversed shear stresses

on the permanent deformation behaviour. The main conclusions of the investigations performed are listed below.

9.1 PERMANENT DEFORMATION RESISTANCE OF GEO-SYNTHETIC REINFORCED GRANULAR BASES

Four series of tests involving a total of 17 different flexible pavement sections with thin asphalt surfacings were carried out to investigate the conditions under which the permanent deformation resistance of the geosynthetic-reinforced granular bases could be improved. The tests examined the effects of prerutting and prestressing geosynthetics as well as the geosynthetic location. Two types of geosynthetics, a stiff geotextile and a geogrid with lower stiffnesses were used. As a result of the tests the following conclusions are drawn:

1. The permanent deformation resistance of most geosynthetic-reinforced granular bases used in the experiments was improved. However, a large range of level of improvement was observed, from almost none to a reduction in permanent deformation by over 80%.

2. The improvement level was found to depend largely on the quality and thickness of the granular base and the location of the geosynthetic within the base.

3. For a weak granular base, such as that constructed of sand and gravel, with low elastic stiffness, significant improvement in permanent deformation resistance should be expected with the installation of a geosynthetic either at the middle or bottom of the layer. Because of the generally large vertical deformations and

high induced stresses which are associated with this type of granular material, the use of a stiffer geosynthetic is likely to produce higher levels of improvement.

4. In reinforced granular bases with high thicknesses of good quality materials, the location of the geosynthetic was found to have a dominant effect on the level of improvement of the permanent deformation resistance. Very little to no benefit may be obtained if the location of the geosynthetic is too far down the layer. From a practical rather than a theoretical point of view, placement of geosynthetics at the middle of a base layer which does not exceed 200mm in thickness, may give an optimum improvement.

5. The inclusion of the geogrid generally led to less permanent deformation development in the granular base than the geotextile despite the much lower stiffness of the geogrid. The better level of improvement could be due to the geogrid's ability to interlock with the granular material. The experimental results may also imply that the frictional property rather than the stiffness of geosynthetic is more important under situations similar to those considered in the current investigation.

6. Prerutting of high quality granular bases, both reinforced and unreinforced, resulted in densification of the layer and, hence, improvement in its permanent deformation resistance. Its benefit was found, in some cases, to outweigh that of geosynthetic inclusion. However, prerutting of weak granular material may be detrimental as a result of causing failure to the material.

7. Prestressing of geosynthetics, together with the provision of good anchorage during construction to prevent slippage, resulted in additional improvement in

the permanent deformation resistance of a reinforced granular base in an accelerated experiment. However, the long-term benefit of prestressing can be lost due to stress relaxation.

9.2 PERMANENT STRAIN BEHAVIOUR OF GRANULAR MATERIALS

9.2.1 Large Scale Rutting Tests

From the results of the large scale rutting test carried out in the Slab and Pavement Test Facilities the following conclusions were drawn:

1. The permanent vertical deformation of the granular base subjected to a moving wheel load was at least three times higher than that subjected to a repeated vertical load with the same magnitude of contact stress.

2. The magnitude of a moving wheel load had greater influence on the permanent deformation of the granular base than that of a repeated vertical load.

3. In two out of three pairs of pavement sections, higher permanent deformation were obtained from a bi-directional than uni-directional wheel load. The exceptional pavement sections were less well compacted and, hence, the trend caused by the different modes of loadings was probably masked by the generally high level of permanent deformation.

9.2.2 Repeated Load Hollow Cylinder Tests

The Nottingham repeated load Hollow Cylinder Test Apparatus was successfully modified to include an outer cell, an up-graded electronic control system and a data acquisition system. Eleven hollow cylinder specimens were tested by means of the modified device. To complement these experiments, two tests on the same material used in the HCA tests were carried out using the repeated load triaxial apparatus. The conclusions from these tests were:

1. Reversed shear stresses were found to cause more contractive permanent strains in both the radial and circumferential direction when results were compared with those obtained under triaxial conditions.

2. When stress conditions were approaching failure, the rate of development of all components of permanent strain was found to be significantly increased due to the additional reversed shear stresses.

3. In conditions where the maximum shear stress ratio, $(q/p)_{max}$ used in the stress path was low and when the magnitude of the reversed shear stress was small compared with the normal stresses, the difference between the strain response under the condition with reversed shear stresses and the triaxial condition was less clear. Nonetheless, it appeared that under these circumstances, reversed shear stresses would cause higher permanent contractive volumetric strains but less permanent maximum shear strains.

4. Higher permanent volumetric and maximum shear strains were obtained due to bi-directional than uni-directional shear reversal.

5. Under identical stress conditions, permanent axial strains obtained from both the HCA and the repeated load triaxial apparatus were similar but the permanent horizontal strain obtained from the HCA was much higher.

6. Rotation of the principal stress and strain planes were coincident during resilient tests.

7. The coefficients m, n and β used in the resilient strain contour models, which were obtained by means of a multiple regression analysis from results of repeated load triaxial tests, were found to be identical to those obtained from HCA tests. The constants K1 and G1, however, were found to be respectively 97% and 29% less for results from HCA tests, indicating that lower stiffnesses were obtained during the tests.

8. The contour model and its coefficients, which were obtained from tests under triaxial conditions, could be used to provide reasonably good predictions of the resilient maximum shear strain under stress conditions which involve principal plane rotation and variation in the intermediate principal stress.

9. Resilient volumetric strain was generally underpredicted by the contour model under stress conditions which involved the application of torsional shear stress.

10. The difference between the measured and predicted resilient volumetric strain using the contour model appeared to bear a curvilinear relationship with the normalised value, $\delta b/\eta_m$ which is defined as the change in the intermediate principal stress parameter divided by the mean shear stress ratio, $(q_{oct})/p_m$.

CHAPTER TEN

PRACTICAL IMPLICATIONS OF CURRENT INVESTIGATIONS

Research often fails to change practice because of limited understanding, inflexible standards, mistrust of change or preoccupation with first cost. These appear to apply quite well to the research on the permanent deformation behaviour of granular bases. However, with the trend towards increasing wheel loads and traffic density at a time when there is increasing economic pressure to optimize cost, research in the above-mentioned area will most certainly have good potential to deliver payoff which may exceed the original investment. It is envisaged that the practical implications of the two investigations presented in this thesis may help to fulfill this objective.

10.1 THE USE OF GEOSYNTHETICS

The results of the current investigation imply that there is a role for geosynthetics to play in reducing the permanent deformation of granular bases which serve as load bearing layers. Their use in heavily loaded pavements should be particularly beneficial and their additional cost to the design should be carefully weighted against the possibly more frequent maintenance expenses of the un-reinforced pavement.

Stiffness of the geosynthetic should be considered in conjunction with the type of geosynthetic, as the current investigation indicates that the benefit, as far as reduction in permanent deformation is concerned, due to a stiff geotextile is far less than that due to

a geogrid with much lower stiffness. This implies that the high cost which is normally associated with high stiffness may sometimes not be justified. However, it is still believed that for a given type of geosynthetic with a particular surface characteristic, higher stiffness will result in better improvement in the permanent deformation resistance of the reinforced granular base.

The location of the geosynthetic reinforcement within the granular layer should be considered in conjunction with the total thickness and the number of layers of construction. From a practical standpoint, the geosynthetic should be at the middle or upper third of the granular layer. This requirement may have an impact on the choice of the maximum particle size of the granular material and, possibly, the compaction plant.

While prestressing of geogrid has led to improved performance in a laboratory-scale pavement, it does not imply that similar benefits in normal site practice can be achieved. This is mainly due to the economic and installation problems which are associated with the use of high prestress force and strong anchors. These problems will become more severe when soft subgrade or low quality granular base materials are used. Therefore, the practicality of applying prestress force under these conditions is questionable. In addition to the problems mentioned above, proper allowance should be made for prestress losses due to stress relaxation and other factors which are related to the method of prestressing and the skill and care of the crew performing the work.

10.2 THE USE OF HIGH DENSITY GRANULAR BASES

The use of the prerutted un-reinforced pavement sections and different gradings of granular material in the laboratory tests has created opportunities for the comparison of

the permanent deformation behaviour of granular bases having different densities. The result of the comparison implies that the use of high density granular base, achieved either by means of methods similar to proof-rolling or the use of specially designed dense grading, will generally improve the permanent deformation resistance of the pavement. Furthermore, the suitably prerutted unreinforced granular layer may perform better than those reinforced with stiff geosynthetics which are not prerutted.

Barksdale et al (1989) found that the cost of prerutting a granular base without geosynthetics at one level might be as small as 50% of the inplace cost of a stiff geogrid (Sg =300 kN/m). On the other hand, prestressing the same geogrid would cost up to 5 times that of prerutting. This economic consideration, together with the results from the current investigation have clearly indicated the benefits of using high density granular bases. However, the concept of prerutting has not been tested in full-scale field experiments. Therefore, its true potential as a means to reducing permanent deformation has yet to be examined.

It is worth noting that the above implications assume that the equally important permeability requirement of the granular base can be satisfied by the provision of both a good road surface maintenance programme, to provide crack-free conditions, and adequate drainage at the layer boundaries to prevent build-up of moisture within the granular layer.

10.3 DESIGN OF AN "IDEAL" PAVEMENT SECTION

The last two sections have created the basis for the design of an "ideal" pavement section which has good resistance to permanent deformation. A proposed pavement

cross-section which incorporates the main design features discussed earlier is shown in Figure 10.1.

The granular layer consists of an upper, densely graded, high quality material and a lower, open graded aggregate. The upper layer, which is reinforced with a stiff geogrid, enables maximum rutting resistance to be achieved at the location where stresses are the most severe. Experience from South Africa (Groth, 1985) indicates that, provided this layer is well supported by layers underneath, there is little advantage in increasing the thickness above 150mm. The use of a more permeable lower layer will facilitate drainage both of water from the subgrade and the dense layer above. Although the lower material is less resistant to permanent deformation than the dense upper layer, since it is lower in the construction, the overall rutting potential of the granular layer is unlikely to be significantly affected. Both granular layers should be connected to the side drain so that water can escape.

In the absence of a naturally stiff subgrade, cement or lime treatment of the subgrade material should be carried out. This requirement is necessary in order to provide the good support conditions for the compaction of the granular layers. At formation level, a geotextile can be used as separator to prevent contamination of the lower granular layer by the subgrade material.

10.4 REALISTIC SIMULATION IN LABORATORY TESTING

The availability of the repeated load HCA has shown that a more realistic simulation of a moving wheel load can be carried out in laboratory testing. This simulation, which

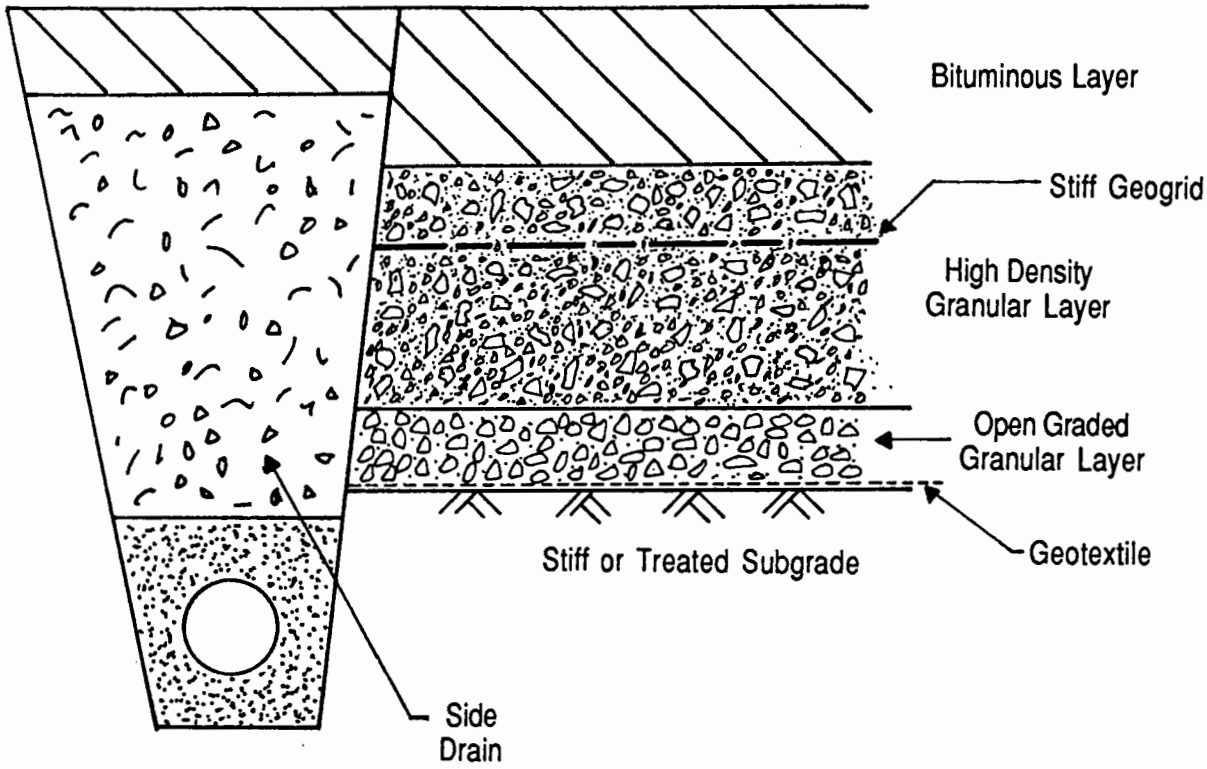

NOT TO SCALE

Figure 10.1 Proposed Cross-section of Pavement with High Resistance to Permanent Deformation.

involves the application of reversed shear stresses to the test specimen, is considered to be particularly important in the study of the permanent deformation behaviour of granular bases subjected to moving traffic.

Because of the HCA's complexities, it will take some time before it can generate sufficient practical data for routine use. However, the current investigation found that under some stress conditions (which are probably material dependent), the results of the permanent strain tests performed by the less complicated repeated load triaxial test apparatus were generally acceptable when compared with those obtained from the HCA. This may imply that under such stress conditions, permanent strain tests performed by means of the HCA are not necessary.

It should not be assumed that permanent strain prediction carried out by means of laboratory tests, even those involving the use of the HCA, is capable of direct correlation with pavement serviceability. The latter is as much a function of the variation in rut along the pavement length as the rut depth itself. The variation may depend on the materials used as well as the standard of construction. Hence, it should be realized that the study of permanent strain behaviour of granular base material would always be bounded by this general framework of pavement behaviour.

CHAPTER ELEVEN

RECOMMENDATION FOR FUTURE WORK

11.1 INTRODUCTION

The permanent deformation behaviour of both reinforced and un-reinforced granular bases under repeated loading is undoubtedly complex, and tests either large or laboratory scale, to characterize it are likely to be both time consuming and demanding of resources. In order to progress this research more efficiently, co-ordination with and systematic exchange of information on, findings from research organizations Worldwide is very desirable.

Realizing that the laboratory and field conditions are very different, both in terms of the state of the granular material and the induced stresses, suitable methods of interpreting laboratory results and comparing them with responses from full scale pavement testing should be developed.

To bridge the gap between laboratory simulated and in-situ conditions, the use of a sophisticated device, such as the repeated load hollow cylinder apparatus has proved to be very valuable and able to produce some important data. The potential of this laboratory device should be further explored and effort to expand its capability should be considered.

In view of the diversity of climate, soils, geology, traffic loading and intensity and road maintenance strategy, attention on research work is more likely to be directed at developing incremental solutions to local problems. However, as a result of the work presented in this thesis, it is felt that the items discussed in the following sections should receive priorities.

11.2 ESTABLISHMENT OF A DATA BASE

The general lack of sufficient resources and the fragmentation of research efforts in the study of the permanent deformation behaviour of granular bases, both reinforced and un-reinforced, have highlighted the need for major co-ordination of the research findings harvested Worldwide. The establishment of a data base containing both the laboratory and in-situ performance of granular materials is very much desirable. Each data file should, ideally, contain the following items of information:

1. Material Classification
   a. Description of the granular material according to an acceptable standard. Emphasis should be placed on mineralogy, shape and surface texture of the particles.
   b. Grading of the specimen.
   c. Density and moisture condition and the method of specimen preparation or compaction of layers.
   d. For full scale or in-situ testing, properties of other pavement layers should be included.

2. Testing Method and Procedure
   a. Type of testing device and instrumentation.
   b. Stress conditions. For laboratory tests, they should include shape of waveform, frequency and duration of rest period. For full scale or in-situ testing, the contact or average stress (which may need to be back-calculated) should be included.
   c. Conditioning procedure prior to main test.

3. Results

   a. Relationship between permanent strain in the granular material and number of repetition of loading.

11.3 FULL SCALE FIELD TRIAL ON GEOSYNTHETIC-REINFORCED GRANULAR BASES

In order to obtain data for validation or improved interpretation of the laboratory results presented in this thesis, full scale field trial on geosynthetic-reinforced pavement sections should be performed. Two full scale field trials are currently being undertaken by the University of Nottingham. The one performed in Wakefield, England contains two bound pavement sections which incorporate granular bases that are reinforced by a stiff geogrid. In the second field trial, which is carried out at Bothkennar, Scotland, ten geosynthetic-reinforced sections of an unbound road are tested. The pavement sections in both full scale trials are heavily instrumented. Therefore, they should provide good opportunities for monitoring the permanent deformation of the granular layers.

11.4 TESTING IN THE HCA

11.4.1 Further Work on the Same Material used in Current Investigations

Test carried out for the current project have established the influence of the reversed shear stresses, both uni- and bi-directional, on the permanent strain behaviour. Although more tests involving other stress paths with reversed shear stresses are warranted, it may be useful to investigate the effect of the intermediate principal stress,

σ_2. This can be achieved by using various differences in inner and outer cell pressures to create a range of anisotropic conditions. The investigation can also include the condition with "jump" rotation of principal planes, similar to that in the triaxial compression-extension tests. It is believed that if high residual stresses exist in the horizontal direction within the granular base, "jump" rotation of the principal stresses can occur under a passing wheel load.

In order to achieve high density, hence high strength, for the material used in the current investigation, a continuous grading with high fines content was used. It would be of interest to investigate the permanent strain behaviour of an open graded specimen which may be expected to have much better drainage properties. The requirement of both good strength and good permeability for granular bases is inevitably contradictory. Hence, it would be useful to compare the performance of specimens having these two different gradings.

11.4.2 Work on Other Materials

A great degree of realism was attached to the choice of the type and grading of the material used in this project. As a result, a material widely used in the highway industry, a scale down version of a realistic grading and a correspondingly high density were selected. However, these choices may not be ideal in the theoretical study of the various fundamental mechanisms of granular material behaviour. Furthermore, comparison of results with other research organizations would be difficult if different categories of materials were tested. Hence, it would be useful if future test programmes could incorporate testing of some model materials such as the well researched Leighton Buzzard sand and other similarly "well-known" materials. Testing of single sized

material such as that used by Ansell (1977) and Shaw (1980) in their cyclic simple shear apparatus should also generate useful results for comparison.

11.5 FURTHER DEVELOPMENT OF THE HCA

11.5.1 Performance of the Modified HCA

The upgrading of the electronic control unit has resulted in much better control of the loading system. The output of both the vertical and torsional load cells followed the command signal satisfactorily at various phase angle shift at the test frequency of 0.5 Hz or lower. Good performance was also observed at frequency of 1 Hz. However, tests carried out at frequencies higher than this level are not recommended. Stability of the system was in general good provided the appropriate gain setting was selected according to the stiffness of the specimen.

The capability of the data acquisition system was generally satisfactory despite the recording of undesirable "noise". Data could be checked before average values were calculated. This helped to eliminate obviously erroneous data. Other features such as data management, analysis and graphics were very useful. However, there is a need for an A/D convertor with more channels and higher speed of conversion.

In spite of the modifications, some features were still considered to be unsatisfactory and further improvement is needed. They included:

1. The maximum torsional shear stress that can be applied is only 50 kPa. Unless small confining and deviator stresses are used, the effect due to the shear stress may be too small to measure.

2. Cross interference of the two load cells was observed during tests when only one load was cycled. The interference was found to be considerably reduced when both loads were cycled.

3. "Noise" from the LVDT's, especially those mounted at 45 degrees to the vertical was rather significant at low strain levels. This could be due to electrical interference from other sources in the laboratory or mechanical damping caused by friction between the shaft and the barrel of the transducer.

4. Control of the stresses imposed on the specimen during the first few cycles requires improvement. This is particularly needed when high stresses and small numbers of cycles are used in the test. A new system which can allow the target stresses to be reached after one cycle should be considered.

11.5.2 Future Development of the HCA

The improvement to the HCA carried out in this project has eliminated a large area of restrictions on the possible stress regime that can be applied to the hollow cylinder specimen. Despite these achievements, in order to fully make use of this torsion-triaxial system, the capability of providing cyclic internal and external cell pressures is highly desirable. More sensors to measure the response of the cell or possibly pore pressures will be needed. The control of such a system will be more complicated and will most certainly require the aid of a computer. However, with the advance of modern electronics and computer programming, such a system should be available at reasonable cost.

REFERENCES

Ansell, P and Brown, S F, (June 1978), *"Cyclic Simple Shear Apparatus for Dry Granular Materials"*, Geotechnical Testing Journal, Vol. 1, No. 2, pp 82-92.

Ansell, P, (1977), *"Cyclic Simple Shear Testing of Granular Material"*, PhD Thesis, University of Nottingham.

Arthur, J R F, Chua, K S and Dunstan, T, (1977), *"Induced Anisotropy in a Sand"*, Geotechnique 27, No. 1, pp 13-30.

ASTM Standard, (1987),*"Soil and Rock: Building Stones: Geotextiles "* , Standard D-15557-78, Vol. 04.08.

ASTM Standard, (1987), *"Resistance to Plastic Flow of Bituminous Mixtures using Marshall Apparatus"*, Standard D1559-20.

Atkinson, J H and Bransby, D L, (1978), *"The Mechanics of Soils: An Introduction to Critical State Soil Mechanics"*, McGraw Hill.

Barksdale, R D and Itari, S Y, (1989), *"Influence of Aggregate Shape on Base Behaviour"* , Paper presented at the meeting of the Transportation Research Board.

Barksdale, R D, Brown, S F and Chan, W K F, (1989), *"Potential Benefits of Geosynthetics in Flexible Pavements"*, National Cooperative Highway Research Program Report 315, Transp. Research Board.

Barksdale, R D, (1972), *"Laboratory Evaluation of Rutting in Basecourse Materials"*, Proc. of 3rd Int. Conf. on the Structural Design of Asphalt Pavements, London, pp 161-174.

Barrett, J R and Smith, D M, (1976), *"Stress History Effects in Base Course Materials"*, Proc. Australian Road Research Board, Vol. 8.

Barrett, J R, (1976), *"Modelling Permanent Strain Behaviour of Unbound Base Course Materials - A Review"*, Division of Applied Geomechanics Technical Paper No. 26, Commonwealth Scientific and Industrial Research Organisation, Australia.

Bell, C A, (1978), *"The Prediction of Permanent Deformation in Flexible Pavements"*, PhD Thesis, University of Nottingham.

Barvashov, V A, Budanov, V G, Fomin, A N, Perkov, J R and Pushkin, V I, *"Deformation of Soil Foundations Reinforced with Pre-Stressed Synthetic Fabric"*, 1st Int. Conf. on use of Fabrics in Geotechnics, Vol. 1, pp 67-70.

Black, W P M and Lister, N W, (1979), *"The Strength of Clay Fill Subgrades: Its Prediction in Relation to Road Performance"*, Department of Environment/Department of Transport, TRRL Laboratory report LR 889, Crowthorne.

Boyce, J R and Brown S F, (1976), *"Measurement of Elastic Strain in Granular Material"*, Geotechnique, 26/4, pp 637-640.

Boyce, J R, (1976), *"The Behaviour of a Granular Material under Repeated Loading"*, PhD Thesis, University of Nottingham.

British Standards Institution, (1985), *"Methods for Determining the Flakiness Index of Coarse Aggregate"*, BS812, Section 105.1.

British Standards Institution, (1980), *"Recommendations for Testing of Aggregates"*, BS5835, Part 1.

British Standards Institution, (1973), *"Specification for Rolled Asphalt (Hot Process) for Roads and Other Paved Areas"*, BS594.

Brown, S F, O'Reilly, M P and Pappin, J W, (April 1989), *"A Repeated Load Triaxial Apparatus for Granular Materials"*, Third Int. Symp. on Unbound Aggregate in Roads (UNBAR3), University of Nottingham, pp 143-158.

Brown, S F and Pappin J W, (1985), *"The Modeling of Granular Materials in Pavements"*, Transportation Research Record 1022, pp 45-51.

Brown, S F, Hughes, D A B and Brodrick, B V, (1985), *"The Use of Polymer Grids for Improved Asphalt Performance"*, Proc. 3rd Eurobitume Symp., Vol. 1, The Hague, pp 223-228.

Brown, S F, Jones, C P D and Brodrick B V, (1982), *"Use of Non-Woven Fabrics in Permanent Road Pavements"*, Proc. ICE, Part 2, Vol. 73, pp 541-563.

Brown, S F and Brodrick, B V, (1981), *"Nottingham Pavement Test Facility"*, Transp. Research Record 810, pp 67-72.

Brown, S F, Brodrick, B V and Pappin, J W, (1980), *"Permanent Deformation of Flexible Pavements"*, Final Technical Report submitted to the US Army, University of Nottingham.

Brown, S F and Brodrick, B V, (1977), *"Stress and Strain Measurements in Flexible Pavements"*, Proc. Conf. on Measurements in Civil Engineering, Newcastle, England.

Brown, S F, (1974), *"Repeated Load Testing of a Granular Material"*, Journal of Technical Engineering Division, ASCE, Vol. 100, No. GT7, July, pp 825-841.

Chaddock, B C J, (1985), *"Deformation of a Haul Road Reinforced with a Geomesh"*, Proc. 2nd Symp. on Unbound Aggregates in Roads, Part 1, pp 93-98.

Chan, W K F and Brown, S F, (1989), *"Granular Bases for Heavily Loaded Pavements"*, 3rd Annual Report submitted to the US Air Force, University of Nottingham.

Crockford, W W, Chua, K M, Yang, W S, Rhee, S K and Senadheera, S P (1988), *"Response and Performance of Thick Granular Layers"*. Final Technical Report submitted to the US Air Force.

Dawson, A R, (1986), *"The Role of Geotextiles in Controlling Sub-base Contamination"*, Proc. 3rd Int. Conf. on Geotextile, Vienna, Austria, pp 593-598.

Department of Transport, (1976), *"Specification for Road and Bridge Works"*, London HMSO.

Descornet, G H D, (1977), *"Repeated Compression Tests on Granular Materials: Modulus and Permanent Deformation"*, Proc. 9th Int. Congress on Soil Mechanics, Tokyo.

Gerrard, C M, Morgan, J R and Richards, B G, (1975), *"An Approach to the Design of Flexible Pavements for Australian Conditions"*, Australian Road Research Report 5 (8).

Groth, P J, (1985)," *The Use of High Density Granular Layers in Road Pavements*", Proc. 2nd Symp. on Unbound Aggregates in Roads, Part 1, pp 99-107.

Hight, D W, Gens A and Symes M J, (1983), *"The Development of a New Hollow Cylinder Apparatus for Investigating Effects of Principal Stress Rotation in Soils"*, Geotechnique 33, No. 4, pp 355-384.

Kadar, P, (1987), *"Accelerated Full Scale Testing of Heavy Duty Pavements - Experience with the Australian Accelerated Loading Facility (ALF)"*, Proc. 6th Int. Conf. - Structural Design of Asphalt Pavements, Ann Arbor, pp 543-549.

Lai, J S and Robnett, Q L, (1981), *"Design and Use of Geotextiles in Road Construction"*, Proc. 3rd Conf. Engineering Assoc. of Asia and Australia, Tai Pei, Taiwan.

Lee, K L and Farhroomand, I, (1967), *"Compressibility and Crushing of Granular Soil in Anisotropic Compression"*, Canadian Geotechnical Journal, Vol. IV, No. 1, pp 68-86.

Lentz, R W and Baladi, G Y, (1980),"*Simplified Procedure to characterize Permanent Strain in Sand subjected to Cyclic Loading*", Proc. Int. Symposium on Soils under Cyclic and Transient Loading, Swansea, pp 89-95.

Lister, N W, (1972), *"The Transient and Long Term Performance of Pavements in Relation to Temperature"*, Proc. 3rd Int. Conf. on Structural Design of Asphalt Pavements, London, pp 94-100.

Loach, S C, (1987), *"Repeated Loading of Fine Grained Soils for Pavement Design"*, PhD Thesis, University of Nottingham.

Maree, J H, Freeme, C R and Kleyn, E G, (1982a), *"Heavy Vehicle Simulator Testing in South Africa"*, Proc. Int. Coll.: Full Scale Pavement Testing, Zurich, pp 53-68.

Maree, J H, Freeme, C R, Van Zyl, N J and Savage, P F, (1982b), *"The Permanent Deformation of Pavements with Untreated Crushed Stone Bases as Measured in Heavy Vehicle Simulator Tests"*, Proc. 11th Australian Road Research Board Conf., Part 2, pp 16-28.

Milligan, G W E, Jewell, R A, Houlsby, G T and Burd, H J, (1989), *"A New Approach to the Design of Unpaved Roads, Part 1"*, Ground Engineering.

Mitchell, J K, (1976), *" Fundamentals of Soil Behaviour"*, John Wiley and Sons Inc.

Morgan, J R, (1972), *"Laboratory Tests on Fine Crushed Rock"*, Proc 6th Australian Road Research Board, Vol. 6, Part 5, pp 179-194.

Murray, R T and McGown, A, (1987), *"Geotextile Test Procedures Background and Sustained Load Testing"*, TRRL Application Guide 5.

O'Reilly, M P, (1985), *"Mechanical Properties of Granular Materials for use in Thermal Energy Stores"*, PhD Thesis, University of Nottingham.

Organisation for Economic Co-operation and Development, (1985), *"Full Scale Pavement Tests"*, Paris.

Pappin, J W, (1979),*"Characteristics of a Granular Material for Pavement Analysis"*, PhD Thesis, University of Nottingham.

Pappin, J W, (1975), *"Pavement Evaluation Project, Griffith, NSW"*, CSIRO Division of Applied Geomechanics, Project Report 2, Melbourne.

Peacock, W H and Seed, H B, (1968), *"Sand Liquefaction under Cyclic Loading Simple Shear Conditions"*, Journal of the Soil Mechanics and Foundations Division, Proc. ASCE, Vol. 90, No. SM3, Proc. Paper 5957, pp 689-708.

Potter, J F and Currer, E C, (1981), *"The Effect of a Strong Fabric Membrane on the Structural Behaviour of a Granular Pavement"*, Transp. and Road Research Laboratory, TRRL Report LR996, Crowthorne.

Powell, J F, Potter, J F, Mayhew, H C and Nunn, M E, (1984), *"The Structural Design of Bituminous Roads"*, TRRL Report LR 1132, Crowthorne.

Raad, L, (1982), *"Reinforcement of Transportation Support System through Fabric Pre-Stressing"*, TRR 755, Transp. Research Board, pp 49-51.

Raymond, G P and Williams, D R, (1978), *"Repeated Load Triaxial Tests on a Dolomite Ballast"*, Proc. ASCE, Vol. 104, No. GT7, pp 1013-1029.

Robnett, Q L, Lai, J S and Murch, L, (1982), *"Effect of Fabric Properties in the Performance and Design of Aggregate-Fabric-Soil Systems"*, Proc. 2nd Int. Conf. on Geotextiles, Vol. II, Las Vegas, pp 381-386.

Rowe, P W, (1962), *"The Stress-Strain Relation for Static Equilibrium of an Assembly of Particles in Contact"*, Proc. of the Royal Society, Vol. A269, pp 500-527.

Ruddock, E C, Potter, J F and McAvoy, A R, (1982), *"A Full Scale Experiment on Granular and Bituminous Road Pavements Laid on Fabrics"*, Proc. 2nd Int. Conf. on Geotextiles, Las Vegas, Vol II, pp 365-370.

Shenton, M J, (1974), *"Deformation of Railway Ballast under Repeated Loading"*, Report RP5, British Railways Research Department.

Silver, M L and Seed, H B, (1971), *"Volume Changes in Sands during Cyclic Loading"*, Journal of the Soil Mechanics and Foundations Division, Proc. ASCE, Vol. 97, No. SM9, Proc. Paper 8354, pp 1171-1182.

Sweere, G T H, Penning, A and Vos, E, (1987), *"Development of a Structural Design Procedure for Asphalt Pavements with Crushed Rubble Base Courses"*, Proc. 6th Int. Conf. on the Structural Design of Asphalt Pavements, Ann Arbor, Michigan, pp 35-49.

Sweere, G T H, (1990)," *Unbound Granular Bases for Roads*", PhD Thesis, Delft University of Technology.

Symes, M J P R, Gens, A and Hight, D W, (1984)," *Undrained Anisotropy and Principal Stress Rotation*", Geotechnique 34, No. 1, pp 11-27.

Symes, M J P R, (1983), *"Rotation of Principal Stresses in Sand"*, PhD Thesis, Imperial College, University of London.

Thom, N H and Dawson, A R, (1989), *"The Permanent Deformation of a Granular Material Modelled using Hollow Cylinder Apparatus"*, Paper submitted to TRB Meeting in Washington DC.

Thom, N H and Brown, S F, (1988), *"The Effect of Grading and Density on the Mechanical Properties of a Crushed Dolomitic Limestone"*, University of Nottingham.

Thom, N H, (1988), *"Design of Road Foundation"* , PhD Thesis, University of Nottingham.

Webster, S L and Watkins, (1977), *"Investigation of Construction Techniques for Tactical Bridge Approach Roads across Soft Ground"*, US Army Engineer Waterways Experimental Station, Vicksburg, Miss., Report S-77-1.

Wong, R K S and Arthur, J R F, (1986)," Sand sheared by Stress with Cyclic Variations in Direction", Geotechnique 36, No.2, pp. 215-226

Wright, D K, Gilbert, P A and Saada, A S, (1978), *"Shear Devices for Determining Dynamic Soil Properties"*, Proc. of American Society of Civil Engineers Speciality Conf. on Earthquake Engineering and Soil Dynamics, Vol. 2, pp 1056-1075, Pasadena, California.

Yeo, K L, (1985), *"The Behaviour of Polymeric Grid used for Soil Reinforcement"*, PhD Thesis, University of Strathclyde.

Youd, T L, (1972), *"Compaction of Sands by Repeated Shear Straining"*, Proc. ASCE Journal of Soil Mechanics and Foundation Division, Vol. 98, SM7, pp 709-725.

Zeevaert, A E, (1980), *"Finite Element Formulations for the Analysis of Interfaces, Non-Linear and Large Displacement Problems in Geotechnical Engineering"*, PhD Thesis, School of Civil Engineering, Georgia Inst. of Tech., Atlanta.

APPENDIX

A TO E

APPENDIX A

LABORATORY TESTING OF PAVEMENT MATERIALS USED IN FULL SCALE EXPERIMENTS IN THE NOTTINGHAM PTF

A.1 Tests on Granular Base Material

Laboratory tests performed on the granular materials consisted mainly of cyclic load triaxial tests, compaction tests, sieve analyses and other index tests.

Repeated Load Triaxial Tests: Brief description of the equipment used is presented in Appendix D. A total of six tests were carried out on recompacted 150 mm diameter samples of the sand and gravel and Type I dolomitic limestone at various moisture contents. The results of earlier testing showed that resilient behaviour of a granular material under repeated loading was very stress dependent and, therefore, non-linear. Hence each of the six tests used 20 stress paths to characterise resilient strain. The ranges of repeated cell pressure and repeated deviator stress used in the tests were 0 to 250 kPa and 0 to 200 kPa respectively. For permanent strain tests, a cell pressure of 50 kPa and a repeated deviator stress of 0 to 200 kPa were used. Up to 2000 stress cycles at a frequency of about 1 Hz were applied to the test samples.

The results for the permanent strain tests for the two types of granular material are shown in Figures A1.1 and A1.2. The results are presented in the form of change of permanent axial and radial strains with the number of stress cycles. Figure A1.1 indicates that the sand and gravel has a rather low resistance to permanent deformation. For the dolomitic limestone, Figure A1.2 indicates that the rate of development of permanent deformation varies with moisture content and as the material approaches saturation, a very rapid increase in the rate of deformation will occur.

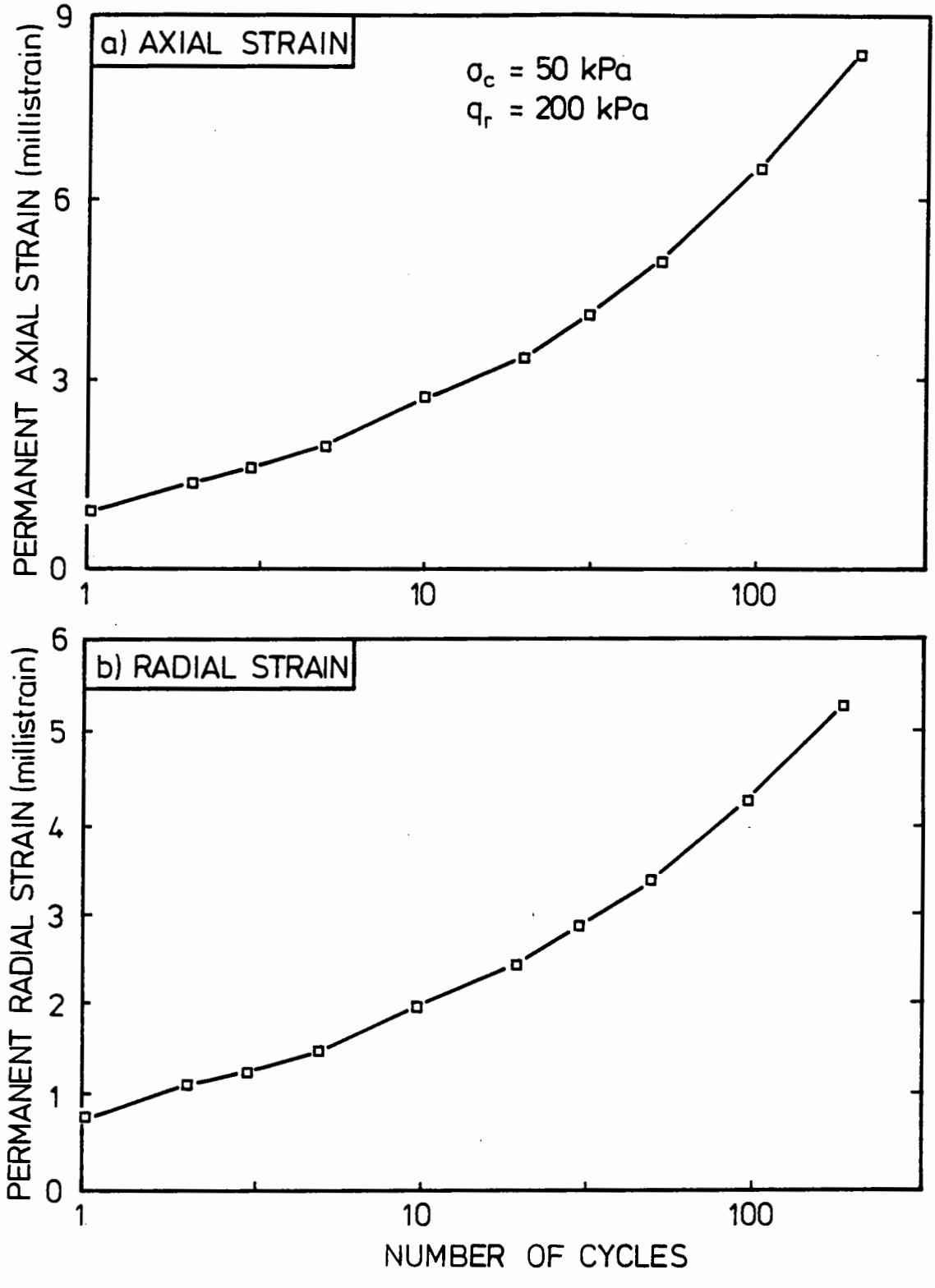

Figure A1.1 Variation of Permanent Axial and Radial Strains with Number of Cycles for Sand and Gravel during Repeated Load Triaxial Test.

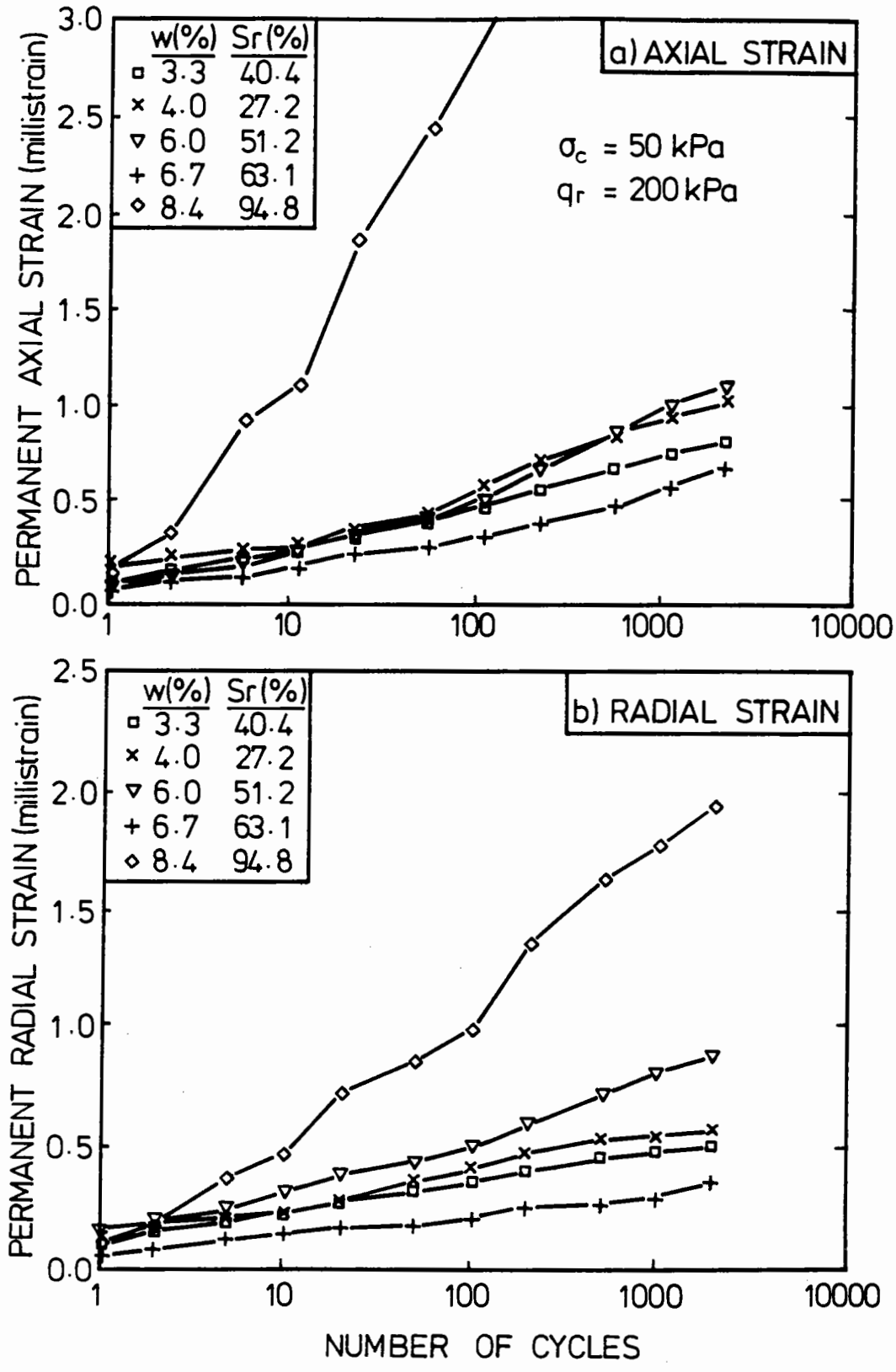

Figure A1.2 Variation of Permanent Axial and Radial Strains with Number of Cycles for Dolomitic Limestone during Repeated Load Triaxial Tests at various Moisture Contents (w) and Degree of Saturation (S_r).

The results of the resilient strain tests, as summarized in Table A1.1 were interpreted by means of the contour model described by equations 8.3 to 8.6 (Jouve et al 1987). The model expressed the bulk modulus, K, and the shear modulus, G, as a function of both p, the mean normal stress, and q, the deviator stress.

Table A-1

Summary of Resilient Strain Tests on Granular Base used in the Pavement Test Facility

Test Number	*Type of Material*	*Dry Density (kg/m3)*	*Moisture Content (%)*	*Volumetric Strain Coefficients*			*Shear Strain Coefficients*	
				K1	*n*	*β*	*G1*	*m*
1	Sand and Gravel	2066	3.7	3040	0.33	0.110	2530	0.33
2	Crushed Limestone	2130	4.0	4785	0.33	0.108	3975	0.33
3	Crushed Limestone	2034	3.3	4900	0.33	0.127	3720	0.33
4	Crushed Limestone	2050	6.0	4130	0.33	0.142	3010	0.33
5	Crushed Limestone	2098	6.7	2975	0.33	0.136	3540	0.33
6	Crushed Limestone	2178	8.4	3800	0.33	0.398	1650	0.33

Note: K1 and G1 are in kPa and the corresponding calculated strains are in fractions.

Compaction Tests: A series of compaction tests were carried out in order to determine the optimum moisture content and maximum dry density of the compacted

material. For the sand and gravel, the test was carried out according to the ASTM D-1557 test method while for the dolomitic limestone, the British Standard Vibrating Hammer method was adopted. The results of the tests for the two materials are shown in Figure A1.3.

Index Tests: Two plasticity index tests were carried out for the fines (less than 425 micron) of each of the two granular materials. The fines for the sand and gravel were found to be non-plastic, while the PI of the fines for the dolomitic limestone was found to be 3%. One flakiness index test BS812 was performed on the crushed dolomitic limestone used in the third series of tests. The result of the test indicated an index of 9% overall while for individual size fractions, the index varied from 3.8 to 16.1%.

A.2 Tests on Silty Clay Subgrade

The silty clay, known as Keuper Marl, has been used extensively at Nottingham in earlier research projects as the subgrade in the PTF. The basic material properties of Keuper Marl used in the current project are given in Table A.2. Repeated load triaxial tests on compacted samples of Keuper Marl were previously performed by Loach (1987) and Bell (1978). One result obtained from Loach's tests is shown in Figure A1.4. This indicates the relationship between resilient modulus and CBR for compacted samples of Keuper Marl and clearly shows the non-linear stiffness characteristic of the soil.

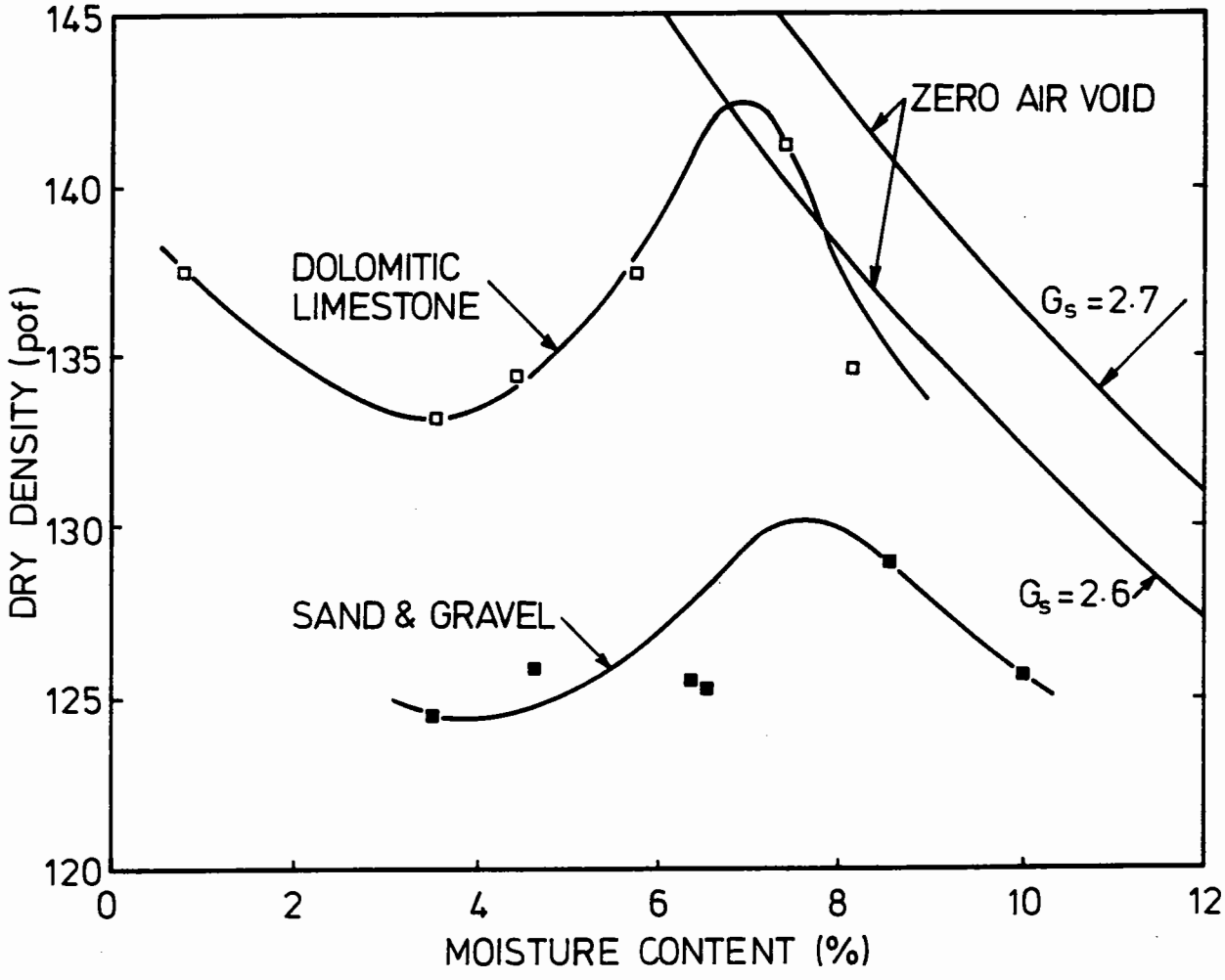

Figure A1.3 Results of Standard Compaction Tests for the Granular Materials.

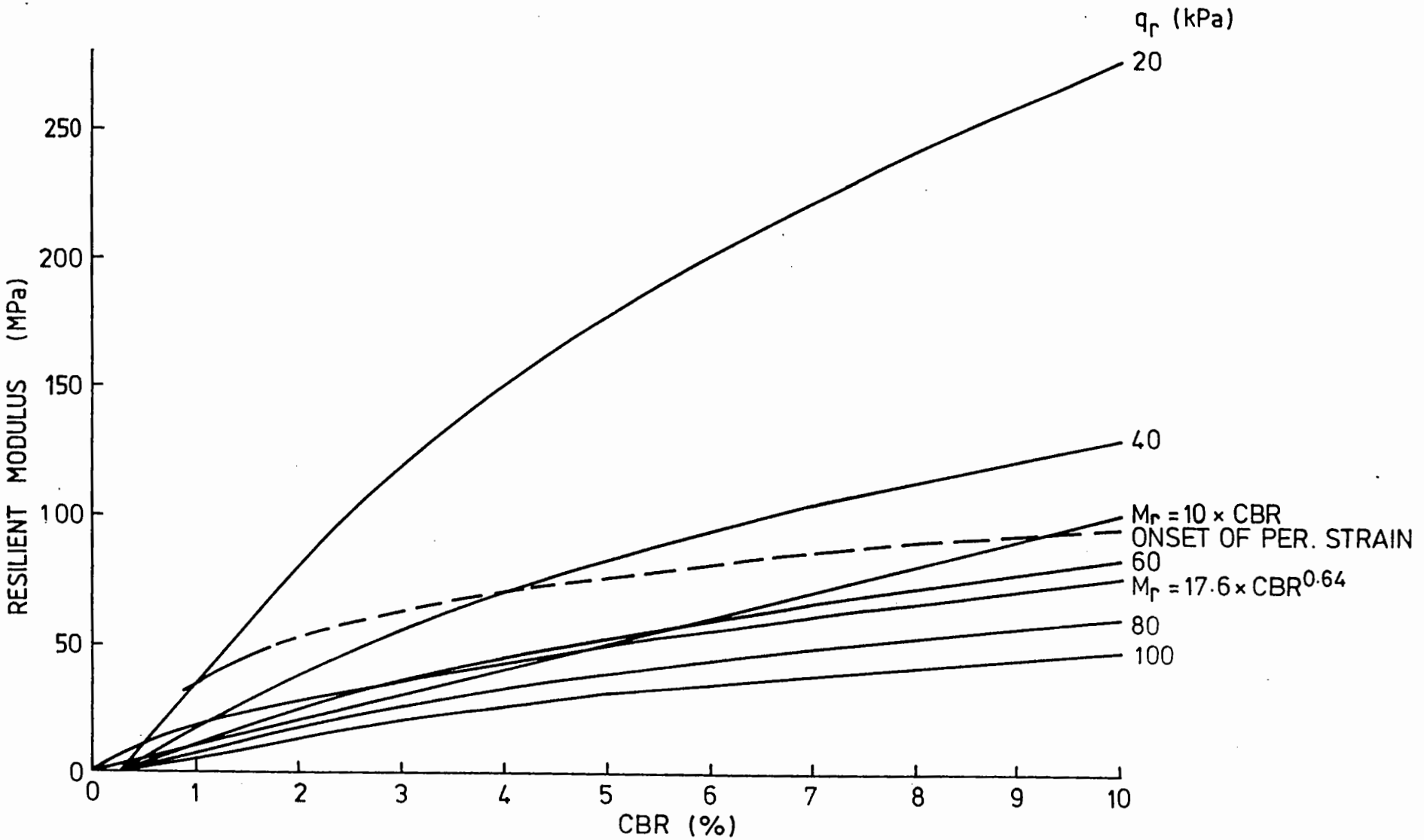

Figure A1.4 The Relationship between Stiffness and CBR for Compacted Samples of Keuper Marl for a Range of Stress Pulse Amplitudes (after Loach 1987).

Table A-2

Results of Classification Tests for Keuper Marl

Unified Soil Classification	CL
Specific Gravity	2.69
% Clay	33
Plastic Limit (%)	18
Liquid Limit (%)	37
Plasticity Index	19
Maximum Dry Density (kg/m^3)	1872
Optimum Moisture Content (%)	15.5

He further suggested the following equation to model the elastic stiffness of compacted Keuper Marl:

$$E_r = \frac{q_r}{A}\left(\frac{(u+\alpha p)}{q_r}\right)^B$$

where u = suction in kPa

p = cell pressure in kPa

$\alpha = 0.3$

E_r = Elastic Stiffness in kPa

q_r = Repeated deviator stress in kPa

$A = 2740$

$B = 2.1$

For the permanent strain behaviour of Keuper Marl, the results obtained by Bell, as shown in Figure A1.5 were found to be the most applicable. Comparison of the index properties between Bell's soil and the one used in the current project showed them to be similar.

A.3 Tests on Geosynthetics

Large Direct Shear Box Tests: 24 large direct shear box tests were performed on the two geosynthetic materials in conjunction with the soil and granular materials. The shear box used for these tests measured 300 mm square by 170 mm high. In each test, the same material was used in both the upper and lower half of the shear box. Compaction was carried out by using a hand-held vibrating hammer. In general, the moisture content and dry density of the material at the time of the large scale pavement test were simulated. The results of the tests are shown in Figure A1.6.

Wide Width Tensile Tests: These tests were carried out at the University of Strathclyde where specialist apparatus was available (Yeo 1985). All tests were conducted at a standard test temperature of 20 °C and were continued until rupture occurred. A standard shearing rate of 2% per minute was used for the geogrid but for the stiff geotextile, because of the requirement of a much higher failure load, the use of a faster rate of 7.5% per minute was necessary. The results of the tests for both materials are shown in Figure A1.7.

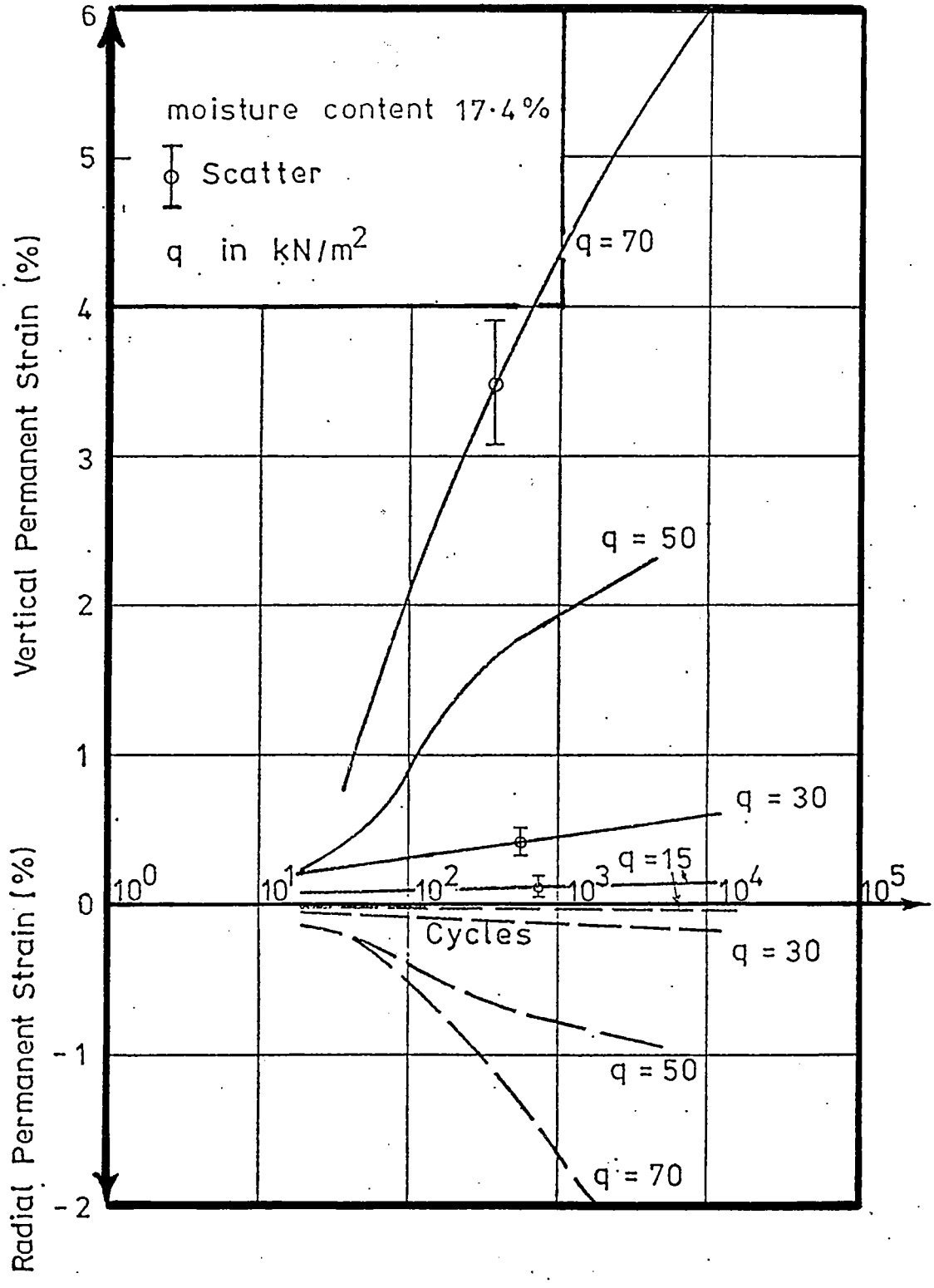

Figure A1.5 Permanent Axial and Radial Strain Responses of Keuper Marl for a Range of Stress Pulse Amplitudes (after Bell 1978).

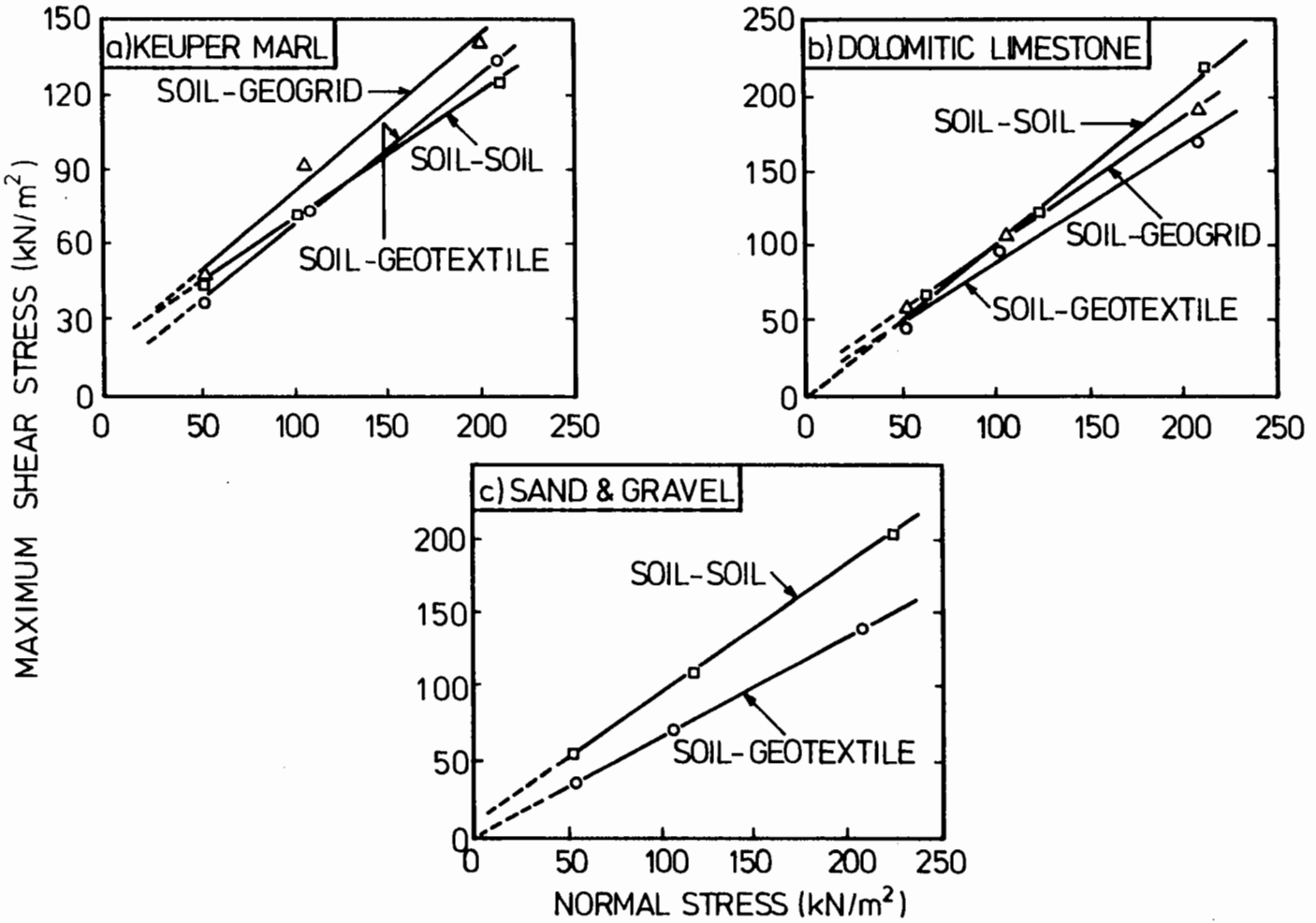

Figure A1.6 Relationships between Normal and Maximum Shear Stress in Large Shear Box Tests.

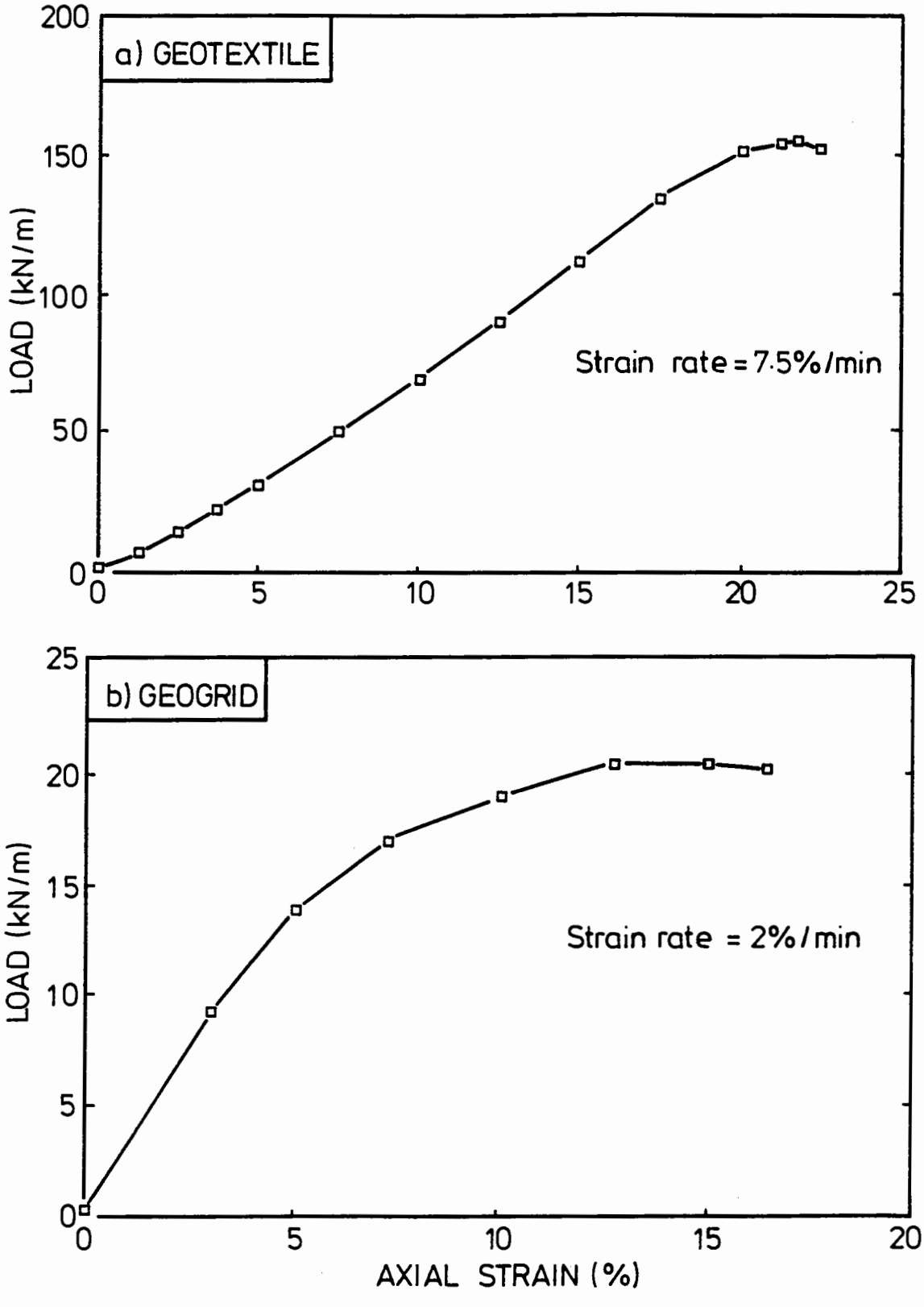

Figure A1.7 Variation of Axial Strain with Load in Wide-width Tensile Tests.

Creep Tests: Background and details of the test were reported by Murray and McGown (1987). All creep tests were carried out in isolation with no confining medium. For each geosynthetic material, up to five separate tests, each with a different sustained load, were performed. For the geogrid, the maximum sustained load corresponded to 60% of the tensile strength of the material. All tests were carried out at 20 °C and, in most cases, lasted for 1000 hours. The results of the two sets of tests during the first 10 hours are shown in Figure A1.8.

A.4 Tests on Asphaltic Materials

Six Marshall samples, made out of the HRA and AC mixes used in the test series were tested. The average test results of the six samples are shown in Table A.3. Two viscosity tests were carried out at Georgia Institute of Technology on the 50 Pen binder used for the asphaltic concrete mix. The viscosity at 60 °C was found to be about 4600 poises.

Table A-3

Comparison of Marshall Test Data for Two Asphaltic Mixes

	Hot Rolled Asphalt	*Asphaltic Concrete*
Binder Content (% by weight)	8	6.5
Mix Density (kg/m^3)	2307	2435
Air Void (%)	6	2.5
VMA (%)	23.6	19
Corrected Stability (kN)	9.03	9.57
Flow (mm)	4.19	4.57

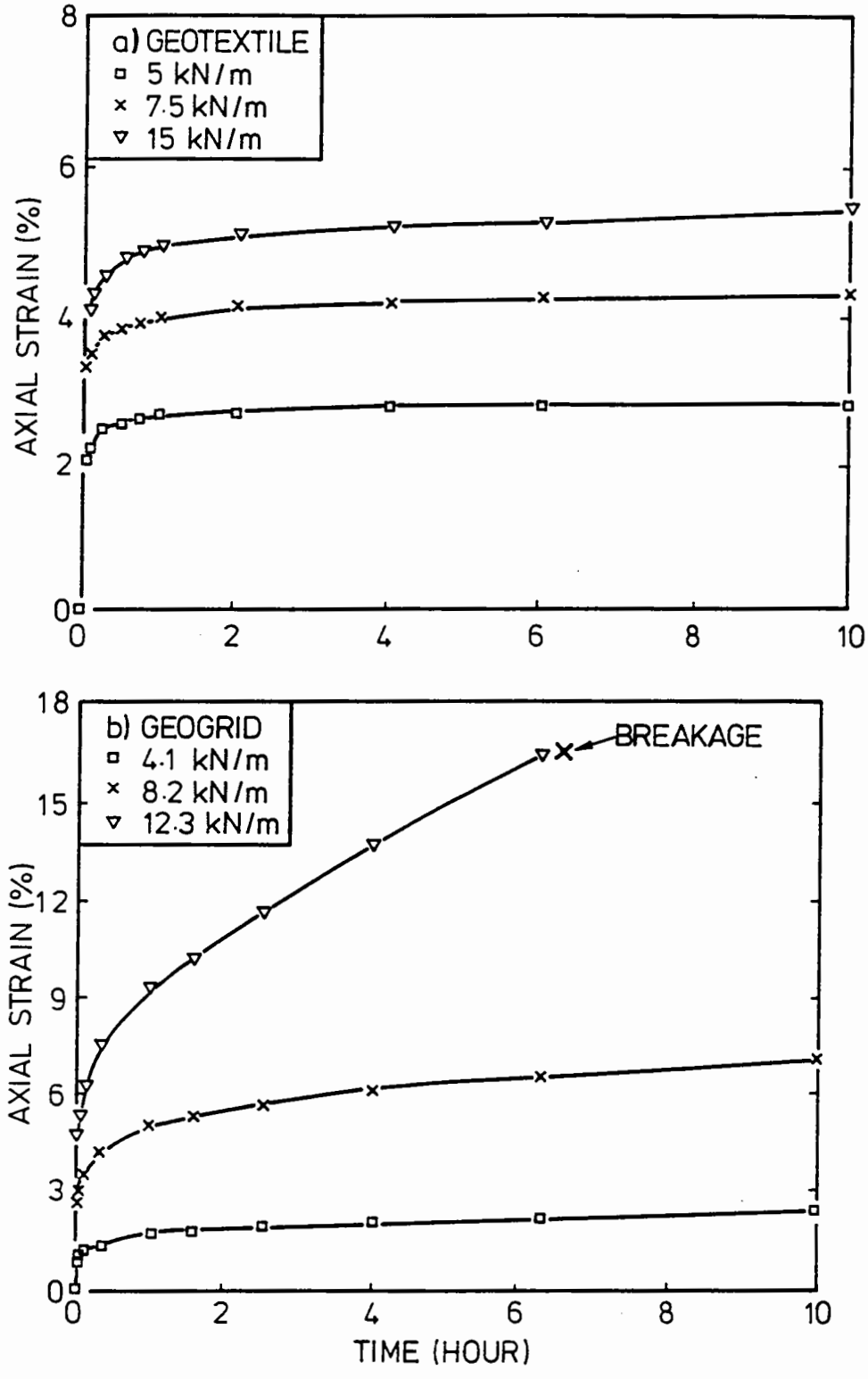

Figure A1.8 Results of Creep Tests for the Geosynthetics at various Sustained Loads during the first 10 Hours.

APPENDIX B

CALIBRATION OF TRANSDUCERS USED IN REPEATED LOAD HOLLOW CYLINDER APPARATUS

Calibration of the transducers used in repeated load HCA tests were carried out on a regular basis of approximately once every two tests. A brief description of the methods used are presented as follows and the results are shown in Table B.1.

B.1 Vertical Load Cell

The vertical load cell was calibrated by means of a standard proving ring with maximum capacity of 14 kN and load-per-division value of approximately 0.011 kN. The vertical compressive load was provided by a standard hydraulic jack and the response of the load cell at regular values of deflection of the proving ring was monitored by a voltmeter. Maximum load of 12 kN, equivalent to approximately 350 kPa in axial stress was used. Linearity between the output voltage and the proving ring deflection was generally observed with coefficient of correlation, R^2, in the region of 0.999.

B.2 Torsional Load Cell

The best method of calibrating the torsional load cell was by means of a pair of hangers and weights connected, via a pulley system to a set of extended steel arms bolted to the load cell. Calibration was carried out in steps of 1 or 2 kg on each hanger, which is equivalent to 1.4 or 2.8 kPa respectively in torsional shear stress. This continued until a total of 35 kg or approximately 50 kPa was reached. Both clockwise and anti-

clockwise loading were performed. It was noted that linearity between the applied moment and the output from the load cell during the initial 30 to 35 kPa in shear stress was generally good. However, beyond this magnitude, some hysteretic effect was observed. Despite this, R^2 of 0.993 to 0.998 were achieved.

B.3 LVDTs

The LVDTs were individually calibrated by means of a micrometer capable of providing reading to 0.0025mm which was equivalent to 17 με for a gauge length of 150mm. The gain setting of the strain gauge amplifier was set initially for a full scale deflection of about 2.5% strain. However, subsequent tests required this to be increased to 4%. Linearity was generally very good for the LVDTs.

B.4 Strain Hoops

Calibration of the two strain hoops was performed simultaneously by means of a specially assembled device consisting of a micrometer and three sets of mounting units. Both compressive and tensile deformations of the strain hoops were calibrated. Good linearity within the range of ±2% strains was obtained.

B.5 Bison Strain Coils

Calibration of the strain coils was carried out according to the instruction manual published by Bison Instruments. It involved the use of the Bison Recorder and a special mounting unit which incorporated a micrometer. Because of the small wall

thickness of the hollow cylinder specimen and in general, small change in thickness, it is not possible to rely on the amplitude value to determine the spacing between coils. Instead, the voltage produced by the small differential movement at a particular balanced position was used. A "CALIBRATION" setting of 500 was chosen. Although the micrometer can resolve movement down to 0.0025mm, due to the small gauge length involved (28 to 30mm), it only represents a strain value of 89 με. However, since the relationships between output voltage and the small differential movement is linear, interpolation can be carried out to determine smaller strain value. This method required that calibration be carried out at a few balanced positions corresponding to the anticipated gauge lengths.

Table B-1

Results of Calibrations for the Transducer used in Repeated Load HCA Tests

Date	*LVDTs (mm/volt)*				*Strain Hoops (mm/volt)*		*Strain Coil (mm/volt)*		*Torsional Load Cell (kPa/Volt)*	*Vertical Load Cell (kPa/Volt)*
	1	*2*	*3*	*4*	*1*	*2*	*1*	*2*		
14.08.89	0.4717	0.4027	0.3534	0.3639	1.146	1.263	0.120	0.112	14.30	169.2
14.09.89	0.4075	0.4139	0.3531	0.4035	1.195	1.329	/	/	13.44	171.5
17.10.89	0.4050	0.4014	0.3550	0.4030	1.225	1.325	0.107	0.111	13.60	172.3
02.01.90	1.1869	1.244	1.3955	1.1584	1.139	1.285	0.112	0.109	13.20	172.0
29.01.90	1.1732	1.2423	1.4311	1.1623	1.170	1.293	/	/	14.08	172.0

Note: "/" means not available.

APPENDIX C

SOFTWARE PROGRAMS FOR THE REPEATED LOAD HCA TEST

The main program for the data acquisition of the repeated load HCA tests is called HCA. The primary functions of the program are:

1. Retrieve data from the specified channels (maximum 8) at specified intervals (2 to 510 milliseconds) for a specified number of times.

2. Based on the input calibration value for each channel, calculate the corresponding stresses and strains. It also calculate all the relevant invariant parameters.

3. Store the raw and/or processed data onto disks.

4. Output test information and key results onto printer.

The total number of scan that can be performed during one run of the program depends on the number of channels selected and cannot be larger than the quotient obtained by dividing 2048 by the number of channels. For each new run, a new data file name in sequential order will be generated. Further analysis or plotting of the data is found to be more efficiently performed by using existing commercially available softwares. To facilitate this, all data files are created such that they can be "imported" by most popular softwares.

The program was written in BASIC language and a listing is presented as follows:

```
10 '                    DATA ACQUISITION FOR THE REPEATED LOAD
20 '                        HOLLOW CYLINDER TEST APPARATUS
30 '                    ******************************************
40 '
50 '
60 'Startup
70 '
80 DEF SEG=0
90 DRIVER1=PEEK(&H4F0)+256*PEEK(&H4F1)
100 DRIVER2=PEEK(&H4F4)+256*PEEK(&H4F5)
110 DEF SEG=DRIVER1 : REM SELECT CARD £1
120 INIT=3 : ABORTIO=6 : DEVCLEAR=9 : LOCAL=12
130 LOCALLOCKOUT=15 : REMOTE=18 : IRESUME=21 : TRIGGER=24
140 OUTPUT=27 : ENTER=30 : STATUS=33 : SETTERMINATOR=36
150 SETTIMEOUT=39 : SERIALPOLL=42 : SRQCHECK=45 : ERRCHECK=48
160 SETEOI=51 : SETTERM=54 : PARALLELPOLL=57 : SRVREQ=60
170 NCINIT=63 : BLOCKOUT=66 : BLOCKIN=69 : BYTESWAP=72
180 TRANSFER=75 : TALK=78 : UNTALK=81 : LISTEN=84
190 UNLISTEN=87 : ATTN=90 : MTA=93 : MLA=96
200 '
210 CALL INIT                                          'initialize driver
220 AD%=9                                              'device address
230 V$=SPACE$(56)                                      'reserve space for data *
240 DIM R(8,256)                                       'data array             *
250 DIM AXSS(256) : DIM TORSS(256) : DIM P(256) : DIM Q(256)
260 DIM OCTASS(256) : DIM ANGSS(256) : DIM AXST(256) : DIM CIRST(256)
270 DIM OBST(256) : DIM RADST(256) : DIM VOLST(256) : DIM SHEARST(256)
280 DIM OCTAST(256) : DIM ANGST (256) : DIM TORST(256):DIM TORP(256)
290 DIM SS1(256) : DIM SS3(256)
300 CHAN=8 : CHAN$="8"                                 '                       *
310 '
320 GOSUB 1170                                          'erase old data files
330 GOSUB 1300                                         'user options
340 GOSUB 460                                          'set device parameters
350 GOSUB 580                                          'retrieve readings
360 GOSUB 2160                                          'read initial data
370 GOSUB 2330                                         'cal stresses
380 GOSUB 2760                                         'cal strains
390 GOSUB 3390                                         'output to printer
400 GOSUB 1520                                         'transfer to disc
410 GOSUB 760                                          'print readings
420 GOSUB 1870                                         'repeat option
430 END
440 '
450 '
460 'Set device parameters
470 '
480 CMD$="A,PA6144,G0,I0,I1,I2,I3,I4,I5,I6,I7,G5"+SCAN$+","+"GD"+DELAY$        '
    *
490 CALL OUTPUT(CMD$,AD%)                              'output command string to device
500 CMD$="GE"                                          'trigger command
```

```
510 LOCATE 23,1 : INPUT "RETURN TO TRIGGER  ",DUM$      'RETURN to trigger
520 CALL OUTPUT(CMD$,AD%)
530 LOCATE 23,1 : PRINT "TAKING READINGS                "
540 GOSUB 1110                                           'wait for SRQ=1
550 SOUND 150,2                                          'beep !
560 RETURN
570 '
580 'Retrieve data
590 '
600 CMD$="PA6144,QI"                                    'reset pointers
610 CALL OUTPUT(CMD$,AD%)
620 '
630 FOR I=1 TO SCAN
640 CALL ENTER(V$,AD%)                                   'get data from A-D
650 R(1,I)=VAL(MID$(V$,1,6))/3277                        'split into channels &
660 R(2,I)=VAL(MID$(V$,8,13))/3277                       'and convert to
670 R(3,I)=VAL(MID$(V$,15,20))/3277                      'voltage
680 R(4,I)=VAL(MID$(V$,22,27))/3277
690 R(5,I)=VAL(MID$(V$,29,34))/3277
700 R(6,I)=VAL(MID$(V$,36,41))/3277
710 R(7,I)=VAL(MID$(V$,43,48))/3277
720 R(8,I)=VAL(MID$(V$,50,55))/3277
730 NEXT
740 RETURN
750 '
760 'Print Results
770 '
780 LOCATE 6,1 : PRINT STRING$(72,45)                    '------
790 LOCATE 7,2 : PRINT "TIME"
800 '
810 FOR J=1 TO 8
820 LOCATE 7,(8+8*(J-1)) :PRINT "CHANNEL"
830 LOCATE 8,(10+8*(J-1)) :PRINT J-1
840 NEXT
850 LOCATE 9,1 : PRINT STRING$(72,45)                    '-------
860 '
870 B=0 : I=1
880 LOCATE (10+B),1 : PRINT (I*DELAY*2)                    'time
890 '
900 FOR J=1 TO CHAN
910 LOCATE (10+B),(8+8*(J-1)) : PRINT USING"£.£££"; R(J,I)          'result
920 NEXT
930 '
940 B=B+1 : I=I+1                                        'next
950 IF B<>14 THEN 1040                                    'check if screen full
960 LOCATE 23,1 : PRINT"RETURN to CONTINUE / ESC to SKIP / ANY OTHER KEY to SCRO
LL BACK"
970 Q$=INKEY$ : IF LEN(Q$)=0 THEN 970                    'wait for input
980 IF ASC(Q$)=27 THEN RETURN                            'IF ESC .....
990 IF ASC(Q$)=13 THEN 1020                               'IF RETURN ....
1000 '
```

```
1010 IF I=15 THEN I=1 ELSE I=I-28                          'scroll back
1020 B=0
1030 VIEW PRINT 9 TO 23 : CLS : VIEW PRINT 1 TO 24         'clear data
1040 IF I=SCAN THEN 1050 ELSE GOTO 880                     'end of results ?
1050 LOCATE 23,1 : PRINT"Press RETURN to CONTINUE - ANY OTHER KEY to SCROLL BACK
"
1060 Q$=INKEY$ : IF LEN(Q$)=0 THEN 1060
1070 IF ASC(Q$)=13 THEN RETURN
1080 IF I<15 THEN I=1 ELSE I=I-14-B
1090 GOTO 1020
1100 '
1110 'SRQ Check
1120 '
1130 CALL SRQCHECK(SRQ)                                    'test SRQ
1140 IF SRQ<>1 THEN 1130
1150 RETURN
1160 '
1170 'Erase Old Data Files
1180 '
1190 '
1200 OPEN "A:TESTX" AS £1 LEN=3                  'holds last result file no.
1210 IF LOF(1)=0 THEN CLOSE :GOTO 1250           'IF does not exist ..
1220 FIELD £1, 3 AS X$                           'define field
1230 GET£1,1 : CLOSE                             'get record
1240 '
1250 CLS
1260 LOCATE 1,25 : PRINT "DATA FILE ";(VAL(X$)+1)
1270 LOCATE 2,25 : PRINT "**************"
1280 RETURN
1290 '
1300 'User Inputs
1310 '
1320 VIEW PRINT 5 TO 23 : CLS : VIEW PRINT 1 TO 24       'clear screen
1330 '
1340 LOCATE 3,1 : PRINT" ZERO STRAIN CRITERIA (A or T) =   "
1350 LOCATE 3,40 : INPUT ZEROCR$
1360 LOCATE 4,1 : PRINT "Interscan Delay  =    "
1370 LOCATE 4,50 : PRINT"MAX = 255"
1380 LOCATE 4,21 : INPUT"",DELAY$
1390 DELAY=VAL(DELAY$)
1400 VIEW PRINT 23 TO 23 : CLS : VIEW PRINT 1 TO 24
1410 IF DELAY > 255 THEN LOCATE 23,1 : PRINT "Delay is too long " : GOTO 1360
1420 '
1430 '
1440 LOCATE 5,1 : PRINT "Scans   =    "
1450 LOCATE 5,50 : PRINT "MAX = 256"                     '       *
1460 LOCATE 5,12,0,7 : INPUT"",SCAN$
1470 SCAN=VAL(SCAN$)
1480 IF SCAN>256 THEN LOCATE 23,1 : PRINT "Too many scans " : GOTO 1440 '*
1490 VIEW PRINT 23 TO 23 : CLS : VIEW PRINT 1 TO 24
1500 RETURN
```

```
1510 '
1520 'Transfer Data to Disc
1530 '
1540 OPEN "A:TESTX" AS £1 LEN=3
1550 FIELD £1,3 AS X$
1560 GET £1,1
1570 Y$=STR$(VAL(X$)+1) : L=LEN(Y$) : Y$=RIGHT$(Y$,L-1)
1580 '
1590 OPEN "A:RES"+Y$+".PRN" FOR OUTPUT AS £2            'open data file
1600 PRINT £2,CHR$(34);"DATA FILE =";CHR$(34);(VAL(X$)+1)
1610 PRINT £2,CHR$(34);"No.Scans = ";CHR$(34);SCAN$
1620 PRINT £2,CHR$(34);"Delay = ";CHR$(34);DELAY$
1630 '
1640 GOSUB 2050                                         'experimental conditions
1650 '
1660 PRINT £2,CHR$(34);"   TIME     AXSS    TORSS      P         Q       TORP
OCTASS";CHR$(34)
1670 FOR I=LOW TO HIGH
1680 PRINT £2,(I*DELAY*2),AXSS(I),TORSS(I),P(I),Q(I),TORP(I),OCTASS(I),ANGSS(I),
AXST(I),CIRST(I),OBST(I),TORST(I),RADST(I),VOLST(I),SHEARST(I),OCTAST(I),ANGST(I
),SS1(I),SS3(I),RADSS 'store result *
1690 NEXT
1700 '
1710 OPEN "A:DAT"+Y$+".PRN" FOR OUTPUT AS £3
1720 PRINT £3,CHR$(34);"DATA FILE =";CHR$(34);(VAL(X$)+1)
1730 PRINT £3,CHR$(34);"No.Scans = ";CHR$(34);SCAN$
1740 PRINT £3,CHR$(34);"Delay = ";CHR$(34);DELAY$
1750 FOR J=1 TO 5
1760 PRINT £3,CHR$(34),C$(J),CHR$(34)                   'save on disc
1770 NEXT
1780 PRINT £3,CHR$(34);"   TIME   CHAN 0   CHAN 1   CHAN 2   CHAN 3   CHAN 4   C
HAN 5   CHAN 6   CHAN 7  ";CHR$(34)
1790 FOR I=1 TO SCAN
1800 PRINT £3,(I*DELAY*2),R(1,I),R(2,I),R(3,I),R(4,I),R(5,I),R(6,I),R(7,I),R(8,I
)
1810 NEXT
1820 LSET X$=Y$                                         'store latest file no.
1830 PUT £1,1                                           'record on disc
1840 CLOSE                                              'close all files
1850 RETURN
1860 '
1870 'Repeat Data Collection
1880 '
1890 LOCATE 23,1 : PRINT "Press ANY KEY to use same settings - RETURN otherwise
                  "
1900 Q$=INKEY$
1910 IF LEN(Q$)=0 THEN 1900
1920 IF ASC(Q$)=13 THEN 1970
1930 VIEW PRINT 5 TO 23 : CLS : VIEW PRINT 1 TO 24
1940 LOCATE 1,35 : PRINT (VAL(Y$)+1) : GOTO 340        'print new file no.
1950 '
1960 '
1970 VIEW PRINT 5 TO 23 : CLS : VIEW PRINT 1 TO 24
1980 LOCATE 23,1 : PRINT " Press RETURN to END - ANY KEY otherwise"
1990 Q$=INKEY$
2000 IF LEN(Q$)=0 THEN 1990
```

```
2010 VIEW PRINT 5 TO 23 : CLS : VIEW PRINT 1 TO 24
2020 IF ASC(Q$)<>13 THEN LOCATE 1,35 : PRINT (VAL(Y$)+1) : GOTO 330
2030 RETURN
2040 '
2050 'Record Exprimental Conditions
2060 '
2070 VIEW PRINT 6 TO 23 : CLS : VIEW PRINT 1 TO 24
2080 FOR J=1 TO 5
2090 LOCATE (6+J*2),1 : PRINT "Condition  ";J            'user prompt
2100 LOCATE (6+2*J),16 : INPUT"",C$(J)
2110 PRINT £2,CHR$(34),C$(J),CHR$(34)                   'save on disc
2120 NEXT
2130 VIEW PRINT 6 TO 23 : CLS : VIEW PRINT 1 TO 24
2140 RETURN
2150 '
2160 '
2170 ' READ INITIAL DATA
2180 '
2190 DAY$ ="19TH JANUARY 1990 "
2200 SAMPLE$="SAMPLE NUMBER 6 (PERMANENT STRAIN TEST)"
2210 AXZERO= -1.000001E-02
2220 TORZERO=-0!
2230 POUT= 100 :PIN=100
2240 CAL1=172 : CAL2=-13: CAL5=-9346:CAL6=8294:CAL7=9429:CAL8=8840
2250 CAL4=-4790: CAL3=3620
2260 COIL=.52
2270 HOOP=-1.529
2280 LVDT1=1.989
2290 LVDT2=-2.084
2300 LVDT3=-2.909
2310 LVDT4=-2.305
2320 RETURN
2330 'CALCULATE STRESSES AND FIND MAX.AND MIN. STRESSES
2340 RADSS=3.96825*(POUT*.14+PIN*.112)
2350 CIRSS=35.71429*(POUT*.14-PIN*.112)
2360 FOR I=1 TO SCAN
2370 AXSS(I)=(R(1,I)-AXZERO)*CAL1+141.72*(.0196*POUT-.01254*PIN)
2380 TORSS(I)=(R(2,I)-TORZERO)*CAL2
2390 MOHRRA= SQR(((AXSS(I)-CIRSS)/2)^2+TORSS(I)^2)
2400 MOHRCE= (AXSS(I)+CIRSS)/2
2410 P(I)= (AXSS(I)+RADSS+CIRSS)/3
2420 Q(I)=MOHRRA
2430 SS1(I)=MOHRRA+MOHRCE
2440 SS3(I)=MOHRCE-MOHRRA
2450 OCTASS(I)=SQR((SS1(I)-RADSS)^2+(RADSS-SS3(I))^2+(SS1(I)-SS3(I))^2)*.7071
2460 ANGSS(I)=ATN(TORSS(I)/(SS1(I)-CIRSS))*57.296
2470 NEXT I
2480 '
2490 'FIND MAX AND MIN STRESSES
2500 '
```

```
2510 MAX1=-99999! : MIN1=99999!:MINI1=99999! 'FOR AXIAL STRESS
2520 MAX2=-99999! : MIN2=99999!:MINI2=99999!     'FOR TORSIONAL STRESS
2530 MAX11=-99999! : MIN11= 99999!     'FOR STRESS ANGLE
2540 '
2550 FOR I=1 TO SCAN
2560 IF ABS(AXSS(I))<=MIN1 THEN MIN1=ABS(AXSS(I)): MINSS= I
2570 IF ABS(TORSS(I))<=MIN2 THEN MIN2=ABS(TORSS(I)): MINTOR= I
2580 NEXT I
2590 IF (ZEROCR$ = "A") THEN KK=MINSS
2600 IF (ZEROCR$ = "T") THEN KK=MINTOR
2610 HIGH=KK+16
2620 LOW=KK-16
2630 IF LOW<1 THEN LOW=1:HIGH=32:GOTO 2650
2640 IF HIGH>SCAN THEN LOW=SCAN-32:HIGH=SCAN
2650 FOR I=LOW TO HIGH
2660 IF AXSS(I)>MAX1 THEN MAX1=AXSS(I) : MAXSS= I
2670 IF AXSS(I)<MINI1 THEN MINI1=AXSS(I):MSS=I
2680 IF TORSS(I)>MAX2 THEN MAX2=TORSS(I):MAXTOR= I
2690 IF TORSS(I)<MINI2 THEN MINI2=TORSS(I):MTOR=I
2700 IF ANGSS(I)>MAX11 THEN MAX11=ANGSS(I)
2710 IF ANGSS(I)<MIN11 THEN MIN11=ANGSS(I)
2720 NEXT I
2730 IF (ZEROCR$ = "A") THEN LL=MAXSS: MM=MSS
2740 IF (ZEROCR$ = "T") THEN LL=MAXTOR:MM=MTOR
2750 RETURN
2760 '
2770 'CALCULATE RESILIENT STRAINS
2780 '
2790 FOR I=LOW TO HIGH
2800 TORP(I)=2*TORSS(I)/(P(I)+P(KK))
2810 AXST(I)=((R(6,I)-R(6,KK))*CAL6+(R(7,I)-R(7,KK))*CAL7)/2
2820 CIRST(I)=(R(4,I)-R(4,KK))*CAL4
2830 OBST(I)=((R(5,I)-R(5,KK))*CAL5+(R(8,I)-R(8,KK))*CAL8)/2
2840 RADST(I)=(R(3,I)-R(3,KK))*CAL3
2850 TORST(I)=-1*(2*OBST(I)-AXST(I)-CIRST(I))/2
2860 MOHRR=SQR(((AXST(I)-CIRST(I))/2)^2+TORST(I)^2)
2870 MOHRC=(AXST(I)+CIRST(I))/2
2880 VOLST(I)=AXST(I)+CIRST(I)+RADST(I)
2890 SHEARST(I)=MOHRR
2900 ST1=MOHRR+MOHRC
2910 ST3=MOHRC-MOHRR
2920 OCTAST(I)=SQR((ST1-ST3)^2+(ST1-RADST(I))^2+(RADST(I)-ST3)^2)*.4714
2930 ANGST(I)=ATN(TORST(I)/(ST1-CIRST(I)+1))*57.296
2940 NEXT I
2950 '
2960 'CALCULATE STRAIN and STRESS INVARIANTS AT MAXIMUM STRESS
2970 '
2980 P1=P(KK): P2=P(LL): Q1=Q(KK): Q2=Q(LL)
2990 GP1=Q1/P1 : GP2=Q2/P2
3000 DGP=GP2-GP1:  GPM=(Q2+Q1)/(P1+P2)
```

```
3010 L2MX=(R(6,LL)-R(6,KK))*CAL6
3020 L3MX=(R(7,LL)-R(7,KK))*CAL7
3030 AXSTMX=((R(6,LL)-R(6,KK))*CAL6+(R(7,LL)-R(7,KK))*CAL7)/2
3040 CIRSTMX=(R(4,LL)-R(4,KK))*CAL4
3050 L1MX=(R(5,LL)-R(5,KK))*CAL5
3060 L4MX=(R(8,LL)-R(8,KK))*CAL8
3070 OBSTMX=((R(5,LL)-R(5,KK))*CAL5+(R(8,LL)-R(8,KK))*CAL8)/2
3080 RADSTMX=(R(3,LL)-R(3,KK))*CAL3
3090 TORSTMX=-1*(2*OBSTMX-AXSTMX-CIRSTMX)/2
3100 MOHRR=SQR(((AXSTMX-CIRSTMX)/2)^2+TORSTMX^2)
3110 MOHRC=(AXSTMX+CIRSTMX)/2
3120 VOLSTMX=AXSTMX+CIRSTMX+RADSTMX
3130 SHEARMX=MOHRR
3140 ST1=MOHRR+MOHRC
3150 ST3=MOHRC-MOHRR
3160 OCTASTMX=SQR((ST1-ST3)^2+(ST1-RADSTMX)^2+(RADSTMX-ST3)^2)*.4714
3170 ANGSTMX=ATN(TORSTMX/(ST1-CIRSTMX))*57.296
3180 '
3190 'CALCULATE PERMANENT STRAIN AT CURRENT MINIMUM STRESS LEVEL
3200 '
3210 PL2=(R(6,KK)-LVDT2)*CAL6
3220 PL3=(R(7,KK)-LVDT3)*CAL7
3230 AXSTPX=((R(6,KK)-LVDT2)*CAL6+(R(7,KK)-LVDT3)*CAL7)/2
3240 CIRSTPX=(R(4,KK)-HOOP)*CAL4
3250 PL1=(R(5,KK)-LVDT1)*CAL5
3260 PL4=(R(8,KK)-LVDT4)*CAL8
3270 OBSTPX=((R(5,KK)-LVDT1)*CAL5+(R(8,KK)-LVDT4)*CAL8)/2
3280 RADSTPX=(R(3,KK)-COIL)*CAL3
3290 TORSTPX=-1*(2*OBSTPX-AXSTPX-CIRSTPX)/2
3300 MOHRR=SQR(((AXSTPX-CIRSTPX)/2)^2+TORSTPX^2)
3310 MOHRC=(AXSTPX+CIRSTPX)/2
3320 VOLSTPX=AXSTPX+CIRSTPX+RADSTPX
3330 SHEARPX=MOHRR
3340 ST1=MOHRR+MOHRC
3350 ST3=MOHRC-MOHRR
3360 OCTASTPX=SQR((ST1-ST3)^2+(ST1-RADSTPX)^2+(RADSTPX-ST3)^2)*.4714
3370 ANGSTPX=ATN(TORSTPX/(ST1-CIRSTPX))*57.296
3380 RETURN
3390 '
3400 'SEND RESULTS AND DATA TO PRINT
3410 '
3420 LPRINT "***********  DATA  FILE ";(VAL(X$)+1)
3430 LPRINT
3440 LPRINT "DATE :"; DAY$
3450 LPRINT "SAMPLE DESCRIPTION :"; SAMPLE$
3460 LPRINT
3470 LPRINT "************************  SET-UP DATA  ************************"
3480 LPRINT
3490 LPRINT
3500 LPRINT "CAL FACTOR & IN.VOLTAGE FOR AXIAL STRESS       =";CAL1,AXZERO
3510 LPRINT "CAL FACTOR & IN.VOLTAGE FOR TORSIONAL STRESS   =";CAL2,TORZERO
3520 LPRINT "CAL FACTOR & IN.VOL FOR AXIAL STRAIN (LVDT2)   =";CAL6,LVDT2
```

```
3530 LPRINT "CAL FACTOR & IN.VOL FOR AXIAL STRAIN (LVDT3)   =";CAL7,LVDT3
3540 LPRINT "CAL FACTOR & IN.VOL FOR CIRCUM. STRAIN (HOOP)  =";CAL4,HOOP
3550 LPRINT "CAL FACTOR & IN.VOL FOR 45-DEG STRAIN (LVDT1)  =";CAL5,LVDT1
3560 LPRINT "CAL FACTOR & IN.VOL FOR 45-DEG STRAIN (LVDT4)  =";CAL8,LVDT4
3570 LPRINT "CAL FACTOR & IN.VOL FOR RADIAL STRAIN (COIL)   =";CAL3,COIL
3580 LPRINT
3590 LPRINT "********************  LOAD DATA  *************************"
3600 LPRINT
3610 LPRINT "INNER CELL PRESSURE(kPa)                       =";PIN
3620 LPRINT "OUTER CELL PRESSURE (kPa)                      =";POUT
3630 LPRINT "MAXIMUM AXIAL STRESS (kPa)                     =";MAX1
3640 LPRINT "MINIMUM AXIAL STRESS (kPa)                     =";MINI1
3650 LPRINT "MAXIMUM TORSIONAL STRESS (kPa)                 =";MAX2
3660 LPRINT "MINIMUM TORSIONAL STRESS (kPa)                 =";MINI2
3670 LPRINT "P one      (kPa)                               =";P1
3680 LPRINT "P two      (kPa)                               =";P2
3690 LPRINT "Q one      (kPa)                               =";Q1
3700 LPRINT "Q two      (kPa)                               =";Q2
3710 LPRINT "(Q/P) one   &  (Q/P) two                       =";QP1,QP2
3720 LPRINT "CHANGE  &  MEAN (Q/P)                          =";DQP,QPM
3730 LPRINT
3740 LPRINT "MAXIMUM PRINCIPAL STRESS ROTATION (DEGREE)     =";MAX11
3750 LPRINT "MINIMUM PRINCIPAL STRESS ROTATION (DEGREE)     =";MIN11
3760 LPRINT
3770 LPRINT "*************************  STRAIN DATA  *************************"
3780 LPRINT
3790 IF(ZEROCR$="A") THEN LPRINT"ZERO STRAINS ASSUMED AT ZERO or ABSOLUTE MINIMU
M AXIAL STRESS"
3800 IF(ZEROCR$="T") THEN LPRINT"ZERO STRAINS ASSUMED AT ZERO or ABSOLUTE MINIMU
M TORSIONAL STRESS"
3810 LPRINT
3820 LPRINT "MAXIMUM STRESS OBTAINED AT SCAN NUMBER"; LL
3830 LPRINT "MINIMUM STRESS OBTAINED AT SCAN NUMBER"; MM
3840 LPRINT "ZERO STRAIN OBTAINED AT SCAN NUMBER";KK
3850 LPRINT
3860 LPRINT "RESILIENT STRAINS AT MAXIMUM STRESS ARE AS FOLLOWS:"
3870 LPRINT "RESILIENT AX STRAIN (MICROSTRAIN) (AV/L2/L3)   =";AXSTMX,L2MX,L3MX
3880 LPRINT "RESILIENT CIRCUMFERENTIAL STRAIN (MICROSTRAIN) =";CIRSTMX
3890 LPRINT "RESILIENT RADIAL STRAIN (MICROSTRAIN)          =";RADSTMX
3900 LPRINT "RESILIENT 45 STRAIN (MICROSTRAIN) (AV/L1/L4)   =";OBSTMX,L1MX,L4MX
3910 LPRINT "RESILIENT TORSIONAL STRAIN (MICROSTRAIN)       =";TORSTMX
3920 LPRINT "RESILIENT VOLUMATRIC STRAIN (MICROSTRAIN)      =";VOLSTMX
3930 LPRINT "RESILIENT MAX.SHEAR STRAIN (MICROSTRAIN)       =";SHEARMX
3940 LPRINT "ANGLE OF STRAIN INCREMENT ROTATION             =";ANGSTMX
3950 LPRINT
3960 LPRINT "ACCUM. PERMANENT STRAINS AT CURRENT MINIMUM STRESS ARE AS FOLLOWS:"
3970 LPRINT
3980 LPRINT "PERMANENT AX STRAIN (MICROSTRAIN) (AV/L2/L3)   =";AXSTPX,PL2,PL3
3990 LPRINT "PERMANENT CIRCUMFERENTIAL STRAIN (MICROSTRAIN) =";CIRSTPX
4000 LPRINT "PERMANENT 45 STRAIN (MICROSTRAIN) (AV/L1/L4)   =";OBSTPX,PL1,PL4
4010 LPRINT "PERMANENT RADIAL STRAIN (MICROSTRAIN)          =";RADSTPX
4020 LPRINT "PERMANENT SHEAR STRAIN (MICROSTRAIN)           =";SHEARPX
4030 LPRINT "PERMANENT VOLUMATRIC STRAIN (MICROSTRAIN)      =";VOLSTPX
4040 RETURN
```

APPENDIX D

REPEATED LOAD TRIAXIAL TEST APPARATUS

Details of the repeated load triaxial test apparatus which can accommodate test specimen with diameter of 150mm are shown in Figures D1.1 and D1.2. The axial load is applied to the specimen by a servo-hydraulic actuator and monitored by a strain gauged load cell located at the bottom section of the loading ram. The confining pressure which is also servo-hydraulically controlled is applied through a non-conducting medium of silicone oil and is monitored by a thin wall pressure cell.

For repeated loading, a waveform generator, capable of providing sinusoidal, square or triangular waveforms was used to generated the required command signals. During testing, the feedback signals from the two monitoring devices are compared with the command signal. An error message is then relayed to the servo-valves so that the necessary adjustment may be made. This arrangement ensures that the required loading conditions are achieved.

To measure deformation of the specimen, an on-sample instrumentation technique is used. This involves using four brass studs which are embedded in the sides of the specimen during sample preparation. The studs allow threaded rods to be attached to the specimen. The rods, in turn, enable the mounting of instruments. Two LVDTs mounted between the two pairs of rods are used to measured axial deformations. For radial deformations, two epoxy hoops incorporating strain gauges are used.

All the stress and strain data are recorded by the new data acquisition system described in Chapter Six. Dedicated software for the repeated load triaxial tests was developed. They are similar to those which are presented in Appendix C for the repeated HCA tests .

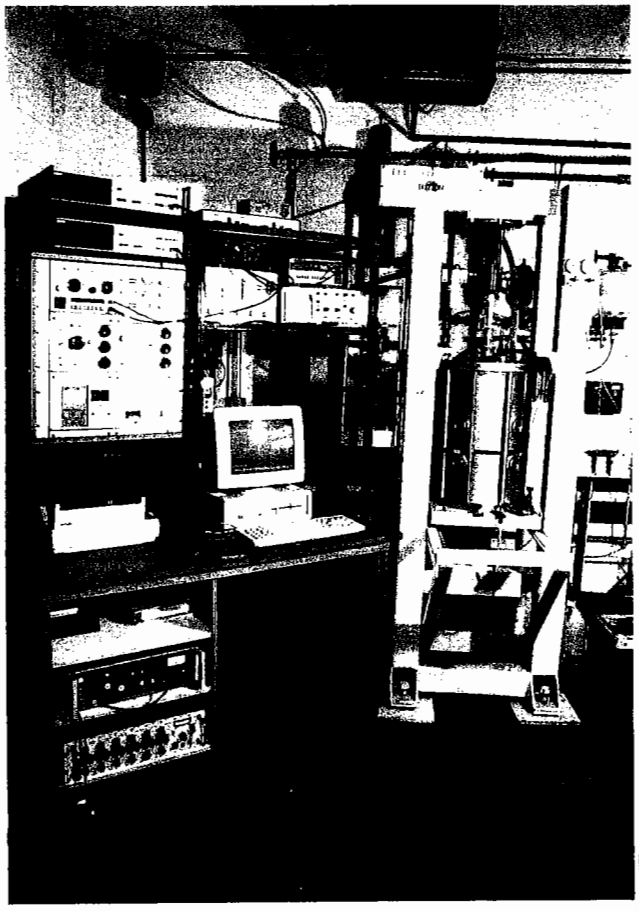

Figure D1.1

Laboratory Set-up of the Repeated Load Triaxial Test Apparatus

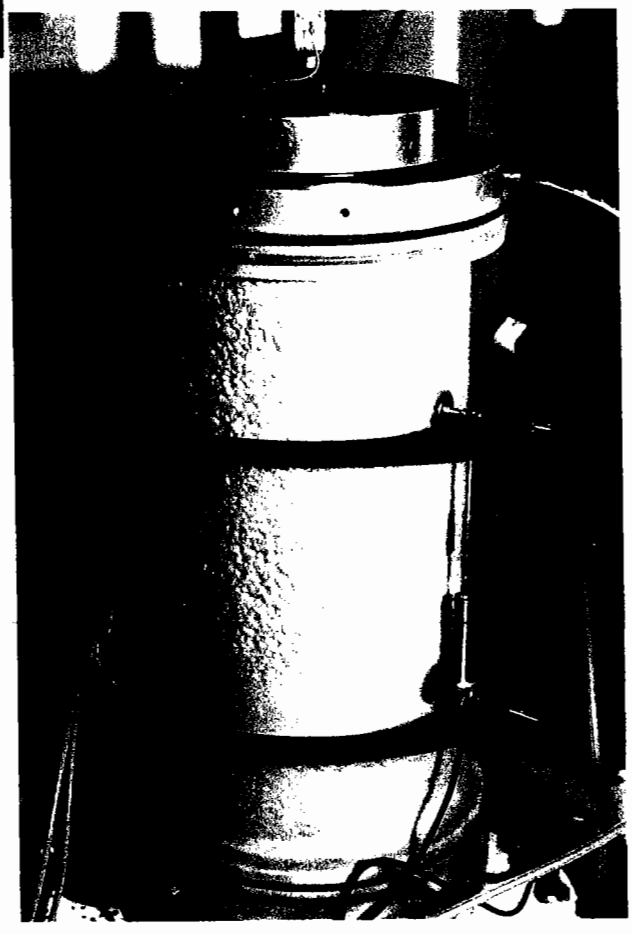

Figure D1.2

150mm-diameter Triaxial Specimen with Instrumentations

APPENDIX E

MEASURED STRESSES AND STRAINS FROM RESILIENT STRAIN TESTS

E.1 Results from Repeated Load Triaxial Tests

FILE NUMBER	INITIAL DEVIATOR STRESS (kPa)	FINAL DEVIATOR STRESS (kPa)	INITIAL CELL PRESSURE (kPa)	FINAL CELL PRESSURE (kPa)	RADIAL STRAIN (με)	AXIAL STRAIN (με)
1	.0	55.0	150.0	150.0	-41.0	170.0
2	.0	101.0	150.0	150.0	-87.0	290.0
3	.0	158.5	150.0	150.0	-149.0	474.0
4	.0	210.0	150.0	150.0	-213.0	628.0
5	.0	54.5	100.0	100.0	-52.0	227.0
6	.0	102.4	100.0	100.0	-134.0	425.0
7	.0	154.8	100.0	100.0	-201.0	585.0
8	.0	50.5	70.0	70.0	-73.0	260.0
9	.0	106.0	70.0	70.0	-236.0	554.0
10	.0	55.0	50.0	50.0	-158.0	428.0
11	.0	58.6	30.0	30.0	-228.0	645.0
12	.0	.0	30.0	80.0	266.3	232.2
13	.0	.0	50.0	100.0	240.9	72.4
14	.0	.0	100.0	150.0	240.1	78.8
15	.0	.0	50.0	150.0	309.8	278.2
16	50.0	50.0	100.0	150.0	204.0	29.6
17	50.0	50.0	50.0	100.0	245.4	39.8
18	100.0	100.0	100.0	150.0	192.5	-20.2
19	.0	227.0	150.0	150.0	-252.0	619.0

E.2 Results from Repeated Load Hollow Cylinder Tests

FILE NUMBER	INITIAL VERTICAL STRESS (kPa)	FINAL VERTICAL STRESS (kPa)	INITIAL TORSIONAL STRESS (kPa)	FINAL TORSIONAL STRESS (kPa)	INITIAL INNER PRESSURE (kPa)	FINAL INNER PRESSURE (kPa)	INITIAL OUTER PRESSURE (kPa)	FINAL OUTER PRESSURE (kPa)	AVERAGE RADIAL STRAIN (με)	AVERAGE CIRCUM. STRAIN (με)	AVERAGE AXIAL STRAIN (με)	AVERAGE 45 DEGREE STRAIN (με)
1	.0	.0	.0	.0	100.0	200.0	100.0	200.0	480.7	-15.3	700.0	-2.9
2	49.6	49.2	.0	.0	100.0	200.0	100.0	200.0	758.0	-12.4	710.0	-59.0
3	101.0	100.1	.0	.0	100.0	200.0	100.0	200.0	677.0	20.0	650.0	-110.0
4	99.8	99.3	.0	.0	100.0	200.0	100.0	200.0	503.3	149.2	650.0	36.0
5	.0	.0	-19.9	-19.9	105.0	100.0	100.0	100.0	-40.7	70.7	.4	61.0
6	.0	.0	20.1	19.9	105.0	100.0	100.0	100.0	-58.5	131.8	6.7	14.3
7	50.7	49.6	-20.1	-19.9	105.0	100.0	100.0	100.0	-58.6	108.2	-66.1	10.3
8	49.7	50.3	.0	.0	110.0	100.0	100.0	100.0	-98.2	286.5	-61.5	9.9
9	.0	.0	.0	-10.6	100.0	100.0	100.0	100.0	-138.6	34.0	482.0	321.0
10	.0	.0	.0	-20.8	100.0	100.0	100.0	100.0	-137.5	39.0	539.1	461.7
11	.0	53.7	.0	.0	100.0	100.0	100.0	100.0	-170.7	-60.8	552.0	426.2
12	.0	54.6	.0	-20.0	100.0	100.0	100.0	100.0	-172.3	-50.5	654.9	506.3
13	.0	.0	.0	-29.0	100.0	100.0	100.0	100.0	-167.4	40.0	567.9	539.5
14	.0	53.7	.0	-29.5	100.0	100.0	100.0	100.0	-164.7	-43.9	608.8	568.0
15	.0	103.6	.0	.0	100.0	100.0	100.0	100.0	-231.0	-125.0	739.2	480.7
16	.0	.0	.0	-38.8	100.0	100.0	100.0	100.0	-154.9	52.0	612.6	603.6
17	49.2	50.9	.0	.0	105.0	100.0	100.0	100.0	17.5	93.7	-49.9	-38.8
18	49.3	49.5	-20.1	-20.0	110.0	100.0	100.0	100.0	-93.4	274.5	-25.8	7.8
19	.0	.0	-39.9	-40.0	105.0	100.0	100.0	100.0	-58.5	125.4	-58.7	71.8
20	99.7	99.2	.0	.0	105.0	100.0	100.0	100.0	-45.8	92.2	98.0	-16.6
21	49.7	50.1	-39.9	-40.0	105.0	100.0	100.0	100.0	-43.8	120.0	71.0	96.6
22	99.3	99.8	-19.9	-19.9	105.0	100.0	100.0	100.0	-42.7	89.6	67.7	14.0
23	.0	152.7	.0	.0	100.0	100.0	100.0	100.0	-310.3	-227.7	883.8	496.9
24	.0	.0	-20.0	-19.9	75.0	70.0	70.0	70.0	-85.3	139.3	90.7	23.4
25	.0	.0	20.0	19.9	75.0	70.0	70.0	70.0	-85.8	217.9	53.2	63.8
26	49.8	50.4	.0	.0	75.0	70.0	70.0	70.0	-102.5	163.3	33.9	23.0
27	51.4	49.9	-19.9	-20.0	75.0	70.0	70.0	70.0	-57.2	132.7	-40.0	70.1
28	.0	.0	.0	-20.5	70.0	70.0	70.0	70.0	100.0	39.0	553.1	493.4
29	.0	51.4	.0	.0	70.0	70.0	70.0	70.0	-186.4	-88.7	643.6	445.3
30	.0	54.4	.0	-19.3	70.0	70.0	70.0	70.0	-169.0	-63.0	620.8	513.9
31	.0	.0	.0	-29.7	70.0	70.0	70.0	70.0	-144.0	59.0	584.9	571.2
32	.0	54.9	.0	-29.8	70.0	70.0	70.0	70.0	-211.4	-47.6	609.2	557.4
33	.0	101.4	.0	.0	70.0	70.0	70.0	70.0	-253.8	-177.9	743.8	473.1
34	.0	102.9	.0	-10.2	70.0	70.0	70.0	70.0	-233.7	-153.0	796.8	509.4
35	.0	.0	.0	.0	50.0	100.0	50.0	100.0	396.5	98.9	700.0	22.8
36	50.4	48.1	.0	.0	50.0	100.0	50.0	100.0	448.5	128.9	650.0	51.4
37	.0	51.8	.0	.0	50.0	50.0	50.0	50.0	-172.8	-98.5	601.2	455.3
38	.0	58.1	.0	-10.4	50.0	50.0	50.0	50.0	-205.4	-81.1	645.7	511.0
39	.0	54.4	.0	-20.1	50.0	50.0	50.0	50.0	-220.7	-47.7	601.3	589.6
40	.0	.0	.0	-20.2	50.0	50.0	50.0	50.0	-153.3	80.0	612.0	556.7
41	.0	.0	.0	.0	30.0	80.0	30.0	80.0	615.0	129.0	800.0	38.0
42	.0	24.6	.0	.0	30.0	30.0	30.0	30.0	-153.3	-62.7	575.6	416.5
43	.0	26.4	.0	-9.3	30.0	30.0	30.0	30.0	-158.2	-47.3	556.0	470.8
44	.0	.0	.0	-9.6	30.0	30.0	30.0	30.0	-131.0	39.0	513.6	464.6
45	.0	102.8	.0	-39.0	150.0	150.0	150.0	150.0	-193.5	-60.0	590.3	466.8

FILE NUMBER	INITIAL VERTICAL STRESS (kPa)	FINAL VERTICAL STRESS (kPa)	INITIAL TORSIONAL STRESS (kPa)	FINAL TORSIONAL STRESS (kPa)	INITIAL INNER PRESSURE (kPa)	FINAL INNER PRESSURE (kPa)	INITIAL OUTER PRESSURE (kPa)	FINAL OUTER PRESSURE (kPa)	AVERAGE RADIAL STRAIN (με)	AVERAGE CIRCUM. STRAIN (με)	AVERAGE AXIAL STRAIN (με)	AVERAGE 45 DEGREE STRAIN (με)
46	.0	148.9	.0	.0	150.0	150.0	150.0	150.0	-179.9	-136.4	730.5	426.7
47	.0	150.4	.0	-20.1	150.0	150.0	150.0	150.0	-225.0	-112.1	759.3	478.4
48	.0	149.4	.0	-39.6	150.0	150.0	150.0	150.0	-241.9	-98.3	717.5	525.0
49	.0	202.4	.0	.0	150.0	150.0	150.0	150.0	-264.1	-212.9	814.8	436.0
50	.0	201.8	.0	-20.0	150.0	150.0	150.0	150.0	-271.7	-179.5	757.1	469.8
51	.0	201.9	.0	-39.0	150.0	150.0	150.0	150.0	-243.5	-157.8	791.6	505.9
52	.0	251.0	.0	.0	150.0	150.0	150.0	150.0	-343.5	-274.3	869.8	446.2
53	.0	253.1	.0	-19.8	150.0	150.0	150.0	150.0	-339.7	-243.7	903.3	497.8
54	.0	254.1	.0	-40.5	150.0	150.0	150.0	150.0	-323.9	-224.7	904.6	521.2
55	.0	.0	-39.8	-39.8	110.0	100.0	100.0	100.0	-143.3	535.1	-21.1	29.5
56	98.6	100.2	.0	.0	110.0	100.0	100.0	100.0	-102.0	342.7	29.1	86.9
57	50.7	49.7	-39.7	-39.8	110.0	100.0	100.0	100.0	-93.5	389.0	-2.8	82.2
58	100.2	100.9	-39.7	-39.7	105.0	100.0	100.0	100.0	-46.8	114.4	55.5	64.2
59	100.5	98.9	-19.9	-19.9	110.0	100.0	100.0	100.0	-79.9	304.4	10.6	45.9
60	99.0	98.9	-39.9	-39.8	110.0	100.0	100.0	100.0	-149.3	589.1	18.2	161.8
61	.0	154.6	.0	-19.8	100.0	100.0	100.0	100.0	-253.3	-187.9	708.6	489.4
62	.0	156.4	.0	-38.8	100.0	100.0	100.0	100.0	-277.7	-178.3	729.4	525.6
63	.0	201.8	.0	.0	100.0	100.0	100.0	100.0	-332.1	-309.4	820.5	409.0
64	.0	204.2	.0	-20.1	100.0	100.0	100.0	100.0	-332.6	-300.8	931.9	471.5
65	.0	203.9	.0	-40.4	100.0	100.0	100.0	100.0	-359.2	-283.9	869.0	532.5
66	48.9	49.7	.0	.0	80.0	70.0	70.0	70.0	-202.6	766.1	35.3	246.4
67	100.5	99.2	.0	.0	75.0	70.0	70.0	70.0	-82.7	223.9	30.6	49.3
68	100.2	101.0	-19.8	-19.9	75.0	70.0	70.0	70.0	-88.6	267.1	-52.5	1.2
69	50.8	49.3	-39.7	-39.8	75.0	70.0	70.0	70.0	-80.2	347.1	-28.0	-6.3
70	.0	104.9	.0	-20.0	70.0	70.0	70.0	70.0	-242.4	-154.3	697.6	490.0
71	.0	51.6	.0	-39.9	70.0	70.0	70.0	70.0	-169.0	-61.9	512.1	557.4
72	.0	.0	.0	-39.7	70.0	70.0	70.0	70.0	-137.0	100.0	433.4	617.8
73	.0	101.9	.0	-39.5	70.0	70.0	70.0	70.0	-266.9	-119.9	689.2	573.5
74	.0	152.5	.0	.0	70.0	70.0	70.0	70.0	-306.5	-276.2	841.6	394.3
75	.0	151.3	.0	-19.9	70.0	70.0	70.0	70.0	-291.9	-234.9	757.7	491.7
76	.0	.0	-20.0	-20.0	55.0	50.0	50.0	50.0	-108.9	530.6	23.9	134.3
77	49.6	50.9	.0	.0	55.0	50.0	50.0	50.0	-68.9	313.3	-15.8	48.7
78	49.7	51.3	-19.8	-19.9	55.0	50.0	50.0	50.0	-115.6	417.5	47.1	54.2
79	50.9	49.5	19.9	19.8	55.0	50.0	50.0	50.0	-154.9	510.2	58.1	238.6
80	.0	52.8	.0	-30.4	50.0	50.0	50.0	50.0	-222.8	-74.3	549.2	568.9
81	.0	.0	.0	-29.3	50.0	50.0	50.0	50.0	-157.1	105.0	352.8	597.0
82	.0	105.2	.0	.0	50.0	50.0	50.0	50.0	-295.1	-232.7	825.1	396.7
83	.0	100.6	.0	-20.8	50.0	50.0	50.0	50.0	-287.0	-167.5	700.7	488.5
84	.0	50.0	.0	.0	30.0	30.0	30.0	30.0	-231.0	-137.1	617.1	392.7
85	.0	47.9	.0	-9.9	30.0	30.0	30.0	30.0	-204.3	-110.7	550.6	460.0
86	.0	52.2	.0	-21.2	30.0	30.0	30.0	30.0	-248.4	-111.6	580.7	548.8
87	199.1	198.8	.0	.0	105.0	100.0	100.0	100.0	-31.9	108.4	50.8	36.5
88	200.0	198.2	-19.9	-19.9	105.0	100.0	100.0	100.0	-43.8	98.3	40.4	28.7
89	198.3	199.5	-39.7	-39.9	105.0	100.0	100.0	100.0	-77.7	159.8	14.6	76.6
90	199.0	199.7	39.9	39.9	105.0	100.0	100.0	100.0	-29.6	175.4	-8.7	62.9
91	201.5	197.1	.0	.0	110.0	100.0	100.0	100.0	-104.7	424.0	16.1	156.0
92	.0	254.4	.0	.0	100.0	100.0	100.0	100.0	-442.9	-445.2	972.6	401.2
93	.0	253.7	.0	-20.1	100.0	100.0	100.0	100.0	-434.2	-404.6	1,066.9	454.7
94	.0	248.6	.0	-39.9	100.0	100.0	100.0	100.0	-406.5	-348.0	1,064.9	551.1
95	.0	.0	-39.8	-40.0	75.0	70.0	70.0	70.0	-83.5	463.5	5.0	141.0

FILE NUMBER	INITIAL VERTICAL STRESS (kPa)	FINAL VERTICAL STRESS (kPa)	INITIAL TORSIONAL STRESS (kPa)	FINAL TORSIONAL STRESS (kPa)	INITIAL INNER PRESSURE (kPa)	FINAL INNER PRESSURE (kPa)	INITIAL OUTER PRESSURE (kPa)	FINAL OUTER PRESSURE (kPa)	AVERAGE RADIAL STRAIN (με)	AVERAGE CIRCUM. STRAIN (με)	AVERAGE AXIAL STRAIN (με)	AVERAGE 45 DEGREE STRAIN (με)
96	99.5	99.5	-39.8	-39.8	75.0	70.0	70.0	70.0	-112.2	217.7	129.9	57.1
97	98.8	99.6	.0	.0	80.0	70.0	70.0	70.0	-200.7	826.5	42.5	244.0
98	99.7	99.8	-20.0	-20.0	80.0	70.0	70.0	70.0	-156.4	703.4	.3	219.2
99	.0	154.8	.0	-39.5	70.0	70.0	70.0	70.0	-367.9	-265.0	938.6	380.2
100	.0	202.3	.0	.0	70.0	70.0	70.0	70.0	-441.3	-406.8	973.8	415.8
101	.0	198.9	.0	-20.1	70.0	70.0	70.0	70.0	-430.4	-351.7	1,028.2	497.7
102	98.8	99.3	.0	.0	55.0	50.0	50.0	50.0	-70.4	344.9	64.0	127.0
103	.0	106.9	.0	-30.5	50.0	50.0	50.0	50.0	-380.4	-229.1	836.0	583.6
104	.0	55.4	.0	-39.6	50.0	50.0	50.0	50.0	-238.6	-132.6	523.6	666.9
105	.0	153.3	.0	.0	50.0	50.0	50.0	50.0	-407.1	-428.2	1,004.6	397.4
106	.0	.0	.0	-20.1	30.0	30.0	30.0	30.0	-153.8	-114.7	349.5	546.5
107	20.0	20.0	.0	-19.5	110.0	110.0	100.0	100.0	132.6	25.0	318.8	458.4
108	24.0	76.0	.0	.0	110.0	110.0	100.0	100.0	-171.7	-74.2	365.7	405.0
109	24.0	24.0	.0	-39.5	110.0	110.0	100.0	100.0	121.0	-70.3	346.0	630.5
110	25.0	125.0	.0	.0	110.0	110.0	100.0	100.0	-222.3	-157.5	554.7	381.2
111	24.0	126.0	.0	-19.5	110.0	110.0	100.0	100.0	-202.2	-137.2	562.8	428.2
112	23.0	198.0	.0	.0	110.0	110.0	100.0	100.0	-305.4	-360.7	689.6	403.4
113	20.0	202.0	.0	-39.1	110.0	110.0	100.0	100.0	-337.5	-371.9	776.0	501.6
114	23.0	75.0	.0	.0	80.0	80.0	70.0	70.0	-223.9	-110.3	413.1	404.3
115	25.0	77.0	.0	-20.5	80.0	80.0	70.0	70.0	-207.1	-122.2	398.7	504.1
116	23.0	125.0	.0	.0	80.0	80.0	70.0	70.0	-250.0	-238.2	561.6	392.1
117	23.0	127.0	.0	-19.7	80.0	80.0	70.0	70.0	-280.4	-247.4	553.7	491.7
118	24.0	126.0	.0	-39.7	80.0	80.0	70.0	70.0	-267.2	-524.1	503.1	641.7
119	24.0	175.0	.0	.0	80.0	80.0	70.0	70.0	-338.6	-449.9	659.4	436.8
120	.0	.0	-19.9	-20.0	100.0	200.0	100.0	200.0	532.9	-103.7	-175.4	-284.4
121	.0	.0	19.9	19.9	100.0	200.0	100.0	200.0	530.7	24.8	44.6	69.1
122	54.1	49.8	-20.0	-20.0	100.0	200.0	100.0	200.0	529.6	26.1	111.2	-47.1
123	.0	.0	-40.1	-39.9	100.0	200.0	100.0	200.0	541.1	-173.9	-23.2	-133.1
124	49.2	51.0	-40.0	-40.0	100.0	200.0	100.0	200.0	495.5	57.3	-20.3	-37.3
125	99.4	100.0	-19.9	-19.9	100.0	200.0	100.0	200.0	492.5	106.7	49.0	-59.7
126	99.8	98.3	-39.9	-39.9	100.0	200.0	100.0	200.0	532.6	129.2	76.6	-28.2
127	.0	.0	-19.9	-19.8	50.0	100.0	50.0	100.0	396.8	98.1	24.4	-25.8
128	50.4	48.8	-19.9	-20.0	50.0	100.0	50.0	100.0	427.3	138.2	57.9	33.8
129	50.8	49.6	19.9	20.0	50.0	100.0	50.0	100.0	444.7	213.4	49.2	99.8
130	.0	.0	-40.0	-39.8	50.0	100.0	50.0	100.0	411.6	65.2	130.1	-132.0
131	50.9	49.5	-40.0	-39.9	50.0	100.0	50.0	100.0	458.4	152.9	-69.8	11.9
132	49.6	49.6	39.8	40.0	50.0	100.0	50.0	100.0	449.1	270.7	4.5	160.3
133	.0	.0	-20.0	-20.0	30.0	80.0	30.0	80.0	588.4	189.0	30.0	-73.6

The range of b-values and angles of principal plane rotation are summarized in Figures E1.1 and E1.2 respectively.

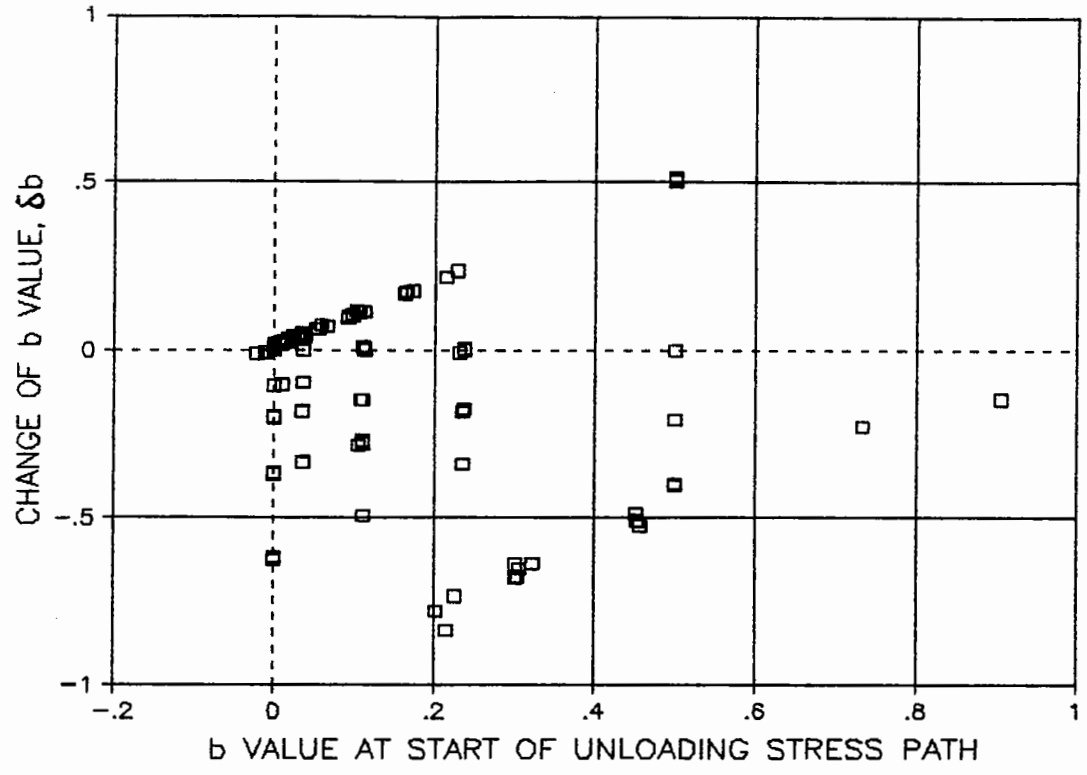

Figure E1.1 Range of b-Values used in Resilient Strain Tests carried out with the Repeated Load Hollow Cylinder Test Apparatus.

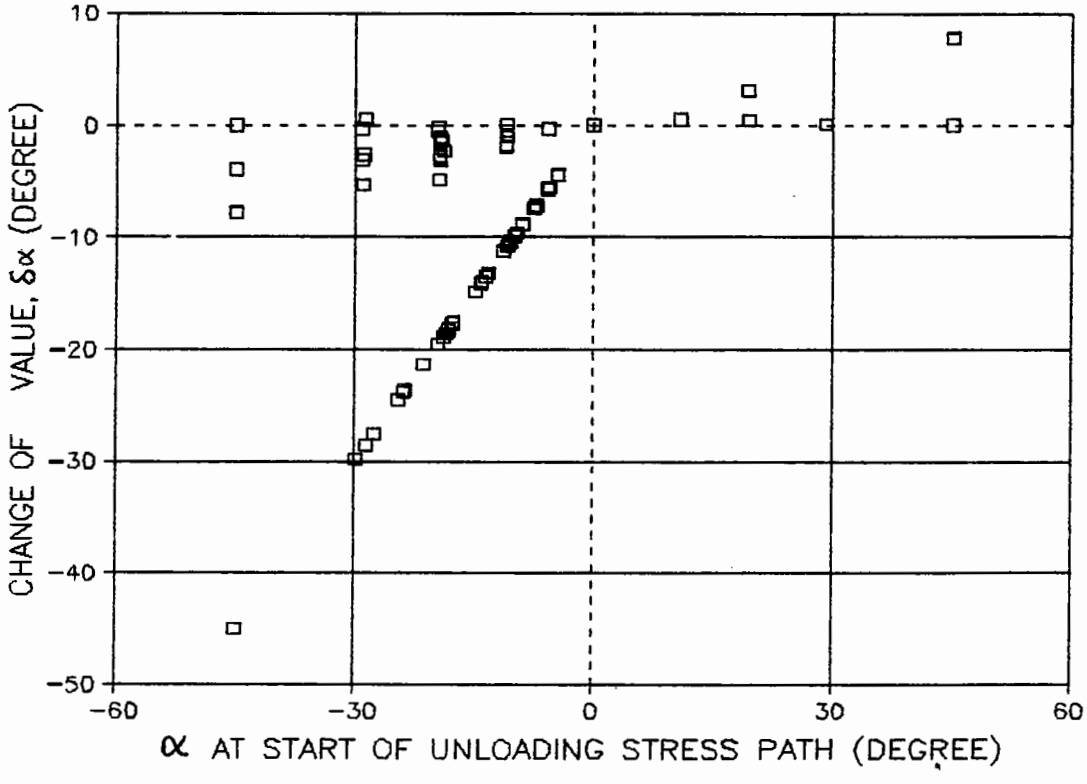

Figure E1.2 Range of Angles of Principal Plane Rotation used in Resilient Strain Tests carried out with the Repeated Load Hollow Cylinder Test Apparatus.